2024 Biennial Report on Seismic Monitoring and Research in Texas

December 2024

The University of Texas at Austin

Bureau of Economic Geology

Mark Shuster, Interim Director

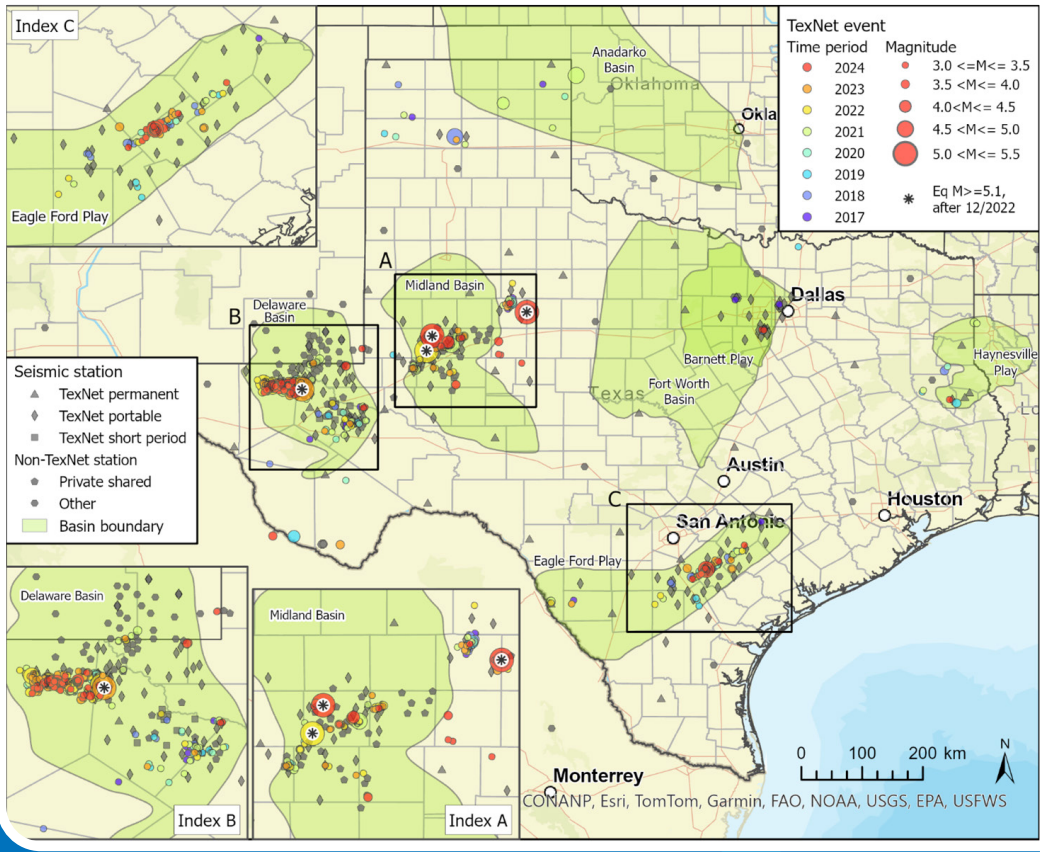

by Alexandros Savvaidis

with contributions from:

Emmanouil Parastatidis, Aaron Averett, Peter Sarkis, Victor Salles, Dino Huang, Katerine Vallejo, Peter Eichhubl, Shuvajit Bhattacharya, Nikolaos Bakirtzis, Elena Kalogirou, Robin Dommisse, Yangkang Chen, Ian Duncan, Jaewook Lee, Jess Domino, Vincent O'Sullivan, Grace Burke, Camilo Muñoz, Constantinos Skevofilax, Bartik Pandel, Ellen M. Rathje, Albert R. Kottke, Yunfeng Chen, Chao Li, Shanshan Yong, Xin'an Wang, Omar M. Saad, M. Beatrice Magnani, Giuseppe Volpe, Michele Mauro, Marco Scuderi, Cristiano Collettini, Mark W. Hildyard, Stella Pytharouli, Oliver Chowns, Andy Nowacki, Iason Grigoratos, Sergey Fomel, Daniel Siervo, Caroline Breton, Fangxue Zhang, Huijian LI, Farzaneh Aziz Zanjani, Yapo Abolé Serge Innocent Oboué, Ramin M. H. Dokht, Yu Jeffrey Gu, Maria Koroni, Jingchuan Wang, Xiuxuan Jiang, Quan Zhang, Wei Chen, Cooper McCabe, Bede Uku, Preston Fleck, Natalie L. Alvarez, Jessica Domino, Heather R. DeShon, Asiye Aziz Zanjani, Vamshi Keranam, Julia Rosenblit, Yeshey Sheldon, Zhong Lu, Liuqing Yang, Hersh Gilbert, Derek L. Schutt, Gabriela Fernández-Viejo, Claire Currie, Pascal Audet, Xing Li, Elizaveta Rybina, and Michelle Lopez

TexNet

Bureau of Economic Geology

TexNet Mission Statement and Objectives

Approved by the Technical Advisory Committee, December 6, 2023.

Mission Statement

Serve as an independent scientific body that monitors earthquake activity, analyzes associated data, and distributes findings and data to government, industry, and the public for their benefit and the benefit of the State of Texas.

Objectives

- Maintain a network of seismometers across Texas that continuously and accurately record earthquake data.
- Exceed the network technical performance metrics established by consultation with the TAC and USGS.
- Strive to reduce the bias and the uncertainty of epicenter and depth estimates.
- Seek to understand causation of seismicity in Texas.
- Maintain, and make available in a timely way, all event catalogs and databases of waveform data and products to stakeholders:
  a. Texas Railroad Commission
  b. Texas Emergency Management, Texas Department of Transportation, Texas Commission Environmental Quality, Texas Groundwater Protection Council, University Lands
  c. Local Communities
  d. Oil and Gas Industry
  e. Academic Research Community
  f. General Public
  g. Media
- Receive and assess input from the stakeholders.
- Seek to understand and quantify the impact and risk to public safety and infrastructure.
- Report to State Legislator, the Governor's office, BEG and The University of Texas at Austin.

TexNet Technical Advisory Committee Members

Brian Stump, Committee Chair – SMU (Southern Methodist University)
Mark Boyd, Committee Member – ConocoPhillips
Chris Hillman, Committee Member – City of Irving
Jeff Nunn, Committee Member – Chevron
Kris Nygaard, Committee Member – ExxonMobile (Retired)
Scott Mitchell, Committee Member – Deep Blue
Aaron Velasco, Committee Member – Railroad Commission of Texas
David Cannon, Committee Member – Diamondback Energy
Larry French, Committee Member – Texas Water Development Board (Retired)
Mark Shuster, Interim Director (ex efficio)

Table of Contents

1.0 Executive Summary

Following a peak in 2022, the level of seismicity greater than magnitude (M_L) 2.5 within Texas has slowly decreased overall (**Figure 1**, Green line). This change has not occurred in all areas as it is mostly driven by a decrease in seismicity within the Delaware Basin. In contrast, the Midland Basin and Eagle Ford area of South Texas have experienced an increase in the frequency and magnitude of seismic events. Also, during 2024, two events above M_L3 were reported in the Dallas-Fort Worth area following a period of five years without such events (**Figure 2**), and two events greater than M_L5 that occurred in the Midland Basin which were widely felt across Texas.

The TexNet network currently operates over 200 stations, versus the original plan for a total of 60 stations, in order to properly characterize all of these seismic events. Due to the rapid increase in seismicity, TexNet funding was increased in 2023 to meet its primary goal of prompt analysis and reporting of all earthquakes down to $M_L1.5$, a metric that has been designed to support stakeholders, including the Railroad Commission of Texas (TRRC) and industry partners.

However, the equipment infrastructure (IT and seismometers) is aging. Most of it is out of warranty and will eventually require replacement, although the current budget has no sustainment funds. The long-term solution for all stakeholders is to request additional funding to provide the necessary resources to meet TexNet's growing monitoring and reporting needs into the future. The current TexNet network provides precise epicenter locations that enable rapid stakeholder response to mitigate possible local impacts. Securing additional short-term funding will ensure that this level of service continues uninterrupted.

Seismic activity in Texas (Figure 2) occurs in seven primary areas: the Permian Basin (~88%), the Eagle Ford area (~9%), the Panhandle, the Dallas-Fort Worth urban area, East Texas, the Cogdell field and the Scurry-Fisher County line (both are near Snyder). All events greater than M_L5 have occurred in the Permian Basin.

The TexNet mission's highest priority is to maintain a network of seismometers which are capable of both accurate and timely recording and reporting of seismicity across Texas, which has motivated the increase in the number of monitoring stations. As a result, the storage space used to archive TexNet data has grown sixteen-fold since 2016, and will continue to increase. During 2024, TexNet has improved its stations' uptime from 90% to 94%, with a goal to support aging equipment and telecommunications, and increase staffing to fulfill USGS standards of 99% uptime.

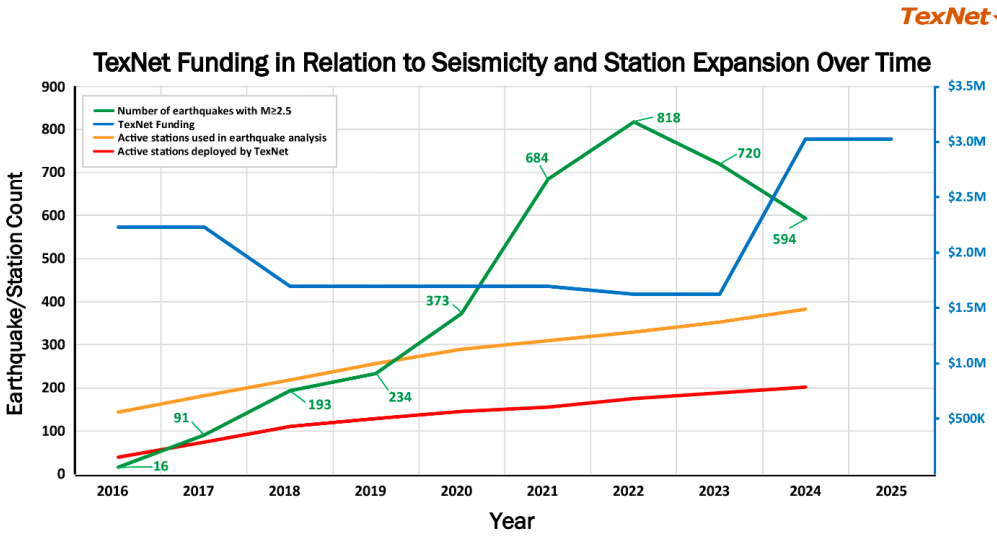

Figure 1. Number of earthquakes of $M_L \geq 2.5$. Number of active stations deployed and maintained by TexNet. Number of stations used in earthquake analysis. Level of TexNet funding.

In key areas of high earthquake risk, TexNet reports all seismicity of $M_L \geq 1$ the next business day. This level of detail is essential to meet the needs of the industry and supports the TRRC in well permitting and mitigation of induced seismicity in urban areas such as Midland and Odessa.

In order to achieve our primary goals over the next two years, TexNet intends to improve the sustainability of its in-the-field infrastructure, improve the analysis of recorded seismic events, and expand event reporting to lower magnitudes by:

(1) Replacing aging seismic monitoring equipment (currently ~85)

(2) Improving and replacing IT infrastructure

(3) Expanding near real-time reporting of events from $M_L 2.5$ down to $M_L 1.5$

(4) Adding auto picked events, and subsequently verified events, to the website

Figure 3 below displays all the seismicity (~30,000 earthquakes) within Texas since 2017. Going forward, TexNet will require the maintenance of the current level of funds at $3 million per year and will request additional funds of $1 million per year for the next two years specifically to upgrade aging equipment. **These funds will allow the State of Texas to ensure timely and accurate reporting of all earthquakes down to $M_L 1.5$.** This lower level of magnitude reporting will also provide the ground motion, earthquake data, and catalogs to the industry and the TRRC to properly and promptly mitigate seismicity risk. *An active and updated network is necessary to capture and document all of these earthquakes for all stakeholders.*

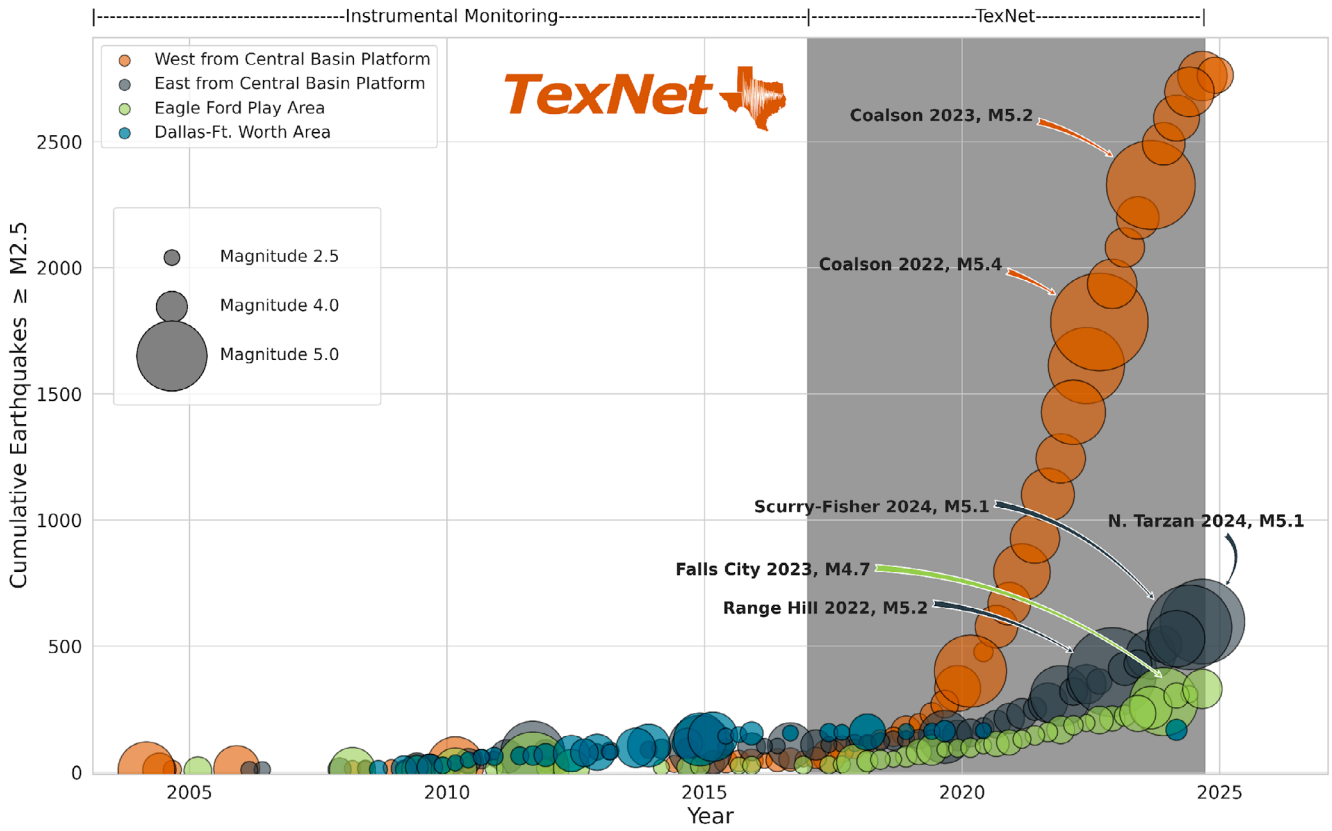

Figure 2. Cumulative number of earthquakes in critical key areas; West from Central Basin Platform (Delaware Basin), East from Central Basin Platform (Midland Basin, Cogdell Field and the Scurry-Fisher County line), Eagle Ford, and Dallas-Ft Worth.

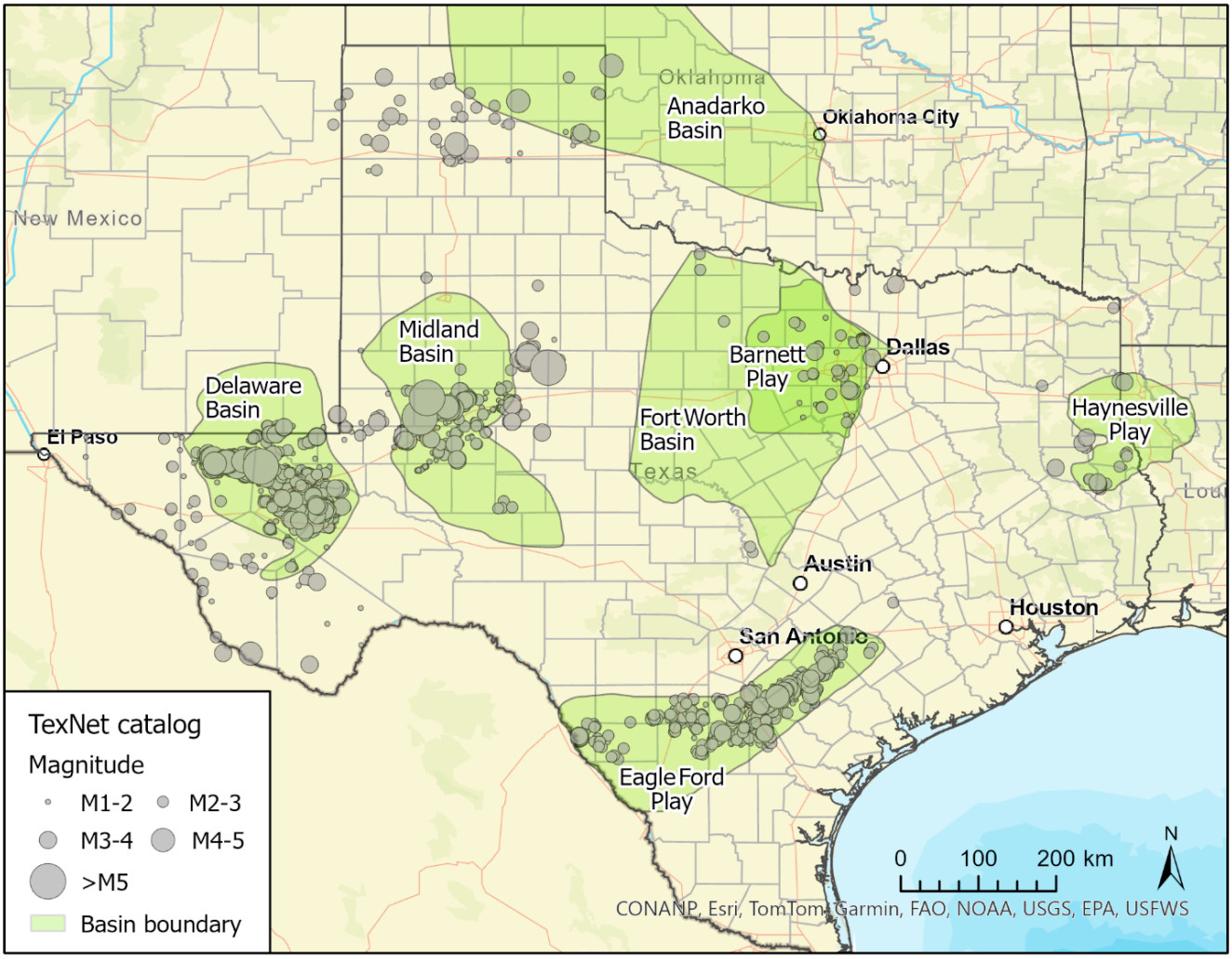

Figure 3. Seismicity in Texas since 2017. Circle size corresponds to earthquake magnitude.

2.0 Impact of TexNet Program on the State of Texas

The TexNet Seismic Monitoring and Seismology Research Program is a multidisciplinary program managed by the Bureau of Economic Geology. **TexNet's mission is to serve as an independent scientific body that monitors earthquake activity, analyzes associated data, and distributes findings and data to government, industry, and the public for their benefit and the benefit of the State of Texas**.

TexNet collects and makes publicly accessible earthquake data, as well as applied research and educational products to the State of Texas, which:

- Quantifies earthquake activity across the state.
- Enables risk mitigation in areas of increased seismicity, and in areas of expected increases in oil and gas operations.
- Informs measures to minimize earthquake activity associated with human activities.
- Reduces impact of possible future earthquakes on both the people and infrastructure of Texas.
- Provides information and outreach that improves the understanding of seismic risk and its avoidance for Texans.

These deliverables are generated as a result of the integrated TexNet process illustrated in **Figure 4**. The process

1. Begins with earthquake monitoring, including the timely and accurate analysis of earthquake activity,
2. Supports understanding of the causes of seismicity, and
3. Delivers information to stakeholders to enable earthquake mitigation, minimizing socioeconomic risks to the State.

The supporting research takes advantage of expertise at The University of Texas at Austin (UTA), Southern Methodist University (SMU), and the University of Houston (UH). This collaboration maximizes the linkage between these different research groups and the operational task.

Monitoring Activities

Seismicity monitoring across the State of Texas currently uses over 200 active TexNet seismic stations and a considerable number of seismic stations deployed from other groups in Texas and neighboring states. Our primary goal is to conduct continuous seismic monitoring across Texas for all events with magnitude greater than or equal to magnitude (M_L) 3.0 in less than 20 minutes. A secondary goal is continuous monitoring and evaluation of events, down to M_L1.5 (with appropriate error quantification) within the next business day, providing a basis for quantifying earthquake activity as it develops for mitigation purposes. These analyses are made publicly available in an earthquake catalog (https://catalog.texnet.beg.utexas.edu), which is the primary source for subsequent operational decisions made by both the Railroad Commission of Texas (TRRC) and industry operators. The earthquake catalog provides primary data for several of our research initiatives as well as data to other researchers within and outside of Texas. Research is designed to reduce bias and modelling errors necessary to improve earthquake locations, including the critical assessment of earthquake depth. Additional goals are to continuously improve the accuracy of surface locations,

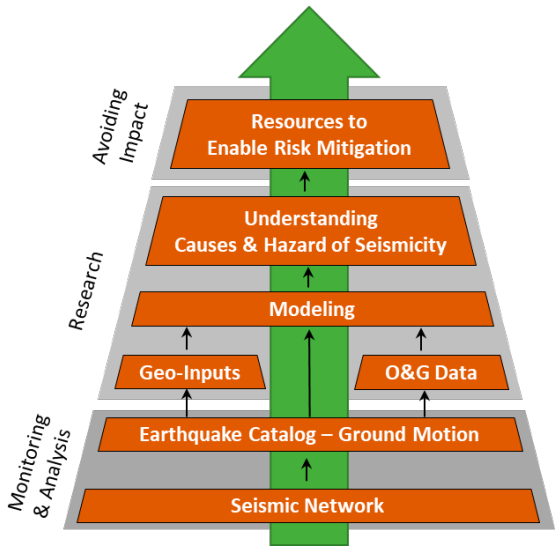

Figure 4. TexNet processes, products, and resources provided to the State of Texas.

and to distinguish the impact of shallow versus deep water disposal on the associated seismicity. Distinguishing between shallow and deep disposal impacts is important to develop mitigation strategies undertaken by the TRRC and the industry.

The acquisition of high-quality seismic data, as well as the compilation, maintenance, and quality control of earthquake catalogs, supports stakeholders in making operational decisions that can reduce the number and intensity of induced earthquakes across Texas. Recent development and distribution of an expanding set of web tools (https://texnet.beg.utexas.edu/) make simple, rapid data distribution publicly available. These tools are part of the TexNet dashboard that provides information to the industry and TRRC to track seismicity across the state, monitor produced water injection, and support risk mitigation in areas of increased seismicity.

Statewide seismicity online catalog to identify seismicity and support migration efforts:
https://catalog.texnet.beg.utexas.edu/

High resolution online catalog to identify and document faults zones:
https://injection.texnet.beg.utexas.edu/

Water injection volumes within SRAs to understand produced water injection:
https://hirescatalog.texnet.beg.utexas.edu/

Geomechanical Injection Scenario Toolkit (GIST) of injection-related earthquakes:
https://gist.texnet.beg.utexas.edu/

Status of all seismic stations used in monitoring:
https://monitor.texnet.beg.utexas.edu/

TexNet operational data combined with statistical, physics-based and Machine Learning (ML) earthquake models quantify areas prone to seismicity and identify factors that might impact future earthquakes. Complementary to an understanding of the causes of seismicity, parameters important in assessing surface hazards and impacts of seismicity are also provided.

Education and Outreach Efforts

By conducting an educational program that shares essential information, TexNet facilitates both an understanding of seismicity risk and approaches for its avoidance. TexNet provides valuable resources to the public, focusing on earthquake monitoring, seismic data analysis, and various online tools. Our goal is to offer comprehensive support, reliable information, and effective solutions to a wide range of stakeholders, including researchers, educators, students, industry professionals, governmental agencies, and the public.

To ensure widespread awareness of our resources, TexNet has established a strong social media presence on platforms such as LinkedIn with 25% of recipients being Texas-based and X. TexNet demonstrates its expertise and shares research materials through these channels. One of notable initiatives in this biennium was promoting the "International ShakeOut Day" and "Earthquake safety and preparedness" through a dedicated social media campaign on LinkedIn. The key messages of this campaign included:

- Sharing essential takeaways about earthquake safety and preparedness, focusing on monitoring, analysis, awareness, prevention, and risk mitigation.
- Visual Content, including social media posts, posters, infographics and other visuals, was designed and published to engage our audience.
- As part of our commitment to raising awareness and improving earthquake preparedness, TexNet explained the ShakeAlert Earthquake Early Warning system and provided guidance on what to do during an earthquake. On October 17th, 2024, the TexNet team, along with over 57 million participants worldwide, took part in the Great ShakeOut Earthquake Preparedness Drill in observance of International ShakeOut Day. We followed the essential earthquake safety protocol: drop, cover, and hold.
- A partner from a local government agency and emergency services, Texas Division of Emergency Management (TDEM) was engaged, and an in-person meeting with TDEM at the Bureau of Economic Geology was hosted.

Informational Outreach includes publishing an informational poster "Be proactive and stay safe" on LinkedIn highlighting the services provided by TexNet, including:

1. Seismicity Monitoring: Earthquake catalogs
2. Earthquake Activity Analysis
3. Earthquake Prevention
4. Seismicity Reasoning Identification: Seismotectonic environment, surface deformation analysis, hazard assessment
5. Risk Assessment
6. Seismicity Awareness
7. Public Outreach
8. Risk Mitigation Strategies

Initiatives and Improvements

During the current biennium (FY 2024-25), we pursued research and delivered products that have significantly improved our understanding of induced earthquakes in Texas as a result of the TexNet Technical Advisory Committee's (TAC) recommendations. Appendix A provides a list of these contributions with brief descriptions of the publications stemming from our work to demonstrate the breadth and depth of this progress. A full list of publications can be accessed at https://texnet.beg.utexas.edu/news/publications.

The fundamental goal of our research during this biennium has been to improve our ability to detect, locate, and analyze earthquakes statewide in an increasingly timely manner. We have also developed and deployed new techniques to improve location accuracy and provide information in a timely manner. Ground motion data are denoised and automatic earthquake location accuracy has been enhanced, when compared to manual earthquake locations. Based on this research, we managed to provide automatic locations at the time of the earthquake that are manually reviewed in the next business day, for events down to M_L1.5 in the Delaware Basin and Eagle Ford Play, and down to M_L1 in the Midland Basin. Also, TexNet 3D geomodelling efforts have provided interpretation to better quantify the depth of seismicity in West Texas.

A Machine Learning (ML) approach was developed during the previous biennium to automatically detect seismic arrivals and use these picks for earthquake detection, reducing human intervention and improving the timely location of the increasing number of earthquakes. The original version of the ML approach produced a total runtime of 217 seconds to identify picks from within 1 minute of data from 99 seismic stations using 15 CPUs. After the applied software was optimized, the total runtime decreased from 217 to 28 seconds (**Figure 5**). This higher efficiency and decreased runtime allows TexNet to use the ML approach in real time and provide timely automated earthquake locations.

As the number of earthquakes across Texas increases, it has been necessary to develop a tool to optimize the selection of seismic station locations. The array design tool takes into consideration fault locations, stress levels/orientation, and subsurface geological information and calculates the optimal station distribution and provides the desired minimum earthquake magnitude detection and location thresholds.

Figure 6 illustrates the best array design that fulfills these criteria for an event detected in an area of interest from at least 5 out of 13 stations with a magnitude of completeness[1] of -0.25, assuming an ambient noise amplitude of less than 10^{-8} m/s. This approach allows us to optimize seismic station locations when different types of information (noise level, fault sensitivity, etc.) are available.

[1] In an earthquake catalog, the magnitude of completeness (Mc) is the minimum magnitude above which all earthquakes within a certain region are reliably recorded (https://corssa.org/en/glossary/).

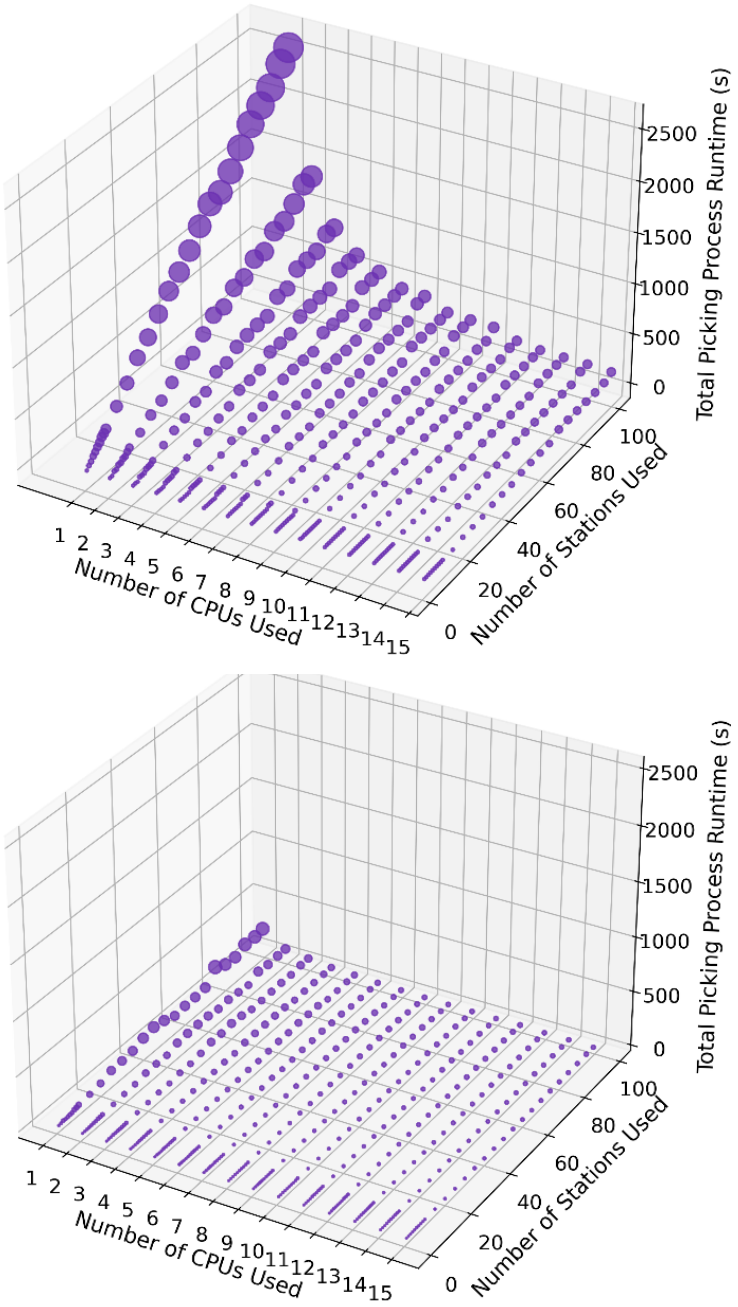

Figure 5. Runtime of optimized Machine Learning (ML) application used in arrival picks and earthquake detection. Benchmarking using the initial code developed (top) and the optimized version (bottom) showing the total runtime for the picker to detect arrival picks.

Figure 7 presents the seismic-strain rate in West Texas (Huang et al., 2024; under review), showing the highest strain rate (≥10Nt-m per year) in areas that currently accommodate most of the high magnitude earthquakes. The areas of high strain rate may be candidates to host additional high magnitude earthquakes. Information such as this help regulators with well permit application decisions and motivates risk mitigation actions.

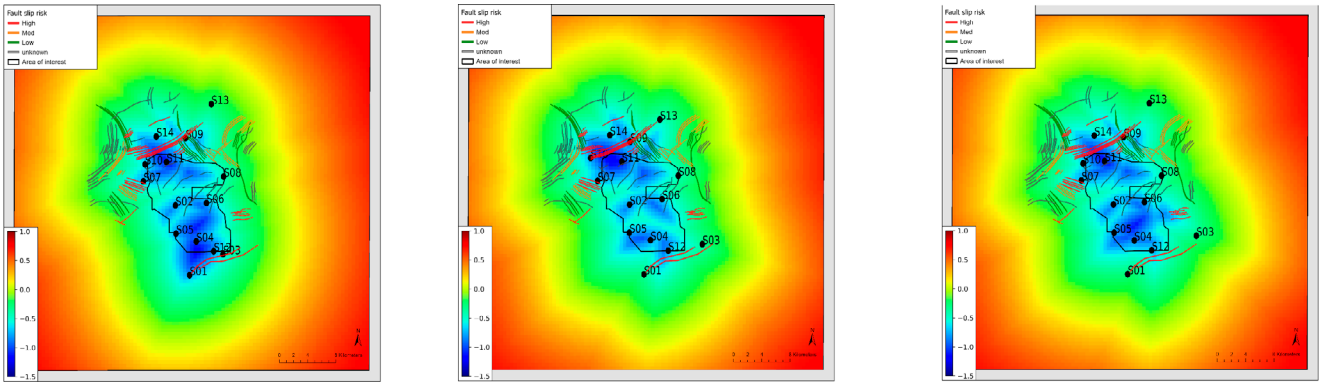

Figure 6. The best solution for an array design with 13 seismic stations that fulfill the criteria of an earthquake event detected in the area of interest from at least five stations and a magnitude of completeness of -0.25 assuming a noise amplitude to be below 10^{-8} m/s. The color scale denotes the expected lowest magnitude threshold.

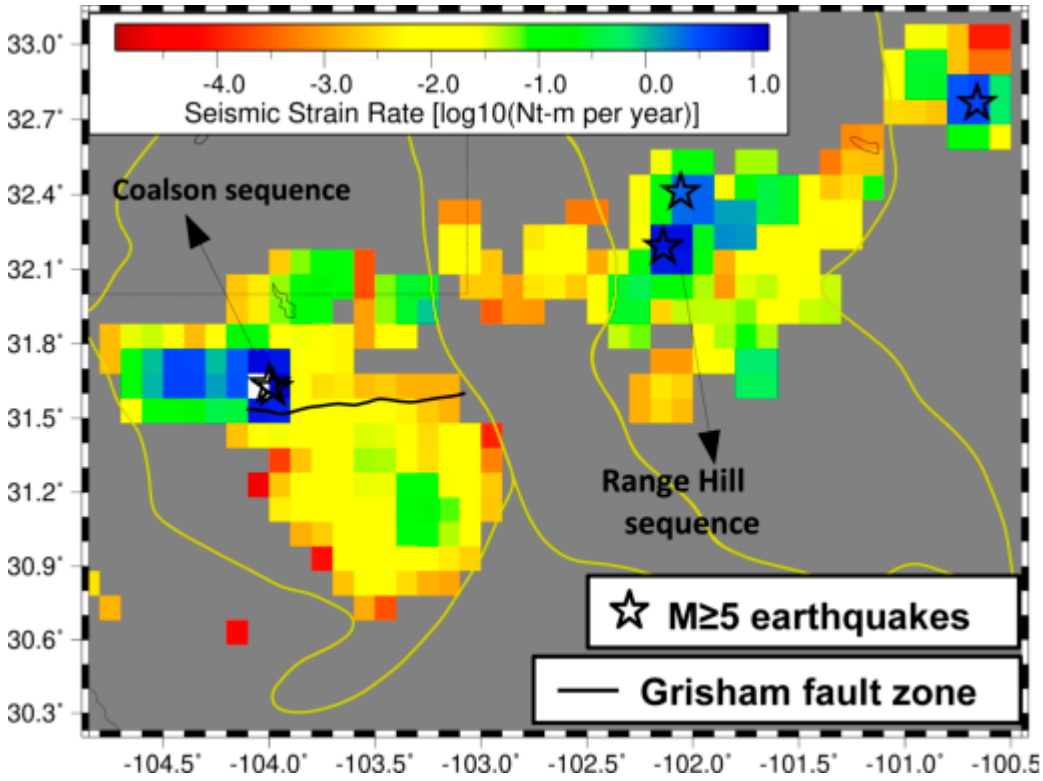

Figure 7. Distribution of seismic strain rate in the Permian Basin. Highest ($M_L \geq 5$) earthquakes are denoted with a star. Boundaries of the Delaware and Midland sub-basins, to the west and east sides, are denoted with yellow line.

Application of TexNet Data to Railroad Commission Actions

In 2021, the Texas Railroad Commission (TRRC) designated the Northern Culberson-Reeves Seismic Response Area (NCR SRA) to respond to the increased seismicity TexNet reported in the area. Within the NCR SRA (**Figure 8**), saltwater disposal operators created an Operator-Led Response Plan (OLRP) on March 1, 2022. The goal of the OLRP was to reduce high-magnitude seismicity by decreasing the number of occurrences to a maximum of M_L3.5 earthquakes no later than December 31st, 2023. This plan was further updated to expand the size of the SRA in response to an M_L5.4 earthquake in November 2022. Based on the occurrence of seven earthquakes with magnitudes ranging from M_L3.6 to M_L5.2 in November and December 2023, The TRRC suspended all disposal well permits into deep strata within the boundaries of the NCR SRA. TexNet real time monitoring and timely earthquake source characterization provided a basis for changing injection limits that ultimately reduced earthquake occurrences in the area.

In September 2021, the TRRC established the Gardendale SRA (**Figure 9**), based on felt earthquakes that occurred between February 2020 and September 2021. Due to TexNet-reported seismic events in December 2021, the TRRC suspended all disposal well permits to deep strata within the boundaries of the SRA. Due to a M_L5.2 earthquake that occurred on December 16th, 2022, RRC enlarged the Gardendale SRA. On May 1st, 2023, an OLRP plan was created responding to the M_L5.2 event (Range Hill). The goal of the OLRP is to reduce high magnitude seismicity, and now there are no more M≥3.5 earthquakes within the SRA.

The TRRC established the Stanton SRA (6) on January 2022, and an OLRP was established on May 15th, 2022, with the objective to eliminate ≥M_L3.5 earthquakes by December 31st, 2023. However, TexNet reported two M_L4.1 earthquakes on November 4th and 5th, 2023 and based on the monitoring information the OLRP was revised. Following the April 10, 2024, M_L4.4 earthquake reported by TexNet, the OLRP plan was further revised, and deep disposal volume limits were decreased by 29 percent across the SRA compared to pre-November 2023. TexNet prompt reporting of seismicity rates in the SRA provided the necessary data for the OLRP updates in order to mitigate the earthquake risk.

In summary, TexNet seismic data and products have proven fundamental to providing the TRRC the basis for adjusting SRAs as well as motivating decisions on response and mitigation plans that have reduced both the number and magnitude of earthquakes in these areas. Specifically, TRRC using TexNet data define SRAs which are used in mitigation by restricting injection.

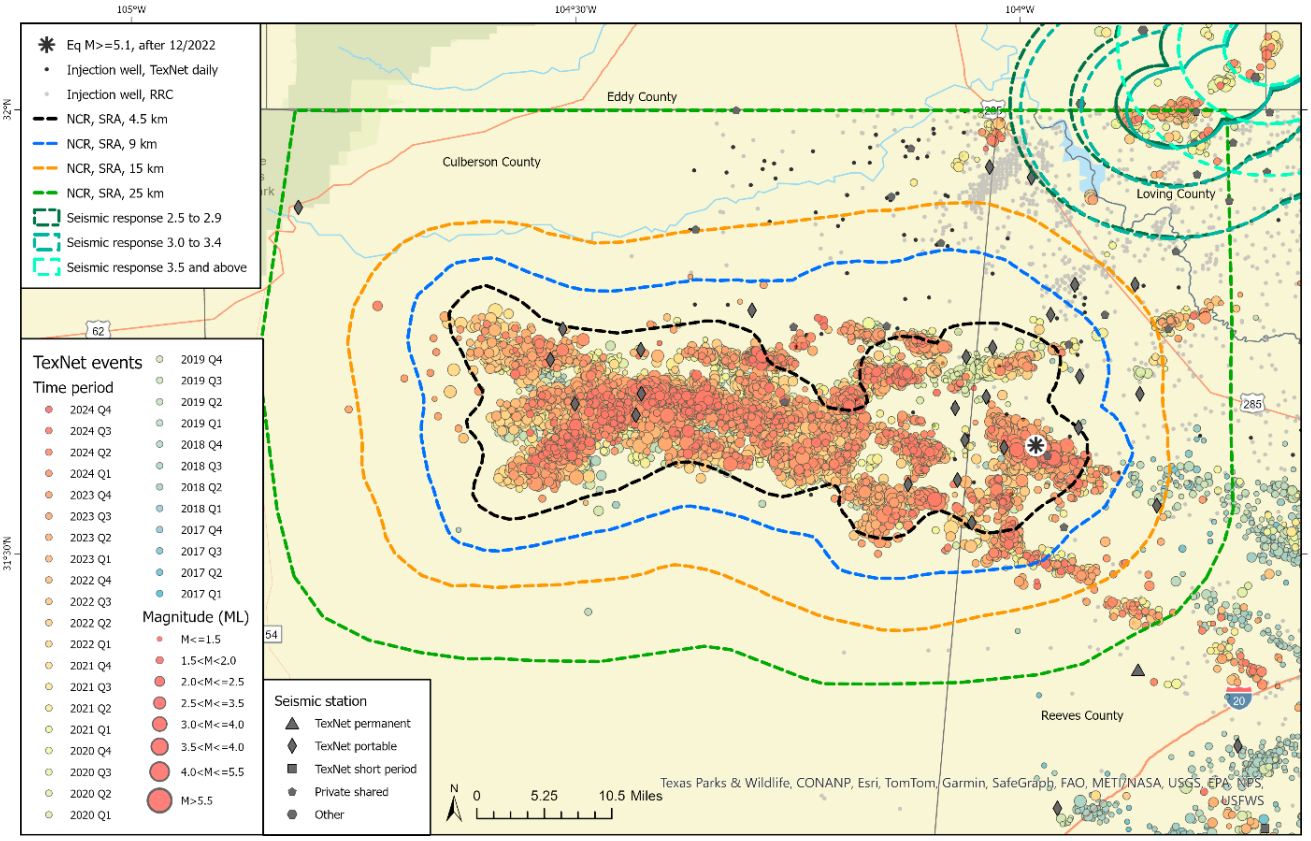

Figure 8. Spatiotemporal distribution of seismicity in North Culberson and Reeves Counties. The SRA defined by the Railroad Commission using TexNet data is denoted with colored isolines. Different guidelines are assigned based on the SRA isoline. Produced water injection wells are denoted with a dot (black dots denote the location of a well for which daily injection volume and pressure data are provided from the operator using the TexNet web tool https://injection.texnet.beg.utexas.edu/). Asterisk denotes the M_L5.2 earthquake of November 08, 2023.

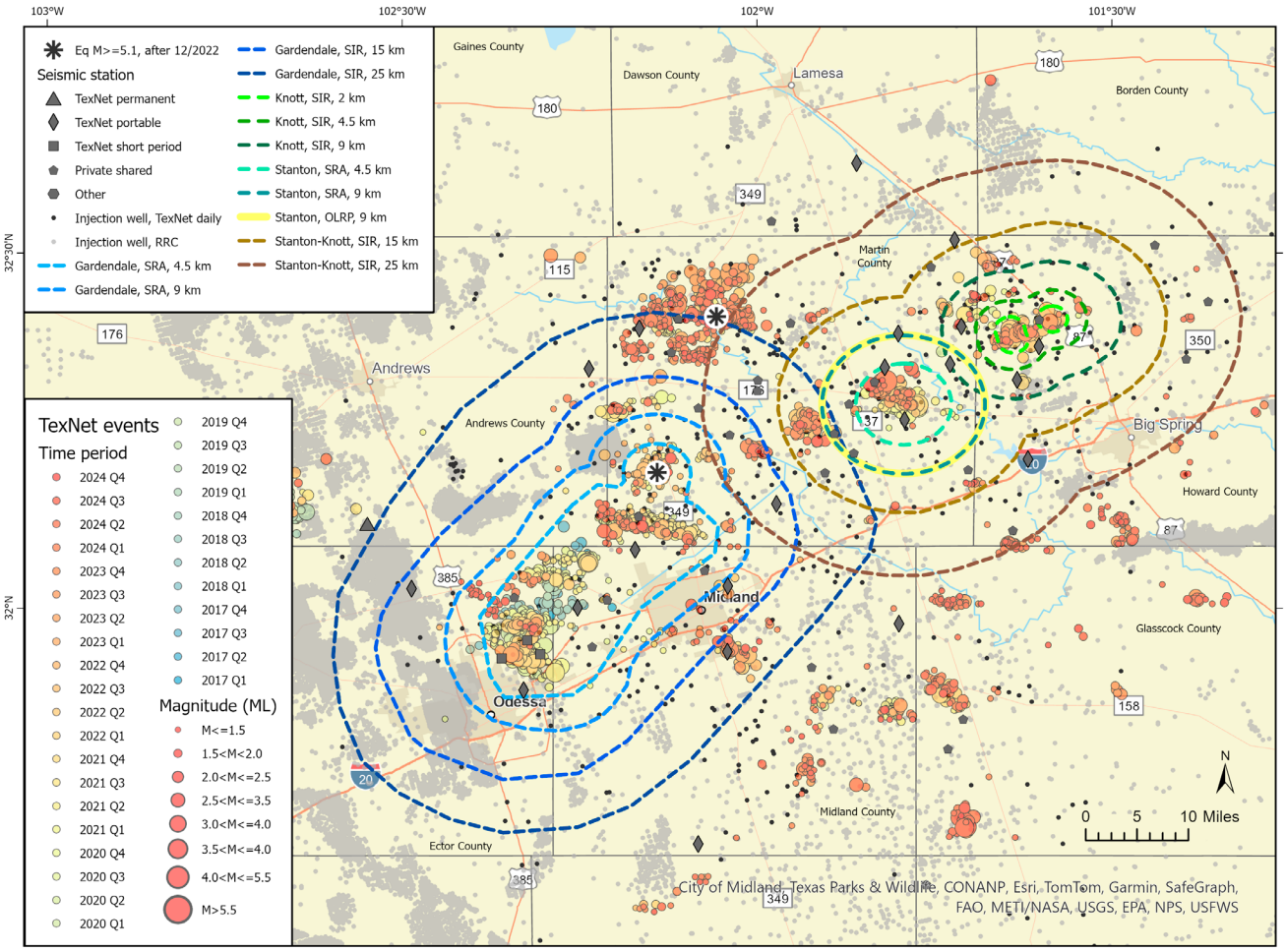

Figure 9. Spatiotemporal distribution of seismicity in the Midland Basin. The Seismic Response Areas (Gardendale to the southwest and Stanton to the northeast) defined by the TRRC using TexNet data are denoted by colored isolines. Different guidelines are assigned based on the SRA isoline for each SRA. Produced water injection wells are denoted with a dot. Black dots denote the location of a well for which daily injection volume and pressure data are provided from the operator using the TexNet web tool https://injection.texnet.beg.utexas.edu. Asterisks denote the M_L5.4 earthquake of December 16, 2022, in the Gardendale SRA, and the M_L5.1 earthquake of September 17, 2024, in the midpoint of the Gardendale and Stanton-Knott SRAs.

3.0 TexNet Budget Utilization: Spending and Next Biennial Request

Summary: Following a peak in 2022, seismicity decreased within the Delaware Basin. In contrast, the Midland Basin and Eagle Ford area of South Texas have experienced an increase in the frequency and magnitude of seismic events. Also, during 2024, two events above M_L3 were reported in the Dallas-Fort Worth area following a period of five years without any similar events, and two events greater than magnitude 5 occurred in the Midland Basin were widely felt across Texas.

The TexNet network currently operates over 200 stations, compared to the original plan for a total of 60 stations in order to properly characterize seismic events. Due to the rapid increase in seismicity, TexNet funding was increased in 2023 to meet its primary goal of prompt analysis and reporting of all earthquakes down to M_L1.5, a metric that has been designed to support stakeholders, including the Railroad Commission of Texas (TRRC) and industry partners. However, the equipment infrastructure (IT and seismometers) is aging. The long-term solution for all stakeholders is to request additional funding to provide the necessary resources to meet TexNet's growing monitoring and reporting needs into the future.

The TexNet mission's highest priority is to maintain a network of seismometers which is capable of both accurate and timely recording and reporting of seismicity across Texas, motivating the increased number of monitoring stations. As a result, the storage space used to archive TexNet data has grown sixteen-fold since 2016, and will continue to increase. During 2024, TexNet has improved its stations' uptime from 90% to 94%, with a goal to improve aging equipment, telecommunications, and staffing to fulfill USGS standards of 99% uptime.

In order to achieve our primary goals over the next two years, TexNet intends to improve the sustainability of its in-the-field infrastructure, improve the analysis of recorded seismic events, and expand event reporting to lower magnitudes by: (1) Replacing aging seismic monitoring equipment (currently ~85), (2) Improving and replacing IT infrastructure, (3) Expanding near real-time reporting of events from M_L2.5 down to M_L1.5, and (4) Adding auto picked events, and subsequently verified events, to the website.

Going forward, **TexNet will require maintaining the current level of funding at $3 million per year** and will request additional funding of $1 million per year specifically to upgrade aging equipment. **These funds will allow the State of Texas to ensure timely and accurate reporting of all earthquakes down to M_L1.5.** This lower level of magnitude reporting will also provide the ground motion, earthquake data, and catalogs to the industry and the TRRC to properly and promptly mitigate seismicity risk. *An active and updated network is necessary to capture and document all of these earthquakes for all stakeholders.*

During the current biennium, TexNet received an additional $1,400,000 per year compared to previous TexNet biennial funds. These funds are being used to increase the number of staff members required to meet the prompt analysis of the growing number of earthquakes across Texas in order to reduce the associated hazards. By the end of FY24 (September 1st, 2023 to August 31st, 2024), TexNet recruited the projected number of needed staff members to complete these taks. As a result, TexNet wi)ll meet its goal of analyzing events down to M_L1.5 in the next business day in early FY25 (September 1st, 2024, to August 31st, 2025), providing the citizens of Texas and its industries critical information for earthquake preparation and mitigation.

Table 1 outlines previous (FY24) and budgeted (FY25) expenses for specific TexNet operational elements. Texas Seismic Network Operations include deployment and maintenance of seismic sensors, telecommunications for data transmission, purchase and operation of TexNet Hub Servers used for both data storage and processing, detection of seismicity, and 24/7 operations necessary to analyze all seismicity events greater than M_L3. Operations costs are primarily used to support personnel, materials, services, seismic and IT equipment, and travel. These costs include salaries of personnel who operate and maintain existing seismometer stations and redeploy portable seismometer stations to detect, locate, and report earthquakes of higher than $M_L1.5$ in the state. Most of the research spending has been on personnel, services, and sub-contracts to Southern Methodist University (SMU) and the University of Houston (UH) focused on more detailed analysis of earthquake patterns and improvements in location including more accurate and precise depth estimates.

A detailed breakdown of FY24 expenses and budgeted FY25 costs for specific categories is provided in **Table 2**. Most of the personnel costs are directed to The University of Texas Bureau of Economic Geology. In FY24, a considerable investment was necessary for IT hardware to ensure timely retrieval, archival, and analysis supporting 24/7 operations. As a result of aging instrumentation, additional expenses were similarly applied to maintenance of existing equipment as well as to the purchase of a limited amount of new equipment for replacements.

Table 1. TexNet Expenses during the 2023-2025 Biennium.

Theme	Project Title	FY24 (Spent)	FY25 (Budgeted)	Project Total
Seismology	T1- Network Operations (Operations)	$1,700,000.00	$2,000,000.00	$3,700,000.00
	T2 - Seismicity Analysis (Operations and Research)	$1,180,000.00	$876,581.55	$2,056,581.55
	T3 - Analysis of Human Operations and Seismicity (Operations and Research)	$47,000.00	$47,927.22	$94,927.22
Seismic Risk Assessment	Earthquake Hazard Assessment (Research)	$50,000.00	$50,000.00	$100,000.00
Databases and Dissemination	Geodatabases and Web Development (Research and Outreach)	$55,000.00	$57,491.23	$112,491.23
Total		**$3,032,000.00**	**$3,032,000.00**	**$6,064,000.00**

Table 2. TexNet Expenses Categories during the current biennium. Amounts provided for FY24 are actual and for FY25 are budgeted.

		Categories	Expensed FY24	Budgeted FY25
1		**Salaries**	**$1,972,967.36**	**$2,315,001.87**
	a	SMU	$194,106.42	$165,000.00
	b	UH	$5,464.08	$0.00
	c	UTA	$1,773,396.86	$2,150,001.87
2		**IT**	**$371,296.68**	**$199,780.13**
	a	Computer-Usage	$46,635.78	$73,971.00
	b	IT-Hardware	$229,820.80	$29,000.00
	c	IT-Services	$94,840.10	$96,809.13
3		**Office and PPE Supplies**	**$8,497.25**	**$10,000.00**
	a	Office-Supplies	$6,472.62	$7,000.00
	b	PPE	$2,024.63	$3,000.00
4		**New Equipment**	**$241,142.49**	**$0.00**
	a	Seismic Stations	$241,142.49	$0.00
5		**Equipment Maintenance**	**$220,407.00**	**$266,705.00**
	a	Seismic Stations Replacements	$181,959.43	$170,000.00
	b	Seismic Stations Maintenance	$38,447.57	$96,705.00
6		**Telecommunications**	**$133,326.49**	**$135,000.00**
	a	Services	$133,326.49	$135,000.00
7		**Travel**	**$81,527.66**	**$105,513.00**
	a	Outreach	$19,589.76	$24,793.00
	b	Fieldwork	$61,937.90	$80,720.00
8		**Balance-Forward**	**$2,835.07**	**$0.00**
		Total	**$3,032,000.00**	**$3,032,000.00**

Since the recruit process of new personnel took several months only a portion of FY24 funds were used to pay the necessary new personnel, it was possible to invest the remaining funds for new IT hardware necessary to process the increasing volume of data associated with the earthquake activity across the State of Texas. In addition, the observed increase in seismicity in key areas (Midland Basin and Eagle Ford) motivated the expenditure of funds for new seismic station hardware necessary to improve the network configuration in these areas in order for precision seismic locations including depth estimates (Figure 2 from Executive Summary). With the completion of the recruitment of all new personnel by the end of FY24, there are no FY25 funds to cover costs associated with any new seismic station additions to TexNet as this part of the budget now goes to the personnel budget. The costs for maintaining existing IT and seismic equipment hardware are retained in the FY25 budget so that operations are not impacted.

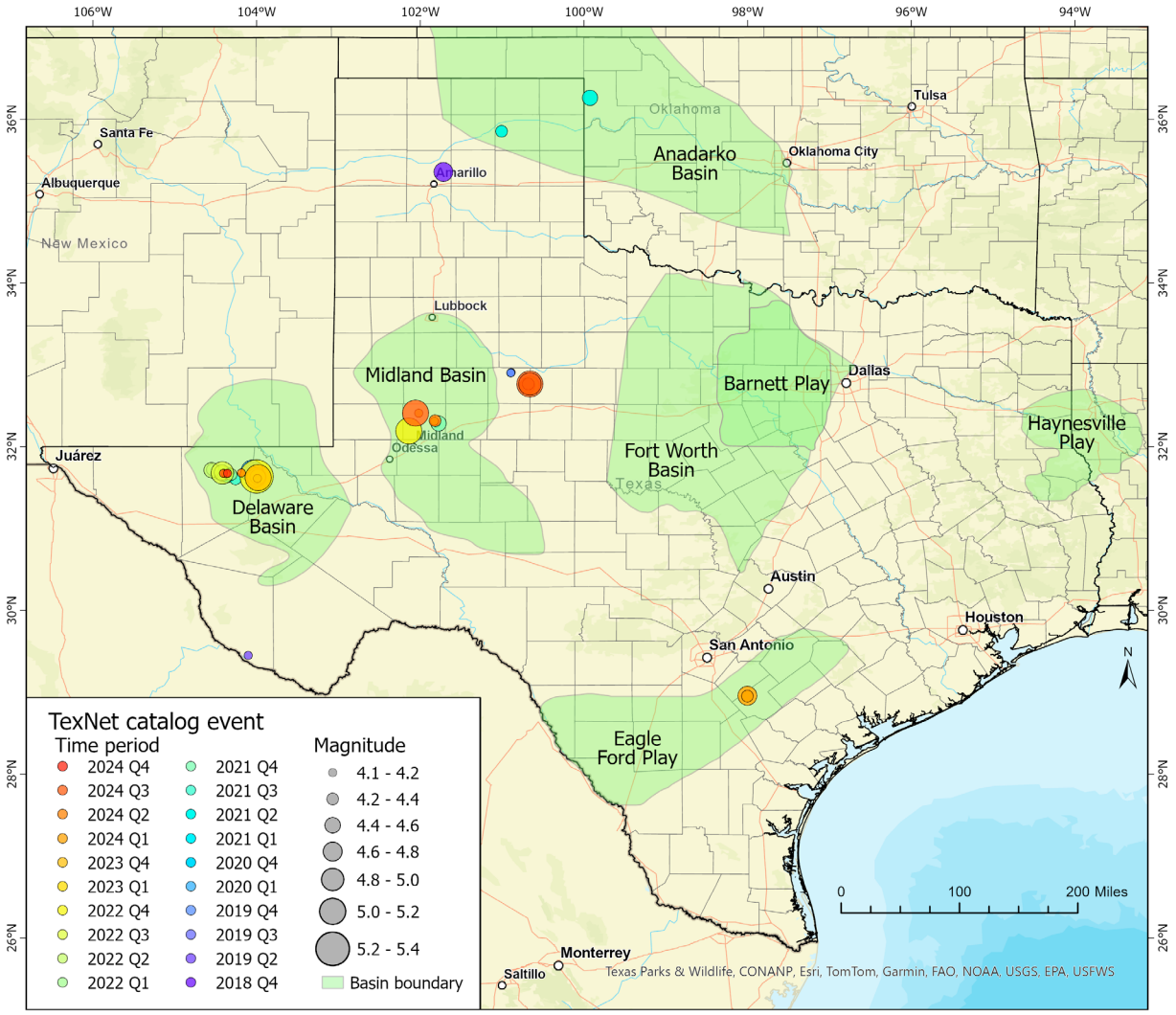

Figure 10. Map showing the 55 highest magnitude earthquakes in Texas from January 2017 to November 2024. Dots are sized by magnitude with color representing the quarter of the year in which they occurred.

Figure 10 displays the 55 largest magnitude earthquakes ($M_L \geq 4.1$) in Texas from January 2017 to November 2024. Out of the 55 events, 21 occurred between Q4 of 2022 and November 2024, documenting the continued high level of seismicity across the State. There are several new areas of new seismicity that now host large magnitude earthquakes including those in the Delaware Basin, the Midland Basin, and its eastern shelf. Additionally, the Eagle Ford Play area had 3 of the highest magnitude earthquakes during 2023 and 2024 since TexNet started in 2017. The increase in seismicity in these new areas necessitates improvements to the network, including the acquisition and deployment of new seismic equipment in those areas.

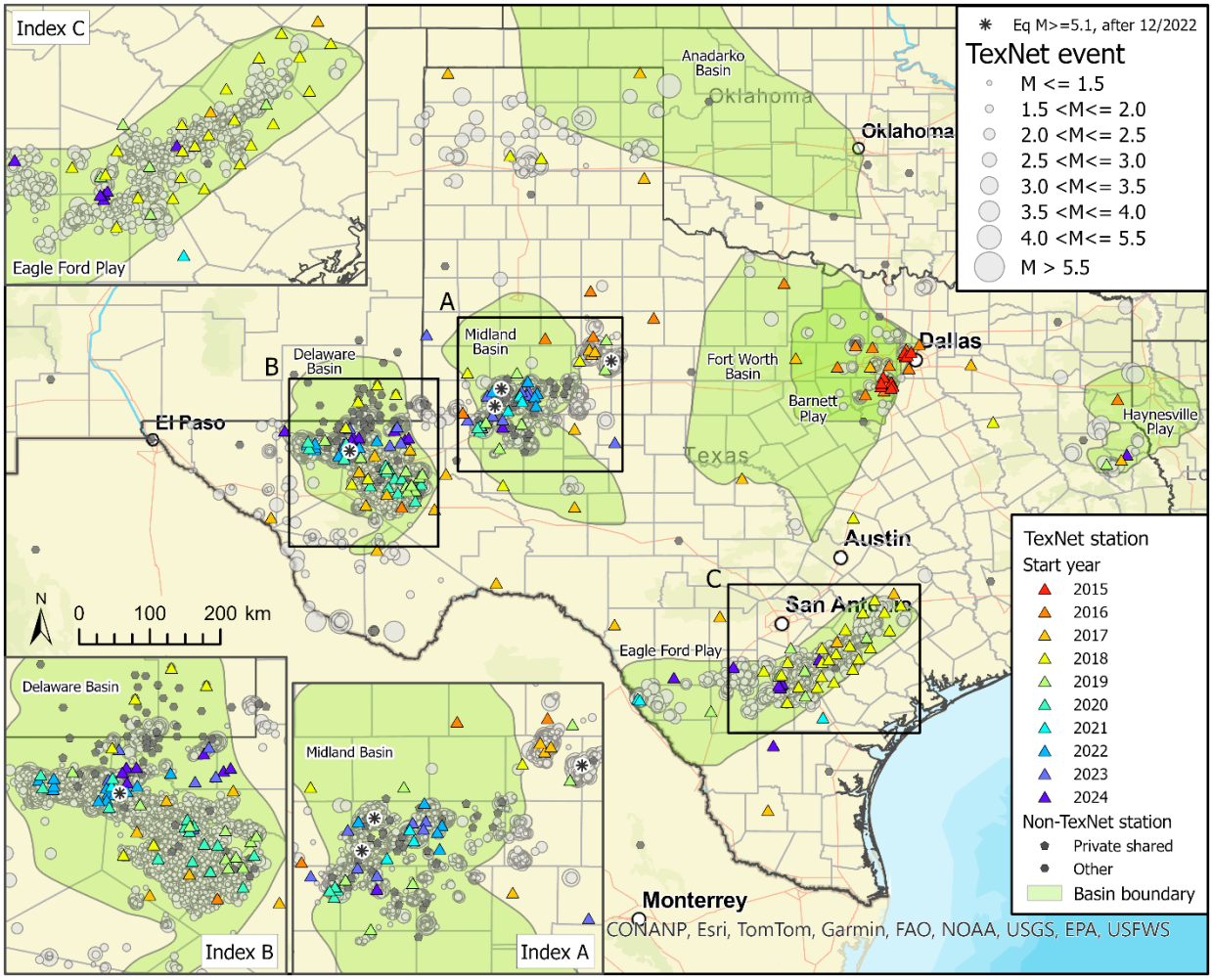

Figure 11. Map showing the seismic stations deployed in the State that TexNet maintains. Stations are color- coded by the year the equipment was purchased. The seismicity since 2017 is shown in comparison to the station distribution.

TexNet deployed the first set of new seismic stations across Texas in 2016. As a result of the aging of this initial instrumentation pool, beginning in 2022, an increasing level of seismic station hardware required extensive repair or replacement. **Figure 11** displays the distribution of seismic station in the State that TexNet maintains. Stations are color-coded by the year the equipment was acquired. Based on this data, by the end of 2024, 85 seismic stations will operate with equipment that is out of warranty, therefore additional funds are necessary for anticipated repairs. TexNet storage needs have increased from 500 Gigabytes in 2016 to 8000 Gigabytes in 2024, and will continue to increase. IT infrastructure, including servers and storage units purchased in 2016 and 2017, will also be out of warranty by the end of 2024 and in need of replacement since their hardware components are no longer available in the market, in order to ensure uninterrupted operation. As a result, IT and seismic equipment needs are anticipated to increase in the next biennium.

For TexNet to fulfill its goals and meet stakeholder's requirements to provide 24/7 operations and improve the understanding of seismicity in the state, we believe an increase in the budget to $8 million for the next biennium (FY26 and FY27) is necessary. This estimated budget increase of $2 million over two years is needed to upgrade existing older IT infrastructure and anticipated repair/replacement of aging seismic station equipment.

4.0 TexNet Seismic Monitoring: Increasing Numbers of Seismic Stations

By 2022, TexNet had increased the number of stations in the State in response to increasing seismicity, increased regulatory requirements, and stakeholders advocating for improvement of earthquake location precision, including depth (Figure 12). At that time, the goal was to densify the network in the Delaware Basin where more than 600 earthquakes of $M_L \geq 2$ occurred in 2022. Also, on November 16, 2022, this area had the highest magnitude earthquake ($M_L 5.4$) in Texas since TexNet's inception.

With industry support, TexNet currently operates and maintains 201 active stations. **Figure 12** summarizes the increase in seismic stations across the State designed to meet the rapid increase in earthquake activity. In addition, the enhanced characterization of the seismicity in the state is leveraged by seismic data from stations deployed and maintained by other groups. These groups include the USGS and industry stations (deployed due to the TRRC incentive to license higher volumes of injecting produced water) as well as seismometers in neighboring states and instruments deployed by a variety of research groups. The total number of seismic stations that TexNet is now archiving and routinely uses in both seismicity analysis and research has increased from 144 stations in 2016 to 383 stations in November 2024. Out of the 383 stations, 64 are deployed and maintained

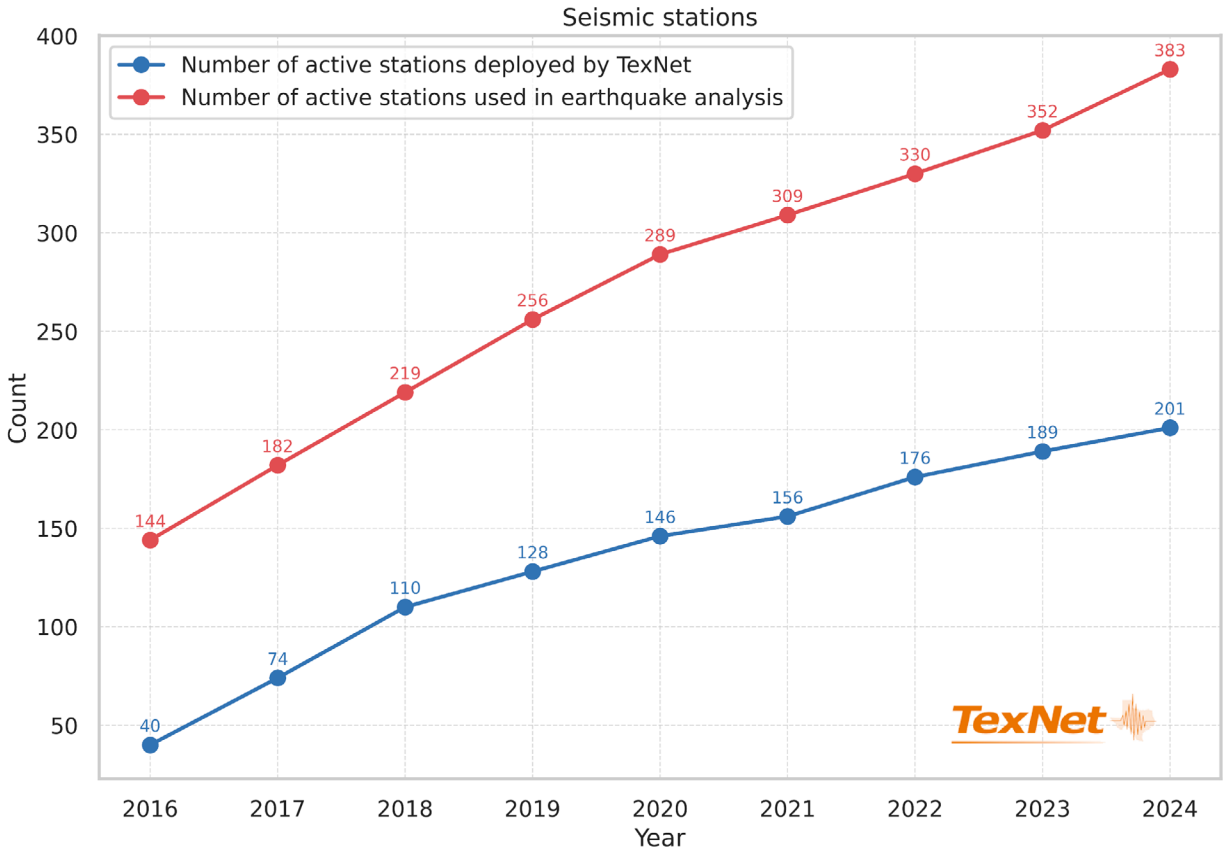

Figure 12. Number of active seismic stations deployed by TexNet as a function of time (blue line) and seismic stations (deployed and maintained by operators, USGS, and neighboring states authorities) from which real-time data are archived and used by TexNet earthquake analysis and research (orange line).

by the industry providing data to TexNet (up from 34 in November 2022). As a result, the associated analyst workload has dramatically increased with the expanding number of stations. Experience demonstrates that this density of stations and amount of data are necessary to extend the monitoring threshold to M_L1.5 as requested by operators and regulators, and even to M_L1 in key areas like the Midland Basin in order to provide precise location and source depth estimates necessary for earthquake mitigation decisions. The ML tools discussed earlier and illustrated in Figure 5 facilitates this processing.

From its inception, TexNet has established standards[2] for seismic monitoring stations, operated a real-time high-quality network, and delivered the necessary ground motion data for daily earthquake analysis. To continue to meet these goals, TexNet deployed an additional 34 stations during 2023–2024 (**Figure 13**) using state funds, private funds, and donations. The strategy TexNet has used in deploying additional resources is driven by increased seismicity in key areas of the state and the locations of industrial operations and/or spatiotemporal seismicity patterns. Critical to these deployments is the location of one or more seismic stations directly above the earthquake activity to improve depth estimates, a critical parameter for mitigation strategies associated with industry activities (Figure 4). Specifically, TexNet deployed 1 station in East Texas, 9 stations in South Texas, 9 stations in Midland Basin, 14 stations in the Delaware Basin, and 1 station north of the Permian Basin, all locations with ongoing and increasing seismicity.

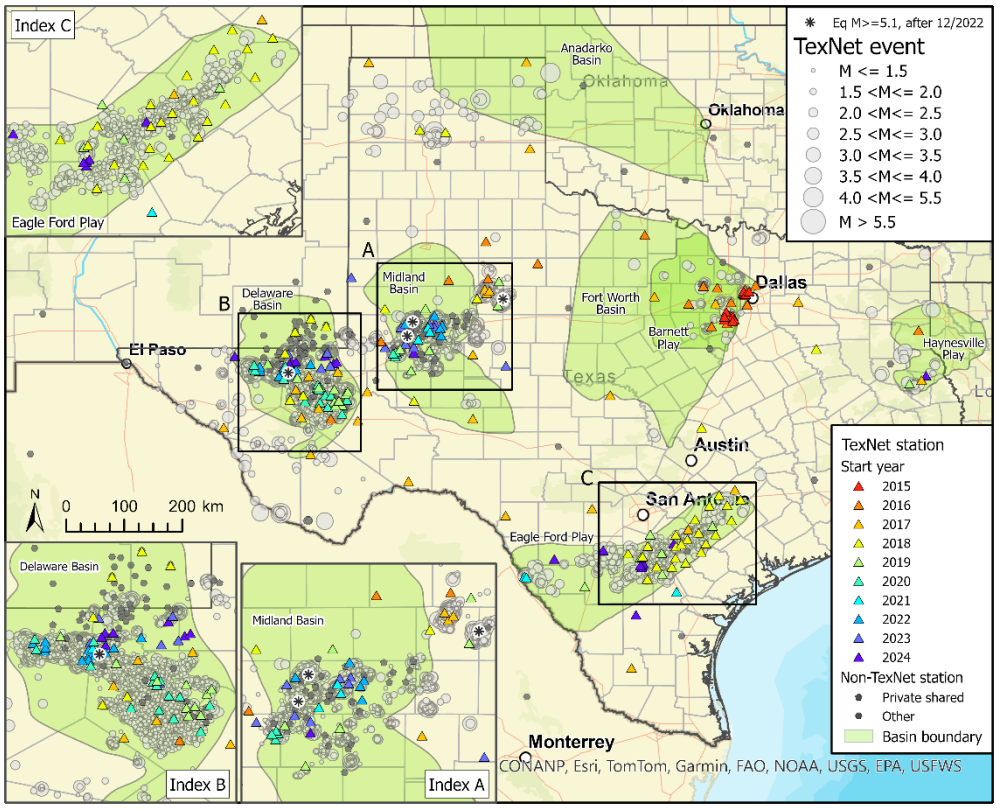

Figure 13. Seismic stations provide real-time waveform data to the TexNet hub for seismicity monitoring. Stations deployed/maintained by TexNet are colored. Asterisks denote the M_L≥5.1 earthquakes that occurred after December 2022.

[2] https://texnet.beg.utexas.edu/operations/seismic-station-requirements

Although the seismicity has slightly decreased in the Delaware Basin, it is important to increase the number of stations to fill the gap close to the border with New Mexico (North Culberson, Reeves, Loving, and Winkler counties, Figure 8). Also, due to the increase of seismicity, the currently small number of stations, and increased regulatory requirements (Permian Basin), stakeholders have requested that TexNet increase the number seismic stations to improve the precision of earthquake locations, including depth estimates, in the Midland Basin and Eagle Ford Play.

To support real-time data acquisition and long-term archival and distribution for more than 200 TexNet stations, additional IT hardware systems were recently purchased, and need to be operated and maintained. To properly support the real-time earthquake monitoring requirements of TexNet, a full backup system for the TexNet Hub was also purchased and installed to handle possible disruption of services at the primary site. This equipment is critical to maintaining TexNet's 24/7 operations under all conditions across Texas.

TexNet continues its operations with on-call staffing based on USGS standards to provide earthquake source information to its stakeholders in a time sensitive manner. As an example of this near, real-time monitoring, we use our online catalog[3], to publish earthquake information for all events of $M_L \geq 3.0$ in less than 20 minutes of their occurrence. Earthquakes with $2.0 \leq M_L < 3.0$ are catalogued in the following weeks. Additional USGS performance standards include a magnitude of completeness for the catalog to $M_L 2$ which based on our stakeholders is being lowered to $M_L 1.5$, and is currently met in the Permian Basin and Eagle Ford Play.

Following the funding increase, TexNet recruited the requested staff, including earthquake analysts, field engineers, and IT/CS personnel. TexNet with the addition of these new people beginning in 2024 provides reporting of seismicity down to $M_L 1.5+$ for the Delaware Basin, Snyder, Eagle Ford, and Dallas-Fort Worth. For key areas like the Midland Basin, the threshold is down to $M_L 1$. The threshold is $M_L 2$ for the rest of the state where the instrument coverage is more sparce.

TexNet stations' uptime has improved from 90% in Q3 of 2022 to 94% in Q3 of 2024. TexNet still needs to improve the stations' uptime to 99% to fulfill USGS standards. If TexNet continues to miss the USGS benchmarks, it could impact its designation as the authoritative source for earthquake information in Texas. To achieve this goal, TexNet needs to replace equipment that is already out of warranty. By the end of 2024, hardware at 85 stations will be out of warranty.

Although our standard products continue to be used daily by our stakeholders, the lack of resources necessary to keep the hardware up-to-date, densify the seismic network and further improve the depth estimation of the seismicity to the levels identified by our oversite Technical Advisory Committee, industry, and the TRRC has significantly impacted our daily and long-term operations. Aging hardware, limited stations, and development of new 3D velocity models still impact the ability of industry to make decisions necessary to protect their investment while meeting TRRC guidance to enable risk mitigation.

[3] https://catalog.texnet.beg.utexas.edu/

5.0 Seismicity in Texas: Increasing Number of Earthquakes

The cumulative number of earthquakes of $M_L \geq 3$ across Texas is updated in **Figure 14**, focusing on key oil and gas production areas documenting the continuous seismicity, as well as the growing number of larger magnitude events. The number of earthquakes reported since 2017 are documented in **Figure 15**. The area west of the Central Basin Platform (Delaware Basin) is still the area with the most seismicity. However, recent seismicity has dropped since 2022. TexNet cataloged 150 and 100 events with $M_L \geq 3$, for 2023 and 2024 respectively, compared to 184 events in 2022. These numbers and the Coalson 2023, $M_L 5.2$ event illustrate that despite the decrease, this area is still an active earthquake zone. $M_L \geq 2.5$ annually).

Seismicity is increasing east of the Central Basin Platform (Midland Basin, Snyder and Scurry-Fisher County line), where TexNet cataloged 45 and 41 events with $M_L \geq 3$ for 2023 and 2024, respectively, compared to 33 in 2022. These numbers, and the two $M_L 5.1$ events in 2024 (Scurry-Fisher and North of Tarzan), illustrate the significance of the increasing frequency and magnitude in seismicity in this area.

The second highest rate of increased seismicity is in the Eagle Ford area where the Fall City $M_L 4.7$ event occurred in 2023, the largest magnitude earthquake in the area since TexNet's creation in 2017. TexNet cataloged 16 and 21, events with $M_L \geq 3$ for 2023 and 2024, respectively, compared to six in 2022. These numbers document an increase of seismicity in this area.

In North Culberson and Reeves Counties, there are 9 earthquakes in the TexNet catalog with $M_L \geq 4.0$ from December 2022 to November 2024, compared to 37 earthquakes with $M_L \geq 4.0$ prior to this time extending back to January of 2020. The highest magnitude ($M_L 5.2$) Coalson earthquake was reported on November 8, 2023, 4.5 miles east of the county line (**Figure 16**; Index B). **Figure 17** shows the spatial distribution of 1215 "Did You Feel It" (DYFI) reports submitted to the USGS from as far as San Antonio and Dallas, and the ground motion data provided by TexNet stations for this earthquake in the Delaware Basin.

East of the Central Basin (Midland Basin and Scurry-Fisher), the TexNet catalog has 12 events with $M_L \geq 4.0$ from December 2022 to November 2024, compared to 2 earthquakes with $M_L \geq 4.0$ prior to this time extending back to January of 2020. The highest magnitude ($M_L 5.2$) earthquake was reported on December 16, 2022, 13 miles north of Midland, Texas (Figure 16; **Index A**). TexNet reported two events of $M_L \geq 5.0$, in 2024, on July 26, 2024 ($M_L 5.1$) in Scurry County, next to the Scurry-Fischer County line, and on September 17, 2024 ($M_L 5.1$) in Martin County, 8 miles Northwest from the city of Tarzan. The distribution of felt intensity estimates for the July 26, 2024 ($M_L 5.1$) earthquake in Scurry County, Hermleigh earthquake, based on 2552 "Did You Feel It" (DYFI) reports is shown in **Figure 18**. Felt reports from as far away as San Antonio, Dallas-Fort Worth, Amarillo, and Midland were submitted to USGS.

The intensity distribution, of the September 17, 2024 ($M_L 5.1$) earthquake in Martin County, based on 1693 DYFI reports submitted to USGS from as far away as San Antonio, Dallas-Fort Worth, and Amarillo, and the ground motion data provided by TexNet stations is shown in **Figure 19**.

These three large earthquakes in just over the last year have been widely felt by residents across Texas, illustrating the rising awareness of earthquake activity. TexNet has provided a basis for understanding this seismicity for Texas.

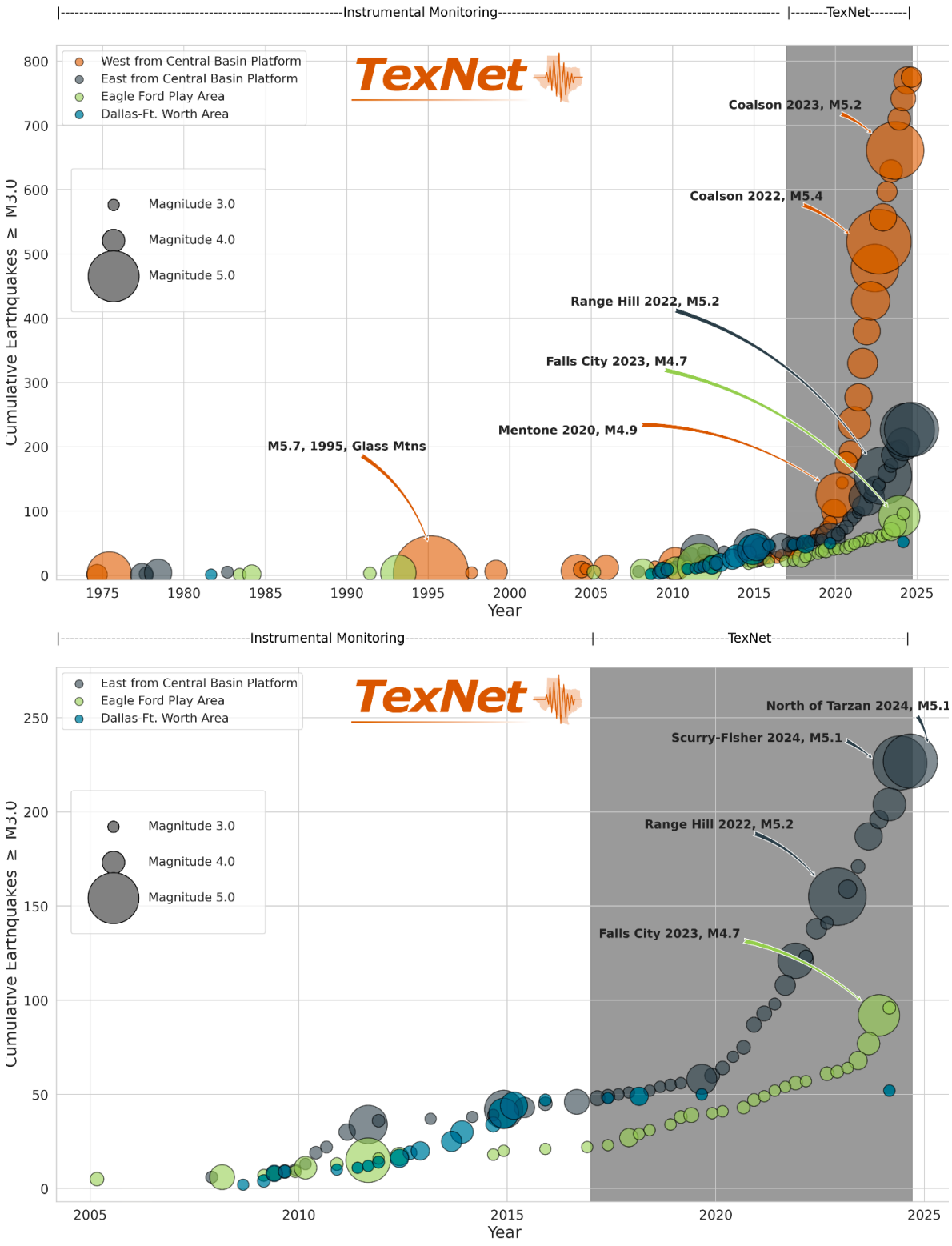

Figure 14. Cumulative number of earthquakes of $M_L \geq 3$ in key oil and gas production areas (top), i.e., West of Central Basin (Delaware Basin; orange color), East of Central Basin Platform (Midland Basin, Snyder and Scurry Fisher County Line; grey line), Eagle Ford (light green line), and Dallas-Fort Worth (green line) from 1975– November 2024. Zoom in time presenting cumulative number of earthquakes (bottom) east of the Central Basin Platform (Midland Basin, Snyder and Scurry Fisher County Line), Eagle Ford, and Dallas-Fort Worth from 2005– November 2024.

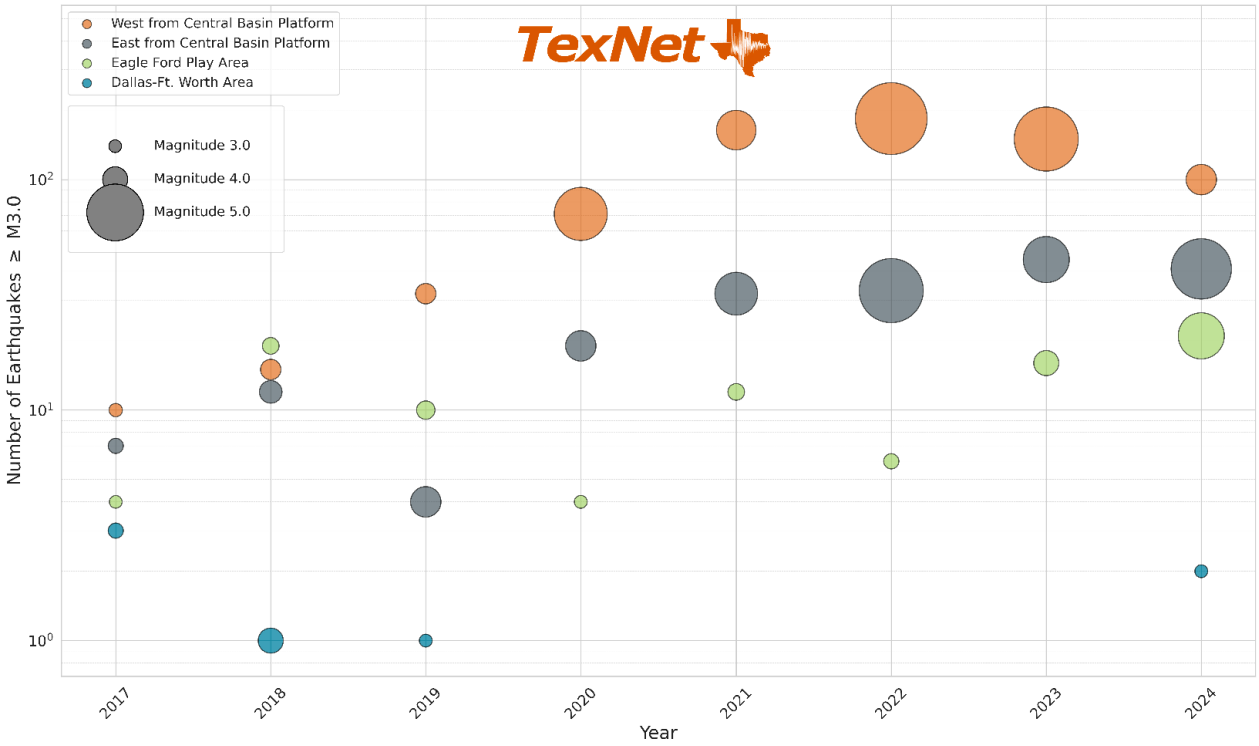

Figure 15. Number of earthquakes with $M_L \geq 3$ in key oil and gas production areas, i.e., West from Central Basin (Delaware Basin; orange color), East of Central Basin Platform (Midland Basin, Snyder and Scurry Fisher County Line; grey line), Eagle Ford (light green line), and Dallas-Fort Worth (green line) from 2017– November 2024. The size of the circles denotes the highest magnitude earthquake in each year and area.

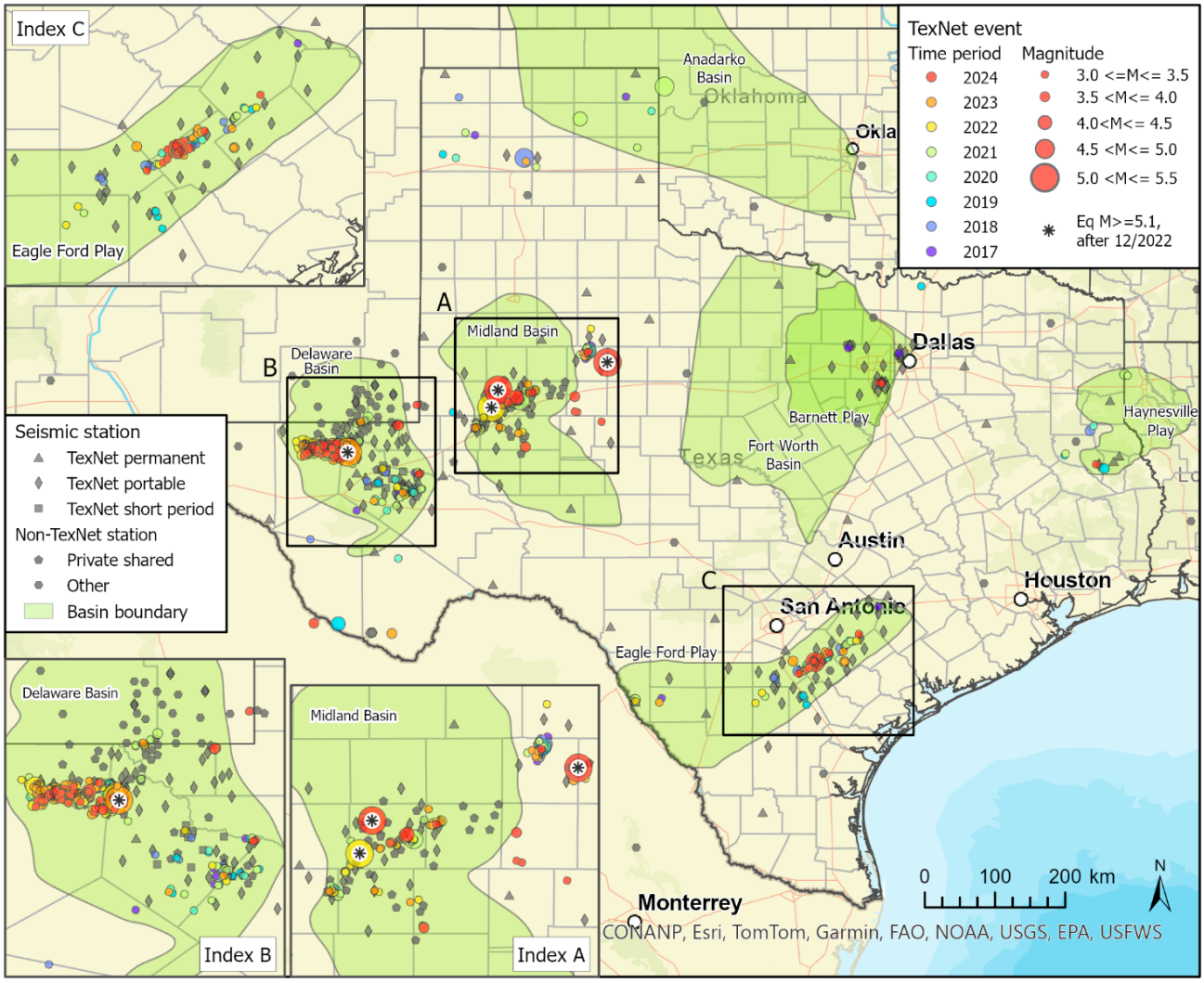

Figure 16. Earthquakes of $M_L \geq 3.0$ since 2017, reported by TexNet until November 2024. Highest magnitude events after December 2023 ($M_L \geq 5.1$) are denoted by an asterisk in a circle. Inset maps A, B and C indicate earthquake locations and sources of data from each area.

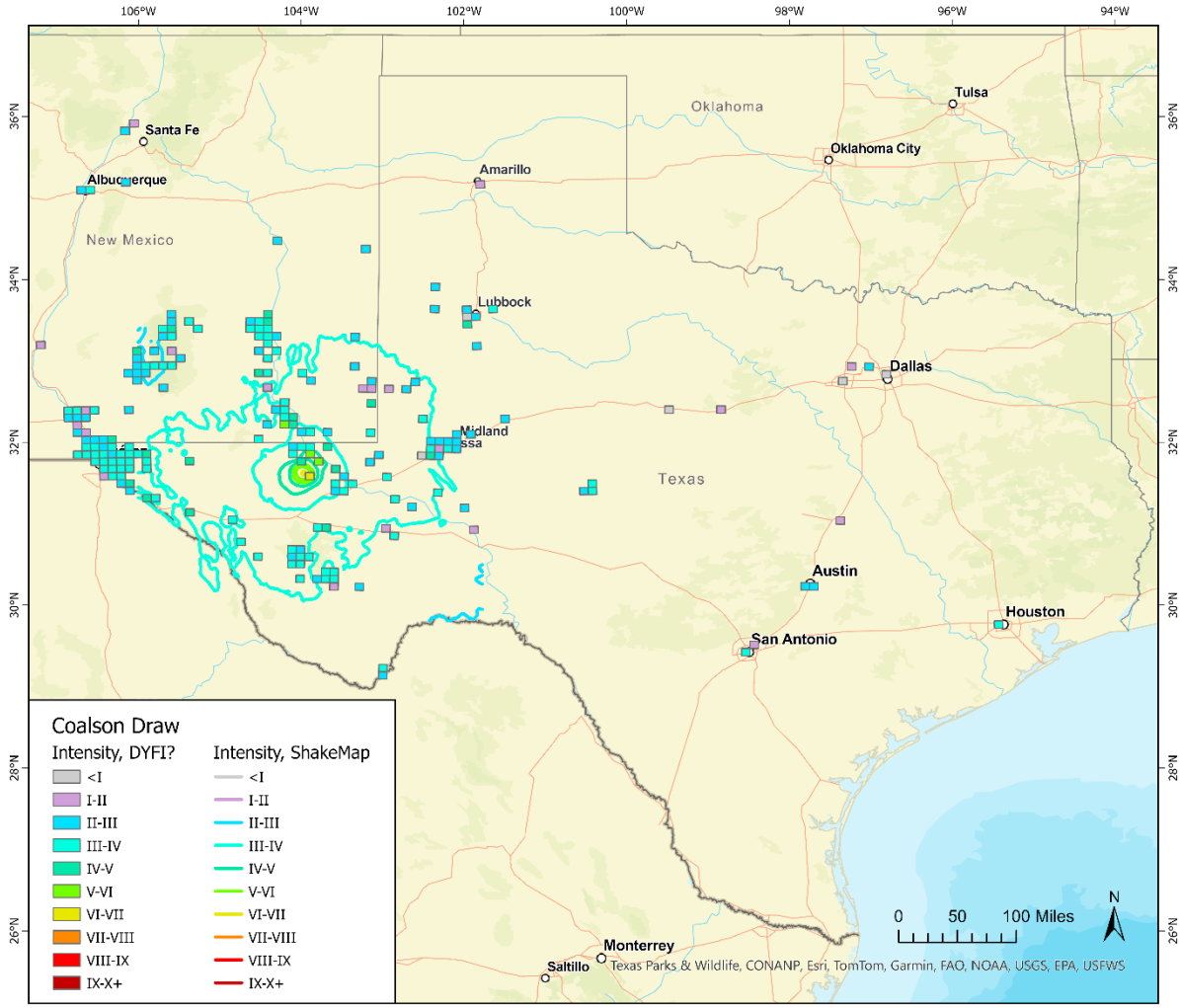

Figure 17. Spatial distribution of intensity[4] estimates for the M_L 5.2 Coalson earthquake in West Texas on November 8, 2023. Intensity is provided at 10 km grid cells based on the Did You Feel It (DYFI) reports provided to USGS, and contoured based on ground motion data provided from TexNet stations. This event was widely felt by residents in Texas and New Mexico.

[4] https://www.usgs.gov/programs/earthquake-hazards/modified-mercalli-intensity-scale

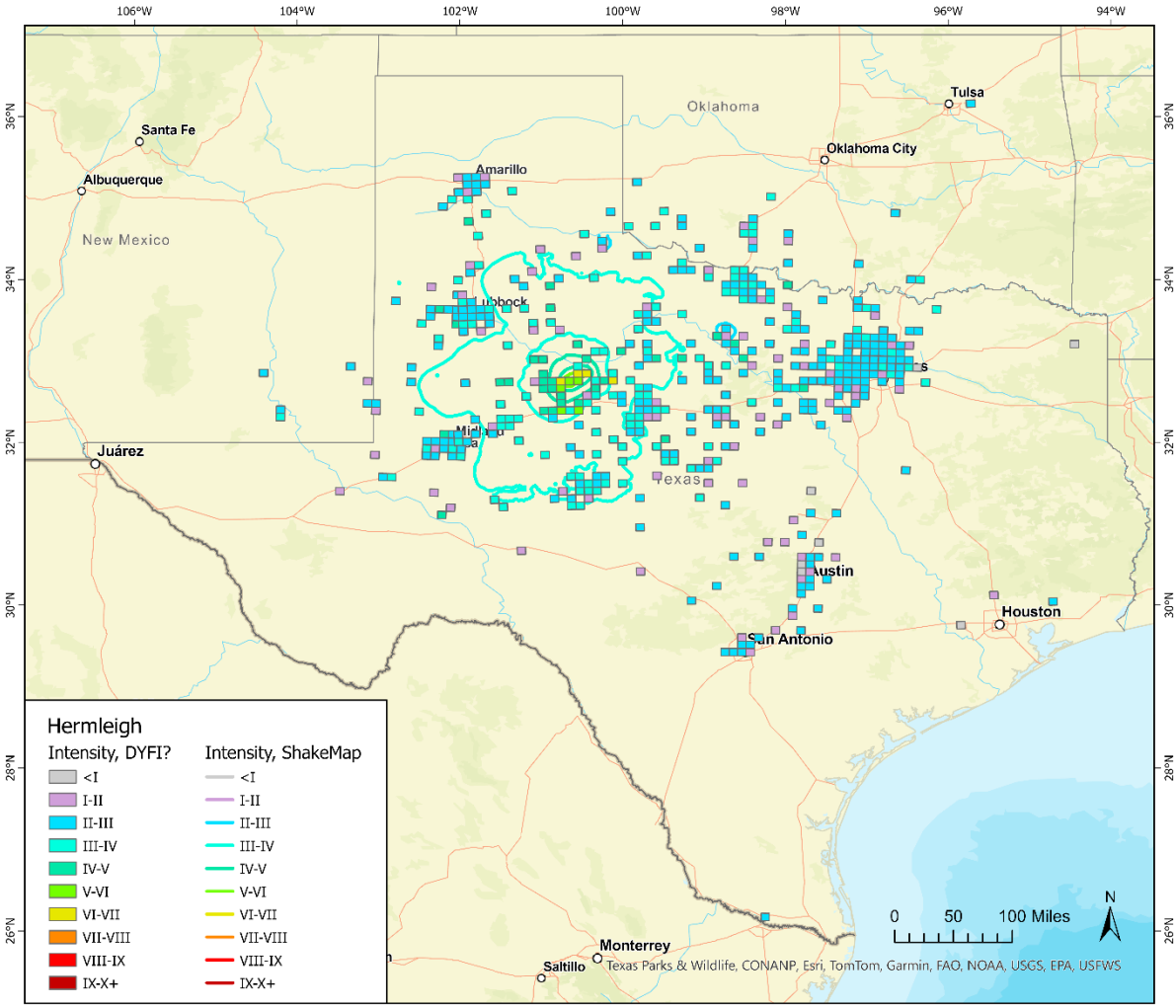

Figure 18. Distribution of ground motion intensity[5] for the M_L 5.1 Scurry County, Hermleigh earthquake in West Texas on July 26, 2024. Intensity is provided at 10 km grid cells based on the DYFI reports provided to USGS and contoured based on ground motion data provided from TexNet stations.

[5] https://www.usgs.gov/programs/earthquake-hazards/modified-mercalli-intensity-scale

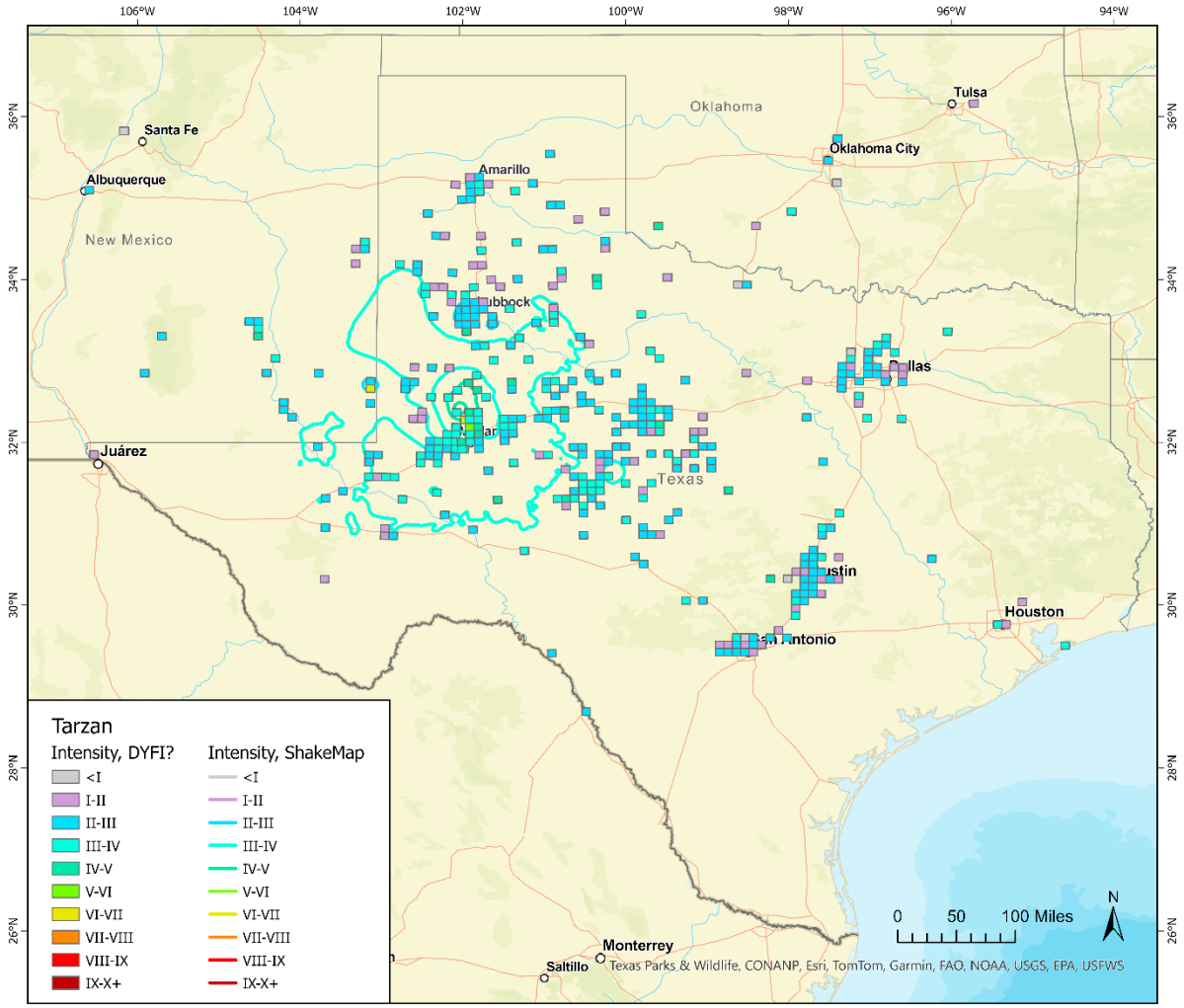

Figure 19. Distribution of ground motion intensity[6] for the M_L 5.1 Martin County (North Tarzan) earthquake in West Texas on September 17, 2024. Intensity is provided at 10 km grid cells based on the DYFI reports provided to USGS and contoured based on ground motion data provided by TexNet.

[6] https://www.usgs.gov/programs/earthquake-hazards/modified-mercalli-intensity-scale

6.0 Web Tools for Stakeholders

TexNet web tools are essential for seismic research and provide valuable educational sources of data for industry, students, educators, and the public interested in seismology. The TexNet web tools continue to provide public access to information regarding the state's seismic activity and to support informed decision-making for policymakers across various sectors, including the oil and gas industry and governmental agencies.

In the following sections, we provide a short description of the TexNet web tools. Those tools complement each other, with the TexNet Earthquake Catalog, the TexNet High Resolution Catalog, serving as the primary source of earthquake information, and the RRC/TexNet Injection & Pressure Reporting Tool as the primary source of daily injection and pressure data. The Fault Slip Potential (FSP) tool uses fault information derived from the high-resolution earthquake catalog and/or additional geological data, and injection information to identify the sensitivity of known fault zones. Further, the Geomechanical Injection Scenario Toolkit (GIST), provides a rapid geomechanical analysis of injection-related earthquakes based on the earthquake catalog and the well injection information provided by TexNet. FSP and GIST are complementary to one another and can use the same input data related to subsurface properties necessary for modelling.

TexNet Earthquake Catalog

The TexNet Earthquake Catalog (https://catalog.texnet.beg.utexas.edu/). is a comprehensive database for various research projects and presents current and historical seismic activity in the state of Texas since 2017, along with station locations in a cartographic format, making information easily accessible to the public. In addition, the TexNet Catalog is a practical resource for monitoring seismicity, as Texas experiences seismic events linked to industrial activities. The high-quality seismic data in the catalog supports academic research, aiding in studies of fault behavior, seismic hazard assessments, and statistical analysis of seismicity contributing to the broader scientific understanding of earthquakes and their implications.

The TexNet Catalog is dynamically updated with current earthquake data, which enables timely analysis and response. Researchers, emergency responders, and stakeholders can access information on seismic events as they happen, giving them real-time insights into seismic activity in the region. This real-time access makes the catalog a critical resource for effective decision-making and risk assessment.

Users can export data in tabular format for general use. The user-friendly interface allows visitors to search, filter, and visualize earthquake locations easily, as well as explore the development of the seismic network over time. TexNet also provides support for scientific inquiries or for access to the application itself.

The catalog's web interface has recently been enhanced with a range of icons to complement the overall design, and a change of color scheme for better contrast and readability (**Figure 20**).

Analytics from the website indicate a solid user base documenting a steady growth over time, with most users from the USA (**Figure 21**).

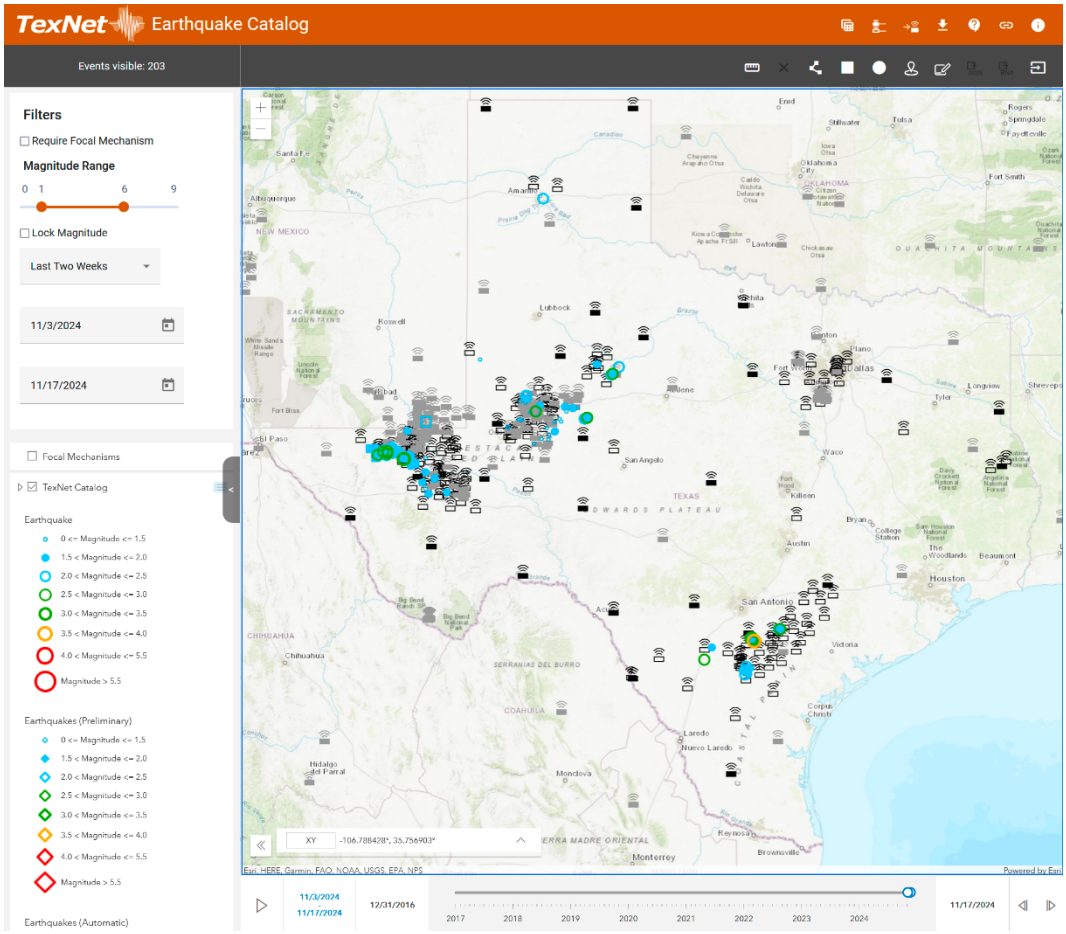

Figure 20. The TexNet Earthquake Catalog website, featuring the newly redesigned interface.

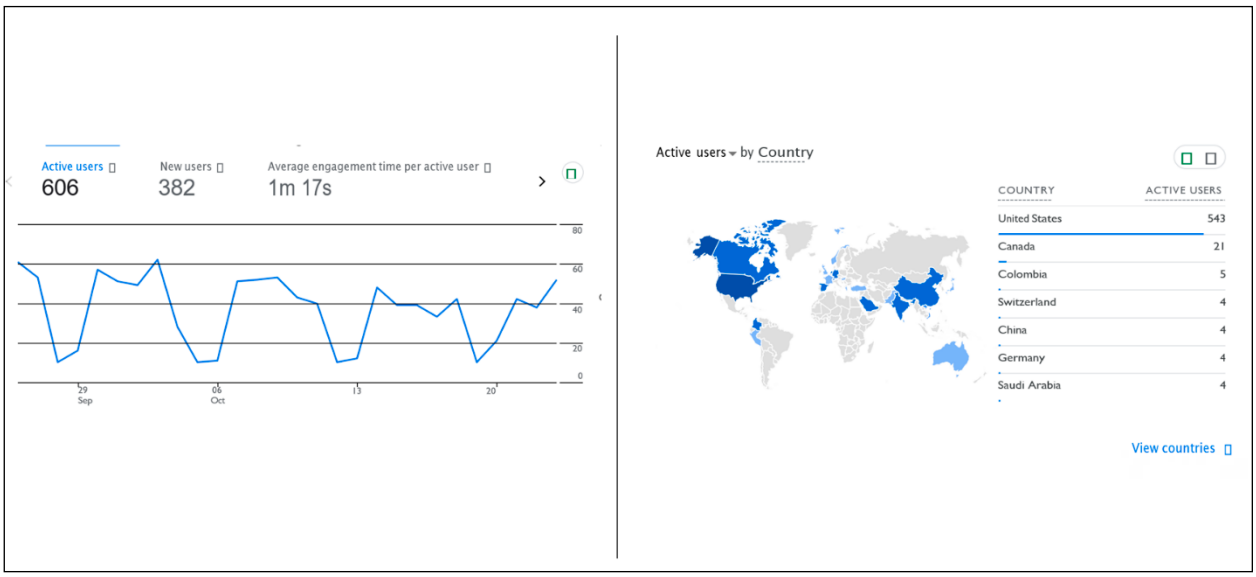

Figure 21. TexNet Earthquake Catalog analytics user base overview for the period of September 26–October 23, 2024. Top: Google Analytics report showing 606 active users, 382 new users, and an average engagement time of 1 minute 17 seconds per active user. Bottom: Distribution of active users by country, with majority in the USA (543 users), followed by Canada (21 users), and fewer than 10 users in other regions.

TexNet High Resolution Earthquake Catalog

The existing TexNet High Resolution Earthquake Catalog (https://hirescatalog.texnet.beg.utexas.edu/) is updated periodically and provides the best characterization of seismicity. The catalog's data is available to the research community and the public. This web tool supports various academic inquiries, such as fault mapping and seismicity migration, and has been cited in multiple research publications:

1. Breton, C., Shensky, M., and Savvaidis, A., 2024, Induced seismicity data prep: Automate data processing and data set production in Texas and New Mexico using Python and ArcGIS Pro tools: Interpretation, doi.org:10.1190/INT-2023-0013.1.
2. Hennings, P. and Young, M., 2023, The TexNet-CISR collaboration and steps toward understanding induced seismicity in Texas, in Recent Seismicity in the Southern Midcontinent, USA: Scientific, Regulatory, and Industry Responses: Geological Society of America, p. 53–71, doi:10.1130/2023.2559(06).
3. Hennings, P., Staniewicz, S., Smye, K., Chen, J., Horne, E., Nicot, J. P., Ge, J., Reedy, R., and Scanlon, B., 2023, Development of complex patterns of anthropogenic uplift and subsidence in the Delaware Basin of West Texas and southeast New Mexico, USA: Science of the Total Environment, v. 903, no. August, p. 166367, doi:10.1016/j.scitotenv.2023.166367.
4. Horne, E. A., and Hennings, P. H., 2024, Delaware Basin 3D Seismic Interpretation Progress Report 1Q2024: Project Introduction, Data Assembly, and Reconnaissance, BEG/CISR - Texas Railroad Commission Contract 455-24-1012: doi:10.18738/T8/ROWA0Y/ZUDHCR.
5. Horne, E. A., Hennings, P. H., Smye, K. M., Staniewicz, S., Chen, J., and Savvaidis, A., 2022, Structural characteristics of shallow faults in the Delaware Basin: Interpretation, v. 10, no. 4, p. T807–T835, doi:10.1190/INT-2022-0005.1.
6. Horne, E. A., Morris, A. P., and Hennings, P. H., 2024, Delaware Basin 3D Seismic Interpretation Progress Report 2Q2024: Fault Interpretation, Characterization, and Fault Slip Potential Analysis - Texas Railroad Commission Contract 455-24-1012: doi:10.18738/T8/ROWA0Y/HST4KF.
7. Huang, G. D., Horne, E. A., Kavoura, F., and Savvaidis, A., 2022, Characteristics of Seismogenic Structures and 3D Stress State of the Delaware Basin of West Texas as Constrained by Earthquake Source Mechanisms: Seismological Research Letters, doi:10.1785/0220220054.
8. Karanam, V., Lu, Z., Kim, J.W., 2023, Hydrocarbon production induced land deformation over Delaware Basin, analysed using persistent scatterer interferometry, IEEE International Geoscience and Remote Sensing Symposium, doi:10.1109/IGARSS52108.2023.10282973.
9. Karanam, V., Lu, Z., 2023, Hydrocarbon production induced land deformation over Permian Basin; analysis using persistent scatterer interferometry and numerical modeling, International Journal of Applied Earth Observation and Geoinformation, doi:10.1016/j.jag.2023.103424.
10. Karanam, V., Lu, Z., Kim, J.W., 2024, Investigation of Oil Well Blowouts Triggered by Wastewater Injection in the Permian Basin, USA: Geophysical Letters, doi:10.1029/2024GL109435.
11. Lee, H. P., Staniewicz, S., Chen, J., Hennings, P., and Olson, J. E., 2023, Subsurface deformation monitoring with InSAR and elastic inversion modeling in west Texas: Geoenergy Science and Engineering, v. 231, doi:10.1016/j.geoen.2023.212299.
12. Morris, A., Smye, K., and Hennings, P., 2024, Hydraulic Fracturing, Fault System Architecture, and the Details of Anthropogenic Earthquakes in the Post-Pennsylvanian Delaware Basin of West Texas: Lithosphere, v. 2024, no. Special 15, doi:10.2113/2024/lithosphere_2024_116.
13. Smart, K. J., Smye, K. M., Cawood, A. J., Ferrill, D. A., Hennings, P. H., and Horne, E. A., 2024, Geomechanical Modeling of Reservoir Dynamics Associated with Shallow Injection and Production in the Delaware Basin: Interpretation, p. 1–46, doi:10.1190/int-2024-0009.1.
14. Smye, K. M., Ge, J., Calle, A., Morris, A., Horne, E. A., Eastwood, R. L., Darvari, R., Nicot, J. P., and Hennings, P., 2024, Role of Deep Fluid Injection in Induced Seismicity in the Delaware Basin, West Texas and Southeast New Mexico: Geochemistry, Geophysics, Geosystems, v. 25, no. 6, doi:10.1029/2023GC011260.

The TexNet High Resolution Earthquake Catalog website also has a strong user base. The majority of users are from the USA (**Figure 22**).

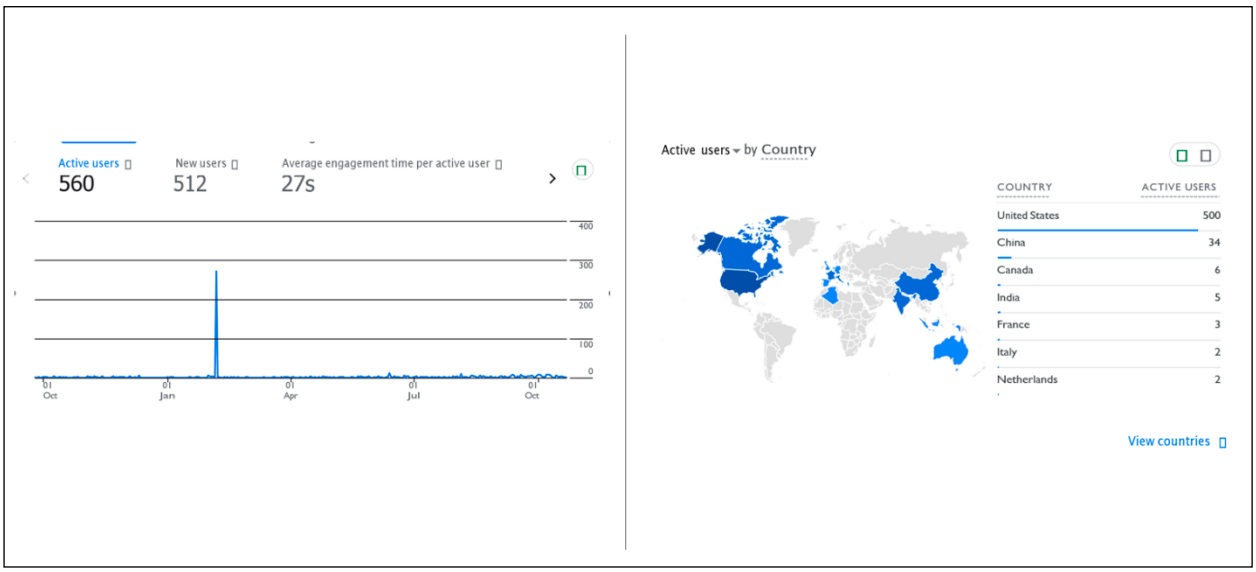

Figure 22. TexNet High Resolution Catalog analytics user base overview for the period of Sep 25, 2023–Oct 22, 2024. Top: Google Analytics report showing 560 active users, 512 new users, and an average engagement time of 27 seconds per active user. Bottom: Distribution of active users by country, with majority in the USA (500 users), followed by China (34 users), and fewer than 10 users in other regions.

RRC/TexNet Injection & Pressure Reporting Tool

The Injection and Pressure Reporting Tool (https://injection.texnet.beg.utexas.edu/) collects and distributes water disposal well injection volume and pressure data, which are submitted by injection well operators. Currently, it has a total of 253 registered users from 179 distinct operators.

As of October 2024, this web application has collected a total of 679,995 daily or monthly injection records for 795 wells. Of those, 252,513 were submitted between October 24, 2023 and October 24, 2024. It has collected a total of 1841 injection pressure records for 36 wells (**Figure 23**). Pressure data collection data started on April 1, 2024.

The RRC/TexNet Injection & Pressure Reporting Tool (**Figure 24**) has introduced several significant updates in 2024 aimed at improving user experience and data management for well operators. These enhancements have been designed with user feedback, ensuring that the tool continues to improve functionality and accessibility for all users.

To streamline the onboarding process for new users, a comprehensive Frequently Asked Questions (FAQ) and Glossary have been added to the portal to familiarize users with the tool's functionalities and terminologies, making navigation smoother and reducing the learning curve associated with the platform. TexNet also provides technical support to users as part of its range of services.

Recognizing the diverse needs of users, the tool now allows users to upload multi-well CSV[7] records, enabling greater flexibility for data input, streamlining data input, and saving time for complex records.

[7] https://www.loc.gov/preservation/digital/formats/fdd/fdd000323.shtml

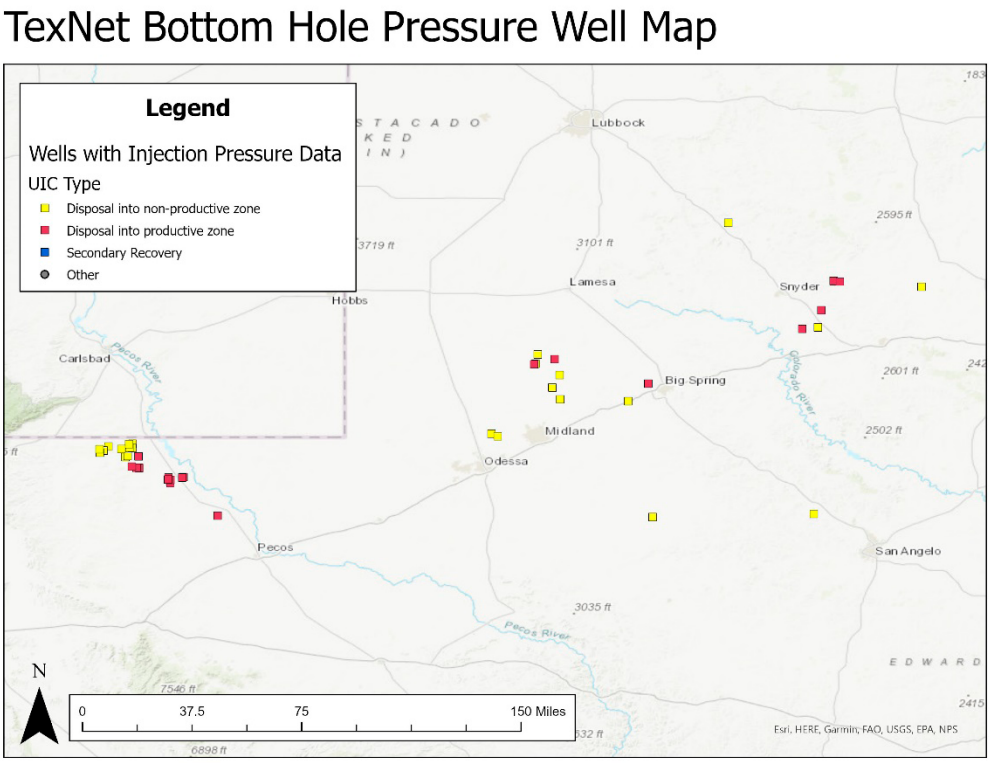

Figure 23. Map of wells where the Injection and Pressure Reporting Tool collects bottom hole pressure data. In total 43 wells have reported injection pressure data, out of the 583 permits that the December 2023 NTO applies to. However, not all permits have active wells and we are working to develop a list of active wells under current compliance.

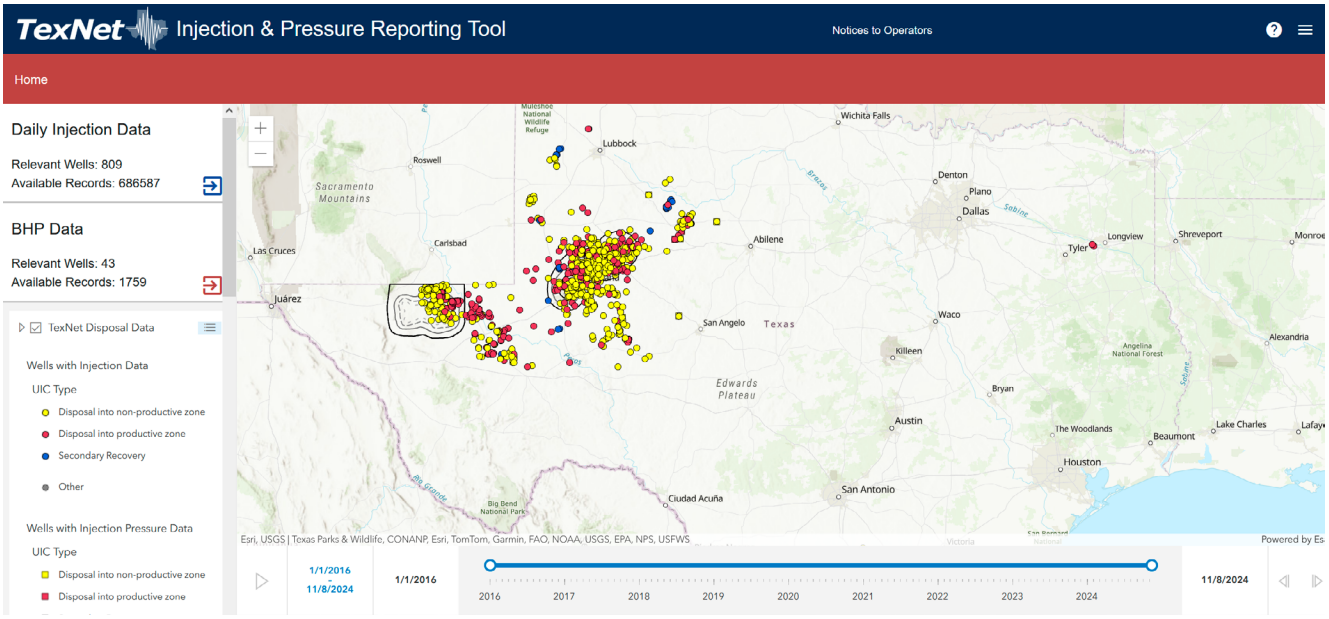

Figure 24. Updated version of the TexNet Injection & Pressure Reporting Tool website featuring the redesigned interface.

In response to user feedback, the tool has also introduced the ability to upload monthly well records supplementing the daily form, which in turn leads to more reliable data and increases flexibility for the well operators. Recent updates to the Injection & Pressure Reporting Tool (Figure 24) have introduced several key improvements aimed at enhancing both functionality and user experience. A new form within the user interface now allows existing administrators to promote other users without directly editing the database. The Excel export feature has been expanded to include circular and rectangular Areas of Interest (AOIs), offering users greater flexibility in spatial data representation. Additionally, the tool now supports multi-well injection and pressure submissions through Excel export and import, simplifying the management of large datasets. The Bottom Hole Pressure (BHP) form has been improved with a more intuitive interface and enhanced data capture capabilities, and the BHP data collection process is now divided into three distinct methods for more precise data analysis, following the Notice to Operators (NTO) requirements[8]. The well table has been updated for better clarity, specifically distinguishing between pre- and post-NTO-permitted wells, while the NTO link has been repositioned for easier navigation. The injection and pressure form has also been refined, with clearer column definitions and units of measure, now aligning with the TRRC H-10 form for consistency. Additionally, more information is pulled from TRRC historical permits, enriching the well data available to users. Finally, a new feature allows users to create custom, user-specific favorites on the "myWells" page, making it easier to access frequently used wells or data. These updates significantly improve the user experience, streamline workflows, and enhance the quality of data available through the tool.

The online tool has also undergone a significant restructuring of multiple pages, driven by feedback from well operators. The results are more intuitive, with portal navigation and enhanced accessibility for colorblind users.

By incorporating user feedback and introducing new functionalities, the tool now stands as a more versatile and efficient resource for those navigating the complexities of injection and pressure reporting. As these updates take effect, users can expect a smoother, more effective approach to managing their well-related data.

[8] https://www.rrc.texas.gov/media/sm5bzzpg/nto-disposal-well-monitoring-reporting-requirements-in-the-permian-basin-12-19-2023.pdf

Geomechanical Injection Scenario Toolkit

The Geomechanical Injection Scenario Toolkit (GIST) is a web application project in development, which provides a rapid, probabilistic geomechanical analysis of injection-related earthquakes based on well injection activities reported in the TexNet Injection Reporting Tool or additional data. The approach, presented in the second International Meeting for Applied Geoscience & Energy in 2022[9], is designed to aid decision-making when responding to seismicity. Originally developed by ExxonMobil, TexNet is now collaborating with them to reimagine GIST as a web application with the potential to incorporate new features.

Moving GIST to the web will greatly increase the tool's usability for a wider audience. Adding a graphical user interface to GIST will allow for a more tailored user experience by consolidating data entry, computations, and visualization. GIST has already undergone several iterations, with considerations for key aspects like legal review, workflow design, element placement, color scheme, and user navigation throughout development (**Figure 25**).

The current timeline aims to have GIST as a part of TexNet web tools as a Minimal Viable Product (MVP) by the end of Q1 2025 (http://gist.texnet.beg.utexas.edu).

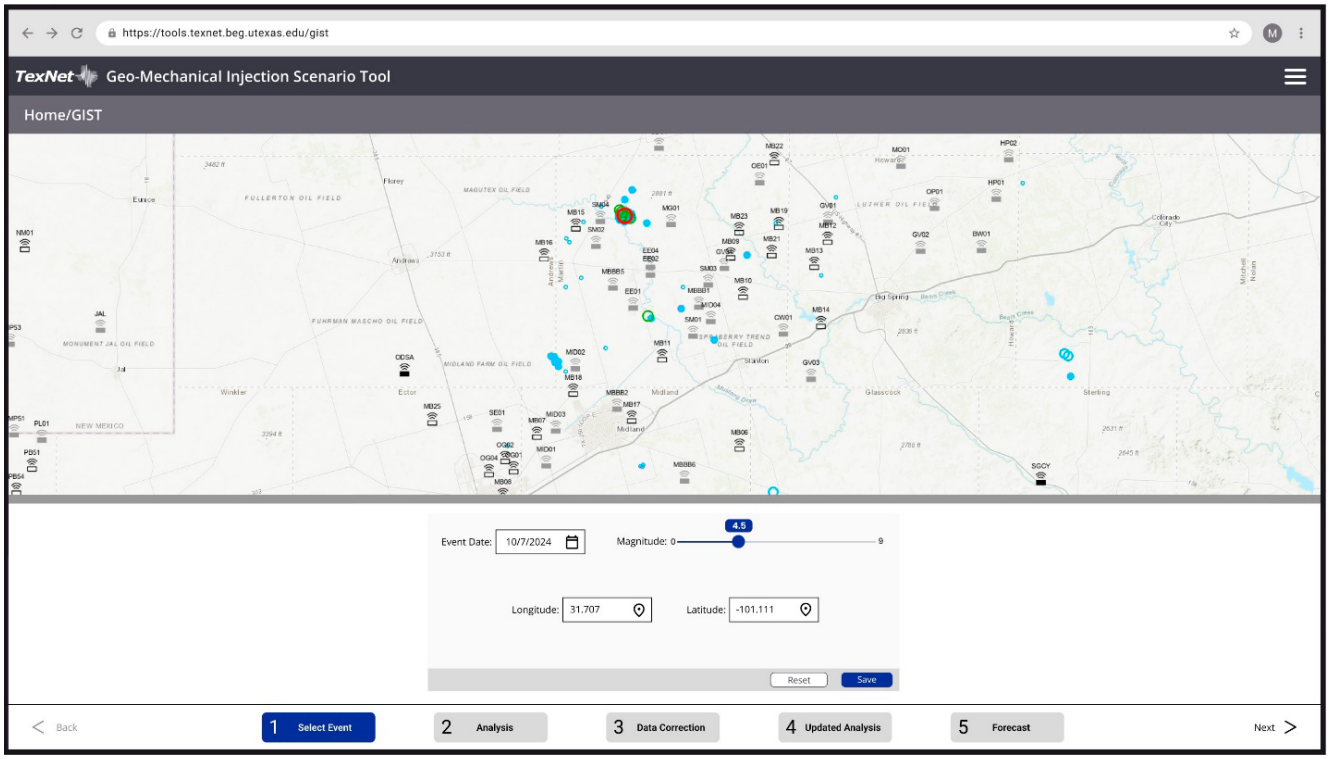

Figure 25. High-fidelity mockup of the first step of GIST, "Select Event."

[9] https://doi.org/10.1190/image2022-3740083.1

Fault Slip Potential Web Tool

Fault Slip Potential (FSP) web tool is another collaborative project that aims to support industry and regulators in their decision making when planning, subsurface related operations.

FSP was originally developed by the Stanford Center for Induced and Triggered Seismicity (SCITS) in collaboration with ExxonMobil to assess the probability of faults slipping due to fluid injection near wells.

The FSP web tool's key functions utilize both a deterministic approach for calculating a single stability for each fault and a probabilistic approach using Quantitative Risk Assessment (QRA), which is a Monte Carlo method used to evaluate the probability of an uncertain outcome when the input parameters themselves are uncertain.

In partnership with ExxonMobil and Decision Geomechanics[10], TexNet is currently redesigning and developing FSP 3.0 as a web-based tool to be integrated into a broader TexNet's web tools portal (**Figure 26**), including more recent developments[11].

A stable version of the FSP web tool is expected to be available within the first half of 2025. Updated documentation will also be provided, explaining the methodologies and tool usage.

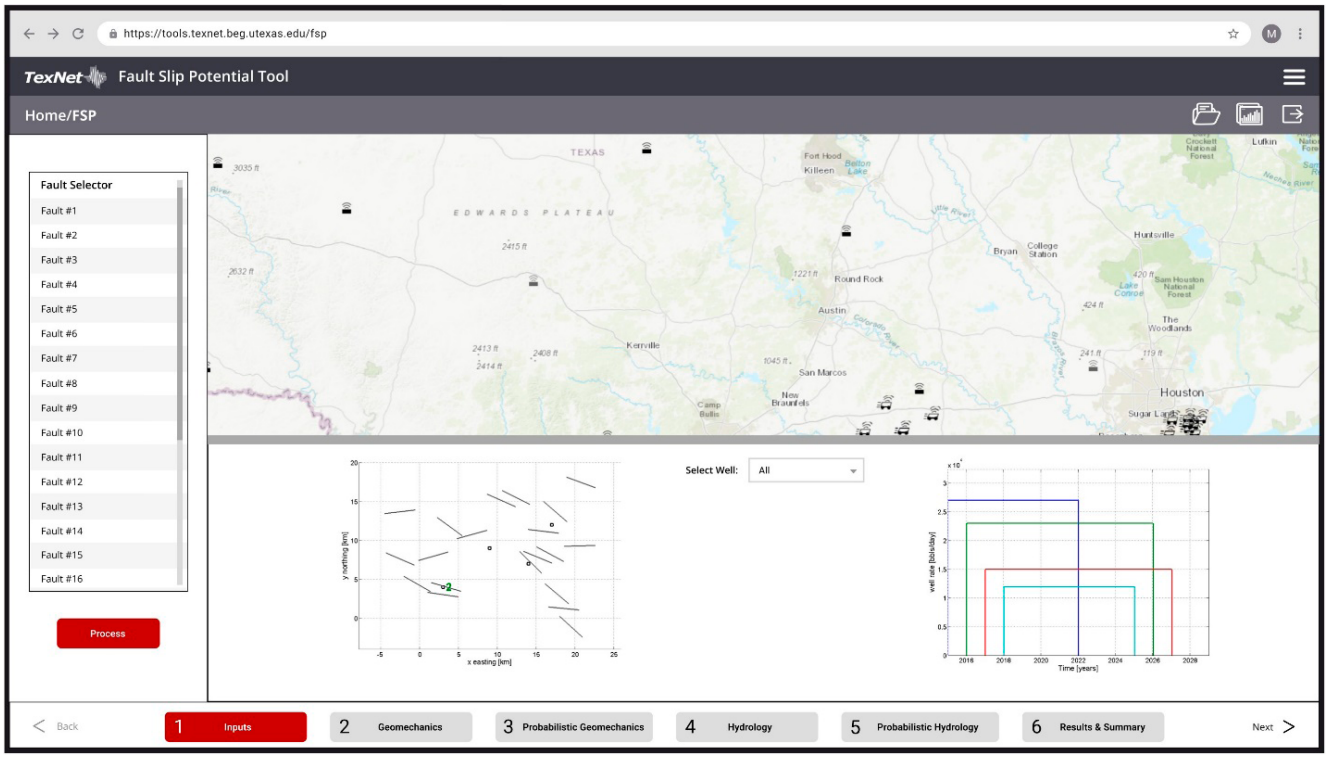

Figure 26. High-fidelity mockup of step one, "Inputs," in FSP Version 3.0.

[10] www.decisiongeomechanics.com
[11] https://imageevent.aapg.org/portals/26/abstracts/2024/4094870.pdf

Web Tools Portal

The Web Tools Platform is an active web project currently under development by TexNet. The Web Tools Portal will allow business logic processes such as GIST and FSP to be hosted on a single website, sharing user accounts and data files between the various tools. This capability allows the user to run them and view their results within a browser, without the need for the complicated setup that custom scientific software often requires. Future tools that were not originally designed as web applications and were written in disparate scripting languages (such as Python, Julia, and MatLab) will be developed and added to the Web Tools Portal, expanding user access.

The portal has been gradually evolving to incorporate additional features and functionalities to ensure scalability for future technological needs. Limited testing is projected for mid-December 2024, with wider availability in 2025.

Secured TexNet funding has facilitated improvements to the existing web tools and supported development of new online tools, creating a combination that will strengthen publicly available resources for seismic monitoring, earthquake analysis, and hazard assessment.

Appendices: Abstracts

Array Design: How Can We Maximize the Event Detectability on Carbon Capture Storage and Geothermal Stimulation Sites?

Emmanouil Parastatidis and Alexandros Savvaidis, The University of Texas at Austin

Presented at ECS 2024 / To be submitted to *The Seismic Record,* 2024

Within recent decades, induced seismicity has become a hot topic because of the increased number of the well stimulation projects in carbon capture storage (CCS), geothermal stimulation, unconventional oil and gas, mining, and dams. As a result, the need to detect as more events with as low magnitude as possible is more imperative than ever, for safety reasons. However, there are two major barriers that minimize our detectability, the first of which pertains to limitations in the geometry of our arrays. These include factors that could affect our setups related to the topography of the area, the limited number of stations, the land restrictions that might be in the area, the access to power grid, and so on. The second barrier relates to the signal quality, such as high ambient noise source nearby, such as busy roads, trees, weather conditions, and other noise.

How can we overcome those limitations? The newly developed ML and DL algorithms are providing very promising results, and we have reduced the magnitude of completeness on existing arrays, such as the one in the graph from north Texas, which has reduced the magnitude of completeness from 1 to 0.2 using EQCCT (O. M. Saad et al., 2023). But what are the hardware capabilities? What is the minimum magnitude for which our array can record based on the existing geometry, or how can we design an array to meet our needs?

To answer this question, we propose a probabilistic method to help us design an array that can achieve maximum performance. Our approach is done in two stages. At first, we use numerical models to test the wave attenuation due to the presence of faults, creating a dense grid with multiple receivers and multiple sources. Then we use the cumulative normalized peak amplitude for each receiver and create a map with expected high and low amplitude (**Fig. 1a**). The next stage of our method uses the results from the modeling stage, and on that map, we set up areas of interest such as areas with higher risk of seismicity due to nearby faults that are critically stressed or areas where injection is taking place, and we assign a weight value on these grid points. The next step is to select the areas we need to avoid due to land restrictions, noisy areas nearby highways, or areas with extreme topography (flooded areas, steep cliffs.) and set a minimum distance among the stations (**Fig. 1b**). Once the grid and the weight values for each point are set and we provide the number of stations that we want to install, then the algorithm generates multiple scenarios with different array geometries, which are used as input arrays for the magnitude sensitivity analysis. For the next step of our approach, we need to calculate the moment magnitude (m) for each grid point for each station of each input design. To do that we use the following three equations (Y. Freudenreich et al., 2011),

$$M_o = \frac{\dot{u}\left(8\pi^2 \rho \alpha^3 R(x,\xi)\right)}{F(\theta,\phi)\omega_c^2 \; exp\{-\pi \Delta T(x,\xi)\omega_c/4Q\}}$$

$$\Delta\sigma = \frac{7}{16}\left(\frac{\omega_c}{k\beta}\right)^3 M_o$$

$$m = \frac{2}{3}\log_{10} M_o - 6.03$$

where M_o is the seismic moment, $\dot{u}$ is the amplitude threshold above noise level in m/s, a is P-wave

where M_o is the seismic moment, $\dot{u}$ is the amplitude threshold above noise level in m/s, a is P-wave velocity, ρ is the density, $R(x,\xi)$ is the distance between the station and theoretical source, F is the radiation pattern, ω_c is the corner frequency, $\Delta T(x,\xi)$ is the travel time between source and receiver, Q is the quality factor for wave attenuation, $\Delta\sigma$ is the stress drop k is a constant (0.37), and β is the S-wave velocity. When the magnitude sensitivity analysis for all the different arrays geometries is complete, the algorithm selects the array designs that better meet the criteria, such as minimum number of stations to pick the event and median magnitude inside the area of interest. In the example presented in the figure below. the top three results are presented in **Figure 1c, 1d , and 1e,** where the criteria are that the event must be picked by at least five stations and have a median magnitude of -0.5 inside the yellow and red areas (**Figure 1b).**

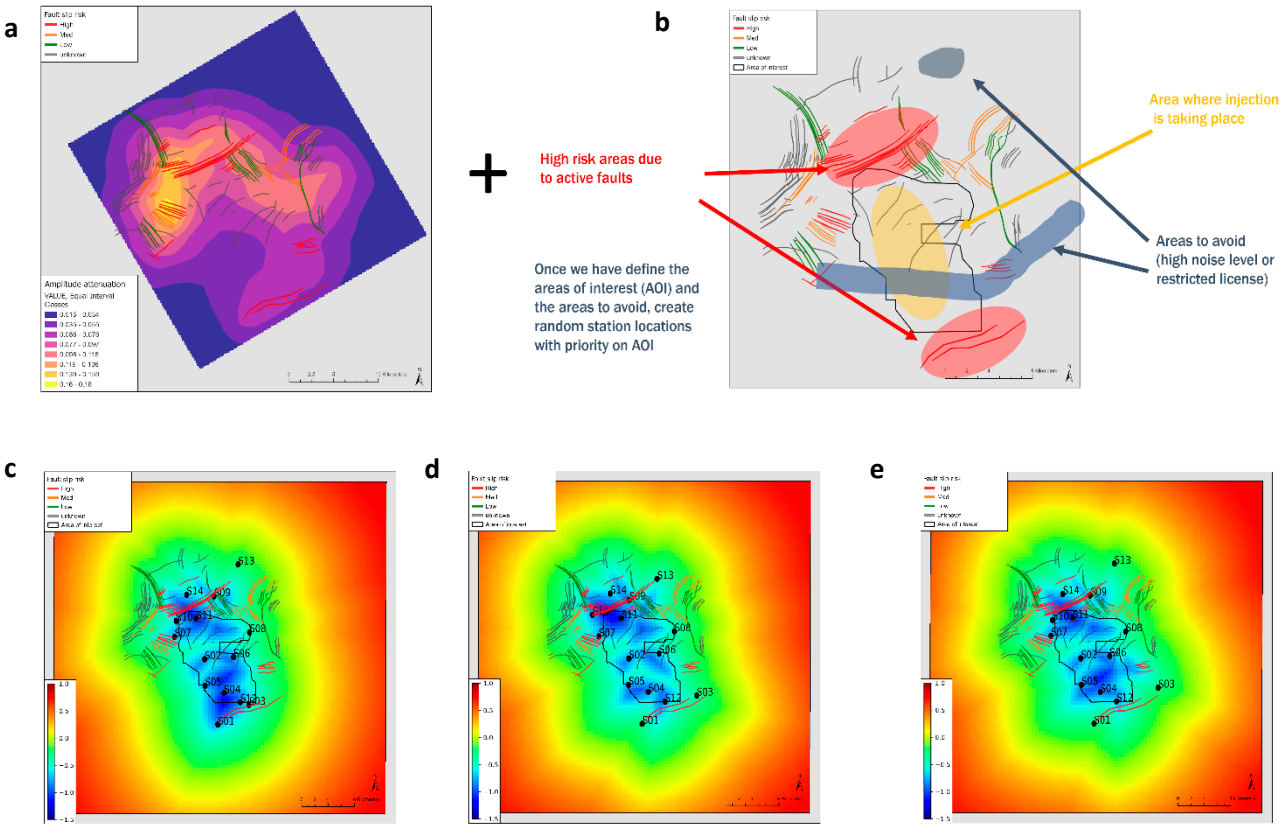

Figure 1. Methodology we follow in designing an array of 14 stations for a future CCS project. **a.** The result of the cumulative normalized peak amplitude, where yellow represents higher amplitude and purple is lower amplitude. Example of the numerical modeling stage: the red, yellow. and green lines are the mapped faults in the area of interest, which are used for modeling. In these scenarios we assume 256 receivers to record the waveforms in an equally spaced (1.8-km) grid and 80 source locations along the faults; for simplification we use a single-layer, homogeneous isotropic medium. **b.** Example of how we set up the areas of interest; red is the high-risk areas due to faults that can be critically stressed, yellow is the area where injection is taking place, and gray areas are the locations we must avoid due to highways that could create higher noise levels on our recordings, or restricted-license areas. **c., d., and e.** Examples of the magnitude sensitivity analysis outputs, which fulfill the criteria to have a detectable event by at least five stations with a median magnitude of M = -0.5 inside the area of interest (E. Parastatidis et al., 2024).

Seismic-network expansion in Midland Basin

Daniel Siervo, Alexandros Savvaidis, Cari Breton, and Dino Huang
Bureau of Economic Geology, The University of Texas at Austin

This study focused on enhancing coverage of seismic networks in the Midland Basin, Texas, to better monitor and understand seismic activity linked to industrial activities involving wastewater injection. Analysis was based on earthquake data recorded by TexNet from January 13, 2017, through May 28, 2024, and involved a total of 12,417 seismic events (comprehensive catalog), including both manually located earthquakes and detected events (lower magnitude automatic event solutions, confirmed by an analyst). Quality filters, such as depth, RMS, and azimuthal gap, were applied to create a refined catalog of 8,278 events.

The primary objective of the study was to map priority areas for seismic-station deployment using both comprehensive and refined catalogs. We employed a data-driven approach that leveraged historical TexNet data, current seismic network geometry, and injection data. The BallTree algorithm was applied to the earthquake catalogs to filter events within a 500-m proximity, reducing redundancy while preserving earthquake-distribution patterns. Further, we computed distances between seismic events and existing seismic stations using the haversine formula to identify events lacking a station within 4 or 10 km, these events are referred to as subject events hereafter.

The area of interest (AOI) was discretized into a grid with 0.01° spacing, representing potential locations for seismic stations. Each grid point was evaluated for its ability to provide coverage to at least two subject events. Results were mapped (Figure 1) to indicate the grid points capable of cover previously uncovered events. Dark- and light-golden-yellow dots represent areas where new stations could improve coverage within 4 and 10 km, respectively.

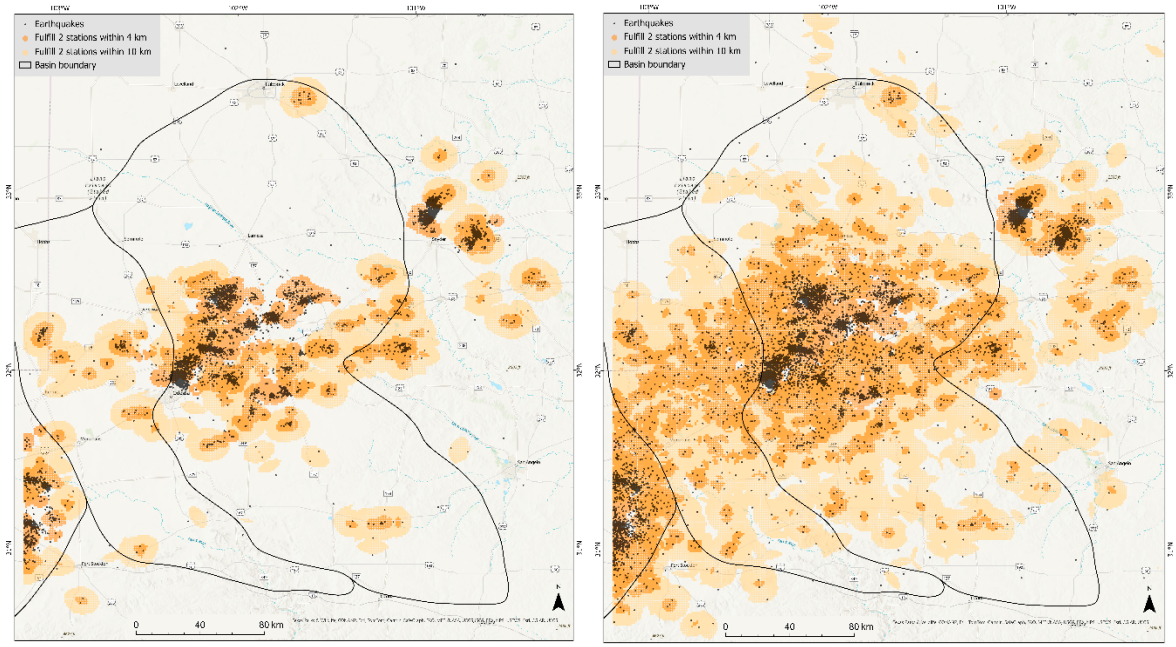

Figure 1. Coverage maps for (left) refined and (right) comprehensive catalogs. Light-golden-yellow dots = locations where placing a station would cover at least two seismic events previously >10 km away from any station. Dark-golden-yellow dots = locations ensuring coverage within 4 km of at least two previously uncovered events.

To further guide the network-expansion assessment, we overlaid saltwater-disposal injection-well locations onto these coverage maps. Four priority areas were identified on the basis of seismicity density and proximity to injection wells. These areas were categorized as very high, high, medium, and low priority, with the highest priority focusing on regions exhibiting both recent seismic activity and high-volume injection wells.

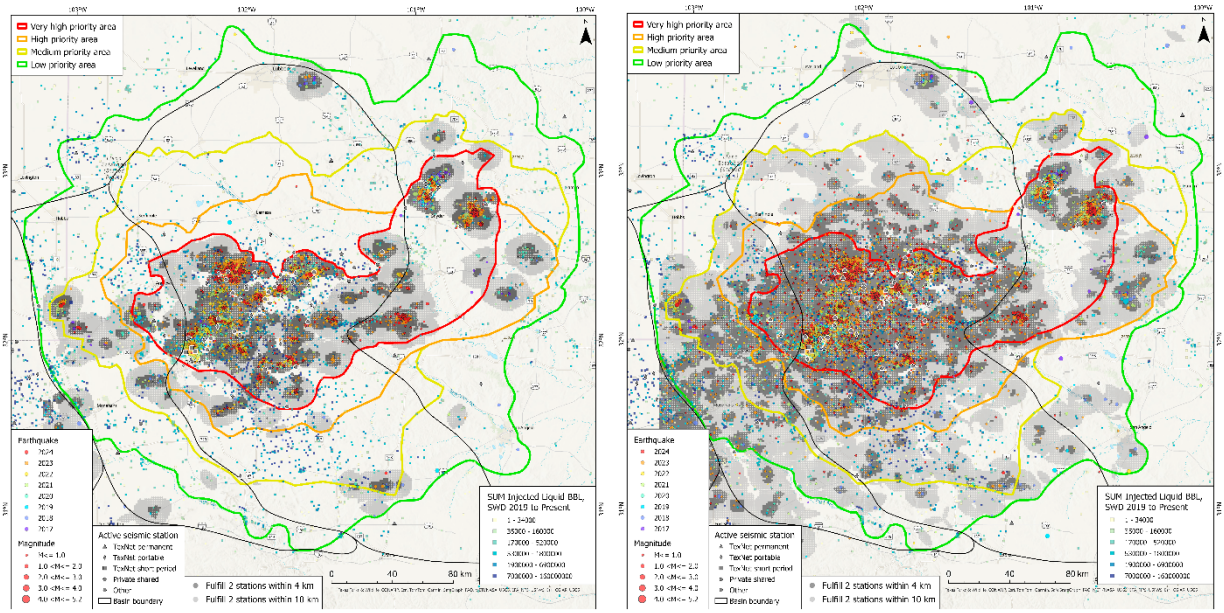

Figure 2. Priority areas for deployment of new seismic stations showing coverage map of (left) refined and (right) comprehensive catalogs **and** SWD injection wells. Maps highlight areas of very high, high, medium, and low priority for station placement on the basis of distribution of seismic events and injection wells.

Methodological integration of injection-well data with seismic-event coverage provides a robust framework for expansion of the seismic network in the Midland Basin. Expanding the seismic network in key areas is crucial to statewide efforts toward enhancing the precision of seismic monitoring, particularly in regions prone to anthropogenic seismic activity.

Optimizing Seismic Event Detection with EQCCT in the Midland Basin, Texas

Victor Salles and Alexandros Savvaidis

EQCCT is a machine learning algorithm developed to detect seismic wave arrivals in seismograms. In its original workflow, EQCCT applies a standard bandpass filter (1Hz–45Hz) to waveform data. However, this fixed filter may not be optimal for every region, as local conditions and signal characteristics can vary widely. To improve detection accuracy, we analyzed a dataset of 996 manually located events in the Midland Basin, with magnitudes between M1 and M3, totaling more than 23,000 manually picked wave arrivals. By performing a signal-to-noise ratio (SNR) analysis across various highpass and lowpass frequency combinations, we identified the top 10 filters for each wave arrival. We then calculated the median of these top filters to set a unique, optimized filter for each station and event. To further refine the filtering process, we looked at the range of highpass and lowpass values across stations with more than 100 event detections, visualized through boxplots (Fig. 1). This led us to test three custom filters for each station: (1) a narrow band based on median highpass and lowpass values, (2) a broader band using the first and third quartiles for highpass and lowpass, respectively, and (3) an even broader band using the minimum values for highpass and maximum for lowpass. The last filter configuration provided the best results in terms of automatic event detection.

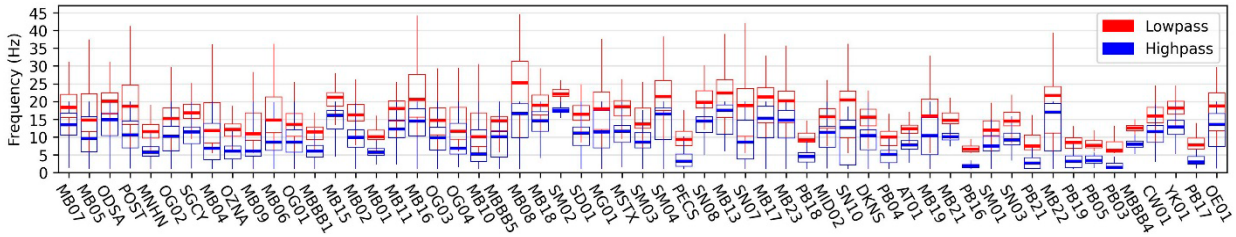

Figure 1. Boxplot of highpass and lowpass frequency distributions for each station with more than 100 event detections. Red boxes represent lowpass frequencies, and blue boxes represent highpass frequencies. These distributions were used to define custom station-specific bandpass filters based on SNR analysis.

The effectiveness of the filtering approach was evaluated by comparing EQCCT's detection results against Midland Basin's manual catalog with 124 events in January/24 (Fig. 2). This catalog comprehends 89 final and 35 reported events. Reported events are real seismic events that do not fulfill all quality criteria (e.g. azimuthal gap, RMS, location uncertainties).

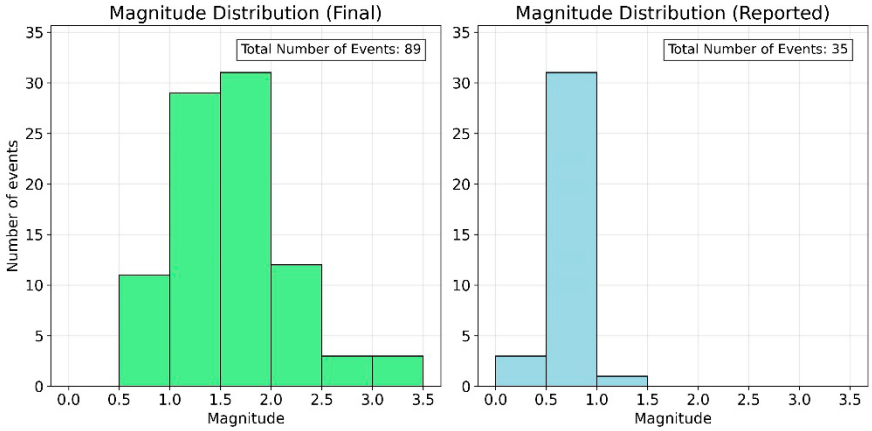

Figure 2. Magnitude distribution of the Midland's January manual catalog, colored by evaluation status (final or reported).

Initially, using the previous EQCCT workflow, 63 events were automatically located (42 final and 21 reported). By implementing the custom station frequency filters workflow, we successfully located all "final" events and 31 out of the 35 "reported" events in the reference catalog, as shown in Fig. 3.

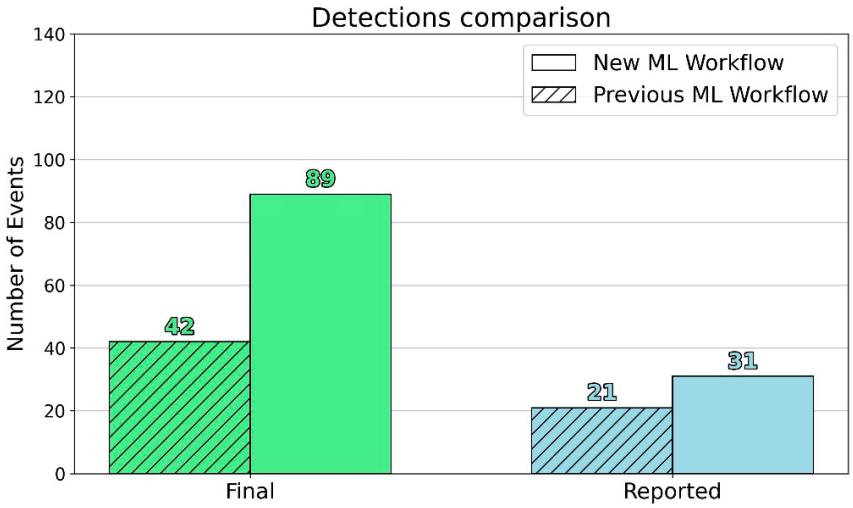

Figure 3. Comparison of earthquake detections between the previous and new EQCCT workflows. The new workflow successfully detected 100% of the final events (89) and 89% of the reported events (35) in the reference catalog.

The four events that were not automatically located had their wave arrivals successfully detected by EQCCT; however, the algorithm responsible for pick association failed to create a new origin. This suggests that fine-tuning the association process is necessary, including experimenting with different algorithms to evaluate their effectiveness in locating earthquakes using EQCCT picks.

The new workflow not only enabled the detection of more events when compared to the reference catalog, but also increased the detection of lower-magnitude events. It effectively lowered the catalog's magnitude of completeness, with an increase in detections for events with magnitudes ranging from 0 to 1.5 (Fig. 4). Similar approaches should be applied to each area of interest, with the goal of enhancing the signal-to-noise ratio of events by accounting for local noise conditions and the specific seismicity characteristics.

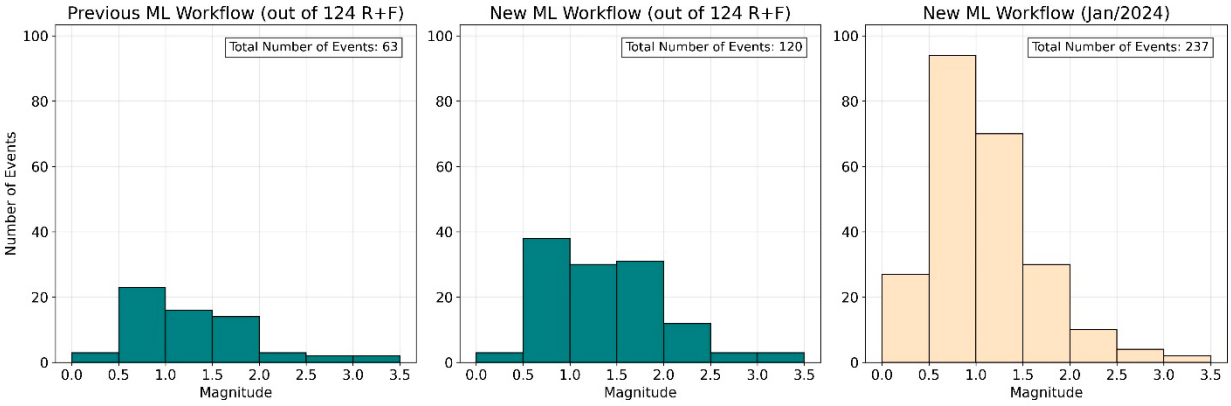

Figure 4. Magnitude distribution of events located using the previous workflow (left) and the new workflow (middle), compared to the 124 events in the Midland Basin's manual catalog (January 2024). The new workflow (right) shows a significant increase in detections of lower-magnitude events when considering all located events in the Midland Basin in January/2024.

Optimizing EQCCT for Real-Time Seismic Event Detection in Resource-Constrained Networks

C. Skevofilax, V. Salles, C. Munoz, Y. Chen, O. Saad, A. Savvaidis

TexNet is developing a software framework to deploy the EarthQuake Compact Convolutional Transformer (EQCCT) machine learning (ML) model for real-time earthquake phase detection across its seismic station network. This initiative seeks to establish a state-of-the-art, real-time seismic event detection system for the State of Texas, with potential for applications in other regions worldwide.

Currently, TexNet is using EQCCT to process historical seismic waveforms (baselineEQCCT). However, the baselineEQCCT algorithm lacks the computational speed necessary for real-time deployment across TexNet's network of more than 300 stations, particularly in limited-computing resource environments (Fig. 1). To address this limitation, computational process parallelization has been integrated into the algorithm, now referred to as stationRayEQCCT. These enhancements have significantly-improved runtime performance, reducing total processing times by as much as 90.7% and greatly improving the efficiency of seismic phase-picking operations (Fig. 2). These findings position TexNet to implement a robust, real-time ML-based seismic monitoring system.

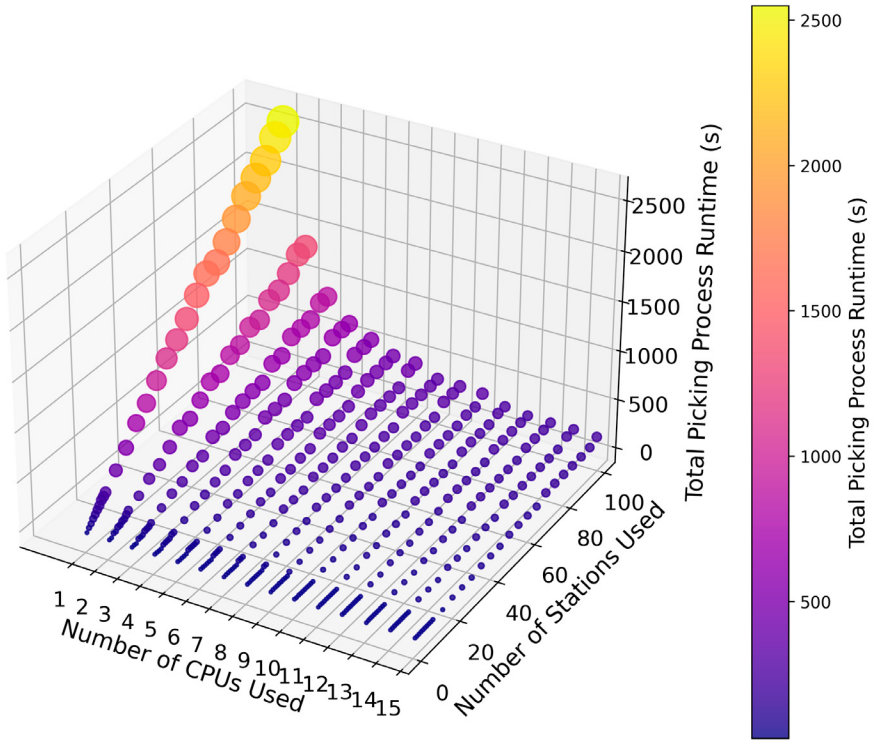

Figure 1. BaselineEQCCT Real-Time Simulation Performance.

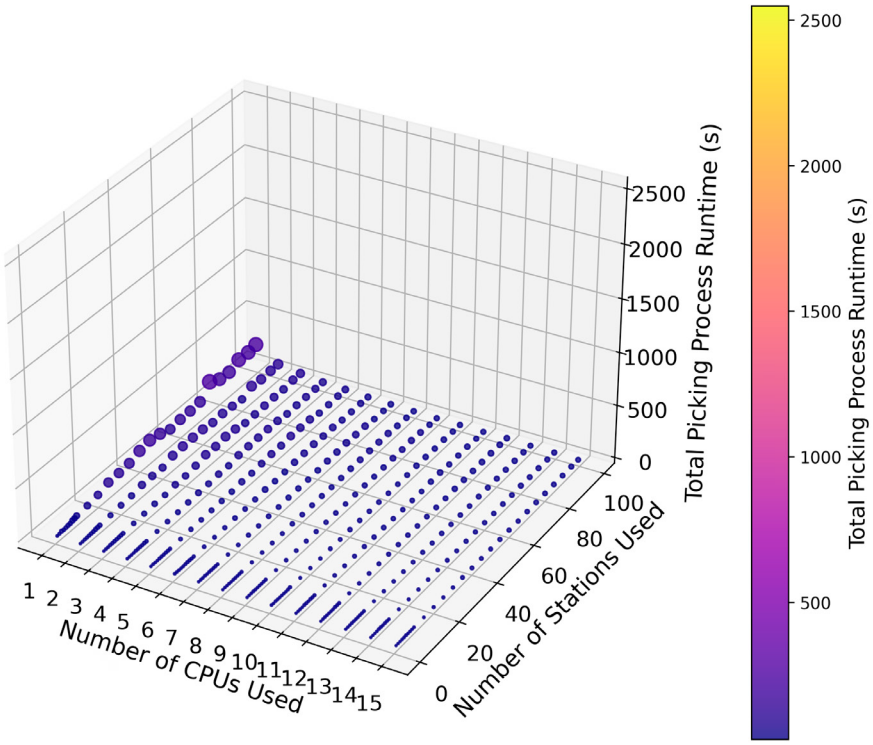

Figure 2. StationRayEQCCT Optimal Configurations Real-Time Simulated Performance.

Implementation of AI/ML Detection of Seismicity as a Real-time SeisComP Module

Camilo Muñoz[1], Victor Salles[1], Constantinos Skevofilax[1], Alexandros Savvaidis[1]
[1]Bureau of Economic Geology, The University of Texas at Austin.

The use of deep-learning techniques for detecting seismic events has increased in recent years. Among recent advancements, the Earthquake Compact Convolutional Transformer (EQCCT) algorithm stands out due to its efficiency and reliability. A persistent challenge for all machine learning methodologies in seismology lies in facilitating real-time application rather than limiting their utility to post-event analysis. In 2023, the Texas Seismological Network (TexNet), which currently comprises more than 200 stations across Texas, integrated an EQCCT-based earthquake detection routine in its most seismically active regions, in addition to the traditional STA/LTA method. Studies of Texas seismicity indicate that EQCCT enabled the detection and location of 50 times more earthquakes in Texas (primarily of magnitudes below 1) compared to the STA/LTA method.

TexNet utilizes SeisComP software for the acquisition, processing, and disseminating of seismological data. One of the main advantages of this software lies in its modular structure, which allows independent execution of various tasks while maintaining integration with SeisComPs data broadcasting and messaging system. We developed a new SeisComP module, sceqcct, to integrate the deep-learning-based wave arrival detection approach alongside other SeisComP processes.

sceqcct can process real-time data by accessing streams through one of the SeisComP RecordStream interfaces (Fig. 1). This capability enables the module to generate picks using the EQCCT algorithm with a delay of less than 30 seconds from the onset time, allowing seamless integration into real-time workflows. Additionally, the module offers an option to operate in playback mode, utilizing archived waveform data.

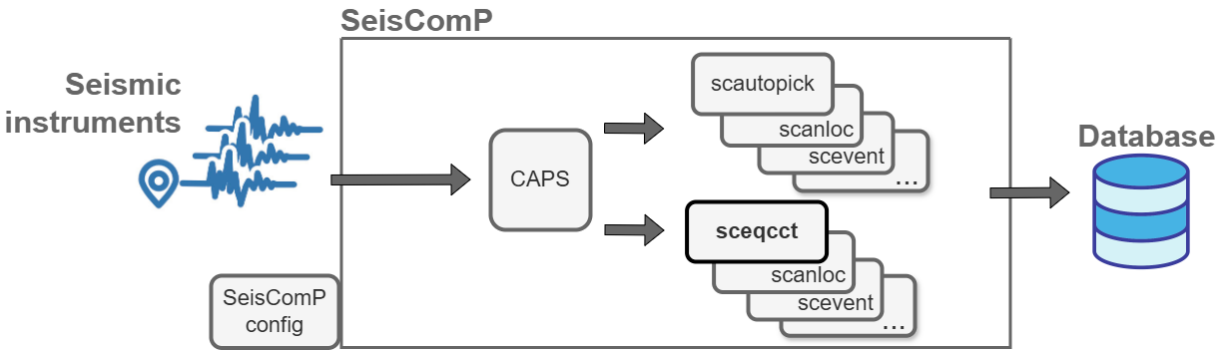

Figure 1. sceqcct is feeding with data from the acquisition module CAPS using the SeisComP record stream interface.

Since its implementation in TexNet in 2023, EQCCT has produced files containing the algorithm outputs in plain text or XML format, listing all detected events. The use of sceqcct, however, eliminates the need for separate output files by generating SeisComP objects (picks) that are sent directly to the SeisComP messaging system. These picks are immediately accessible to any module subscribed to by the appropriate messaging group. The combination of real-time data processing and integration with the messaging system increases the number of events detected in real-time and reduces computation time and resource usage. Utilizing the module eliminates the need to manage waveform data files or generate output files, thereby greatly streamlining the process.

To evaluate the sceqcct performance, we compared its results against the current EQCCT instance running in production in playback mode. Picks associated with events from both the real-time module

(sceqcct) and playback show a high similarity (Fig. 2a). For all magnitude and epicentral distance ranges, similarity is above 85%. The similarity increases with higher magnitude and lower epicentral distance values, as expected. Events comparison revealed a noticeable similarity in the number of detected events along all magnitude ranges, 100% for events with magnitudes greater than 1.2 and some slight differences for lower magnitude events (Fig. 2b).

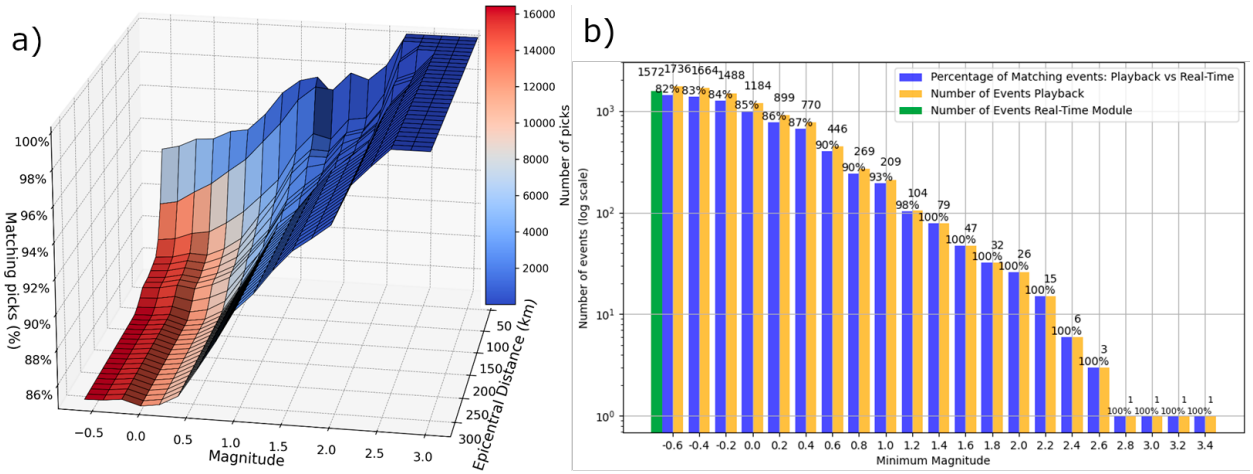

Figure 2. a) Comparison of picks associated with events: playback versus real-time module. b) Comparison of events produced by: playback versus real-time module.

The discrepancies in picks and events between real-time and playback executions are mainly due to the non-availability of all data in the real-time mode and also to the finer segmentation of data in real-time mode.

As expected, creation times are much lower when using the real-time implementation than when using playback. Using sceqcct, the event creation times were less than 100 seconds for most of the events, compared to values close to 500 seconds using the current playback mode implementation (Fig. 3).

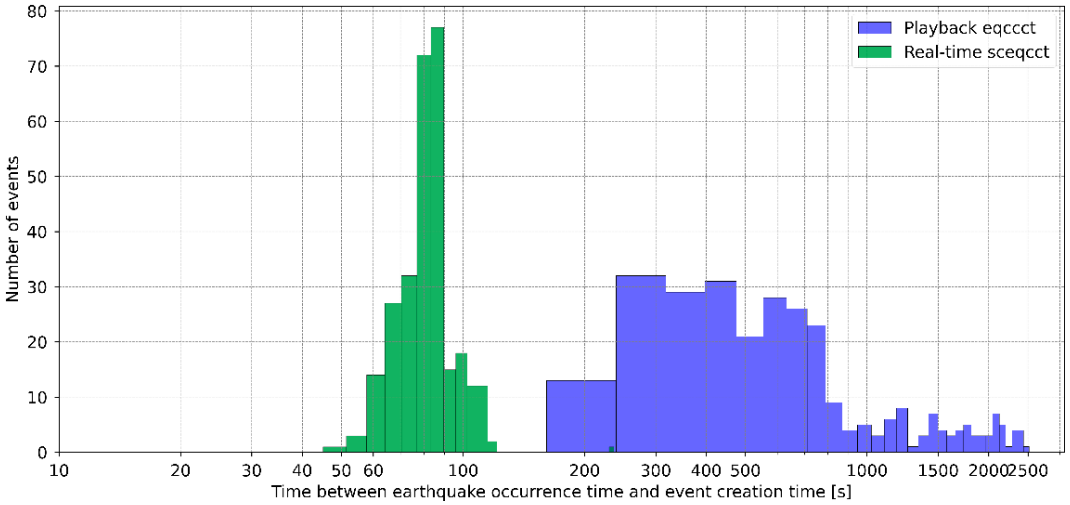

Figure 3. Comparison of event creation times between real-time and playback executions.

Incorporating this as a SeisComP module could also benefit other seismological centers, as this software is the most stable and widely used for real-time earthquake monitoring, making the installation and integration of sceqcct into any SeisComP system straightforward. Furthermore, both the SeisComP module and the predictor utilizing EQCCT are developed in Python, facilitating community contributions due to the language's popularity and extensive use.

Pyseistr: A Python package for structural denoising and interpolation of multichannel seismic data

***Yangkang Chen**, The University of Texas at Austin, **Alexandros Savvaidis**, The University of Texas at Austin, **Sergey Fomel**, The University of Texas at Austin, **Yunfeng Chen**, Zhejiang University, **Omar M. Saad**, KAUST, **Yapo Abolé Serge Innocent Oboué**, Zhejiang University, **Quan Zhang**, Zhejiang University, and **Wei Chen**, Yantze University*

Published in Seismological Research Letters, 2023, 94(1), 1703–1714.

New sensing techniques such as nodal geophones and distributed acoustic sensing enable a spatial-sampling ratio that has been unprecedentedly high in earthquake seismology. The much higher sampling of seismic wavefields that is close to the level in exploration seismology calls for a unified processing approach for multichannel seismic data, regardless of the research interest—for example, oil- and gas-oriented or earthquake-study oriented interest. We created the first Python package for multichannel seismic data to benefit both communities—that is, exploration and earthquake seismology—called Pyseistr. Pyseistr is a Python package designed to make full use of structural patterns in multichannel seismic data to facilitate data processing. The Pyseistr package currently includes several fundamental functions such as slope estimation, structural mean and median filtering, and structural reconstruction of missing data. The Pyseistr package is continuously updated to include more functions to benefit both exploration and earthquake communities. The open-source repository can be found at https://github.com/aaspip/pyseistr.

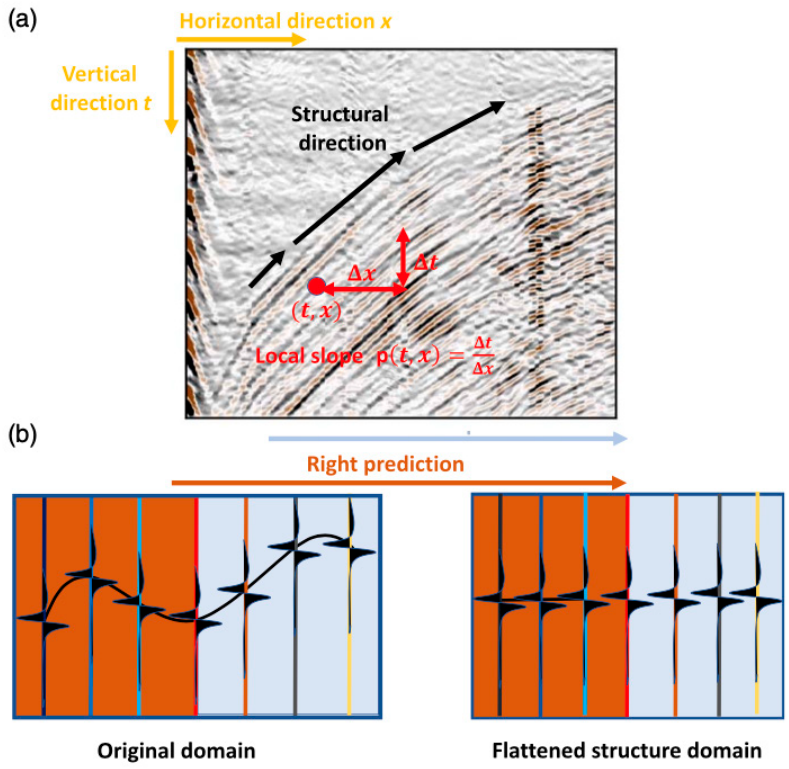

Figure 1. Principles of Pyseistr. (a) Demonstration of structural filtering. (b) Demonstration of flattening process.

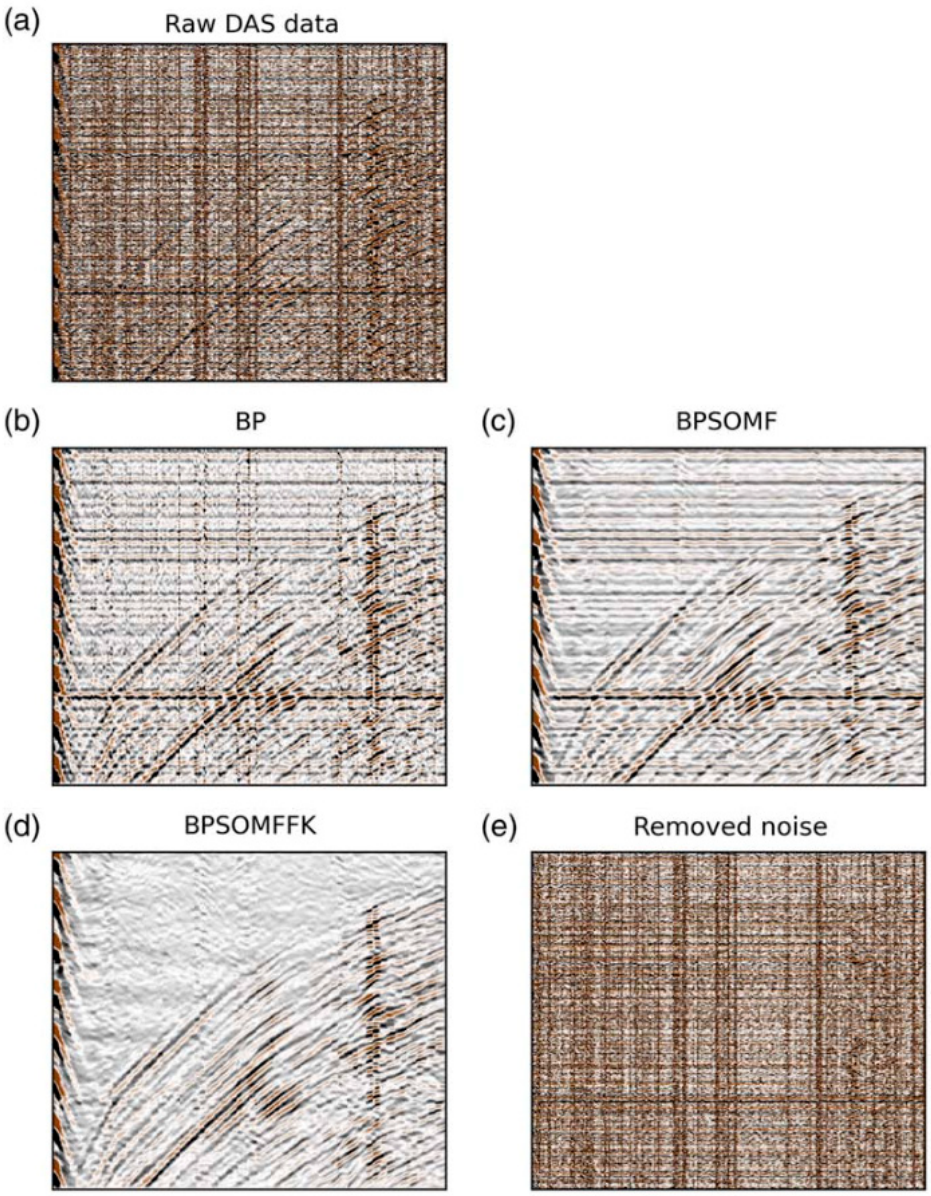

Figure 2. Example of cascaded structure-oriented filtering workflow on passive seismic dataset. (a) Raw distributed-acoustic sensing (DAS) dataset from frontier observatory for research in geothermal energy (FORGE) project with file name "FORGE_78-32_iDASv3-P11_UTC190426070723.sgy." (b) Filtered data using band-pass (BP) filter. (c) Filtered data using cascaded BP and SOMF filter. (d) Filtered data using cascaded BP, SOMF, and frequency-wavenumber (f-k) filter. (e) Removed noise. Figure can be reproduced through script "test_pyseistr_das.py" in "demo" folder.

Pyekfmm: A python package for 3D fast-marching-based traveltime calculation and its applications in seismology

***Yangkang Chen**, The University of Texas at Austin, **Yunfeng Chen**, Zhejiang University, **Sergey Fomel**, The University of Texas at Austin, **Alexandros Savvaidis**, The University of Texas at Austin, **Omar M. Saad**, KAUST, and **Yapo Abolé Serge Innocent Oboué**, Zhejiang University*

Published in Seismological Research Letters, 2023, 94(1), 2050–2059.

We created a multifunctional, open-source package—pyekfmm for eikonal-based, traveltime calculation in 2D and 3D heterogeneous anisotropic media that was based on the well-documented fast-marching method. Diverging from existing traveltime-calculation packages, the pyekfmm package offers a seamless compilation of backbone C programs in the Python environment through a state-of-the-art pip installation. As a result, users can use the pyekfmm package for different scientific purposes with the convenience enabled by Python interfaces and with the efficiency offered by C programs. The pyekfmm package offers the option of traveltime calculation to second-order accuracy. More important, the pyekfmm package provides the option for traveltime calculation in anisotropic media, enabling its exclusive applications in special cases in which strong anisotropy exists. We have introduced mathematical principles and the structure of the package in detail. To demonstrate, we applied its potential to a wide spectrum of applications, including traveltime calculation in different situations with increasing complexities, ray tracing, earthquake-source location, relocation, and surface-wave tomography. The open-source repository HYPERLINK "can be found at https://github.com/aaspip/pyekfmm.

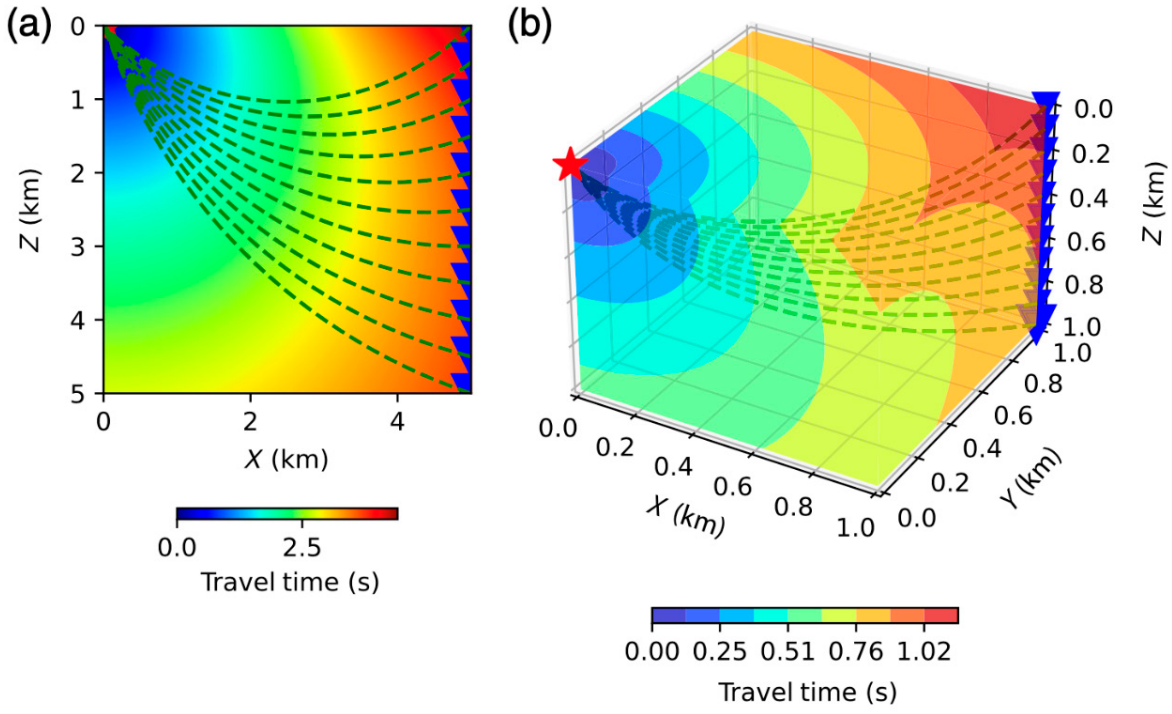

Figure 1. Traveltime calculation and ray-tracing examples in (a) 2D and (b) 3D media with vertically increasing velocities.

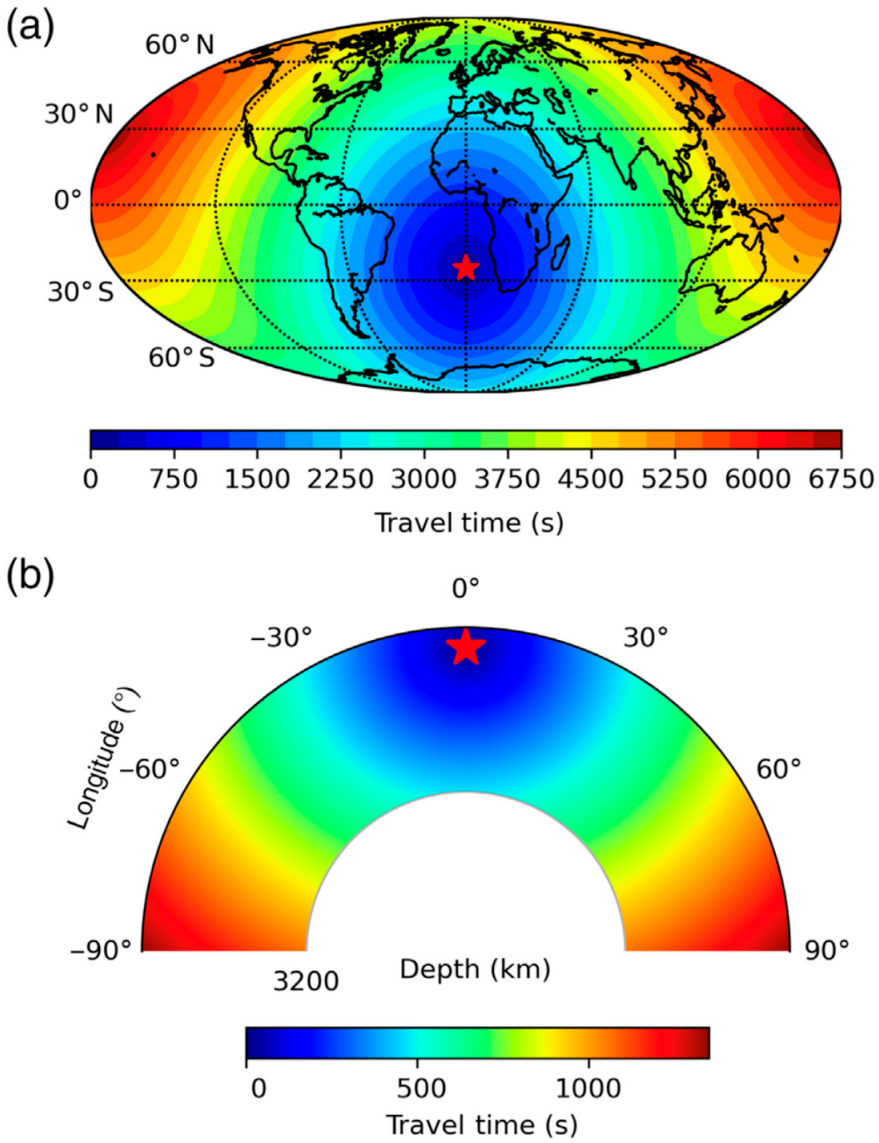

Figure 2. Traveltime calculation for global Earth. (a) We assume an event at latitude −25˚, longitude 0˚, depth 0 km, and constant surface-wave velocity of 3.0 km/s. (b) We assume an event at latitude −25˚, longitude 0˚, and depth 400 km with a constant P-wave velocity of 6 km/s.

TXED: Texas earthquake dataset for AI

***Yangkang Chen**, The University of Texas at Austin, **Alexandros Savvaidis**, The University of Texas at Austin, **Omar M. Saad**, KAUST, **Guo-Chin Dino Huang**, The University of Texas at Austin, **Daniel Siervo**, The University of Texas at Austin, **Vincent O'Sullivan**, The University of Texas at Austin, **Cooper McCabe**, The University of Texas at Austin, **Bede Uku**, The University of Texas at Austin, **Preston Fleck**, The University of Texas at Austin, **Grace Burke**, The University of Texas at Austin, **Natalie L. Alvarez**, The University of Texas at Austin, **Jessica Domino**, The University of Texas at Austin, and **Iason Grigoratos**, ETH Zurich*

Published in Seismological Research Letters, 2024, 95(4), 2013–2022.

Machine-learning (ML) seismology relies on large datasets with high-fidelity labels from humans to train generalized models. Among the seismological applications of ML, earthquake detection and P- and S-wave-arrival picking are the most widely studied, with capabilities that can exceed those of humans. In response, we have compiled a regional artificial intelligence (AI) earthquake dataset (TXED) for the state of Texas. This TXED dataset is composed of earthquake signals with manually picked P- and S-wave-arrival times and manually picked noise waveforms corresponding to more than 20,000 earthquake events spanning from the beginning of the Texas seismological network (TexNet) (January 1, 2017) to date. These data supplement existing worldwide, open-access, seismological AI datasets and represent the signal and noise characteristics of Texas. Direct applications of these TXED datasets include improving performance of a global picking model in Texas by transfer learning using the new dataset. It will also serve as a benchmark dataset for fundamental AI research such as designing seismology-oriented, deep-learning architectures. We plan to continue expanding the TXED dataset as more observations are made by TexNet analysts. The repository can be accessed at https://github.com/chenyk1990/txed. Figure 1 are samples of signal. Figure 2 are signal waveform distribution information. Table 1 lists the attributes of the data

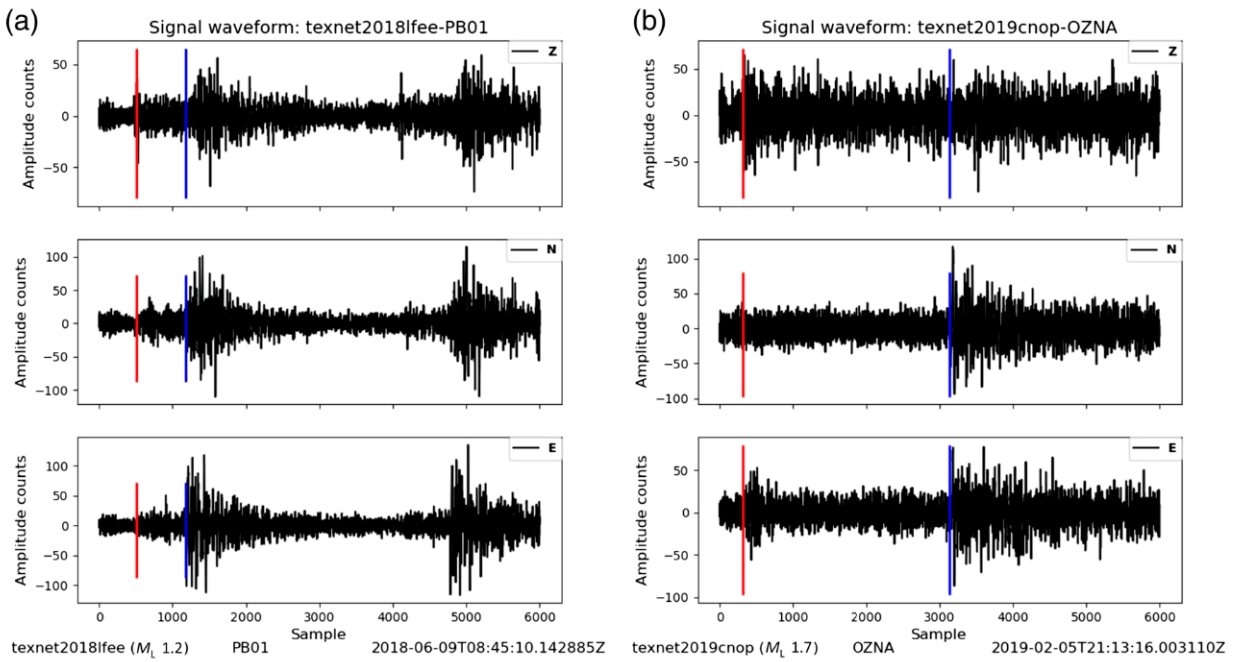

Figure 1. Several signal-waveform examples of small earthquakes.

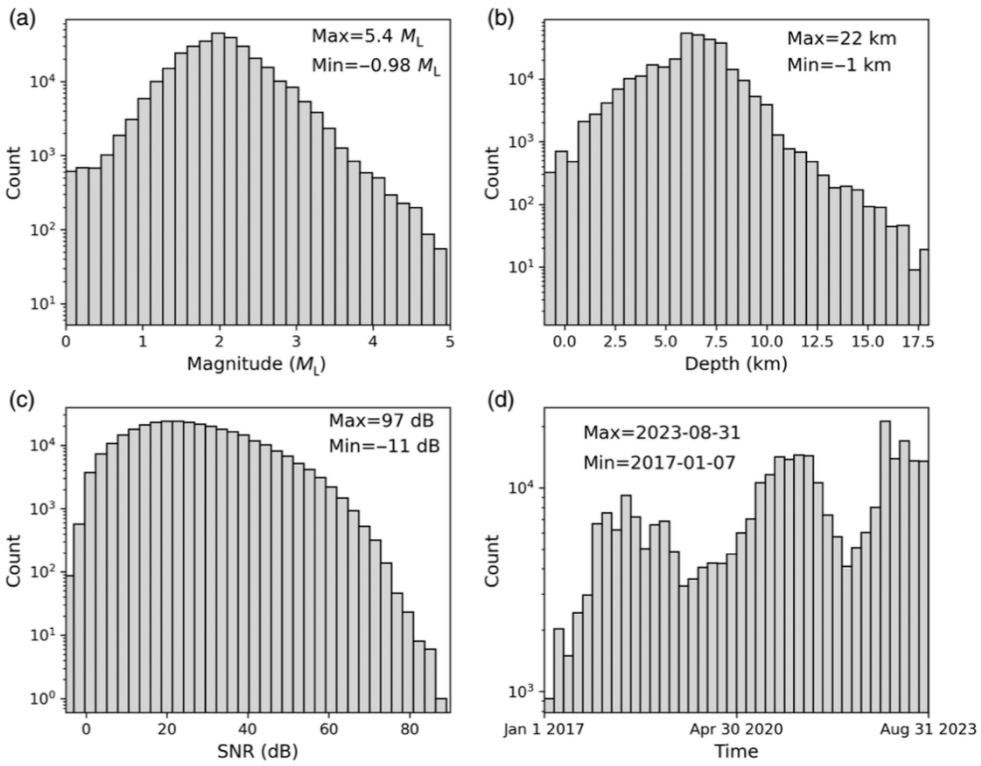

Figure 2. Distribution of signal waveforms. (a) Magnitude distribution. (b) Depth distribution. (c) SNR distribution. (d) Event origin-time distribution. Maximal and minimal values of each scenario indicated in each panel.

TABLE 1
Detailed Description of the Attributes in TXED

Attribute	Description	Example
p_arrival_sample	*P*-wave arrival sample	598
s_arrival_sample	*S*-wave arrival sample	1042
p_arrival_time	*P*-wave arrival time	2023-08-22T13:56:29.453897Z
s_arrival_time	*S*-wave arrival time	2023-08-22T13:56:48.828783Z
p_uncertainty	*P*-wave uncertainty	0.2 s
s_uncertainty	*S*-wave uncertainty	0.3 s
coda_end_sample	Ending sample of the coda	1486
snr_db	Signal-to-noise ratio of three components	[31.37, 31.55, 34.98] dB
trace_category	waveform type (signal or noise)	earthquake_local | noise
ev_longitude	Event longitude	−104.38°
ev_latitude	Event latitude	31.66°
ev_depth	Event depth compared with MSL	7879.71 m
magnitude	Event magnitude	2.67
origin_time	Event origin time	2022-08-12T22:32:20.315720Z
sta_longitude	Station longitude	−104.14°
sta_latitude	Station latitude	31.92°
sta_elevation	Station elevation compared with MSL	914.00 m
station	Station code	PECS
polarity	*P*-wave first-motion polarity	unknown|U|D
causal	Causal factor	unknown|HF|SWDsh|SWDdp

HF, hydraulic fracturing; MSL, mean surface level; SWDdp, deep saltwater disposal; SWDsh, shallow saltwater disposal.

Table 1. Attributes of TXED.

Effect of TXED-assisted transfer learning in triggering far-away stations

Yangkang Chen, The University of Texas at Austin, Alexandros Savvaidis, The University of Texas at Austin, Omar M. Saad, KAUST, and Daniel Siervo, The University of Texas at Austin

Presented at the 85th Annual International Conference and Exhibition, EAGE, 2024.

For training a generalizable model, machine learning (ML) seismology relies on a large-scale database with high-fidelity labels from humans. Among the seismological applications of ML, earthquake detection and P- and S-wave-arrival pickings are the most widely studied, with the most successful results exceeding those from humans. We compiled a regional artificial intelligence (AI) earthquake dataset (TXED) for the state of Texas. The TXED dataset is composed of earthquake signals with manually picked P- and S-wave-arrival times and manually picked noise waveforms corresponding to more than 20,000 earthquake events from the beginning of the Texas seismological network (TexNet) (01/01/2017) to date. Then we applied transfer learning to a pretrained, deep-learning model, EQCCT, using regional TXED data to boost phase-picking performance in regional, continuous waveform data. Error distribution shows that the picking errors, as compared with those of the manual picks, were significantly smaller after the transfer-learning step (Figure 1). Application of the new model after transfer learning to continuous-waveform data in West Texas recorded by TexNet further demonstrated an obviously enhanced detectability using deep-learning approaches. In particular, transfer learning slightly improved detection performance of large-magnitude earthquakes while tremendously improving detection of small events by triggering far-away seismic stations.

For small earthquakes (e.g., M<1.5), we used a Ml=1.29 earthquake event in West Texas on November 7, 2023, as an example. This event was not detected by TexNet but was detected by both EQCCT models (original and fine-tuned). The original EQCCT model detected this event in only 5 stations, whereas the fine-tuned EQCCT model detected this event in 11 stations (Figure 2a, b). Significantly more P- and S-wave picks occurred owing to a more accurate performance of the fine-tuned EQCCT model. According to the station locations (Figure 2c) and owing to the results of the fine-tuned model, we found that the newly triggered stations were mostly farther away than the earthquake-epicenter locations. And although the epicenter locations of the two models were close, their depth difference was larger, around 2 km. We have no reference location from manual quality control, but we think that the hypocenter location of the fine-tuned model is more accurate owing to a larger number of stations and better azimuthal coverage. This scenario is a convincing demonstration that the fine-tuned model can significantly improve detection ability and location fidelity for small-magnitude earthquake events because of more accurate picking in the presence of strong local noise.

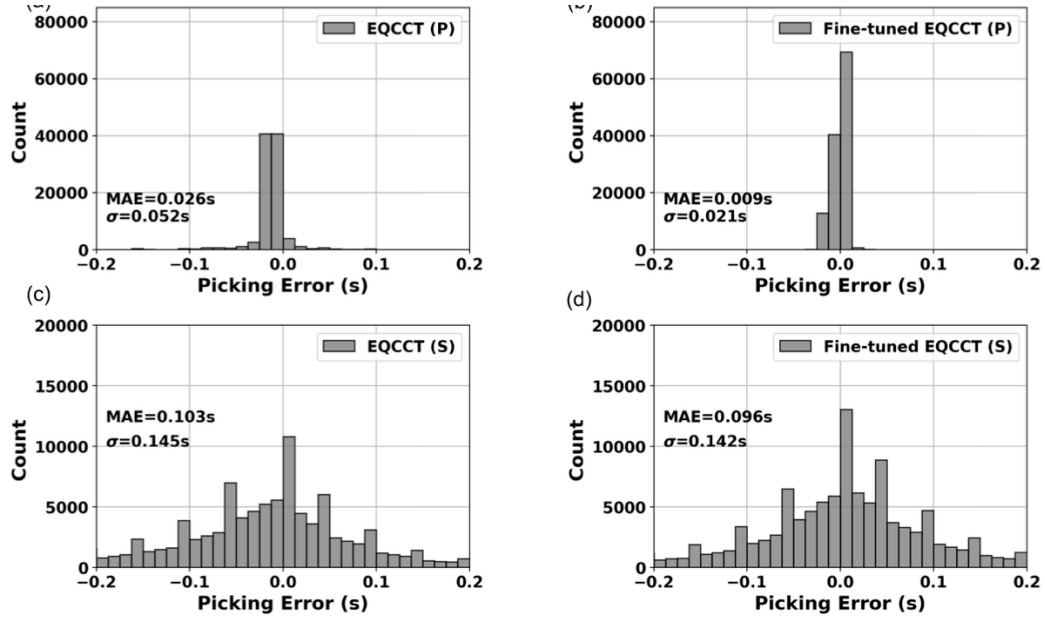

Figure 1. Distribution error of P-wave picks corresponding to (a) pretrained EQCCT and (b) fine-tuned EQCCT models. Distribution error of S-wave picks corresponding to (c) pretrained EQCCT and (d) fine-tuned EQCCT models.

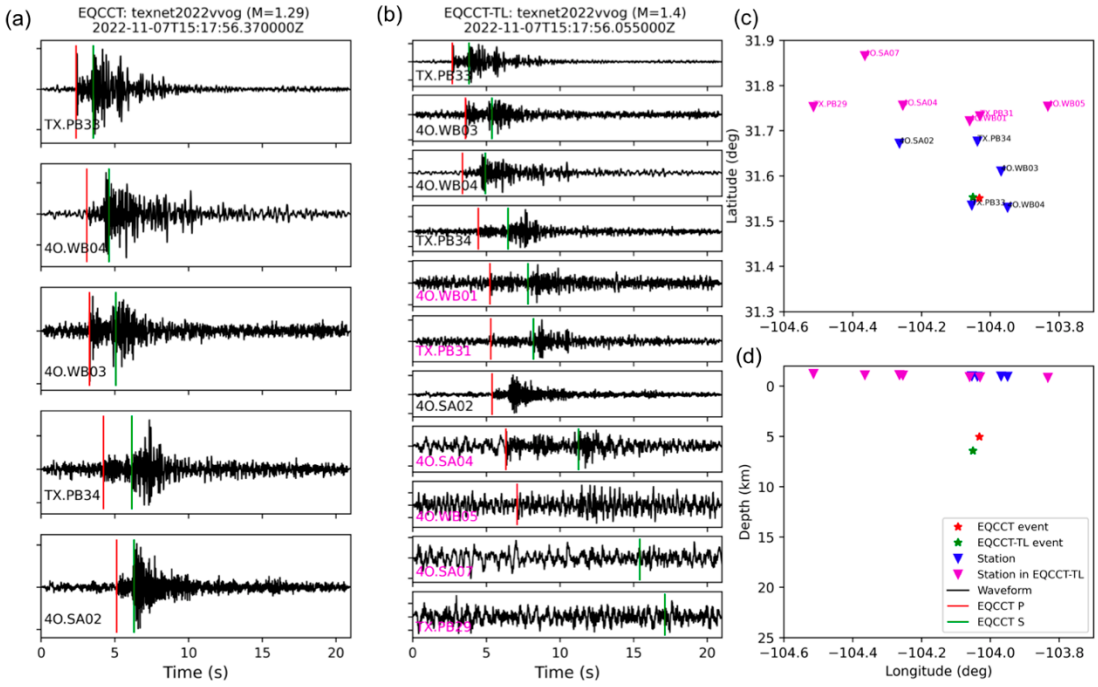

Figure 2. Earthquake-detection comparison for small-earthquake event not in public TexNet catalog. (a) Picking performance for EQCCT model without transfer learning. (b) Picking performance of new model after transfer learning. (c) Earthquake source and station locations on map. (d) Earthquake source and station locations on longitude-depth slice. Transfer-learning model significantly better than original model; e.g., EQCCT detects this event from only 5 stations, whereas EQCCT-TL detects this event from 11 stations. According to map view, most added stations are far away.

Visualizing seismic-network geometry impact: Azimuthal gap and distance improvement through station-placement simulation

Daniel Siervo and Alexandros Savvaidis
Bureau of Economic Geology, The University of Texas at Austin

Two of the most influential parameters determining quality of earthquake location are maximum azimuthal gap and distance to the closest station. This study presents a data-driven methodology for visualizing how placement of hypothetical seismic stations can impact these parameters. The example shown uses TexNet web catalog data from the Midland Basin (2017—2024).

We simulated deployment of additional seismic stations to assess their effect on azimuthal gap and proximity to the nearest station, resulting in two maps. Workflow involved first simulating placement of hypothetical new stations across the region of interest. We then analyzed their impact on existing seismic-event coverage. In the case of GAP computation, only stations within a configurable radius, set to 100 km in this example, were used to assess azimuthal-coverage improvement. Baseline calculations were first performed using current network configuration to determine events with poor azimuthal coverage and large distances to nearest stations. Simulations then added a new station iteratively to calculate the number of events affected for each tested site.

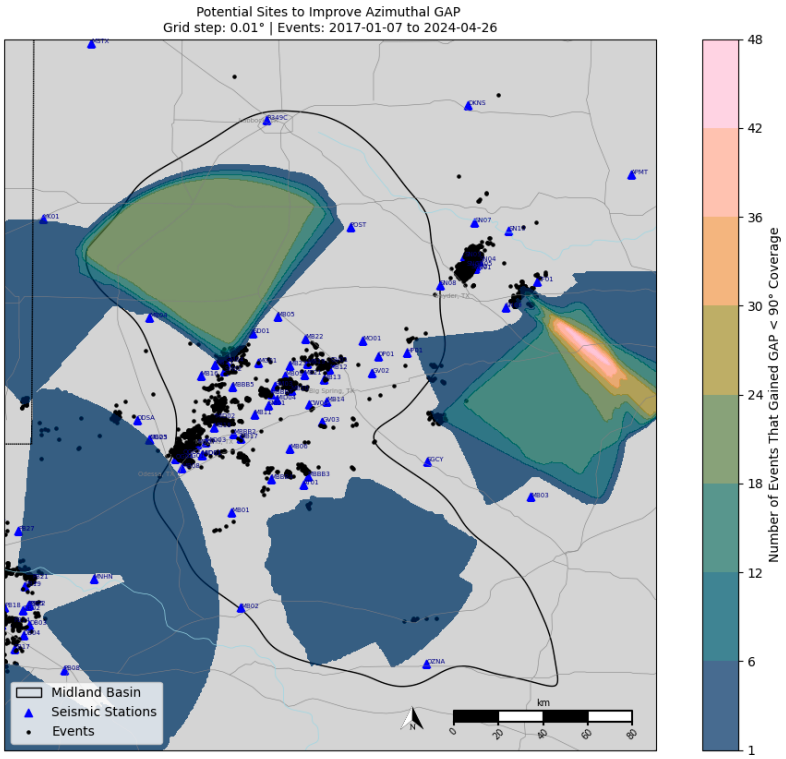

Figure 1. Simulated azimuthal-gap improvement. Regions color-coded to reflect number of seismic events that would have improved gap of <90° if new station were deployed there. Highest impact areas indicated in warmer colors, suggesting sites where new station could lead to reductions in azimuthal gaps, thereby improving event-location geometry.

The azimuthal-gap improvement map shows the number of seismic events that would experience a reduction in azimuthal gap to less than 90° if a new station were to be deployed at a given location. Areas where a new station significantly reduced the azimuthal gap are highlighted in colors indicating various levels of improvement. This visualization helps to explain how adding a station in a specific area can enhance azimuthal coverage.

The closest-station distance-improvement map suggests how adding a new station improves the proximity of seismic events to at least one station within a 10-km radius. Colors represent the number of events that now meet this proximity criterion, indicating improved coverage, which should translate to an improvement in accuracy of earthquake locations.

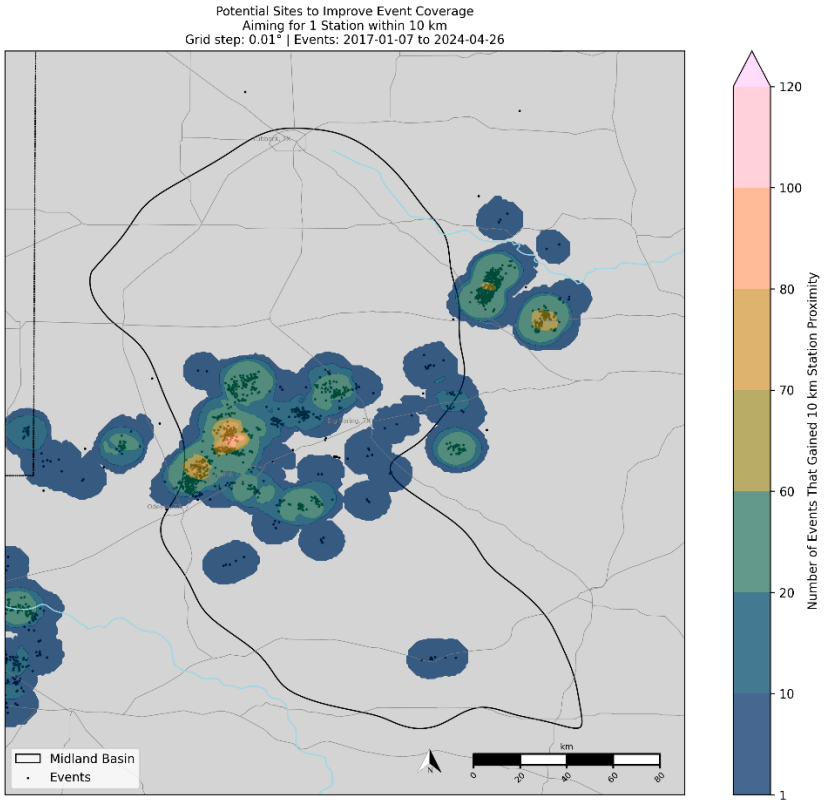

Figure 2. Closest-station distance-improvement map. Illustration of improvements in proximity to closest seismic station within 10-km radius. Colors used to depict number of events that would meet proximity criterion after deployment of new station in specific areas.

Conclusions

Azimuthal-gap and distance-improvement maps provide visualization of how placement of a new station could affect network coverage. These maps can help network planners identify areas where a new station would have the most significant positive impact, whether by reducing azimuthal gap or by providing the nearest station distance to existing events.

QBTransNet: Deep learning earthquake distinction from quarry blasts using dilated convolutional transformer

***Liuqing Yang**, Uppsala University, **Yangkang Chen**, The University of Texas at Austin, **Daniel Siervo**, The University of Texas at Austin, **Katerine Vallejo**, The University of Texas at Austin, and **Alexandros Savvaidis**, The University of Texas at Austin*

Submitted to Seismological Research Letters.

An accurate distinction between naturally and artificially induced earthquake events is crucial to any subsequent data analysis. However, because the signal characteristics of nonseismic events caused by quarry blasts are similar to earthquake events, unreliable and potentially erroneous manual identification, especially in the absence of source location information, may result. We have therefore proposed a reliable, deep-learning-based framework to distinguish between earthquakes and quarry blasts. During the data-preprocessing stage, we applied a continuous wavelet-transform algorithm to the 60-sec, three-channel waveforms extracted from the 10 s before and 50 s after the first arrival time of the P-wave for time-frequency conversion. Our proposed discrimination framework comprises a dilated convolutional transformer (DCT) and a capsule neural network. DCT combines the local perception capability of traditional convolutional neural networks, effectively extracting spatial features from multichannel scalograms. Additionally, the multihead, self-attention module in the transformer dynamically adjusts feature weights across different positions to adaptively focus on significant features—crucial to handling complex background noise and irrelevant information in earthquake and quarry-blast signals. Then we transferred the features extracted by DCT to the capsule neural network for hierarchical feature representation. The dynamic routing mechanism in the this network allows for flexible and adaptive feature propagation and integration between capsules, enabling precise distinction between earthquakes and quarry blasts. We used an artificial intelligence (AI) earthquake dataset recorded by the Texas seismological network (TexNet) to demonstrate the classification performance of the proposed network. Compared with state-of-the-art classification networks, the proposed method has higher reliability and more satisfactory results, with testing accuracy, precision, recall, and F1 score reaching 99.22%, 99.34%, 99.01%, and 99.18%, respectively. We also were able to demonstrate the robustness of the proposed network through a real-time monitoring test.

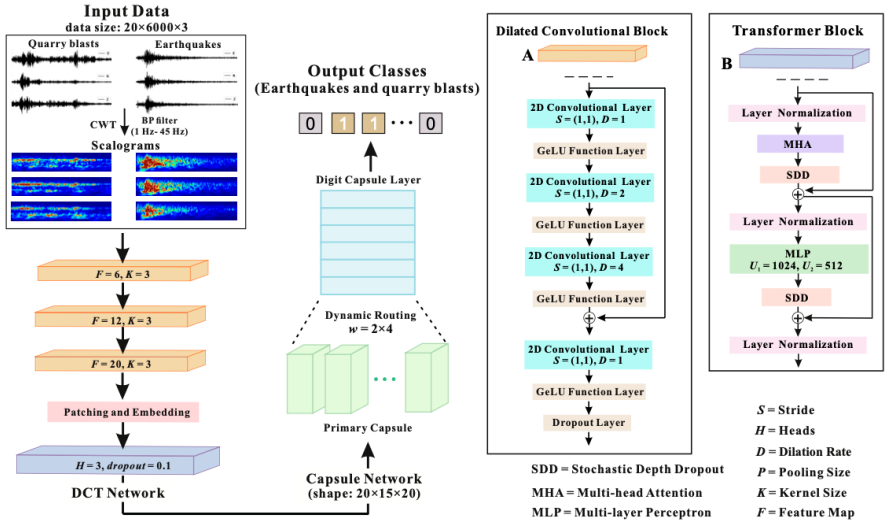

Figure 1. Architecture of proposed QBTransNet for earthquake distinction, consisting of dilated convolutional transformer (DCT) and capsule networks. Frame boxes A and B represent core blocks of DCT network.

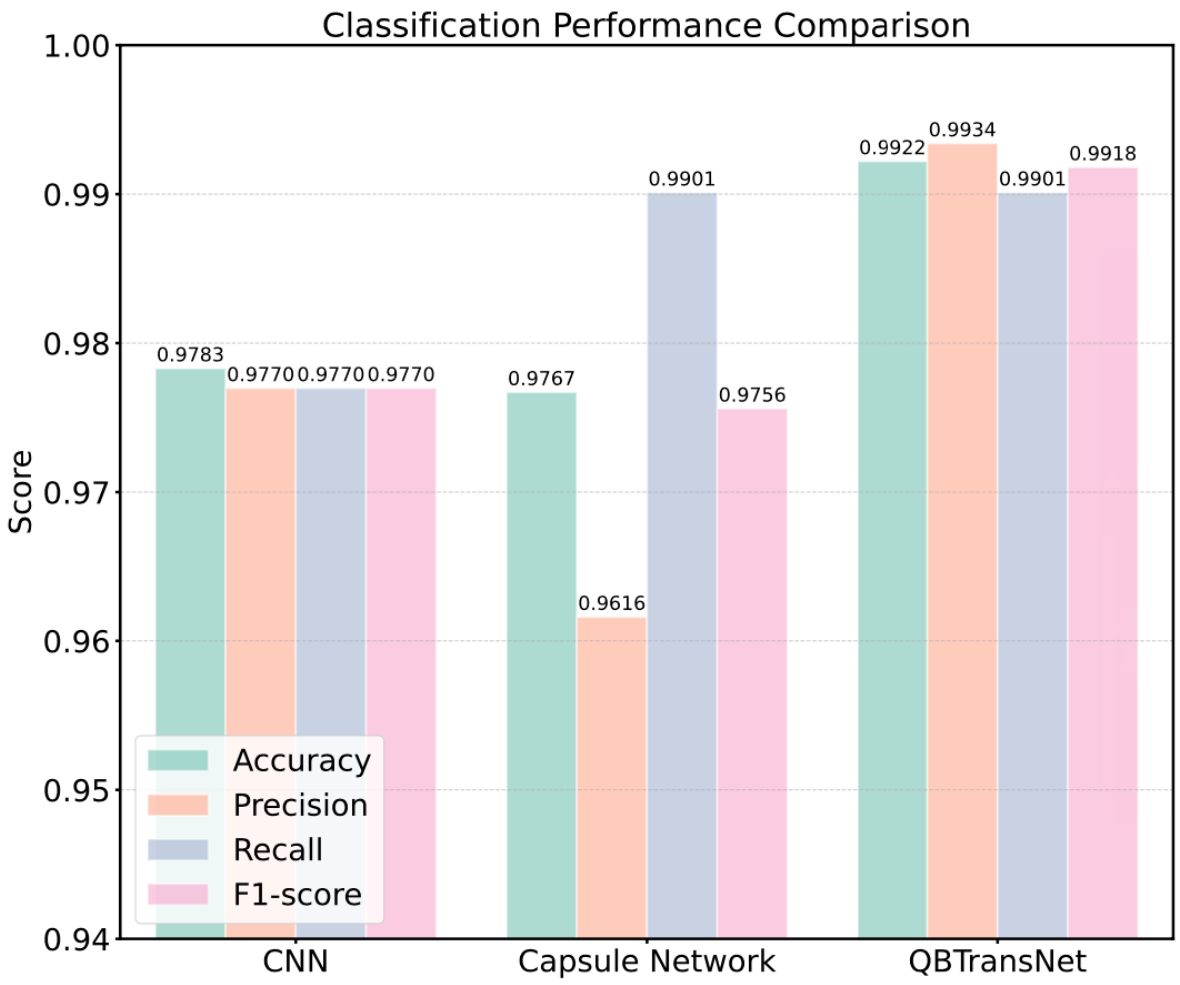

Figure 2. Histogram display of benchmark networks and proposed QBTransNet in different evaluation metrics.

Deep learning for seismic-data compression in distributed acoustic sensing

***Yangkang Chen**, The University of Texas at Austin, **Omar M. Saad**, KAUST, **Yunfeng Chen**, Zhejiang University, and **Alexandros Savvaidis**, The University of Texas at Austin*

Submitted to IEEE Transactions on Geoscience and Remote Sensing

Distributed acoustic sensing (DAS) is emerging in seismic monitoring owing to its ultradense spatial sampling, durability to harsh environments, and sensitivity to weak ground vibration. Compared with traditional nodal geophones that are normally sparsely distributed, DAS offers unprecedented detectability in small-magnitude earthquake events, subtle reservoir dynamics, and other weak signals among various applications. The appealing detectability of weak signals is, however, compromised by the terabyte-scale, daily continuous record that causes prohibitive storage problems. The current solution is to save only segmented data of interest, e.g., a certain length around a target event. Here, we tackled the urgent storage problem of DAS monitoring by designing a deep-learning (DL)-based compression algorithm, which can be split into two major components. First is the encoder, which is based on vision-transformer architecture, wherein an input multichannel DAS dataset goes through an encoding process to output key features from the input. Second is the decoder, in which features are optimally combined to reconstruct data at the original scale. Optimal network parameters were obtained via an unsupervised training process, aiming at minimizing the difference between reconstructed and input data. In the proposed DL-based compression algorithm, only the decoder's weight parameters and extracted features from input data through the encoder were saved on the disk, which was sufficient to reconstruct a high-fidelity dataset. The proposed compression algorithm can reach about 50 times the compression rate for a gigabyte-scale DAS dataset without unsatisfactory reconstruction performance.

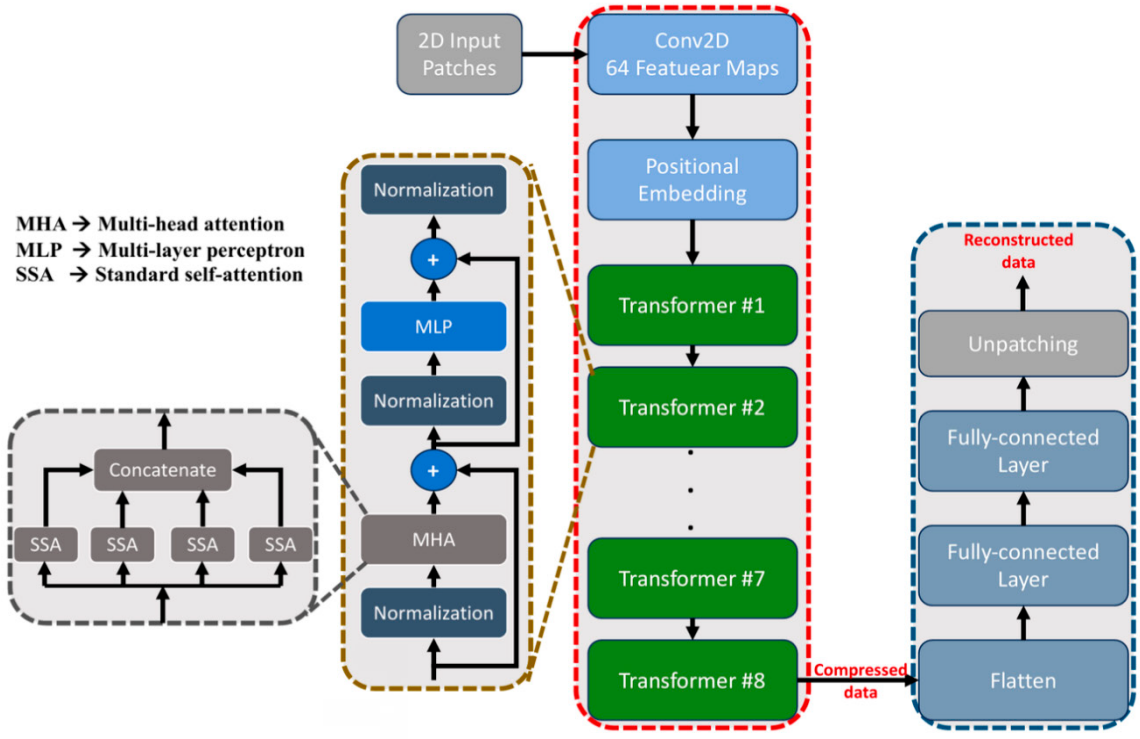

Figure 1. Proposed architecture for vision-transformer-based encoder. Encoder used to extract features from smaller-sized input patches, achieving goal of data compression, which can be input to decoder to reconstruct data at original scale.

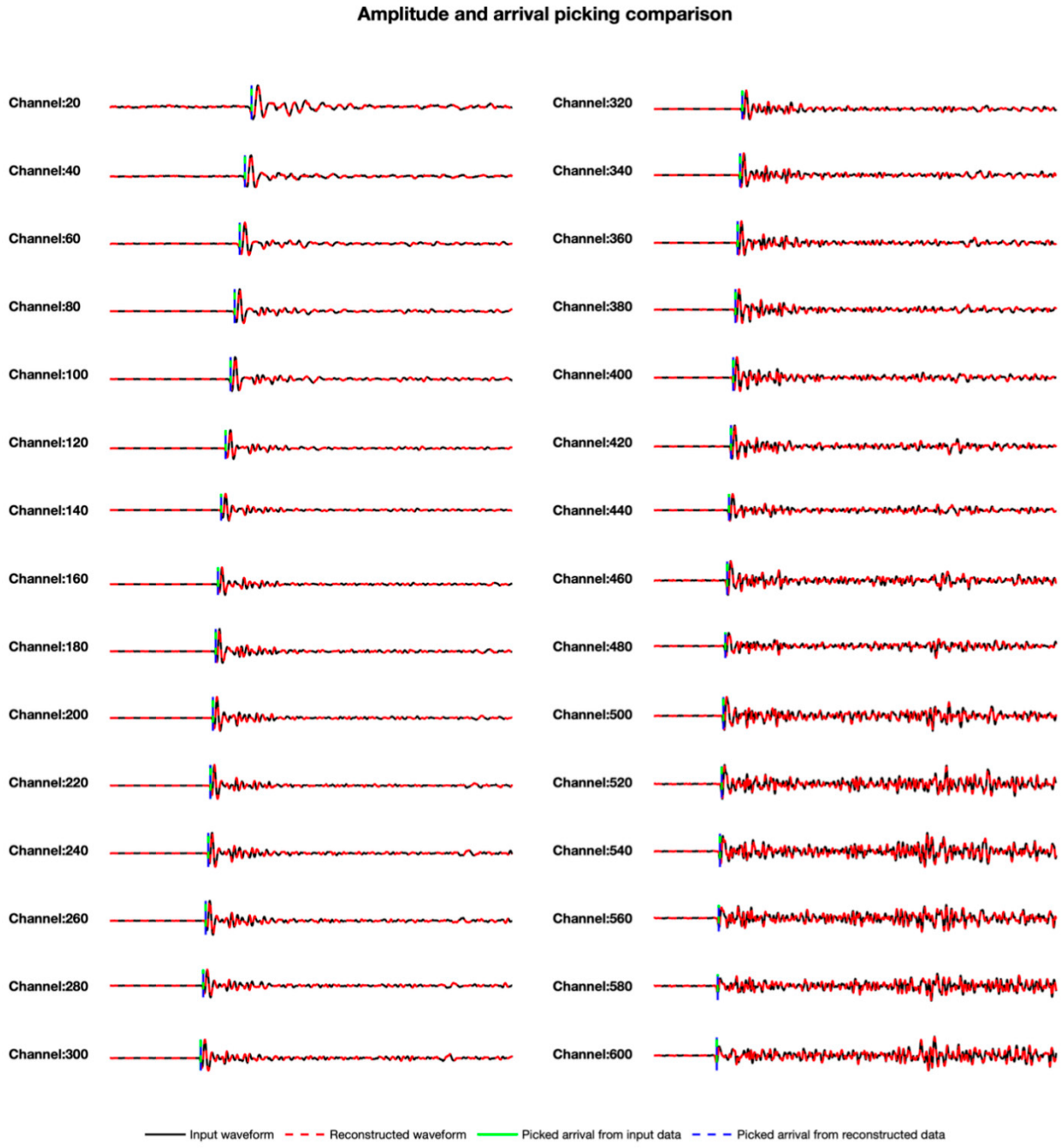

Figure 2. Single-trace amplitude comparison for FORGE data example and P-wave arrival picking comparison. Black and red dashed lines = input and reconstructed traces, which overlap each other, indicating near-perfect reconstruction. Picked arrival times using widely accepted STA/LTA method indistinguishable, showing that compression does not affect following processing or analysis steps.

Thousands of induced earthquakes per month in West Texas detected using EQCCT

Yangkang Chen, The University of Texas at Austin, Alexandros Savvaidis, The University of Texas at Austin, Omar M. Saad, KAUST, Yunfeng Chen, Zhejiang University, Iason Grigoratos, ETH Zurich, Sergey Fomel, The University of Texas at Austin, Daniel Siervo, The University of Texas at Austin, Guo-Chin Dino Huang, The University of Texas at Austin, and Caroline Breton, The University of Texas at Austin

Published in Geosciences, 2024, 14, 114.

West Texas has been a seismically active region in the past decade owing to injection of industrial wastewater and hydrocarbon exploitation. The newly founded Texas seismological network has provided a catalog that characterizes intense seismicity down to a magnitude of 1.5 Ml. However, numerous small-magnitude events (Ml < 1.0) occur every day that are not analyzed or reported, owing to a prohibitively high workload of manual-verification picks using automatic-picking methods. We proposed applying an advanced deep-learning method, the earthquake compact convolutional transformer (EQCCT), to unleash power in analyzing hundreds of small earthquakes per day in West Texas. The EQCCT method is embedded in an integrated-detection-and-location framework to seamlessly output a complete earthquake catalog, given a list of available seismic stations. The EQCCT has enabled us to detect and locate 50 times more earthquakes (mostly smaller than magnitude 1) than we previously could. We applied the EQCCT-embedded detection and location workflow to the Culberson and Mentone earthquake zone (CMEZ) in West Texas and detected thousands of earthquakes per month for 3 consecutive months. Further relocation of the new catalog revealed an unprecedentedly high resolution and precise depiction of shallow and deep, basement-rooted faults. This catalog also offers significant insights into the seismotectonic status of the CMEZ. Association with nearby injection activities also revealed a strong correlation between rate of injected-fluid volume and number of small earthquakes.

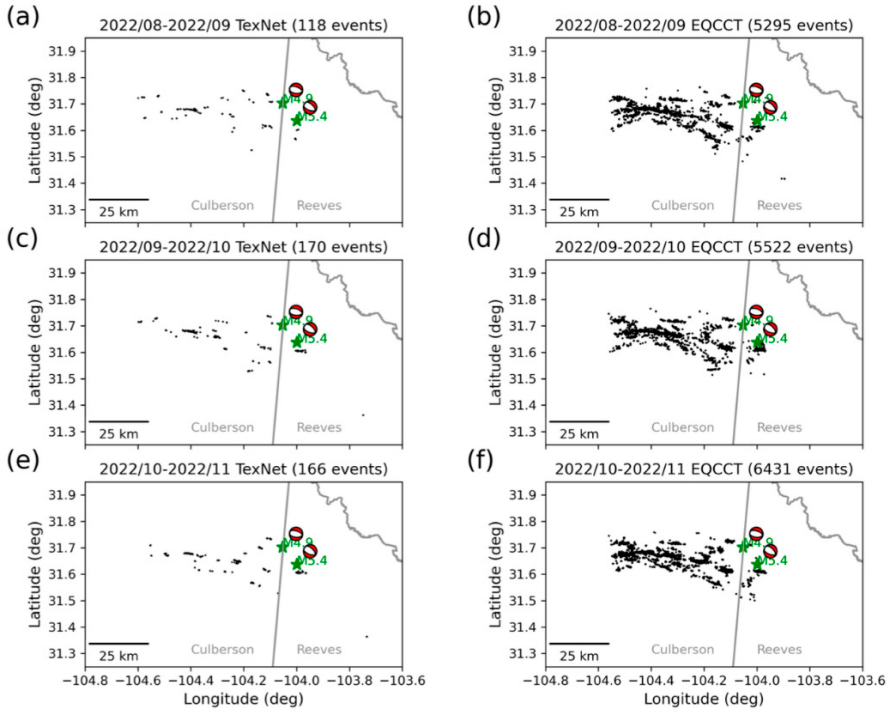

Figure 1. Single-month comparison of relocation results between TexNet and EQCCT catalogs. (a) Relocated TexNet catalog between 2022/08 and 2022/09. (b) Relocated EQCCT catalog between 2022/08 and 2022/09. (c) Relocated TexNet catalog between 2022/09 and 2022/10. (d) Relocated EQCCT catalog between 2022/09 and 2022/10. (e) Relocated TexNet catalog between 2022/10 and 2022/11. (f) Relocated EQCCT catalog between 2022/10 and 2022/11.

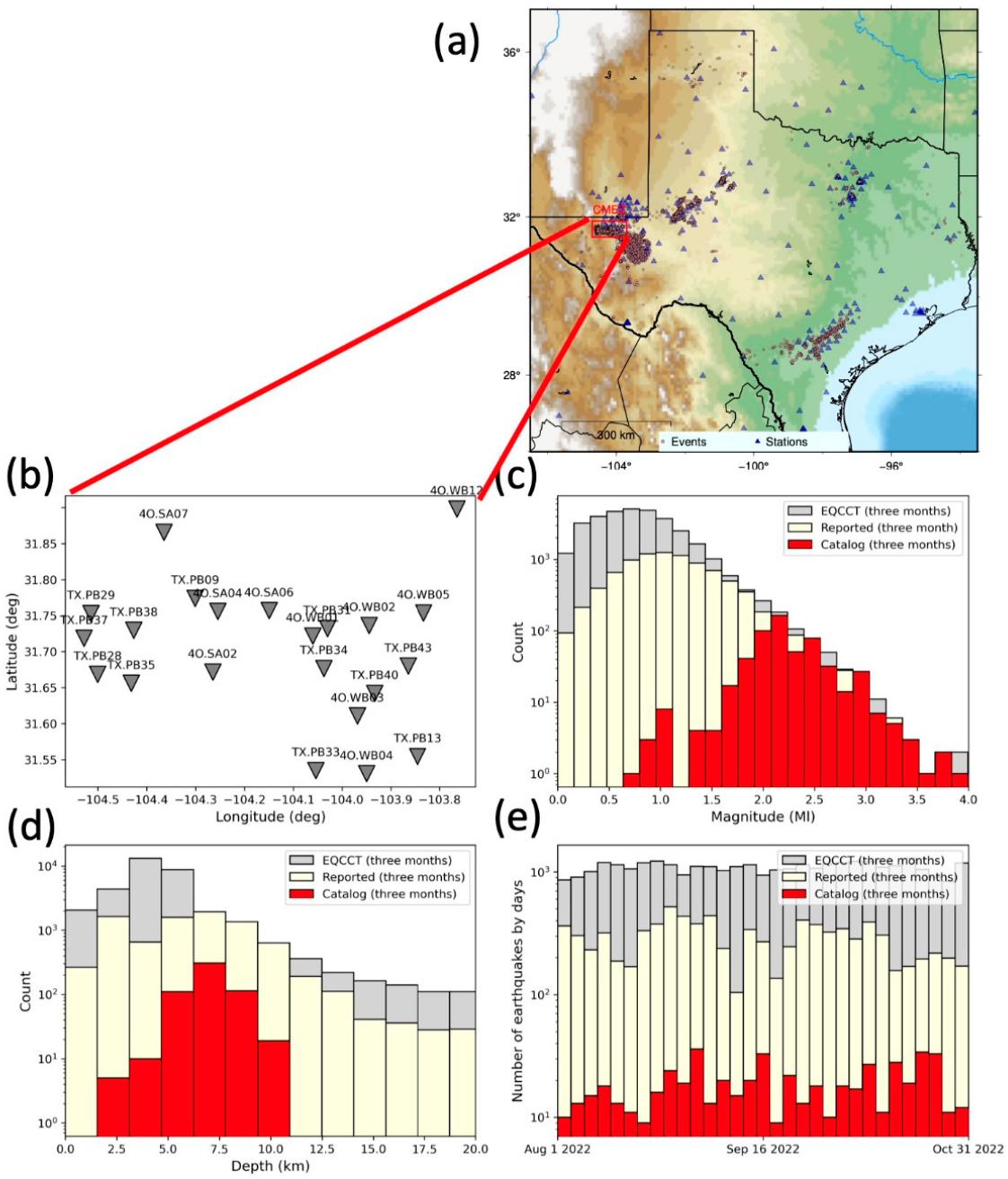

Figure 2. Distribution of events. (a) Map of Texas seismological network. CMEZ = Culberson and Mentone seismic zone, the most seismically active area in Texas. In 2022, 80.85% of Texas seismicity was located in CMEZ. (b) Stations used in detection and location. (c) Magnitude distribution. (d) Depth distribution. (e) Distribution of earthquakes by date; each bin = 3 days. Reported events = those detected by traditional automatic-picker short-term average/long-term average at TexNet but not manually reviewed.

Massive focal mechanisms determined from deep learning in West Texas

***Yangkang Chen**, The University of Texas at Austin, **Alexandros Savvaidis**, The University of Texas at Austin, **Omar M. Saad**, KAUST, **Fangxue Zhang**, Zhejiang University, **Yunfeng Chen**, Zhejiang University, **Dino Huang**, The University of Texas at Austin, **Huijian LI**, KFUPM, and **Farzaneh Aziz Zanjani**, University of Florida*

Published in IEEE Transactions on Geoscience and Remote Sensing, 2024, 57(4), 2249-2262.

Because focal mechanism provides seismological constraints on geological faults that generate earthquakes, it has become crucial to regional seismotectonic research. Focal-mechanism calculation is based on P-wave first-motion polarity and is a widely used method, particularly for small- to moderate-size earthquakes. However, determining P-wave first-motion polarity can be challenging and subjective when dealing with smaller earthquakes. Here, we have proposed a deep-learning method (EQpolarity) for determining P-wave first-motion polarity using vertical-component seismic waveforms. This deep-learning method was trained using a large-scale dataset from southern California, which we then adapted to Texas earthquake data via a transfer-learning method. Original and secondary models obtained 95.43% and 98.82% accuracy in the Texas database, respectively, indicating the effectiveness of transfer learning. We further applied the deep-learning method to thousands of events in the TexNet catalog to determine focal mechanisms. Most focal-mechanism solutions aligned well with strikes, dips, and rakes of known faults that had been explored previously using full-waveform-based methods (Figures 1 and 2). Generation of a large focal-mechanism database offers significant insights into the seismotectonic status of West Texas. The open-source package of EQpolarity can be accessed at https://github.com/chenyk1990/eqpolarity.

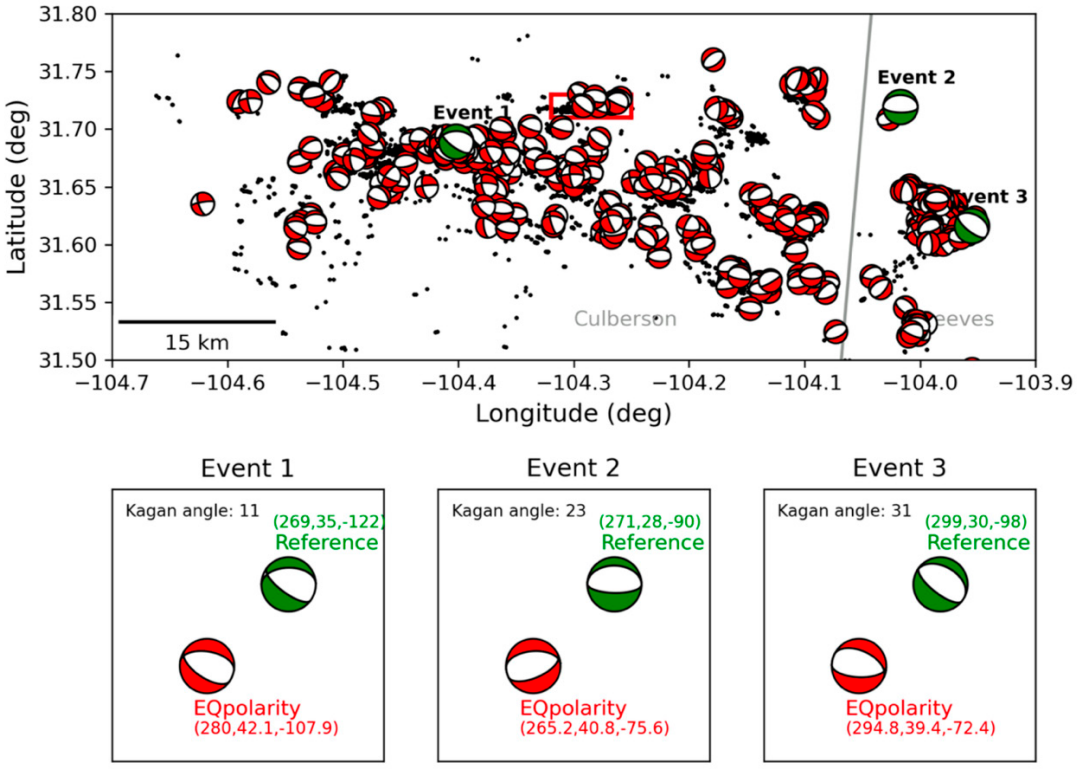

Figure 1. Earthquake application of EQpolarity and HASH to earthquake data from West Texas resulted in numerous focal-mechanism solutions. Here, only 500 focal mechanisms plotted. Area highlighted by red frame box detailed in Figure 2 for comparison of focal-mechanism inversion using different deep-learning architectures.

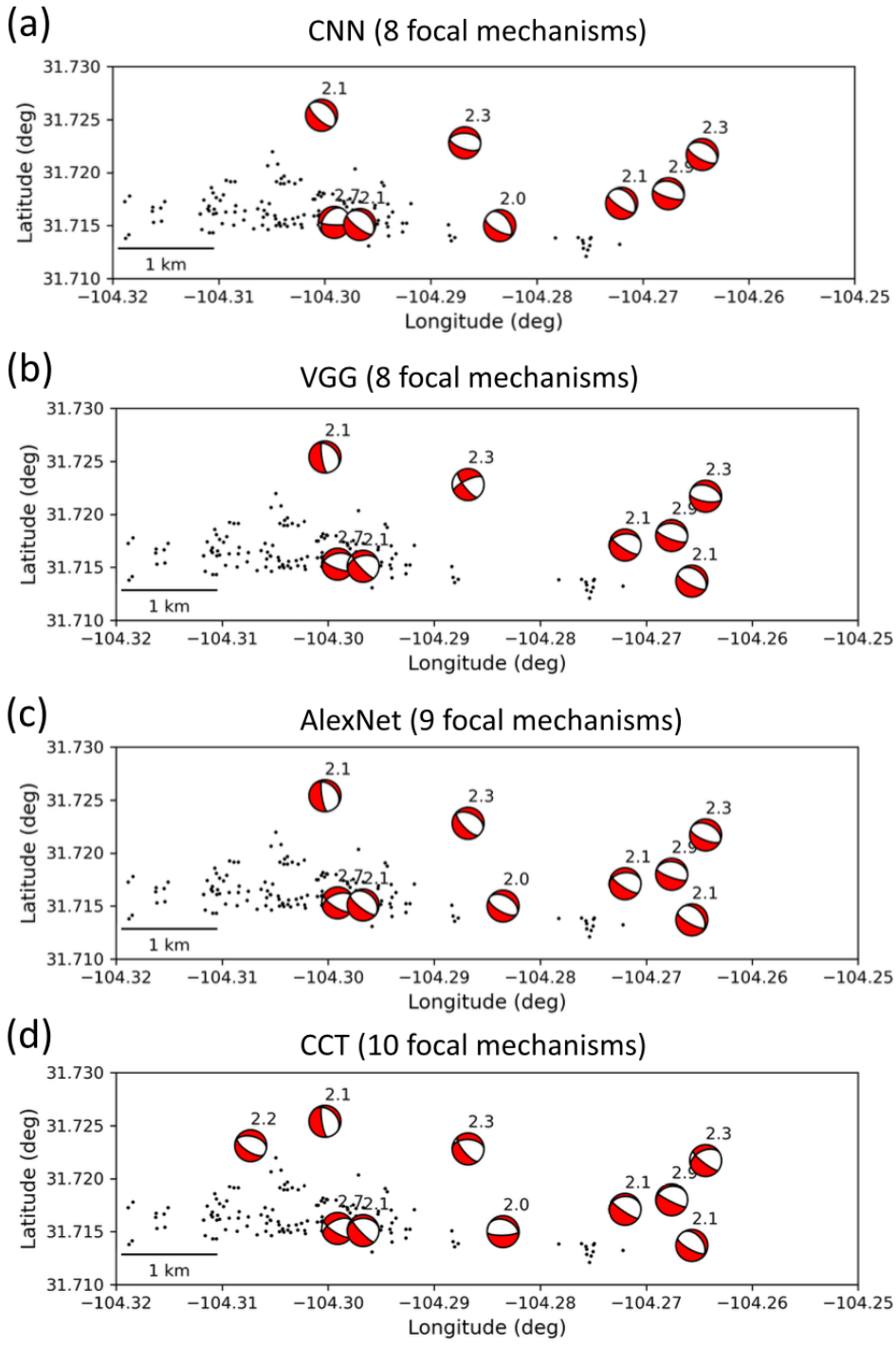

Figure 2. Comparison of different deep-learning architectures in terms of inverted focal mechanisms. (a) Eight inverted focal mechanisms from CNN model. (b) Eight inverted focal mechanisms from VGG model. (c) Nine inverted focal mechanisms from AlexNet model. (d) Ten inverted focal mechanisms from proposed CCT model. Number on each beachball = magnitude of event. All events have small magnitudes.

Moment Tensor Inversion in the Midland Basin using Gisola

Katerine Vallejo

Moment Tensor (MT) calculation is crucial because it provides detailed insights into the mechanics of an earthquake source. It helps elucidate the tectonic setting, reveals changes in the stress field, offers refined estimates of magnitude and depth by analyzing the seismic energy released during the event, and aids in distinguishing between natural and induced seismicity.

As part of TexNet's real-time earthquake monitoring, efforts are underway to implement new tools that maximize the information obtained from earthquake source mechanisms. Gisola is an open-source software that offers full autonomy for automatic real-time MT computation. It is optimized for high-performance inversion computing through multiprocessing on both CPU and GPU (Triantafyllis et al., 2021).

Gisola operates in a series of steps, incorporating multiple quality control parameters for waveform evaluation and filtering of the data used in the MT calculations. These parameters include quality check modules such as signal-to-noise ratio, long-period disturbances, station assessment based on power spectral density measurements, and waveform clipping.

Owing to Gisola's compatibility with TexNet's primary processing software (SeisComP) and FDSN Web Services, incorporating focal mechanism results from Gisola and managing MT data within SeisComP is straightforward. The inversion results can be distributed in various user-friendly formats and shared via a website or email. Integrating Gisola into TexNet's current processing would enhance the catalog with timely and comprehensive focal mechanism data, providing deeper insights into regional tectonics and delivering stakeholders broader earthquake source information.

Tuning specific parameters to the region of interest is crucial to ensuring Gisola's reliable operation. The Midland Basin (MB) was selected as the starting point for tuning and testing due to its significant increase in seismicity in recent years.

Different configuration parameters have been tested, and initial analyses have focused on large-magnitude earthquakes ($M \geq 4.0$) in the MB region. **Figure 1** presents the main results from Gisola's moment tensor inversion for a significant-magnitude event. **Figure** 2 provides a map with the focal mechanisms derived from the MT inversions using Gisola for five earthquakes that occurred in the MB between 2021 and 2024.

The results demonstrated high-quality solutions. However, the input files for these test events were manually downloaded. Additional tuning and configuration are required for the program to operate in real-time and extend its functionality to lower-magnitude events. Computation times for various earthquakes must be assessed and optimized through multiprocessing on both CPU and GPU to enhance inversion performance and ensure reliable results in the shortest possible time.

TexNet

Bureau of Economic Geology
Texas Seismological Network

Moment Tensor Solution

2022-12-16 23:35:28.55 || 32.1729, -102.1407 || 4 km || 5.1 Mw

QuakeML | Text | EMSC

Event ID:	texnet2022yplg	**Evaluation Mode:**	automatic	**Evaluation Status:**	preliminary

Quality Metrics

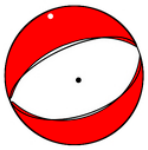

Correlation:	0.85	**Variance Reduction:**	0.72	**Quality:**	A1
DC (%):	99.90	**CLVD (%):**	0.10	**ISO (%):**	0.00
Min Singular:	9.383e-15	**Condition Number:**	2.09	**STVAR:**	0.00
Max Singular:	1.964e-14			**FMVAR:**	4.73

Hypocenter

Origin Time:	2022-12-16 23:35:27.98	**Magnitude:**	5.2 ML(TexNet)
Latitude:	32.1909	**Longitude:**	-102.1407
Depth:	8.2 km		

Centroid

Centroid Time:	2022-12-16 23:35:28.55	**Magnitude:**	5.1 Mw
Latitude:	32.1729	**Longitude:**	-102.1407
Depth:	4.2 km	**Mo (Nm):**	4.944e+16

Figure 1. Moment tensor inversion Gisola results for texnet2022yplg.

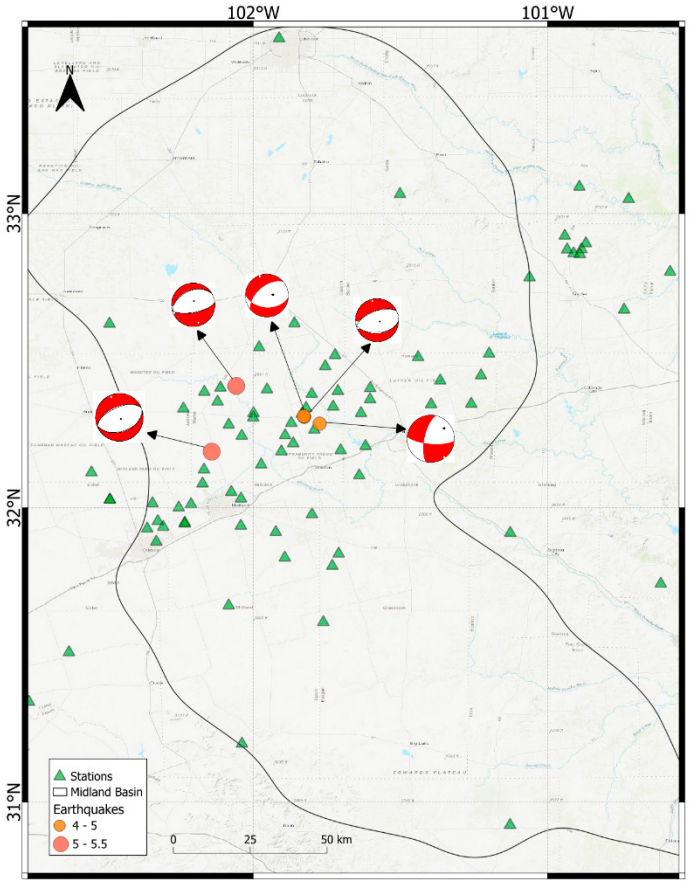

Figure 2. Midland Basin region and focal mechanisms calculated using Gisola (in red) for the interest area.

Mapping the 2-D Stress Field and Crustal Deformation of the Permian Basin

Dino Huang, Yangkang Chen, Alexandros Savvaidis

Bureau of Economic Geology, The University of Texas at Austin

Located in New Mexico and Texas, the greater Permian basin is composed of two subunits – the Delaware and the Midland basins. Induced seismicity in the greater Permian basin has revealed previously unmapped complex seismogenic structures. This study combines previous results and will further define the seismotectonics and the 2-D stress field of the greater Permian basin. Seismicity in the Permian basin is clusteed and has shown different distribution patterns (Fig. 1).

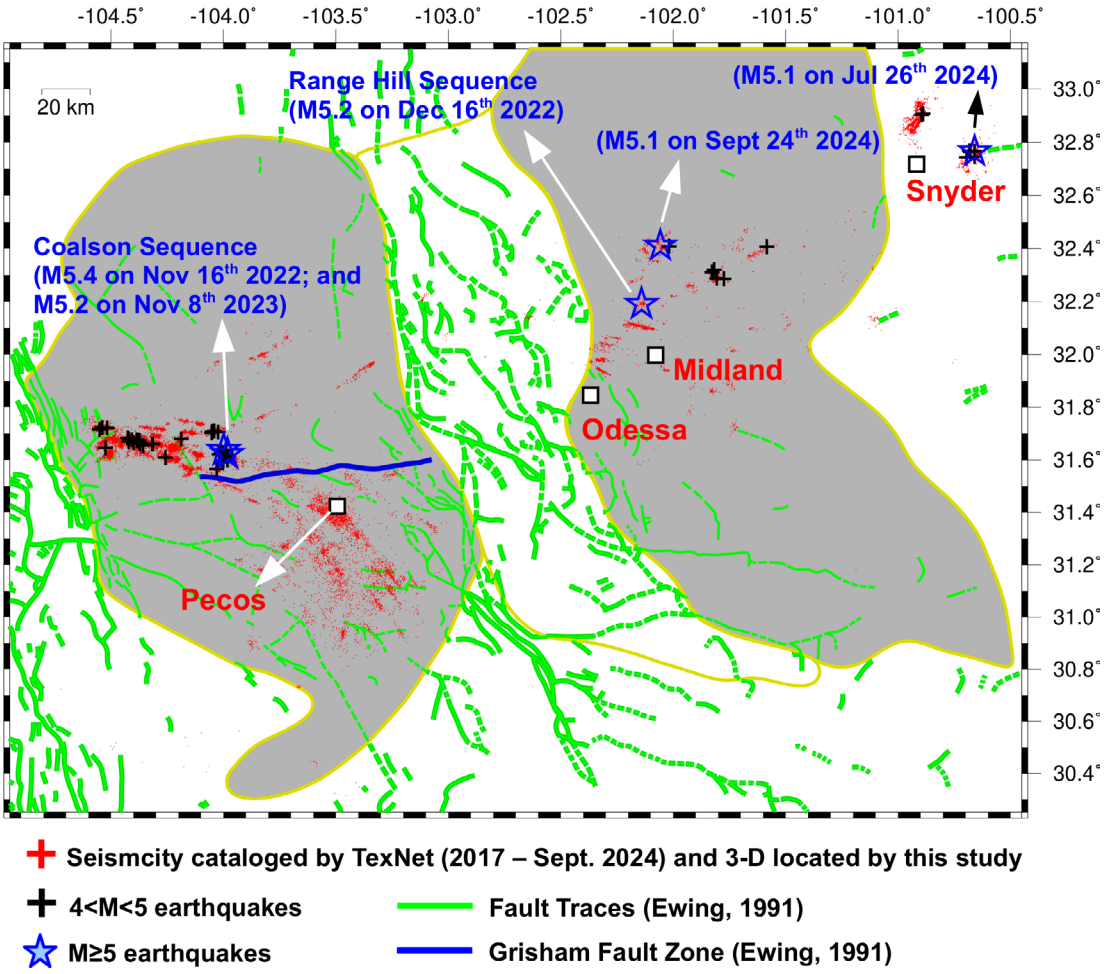

Figure 1. Study area, seismicity distributions, and tectonic history of the greater Permian Basin. TexNet has documented more than 23,600 M⩾1.5 events in our study area from 2017 to September 2024, including five M⩾5 earthquakes (denoted by blue stars). Those M⩾4 earthquakes are concentrated within only a few clusters.

In the Delaware basin, earthquakes form several parallel-trending linear clusters. The extent of hypocentral depths vary greatly across the Grisham fault zone; events located below the basin-basement interface north of the fault zone and more shallowly to the southern Delaware basin (Fig. 2).

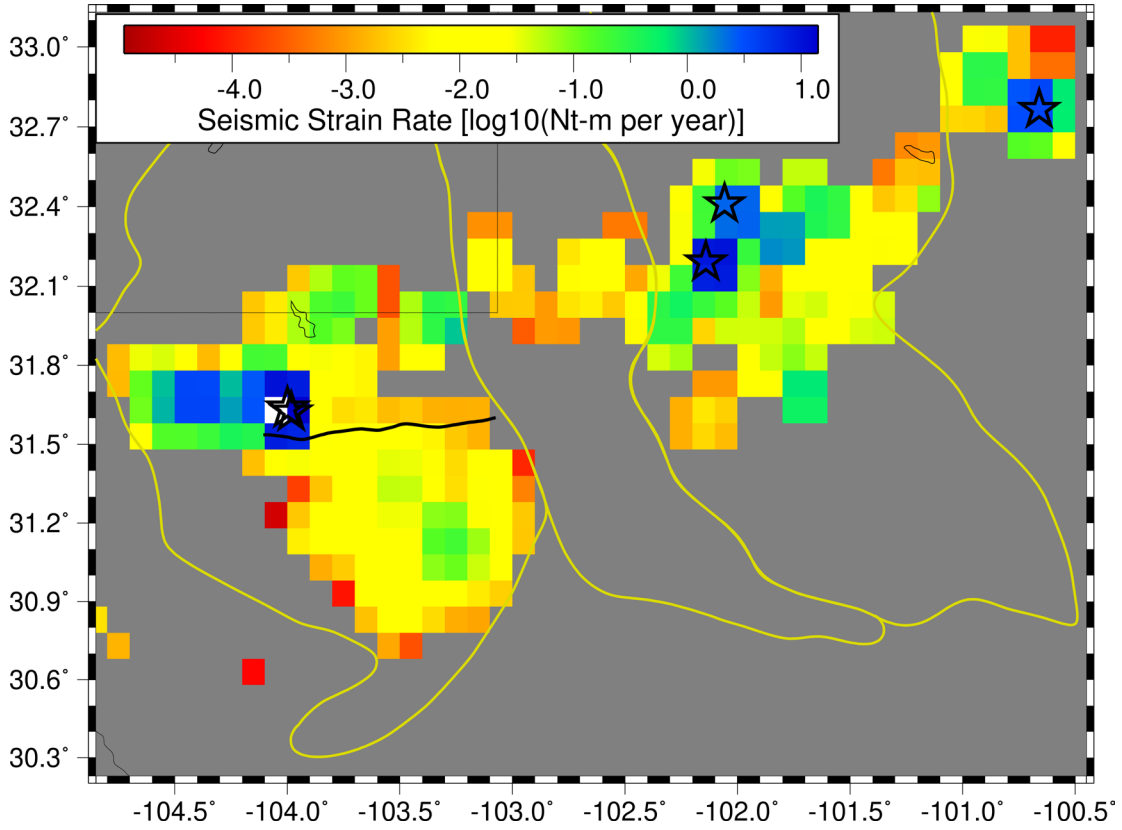

Figure 2. Seismic-strain rate. As expected, the highest seismic strain rate is association with M⩾5 events in two distinct zones.

In contrast, the seismicity distribution presents a different pattern in the Midland basin, where they are geographically concentrated mostly in two subregions: (1) the mid-central part of the Midland basin and (2) the Snyder area, located at the east margin of the basin. Still, most of the seismicity is located in the crystalline basement as well. Most of the seismicity zones contain seismogenic structures commonly presenting linear geometry but with various orientations. In the Snyder area, seismicity concentrated in the top portion of the crystalline basement as well. In addition to analyzing the seismicity distributions, we further grouped focal mechanisms across grid-nodes within the greater Permian basin to perform 2-D stress inversion. We aim to build a stress model. Although the inversion results present the great Permian basin as an extensional tectonic regime, the orientations of stress fields are however diverse across the basin. Both the Delaware and Midland basins are extending in different directions: the Delaware basin is extending in a northeast-southwest direction and accommodated by normal faulting, whereas it is in a northwest-southeast direction and accommodated by a mix of normal and strike-slip faults in the Midland basin. Analysis on the seismic-strain rate has indicated that higher seismic-moment release is concentrated within certain geographic regions where the complex seismogenic structures are revealed by earthquake source mechanisms.

Update on the 3D Permian Basin Faulted Velocity Model

Robin Dommisse, Alexandros Savvaidis, Dino Huang, Yangkang Chen, Ian Duncan, Emmanouil Parastatidis, Jaewook Lee

Accurate velocity models are critical for a variety of subsurface modeling tasks, including depth-conversion of 3D seismic models and earthquake location. The 3D Permian Basin velocity model created in this study uses a unique dataset consisting of more than 20,000 compressional sonic well log curves. The 3D model was validated using 2600 velocity checkshots provided by the Velocity Databank of Houston.

The stratigraphic framework contains more than 50 individual formations, based on more than 2.2 million surface tops for approximately 26,000 wells, modeling the Permian Basin section from surface to basement. The structural framework consists of a fully sealed faulted framework containing more than 2000 faults, including basement-rooted faults and shallower faults. Additional 3D seismic volumes and well logs were shared by operators and vendors and licensed from data providers.

This study focuses on five tasks:

- calculation of p-wave velocity (Vp) from well log sonic (delta T) curves
- creation of a sealed faulted framework using 3D fault surfaces based on published faults
- construction of a stratigraphic framework based on BEG and proprietary operator well top interpretations (Fig. 1)
- determination of distribution of the velocity data along 100-meter-thick sublayers for each of the 50 stratigraphic framework zones (Fig.2)
- validation of the 3D velocity distributions using independent velocity surveys and seismic derived velocity data

The calculation of the velocities from well logs involved sonic-log correction, vintage-based log normalization, and quality assurance. The calculated well log velocities were sampled using the vertical layer structure of the 3D model. Next, we characterized the spatial variance of the velocity data for each of the more than 50 formations. This was done by generating lateral variograms for the velocity in all zones and fault blocks. Multiple equiprobable realizations were investigated to determine scenarios with maximum predictability of velocity data away from the well and seismic velocity control.

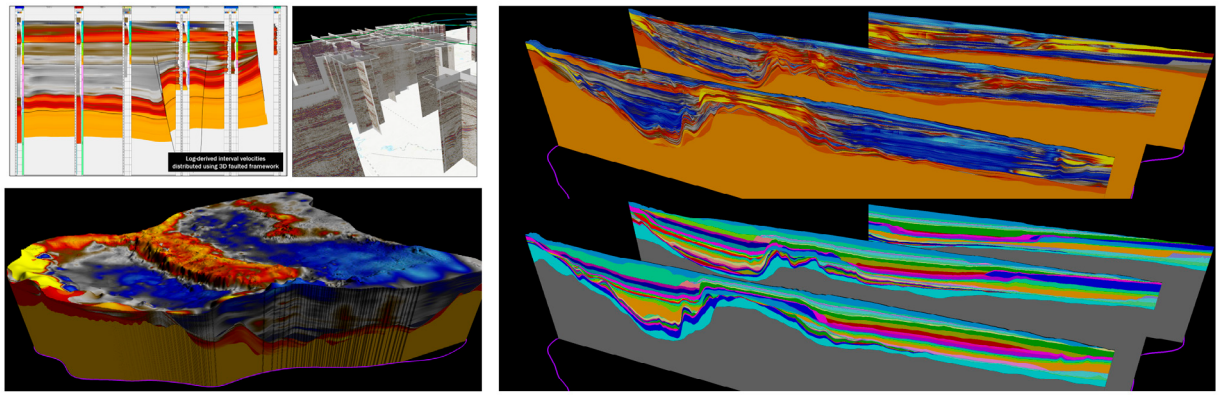

Figure 1. A 2D faulted cross section, 3D model, and fence diagrams showing velocity distributions along the zones of the 3D Permian Basin model. The 3D seismic surveys used in the study are shown in the above right figure.

We used the Eliis Paleoscan software to interpret horizons in 38 available 3D seismic volumes and more than 2000 2D seismic lines which were shared by operators and vendors and licensed from data providers. Depth-depth correction shift values were applied to horizon interpretations for the PSDM velocity volumes. We generated synthetic seismograms for each of the 3D seismic volumes and used well-seismic tie workflows to calculate interval velocities used for additional model validation.

The 3D faults were extracted from the 3D seismic surveys using Deep Learning workflows from the Geophysical Insights Paradise software. We interpreted a fault-fault connection network using the Schlumberger Petrel software, which was used to build a sealed faulted framework. The stratigraphic horizons were faulted using the fault-network definition and subsequently corrected and adjusted for all horizon-fault interfaces using available well log and seismic interpretations.

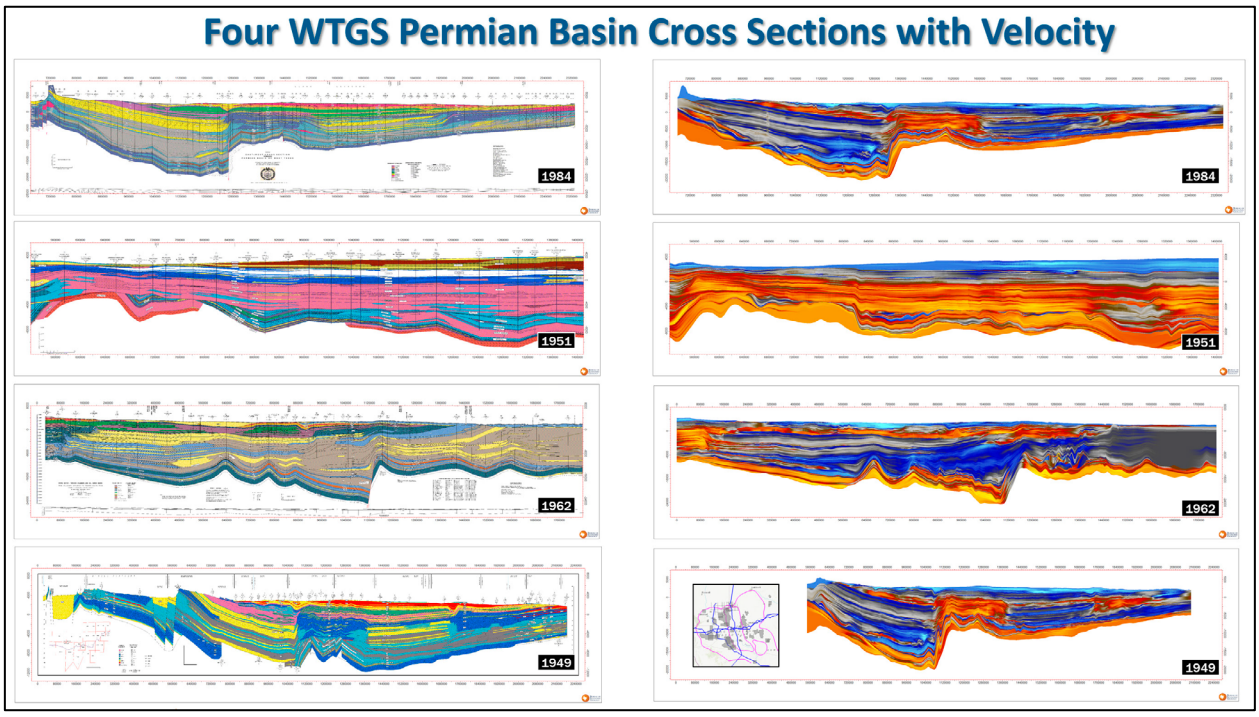

Figure 2. Four historical West Texas Geological Society cross sections (left) compared to p-wave velocities extracted from the 3D Permian Basin Velocity Model.

The result is a unique Permian Basin wide 3D velocity model, consisting of more than 800 million cells, that can be used to more precisely depth-convert 3D seismic volumes and locate 3D earthquake hypocenters.

Basin-scale Prediction of S-wave Sonic Logs Using Machine Learning Techniques from Conventional Logs

J. Lee, Y. Chen, R. Dommisse, G. Huang, and A. Savvaidis

From *Geophysical Prospecting*, 2024, v. 72, no. 7, p. 2557–2579

S-wave velocity plays a crucial role in various applications but often remains unavailable in vintage wells. To address this practical challenge, we propose a machine learning framework utilizing an enhanced bidirectional long short-term memory algorithm for estimating S-wave sonic logs from conventional logs, including P-wave sonic, gamma ray, total porosity, and bulk density. These input logs are selected based on traditional rock physics models, integrating geological and geophysical relations existing in the data.

Our study, encompassing 34 wells across diverse formations in the Delaware Basin, Texas, demonstrates the superiority of machine learning models over traditional methods like Greenberg–Castagna equations, without prior geological and geophysical information (Figure 1). Among these machine learning models, the enhanced bidirectional long short-term memory model with self-attention yields the highest performance, achieving an *R*-squared value of 0.81 (Figure 2). Blind tests on five wells without prior geologic information validate the reliability of our approach (Figure 3). The estimated S-wave velocity values enable the creation of a basin-scale S-wave velocity model through interpolation and extrapolation of these prediction models.

Additionally, the bidirectional long short-term memory model excels not only in predicting S-wave velocity but also in estimating S-wave reflectivity for seismic amplitude variation with offset applications in exploration seismology. In conclusion, these S-wave velocity estimates facilitate the prediction of further elastic properties, aiding in the comprehension of petrophysical and geomechanical property variations within the basin and enhancing earthquake hypocentral depth estimation.

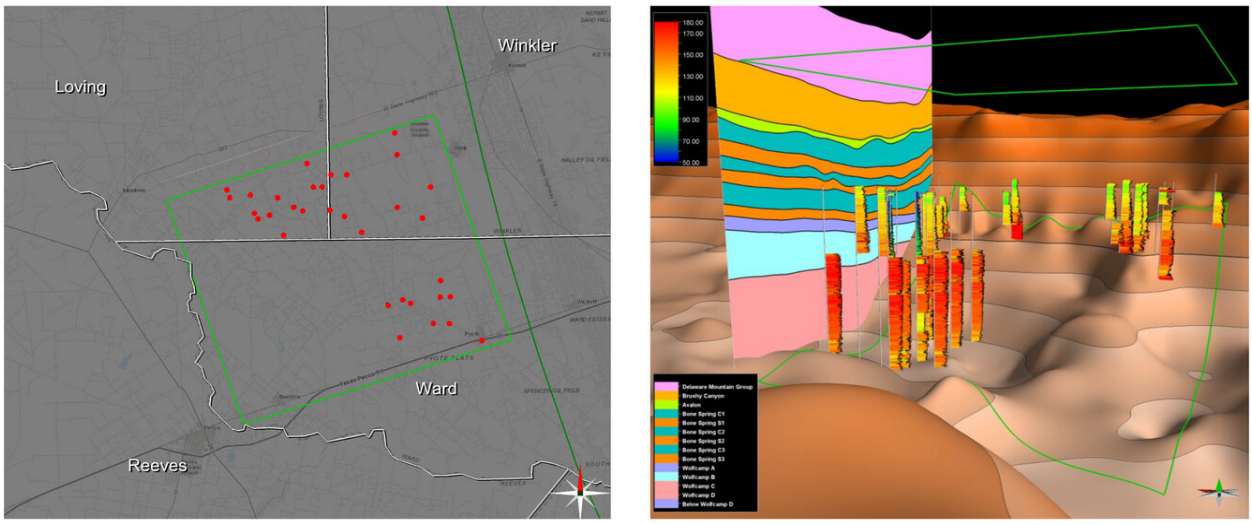

Figure 1. (a) A map of the Delaware Basin study area (indicated by the green box) with 34 well locations shown as red dots. (b) A screenshot of the measurements in the log datasets, including formation interpretations.

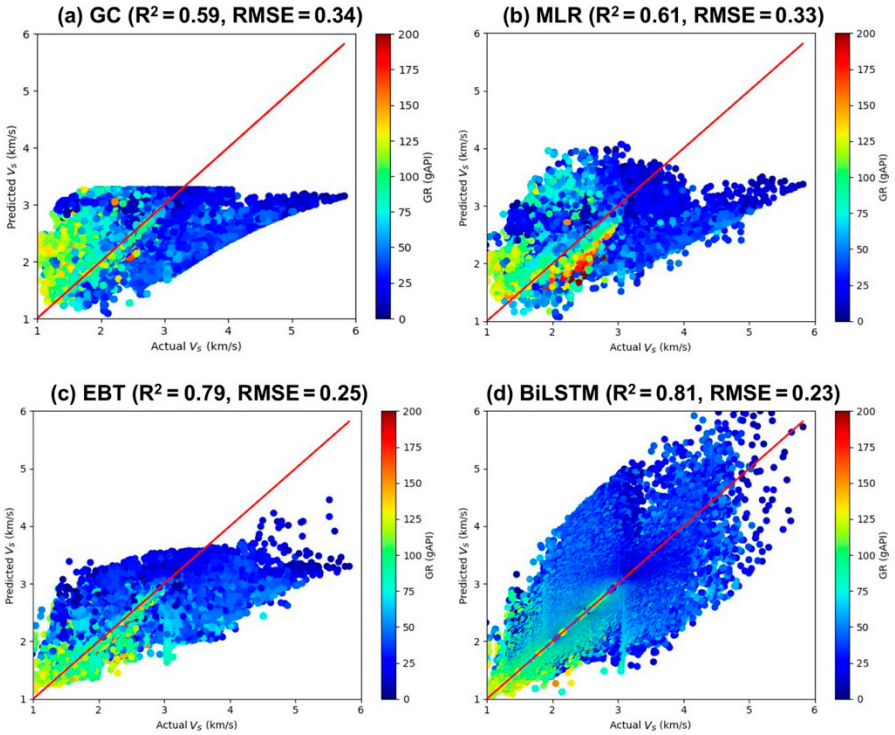

Figure 2. Comparison of predicted versus actual plots for four distinct prediction models: (a) the optimized Greenberg–Castagna (GC) model for with an value of 0.59; (b) the multiple linear regression (MLR) model for with an value of 0.61; (c) the ensembles of bagged trees (EBT) model for with an value of 0.79; and (d) the self-attention bidirectional long short-term memory (BiLSTM) model for with an value of 0.81. GR, gamma ray; RMSE, root mean square error.

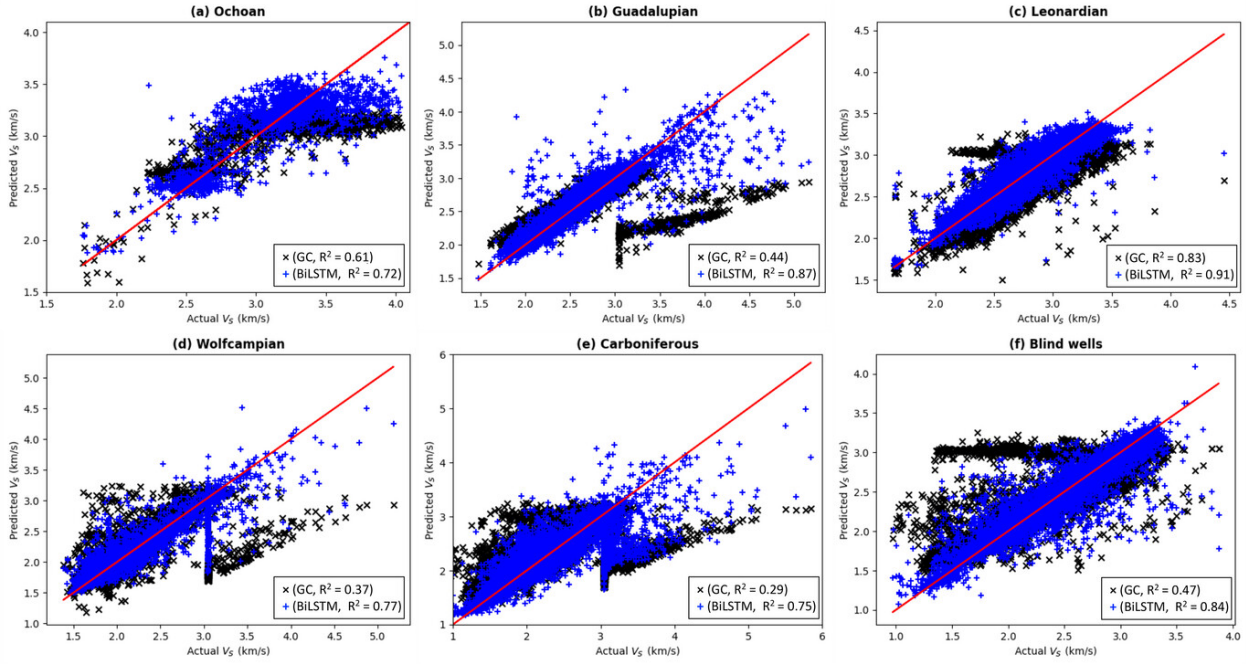

Figure 3. Comparison of predicted versus actual plots for two S-wave velocity () prediction models, the Greenberg-Castagna (GC) model (black ‘x') and bidirectional long short-term memory (BiLSTM) model (blue ‘+'), on (a–e) geologic-age-categorized subgroups and (f) blind wells.

Constructing a Comprehensive 3D S-wave Velocity Model of the Delaware Basin

J. Lee, R. Dommisse, A. Savvaidis

Presented at the 4th International Meeting for Applied Geosciences and Energy (SEG-AAPG), 2024.

State-of-the-art 3D velocity modeling is integral across a spectrum of applications, including stratigraphy, basin-to-regional scale mapping, reservoir characterization, carbon capture and storage, and earthquake relocation. S-wave velocity is a key parameter, offering insights into lithology and rock stiffness due to its diminished susceptibility to pore fluid influence. This study aims to construct a robust and comprehensive 3D S-wave velocity model to unveil the spatial variability of S-wave velocity within the Delaware Basin. Employing an integrated approach, we utilize shear sonic logs from 204 wells spanning the Delaware Basin, extending across West Texas and Southern New Mexico (Figure 1). Additionally, we incorporate data from 16 formation horizons, ranging from surface elevation to subsurface layers, encompassing the Rustler, Lamar, Bell Canyon, Cherry Canyon, Brushy Canyon, Bone Spring, Wolfcamp, Cisco, Strawn, Barnett, Woodford, Fussellman, Montoya, Simpson, and Ellenburger formations. These horizons had been delineated through a comprehensive analysis of stratigraphic records and post-stack seismic data. Initially, we extrapolated the interpreted formation horizons to cover the basin boundary. However, acknowledging the incomplete coverage, we employ a surface resampling method to edit and extrapolate these surfaces. This approach utilizes convergent gridder methods to retain general trends in data-sparse areas while preserving detail where data density allows. Truncations between horizons are delineated to illustrate pinch-out regions, showing a more holistic representation. Hence, we create a 3D grid incorporating the extrapolated horizons and basin boundary. We also scale up the shear velocity logs using the harmonic average method to match grid cell dimensions, assuming that the basin is composed of layered media. Then, we apply seven interpolation methods to a 3D grid derived from the upscaled logs and assess the performance of the seven interpolation methods using eight blind wells in the University Lands (Figure 2). The “Moving Average” method is identified as the best algorithm, as it yielded the lowest mean absolute error (MAE). The developed 3D S-wave velocity model not only enhances our comprehension of petrophysical and geomechanical property variations across the basin but also aids in successful seismic inversion, thereby improving earthquake hypo-central depth estimation and facilitating the derivation of elastic and petrophysical property models from seismic data.

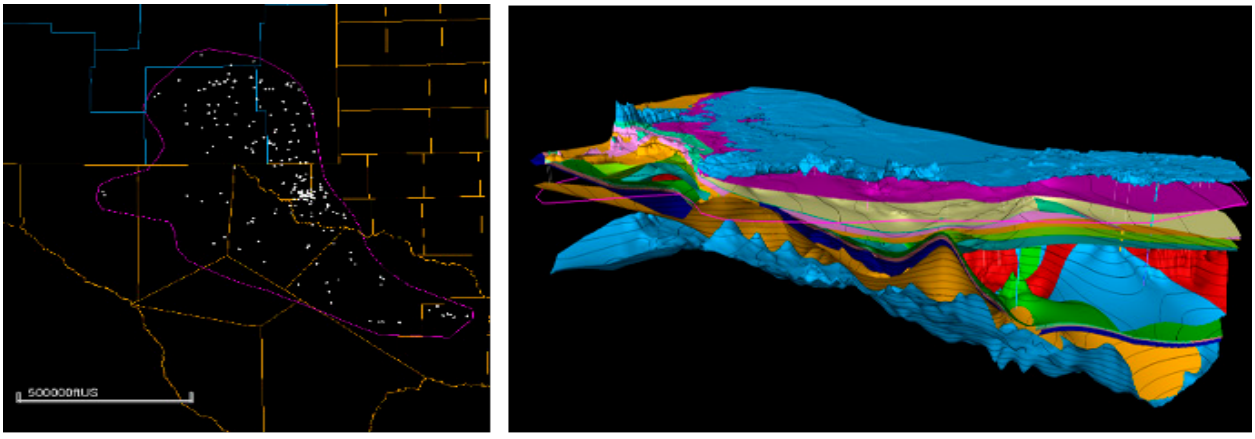

(a) (b)

Figure 1. (a) Geographical extent of the study area in West Texas and Southern New Mexico with well locations, and (b) 17 imported geological horizons in this study. Note that these horizons are interpreted from the well tops and post-stack seismic data and extrapolated within the basin boundary.

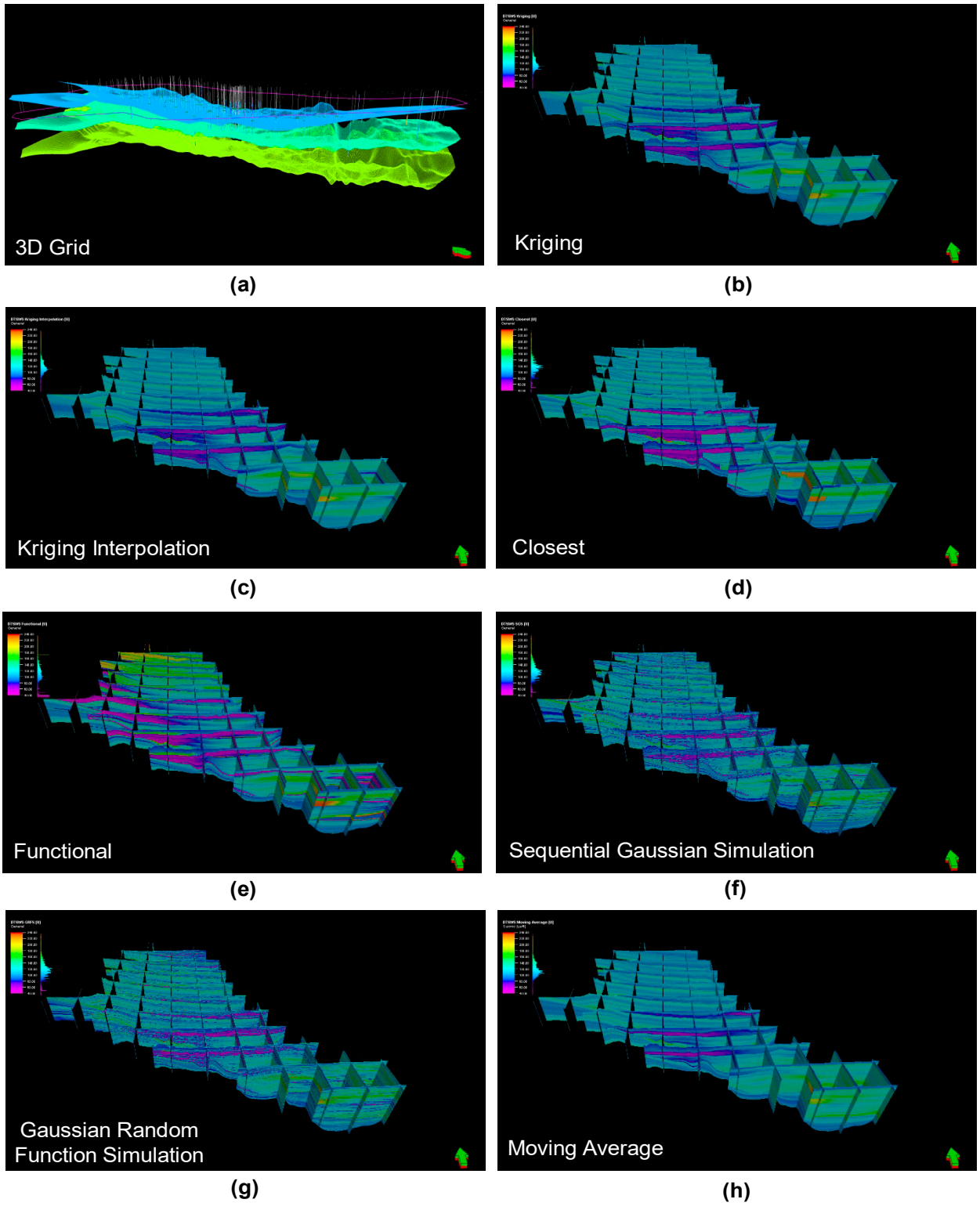

Figure 2. (a) 3D grid generated from the imported horizons and (b–h) Comparison of seven different geostatistical interpolation methods for S-wave velocity distribution in the Delaware Basin: (b) Kriging, (c) Kriging Interpolation, (d) Closest, (e) Functional, (f) Sequential Gaussian Simulation, (g) Gaussian Random Function Simulation, and (h) Moving Average. Note that the "Moving Average" method is identified as the best algorithm, as it yielded the lowest mean absolute error (MAE).

Updates and future work on Midland basin Vs model

Emmanouil Parastatidis, Robin Dommisse, and Alexandros Savvaidis,
The University of Texas at Austin

Work in progress

An accurate velocity model is necessary when it comes to earthquake location. In past years there was a significant progress on creating an accurate and updated velocity model for both P- & S- waves (Vp & Vs) for the Delaware basin (J. Lee et al., 2024; https://doi.org/10.1111/1365-2478.13527). Now we are focusing to create an update velocity model for the Midland basin (Figure 1). The scope of this work is to provide an accurate velocity model for the S-waves for the Midland basin using the available data. There are three main sources of data used for this project (Table 1).

Source	Number of Wells
Velocity Databank Check shots (VDB Check shots) Vp	678
TexNet multi-sourced QC'd sonic logs* Vp & Vs	5021 + 117
Exxon sonic logs ML predicted Vp & Vs (Webb et al., 2024; IMAGE, Houston, USA)	698

Table 1 Summary of the available data we have in the Area of Interest (Figure 1).

During our study for building the Vs model we have come across four main limitations. At first, even though there are plenty of sonic log and check shot data to create a reliable model for Vp, it becomes challenging for producing the Vs model. To avoid such a challenge, we proposed an indirect way to calculate the Vs for the Midland basin. Instead of calculating the Vs directly from the sonic logs and then extrapolate them through the layers, we use the Vp/Vs ratio resulted from the Exxon Mobile sonic logs. Then we extrapolate the Vp/Vs to the entire volume of the focused area. Finally, we use the two Vp models created, one based on check shot data and one on sonic log data and calculate the Vs based on the ratio data (Figure 2a) resulting in two versions for Vs model (Figure 2b & c).

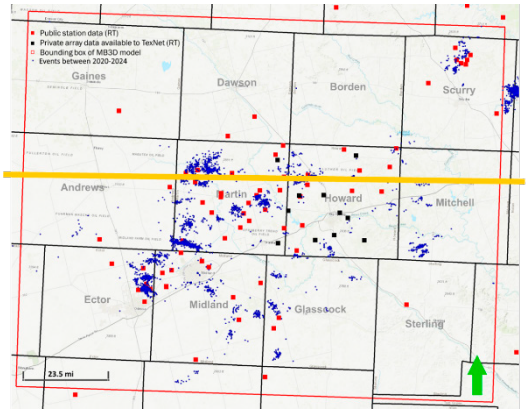

Figure 1 The area of interest for which we have built the Vp and Vs models. The yellow line in the middle is the cross section of the velocity models presented below (Figure 2).

The next limitations have to do with the amount of available sonic log data for the shallow formations (Rustler formation) where, the data limitation creates inconsistent and inverted velocities for that layer. The solution we have proposed was to replace that layer in the model with the data from the check shot data which are denser compared to the sonic log data, for these shallow layers and create a smoother model.

Another topic that we have come across, is the high velocity contrast between bottom layers (Simpson-Ellenburger) and basement. Based on the data we have, which are limited for both check shots and sonic logs, the Simpson formation have inverted velocities (lower velocities than the formations above and below) which is more intense on the sonic log data. This contrast in the velocities is creating extra complexity on calculating the theoretical travel paths and will need to be studied further.

Finally, the velocity model we have built extends up to 40000ft depth in order to be able to calculate theoretical travel paths for the earthquake locations. However, our data from checkshots and sonic logs are penetrating up to the depth of the Ellenburger formation just above the basement at approximately 10000ft depth. To overcome this data shortage, we have proposed two solutions. In the first one, we use data as calculated from Huang et al. (2019); https://doi.org/10.1029/2019JB018351, tomography study.

While in the second approach we use a constant Vp (21000 ft/s) and Vs (12068 ft/s) as calculated from 9 sonic logs that penetrates through the surface of the basement.

Overall, the Check shots model is more appropriate to use on earthquake relocation due to being a smoother velocity model compared to the sonic log derived one and as a result is better on calculating travel paths and also because the waveform frequencies from check shots are closer to earthquake data.

Our next steps on improving the Vp and Vs models will involve filling the gaps of data we currently have with either more data coming from the industry or by using advanced Machine Learning methods in continuation of J. Lee et al., (2024) to predict the Vs from the Vp sonic logs combining the data from other attributes from the well logs, such as gamma rays, density and porosity. Another proposed method to improve the current models is to apply smoothening techniques on the sonic log-based model and calibrate the sonic log data with the check shot data for the common wells. For the data shortage about the basement, we are going to use modeling methods to optimize the velocities. Once we finalize our results, we will apply our methods to extend the model for the rest of the Permian Basin.

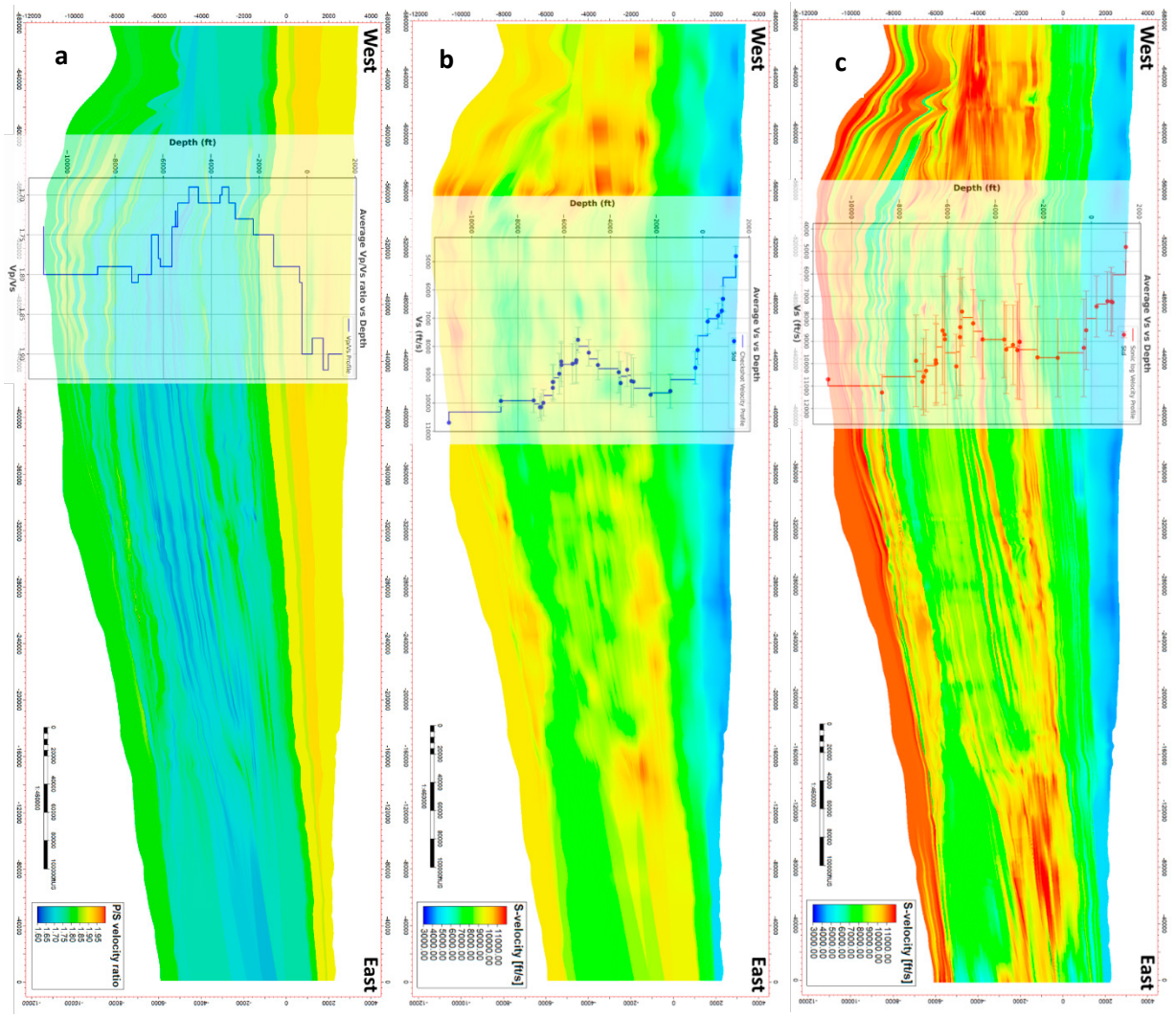

Figure 2. a. Cross section of the Vp/Vs ratio based on Exxon data and vertical average Vp/Vs ratio with depth. b. Cross section of the Vs as derived from Vp Check shots using Vp/Vs ratio and vertical average Vs with standard deviation, versus depth. **c.** Cross section of the Vs derived from Vp Sonic logs using Vp/Vs ratio and vertical average Vs with standard deviation, versus depth, sonic log data have a higher standard deviation per formation compared to the check shot data.

Reference model of crustal thickness and Vp/Vs of western Canada

Quan Zhang, University of Ottawa, Yunfeng Chen, Zhejang University, Hersh Gilbert, University of Calgary, Derek L. Schutt, Colorado State University, Yu Jeffrey Gu, University of Alberta, Gabriela Fernández-Viejo, University of Oviedo, Claire Currie, University of Alberta, Pascal Audet, University of Ottawa, and Yangkang Chen, The University of Texas at Austin

Published in Journal of Geophysical Research: SolidEarth, 129, e2024JB029387

The Canadian Cordillera marks a transition region from the current plate boundary through the Phanerozoic Cordilleran orogen to the Precambrian cratons. During the past 2 decades, knowledge of the subsurface structure of western Canada has been greatly advanced through seismological investigations pioneered by the Lithoprobe project and, more recently, by regional passive seismic arrays. In this study, we constructed a new model (WCANM22) of crustal thickness and P- to S-wave velocity ratio (Vp/Vs) by compiling receiver function data from 473 stations and existing constraints from over 2,600-km-long active source experiments. Our model covers a broad swath (~¼) of the land area of North America (105—140°W, 48—72°N) and shows an overall flat Moho beneath the Cordillera, with an average depth of about 36 km and a standard deviation of 3 km across orogenic belts. This study provides a comprehensive catalog of Vp/Vs in western Canada and reveals a moderate correlation between Poisson's ratio and the age of crustal domains. Average Vp/Vs values are 1.72, 1.79, and 1.82 for the Phanerozoic Cordillera, Proterozoic Cratons, and Archean-aged Medicine Hat Block, respectively, suggesting continued modifications to crustal composition through episodic tectonothermal events. This distinct trend in western Canada sheds new light on the debated role of secular changes in the composition of continental crust.

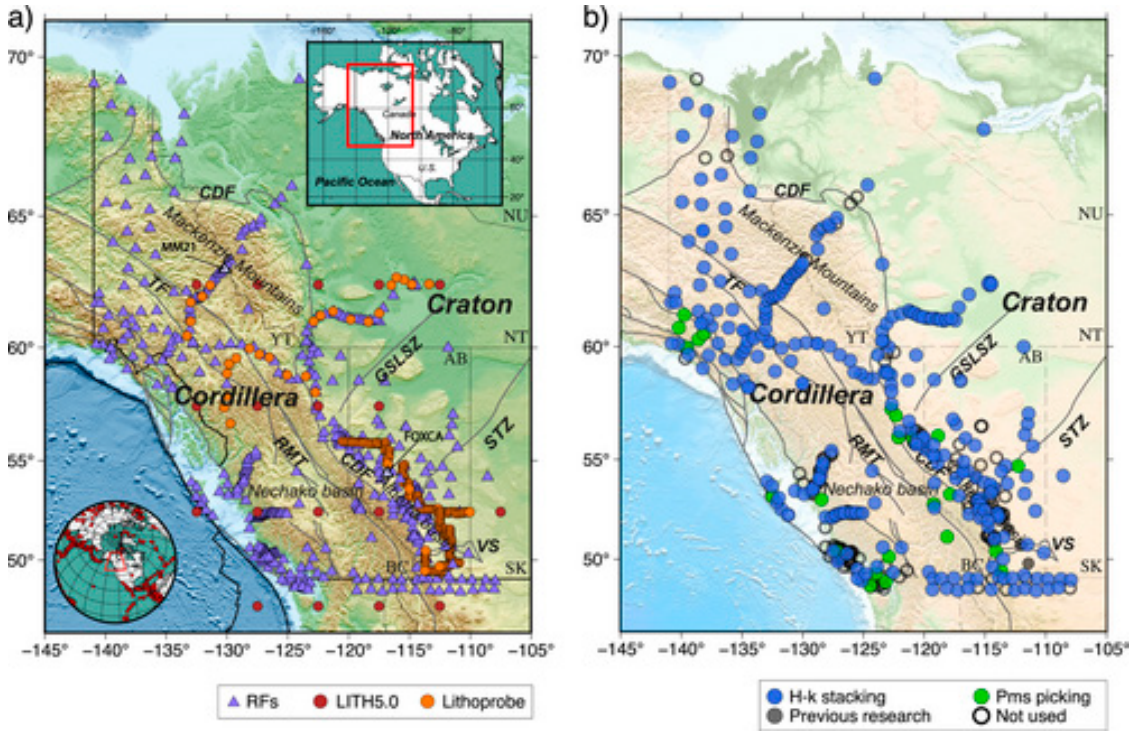

Figure 1. Distribution of seismograph stations in western Canada superimposed on topographic relief map. (a) Triangles = broadband stations (or station groups) used in receiver-function analysis. Circles = sampling points from earlier studies using various seismic imaging methods. Black lines = major faults and geological boundaries (abbreviations same as in Figure 1). Inset: red circles = locations of earthquakes analyzed in this study. (b) Seismograph stations color-coded by crustal parameter estimation, including *H-k* stacking (high quality, blue), *Pms* phase picking (medium quality, green), and directly using reliable measurements from previous studies (gray). Open circles = stations with relatively low data quality ignored in analysis. BC = British Columbia, AB = Alberta, SK = Saskatchewan, YT = Yukon Territory, NT = Northwest Territories, NU = Nunavut.

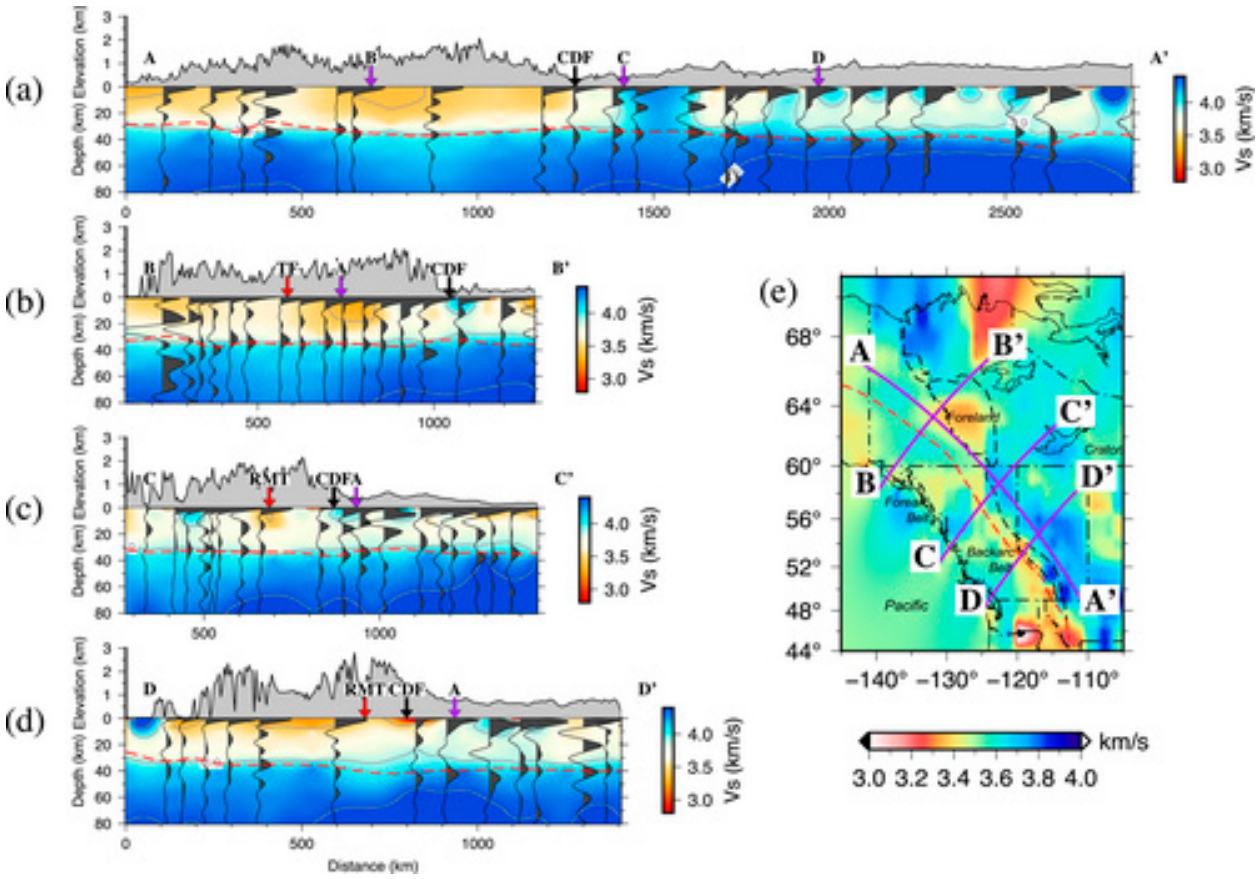

Figure 2. Moho variations (a) along and (b–d) perpendicular to strike of Cordillera. Receiver functions are migrated to depth using shear velocities from CRUST1.0 model. Red dashed line = Moho depth extracted using *H-k* analysis with Kriging interpolation. Background colors = shear velocities from ambient noise tomography. Purple arrows = intersections of profiles. Red and black arrows = locations of Tintina Fault/Rocky Mountain Trench and Cordilleran deformation front (CDF) on profile, respectively. Gray shades = surface elevation obtained from ETOPO1 model. Misalignment of Moho depth with peak location of Moho converted phases (*Pms*) on RFs mainly reflects different V_p/V_s values between CRUST 1.0 used in depth migration and those determined from *H-k* analysis. (e) Shear velocities at 10 km depth . Purple lines = profile locations. Red dashed line = Tintina Fault/Rocky Mountain Trench; black line = CDF.

High-resolution, mantle-transition-zone imaging using multidimensional reconstruction of SS precursors

Yapo Abolé Serge Innocent Oboué*, *Zhejiang University*, *Yunfeng Chen*, *Zhejiang University*, *Ramin M. H. Dokht Geological Survey of Canada*, *Yu Jeffrey Gu*, *Univeristy of Alberta*, *Maria Koroni*, *ETHZürich*, *Jingchuan Wang*, *University of Maryland*, *Xiuxuan Jiang*, *Zhejiang University*, *and Yangkang Chen*, *The University of Texas at Austin

Published in Journal of Geophysical Research: SolidEarth, 129, e2023JB027012.

SS precursors have been extensively utilized in mapping the mantle transition zone (MTZ). However, their applications are often challenged by weak phases that arise from small impedance contrasts of mantle discontinuities, noise contamination, and localized thermal/compositional heterogeneities. We developed a new data-processing workflow for more dependable MTZ imaging by adopting a recently proposed, robust damped rank-reduction (RDRR) method from exploration seismology. This method exploits signal coherency in four-dimensional data and allows simultaneous attenuation of noise and interpolation of missing traces. We utilized synthetic data sets generated using realistic Earth structures and MTZ topography to evaluate the capability of the proposed workflow. Our test results show that the RDRR method can capture topographic variation of mantle discontinuities well, improving the SNR of SS precursor data by an order of magnitude. Application to SS precursors from the western Pacific can successfully remove contaminating noises, mitigate imaging artifacts of small-scale anomalies, and improve lateral coherency of the MTZ structure, revealing a clear first-order structural transition. Compared with earlier global and regional models, our model reveals more structural details, including a localized, thin MTZ near the Changbai Volcano in east Asia. This observation, in conjunction with the reported low-velocity structure in the MTZ in earlier tomographic studies, may support the presence of deep mantle upwelling through a slab gap. In summary, our work enables resolution of MTZ structures with high fidelity and highlights the importance of advanced array methods in improving SS precursor imaging.

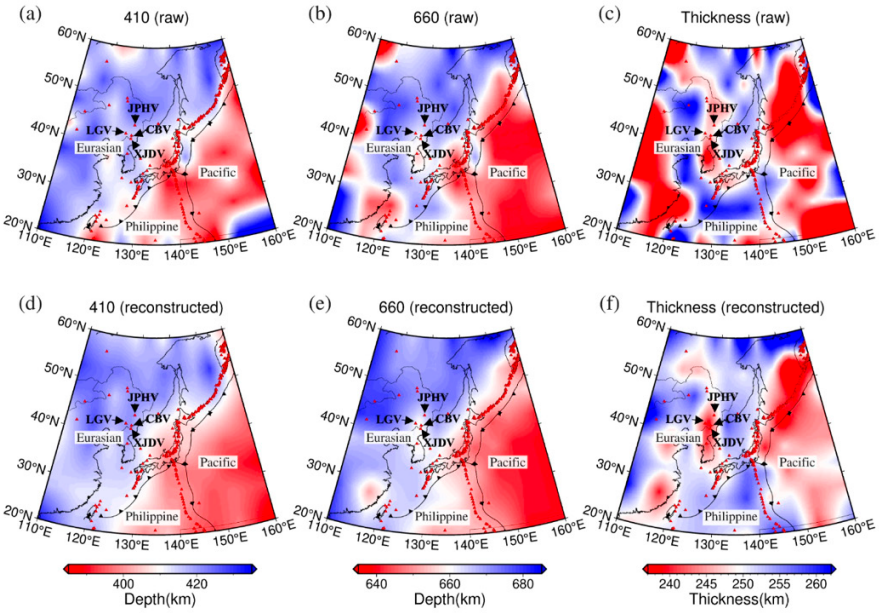

Figure 1. SS precursor imaging results. (a)—(c) Apparent depths of 410 and 660 MTZ discontinuities and MTZ thickness determined from poststack raw data. (d)—(f) Same as a—c, but for poststack reconstructed data. LGV = Longgang Volcano, JPHV = Jingpohu Volcano, CBV = Changbai Volcano, XJDV = Xianjingdao Volcano.

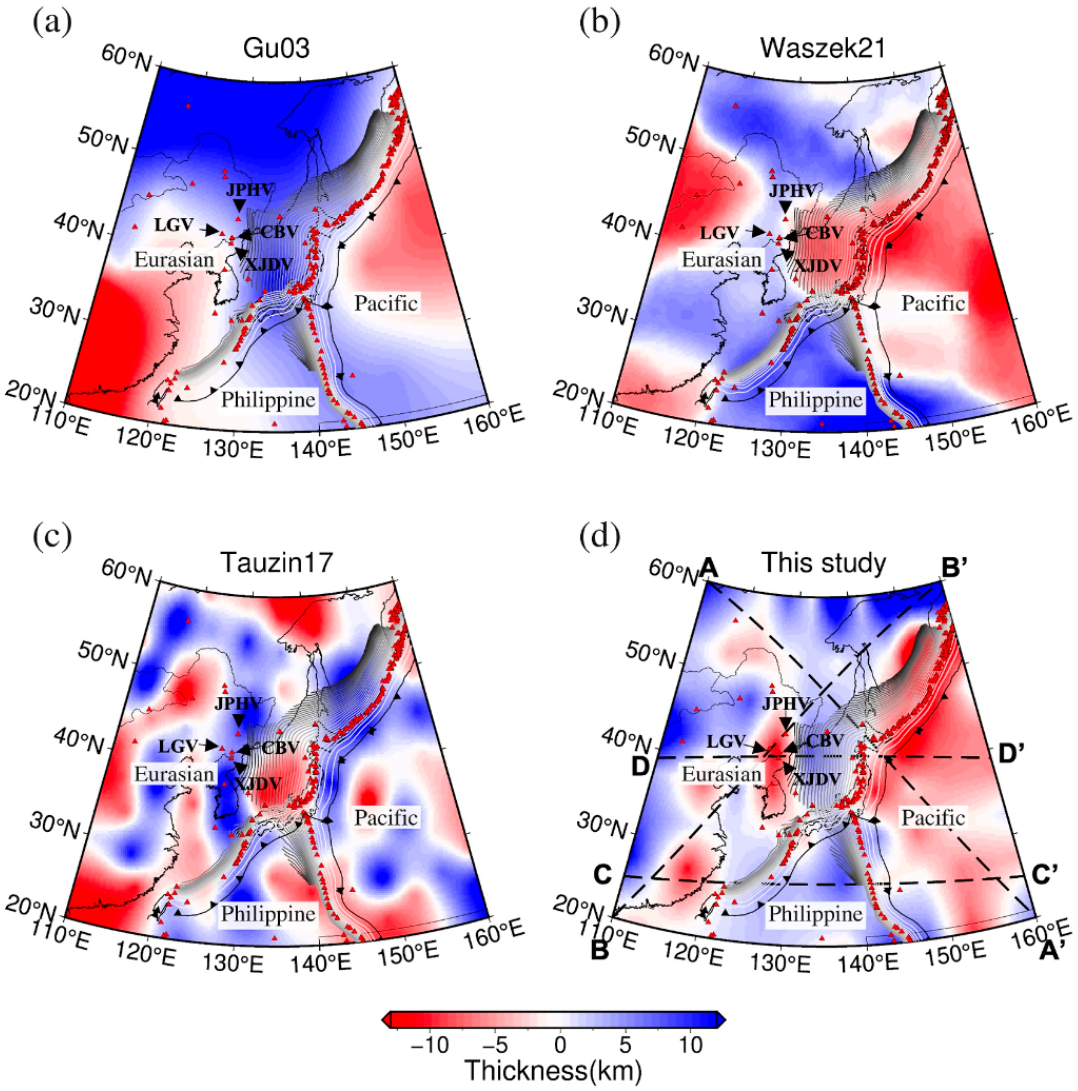

Figure 2. Comparison of MTZ thickness obtained from three earlier models.

Probing frictional properties of Delaware Basin formations: Insights from laboratory experiments

M. Beatrice Magnani, Giuseppe Volpe**, Michele Mauro**, Marco Scuderi**, Cristiano Collettini***
** Roy Huffington Department of Earth Sciences, Southern Methodist University, Dallas, TX*
*** Dipartimento di Scienze della Terra, Università di Roma, La Sapienza, Roma, Italy*

Since 2016, the Delaware Basin in West Texas/SE New Mexico has experienced a marked increase in seismic activity, primarily related to subsurface injection of wastewater into shallow and deep formations, as well as oil and gas production via hydrofracture. However, details of how these industry practices connect with seismicity have recently become well understood. To investigate these connections, we tested the frictional properties of rocks belonging to stratigraphic succession of the Delaware Basin (Texas) from the crystalline basement to formations of the Delaware Mountain Group (DMG). We tested the following 11 lithologies: intact and weathered granite from the crystalline basement, dolostones and limestones from the Ellenburger Formation, dolostones from the Atoka Formation, shales from the Wolfcamp Formation, shales and limestones from the Bone Spring Formation, siltstones from the Cherry Canyon Formation, and siltstones and sandstones from the Bell Canyon Formation. To perform frictional experiments, we crushed, powdered, and sieved rock samples below 125 μm to produce an analog fault gouge. Before testing the gouges, we characterized their mineralogical composition using X-ray powder diffraction analysis (XRpD). We next estimated content and number of mineral phases occurring in the tested materials by calculating peak areas and using mineral intensity factors as calibration constants. XRpD analysis of the gouge provided mineral assemblages characterized by a mixture of tectosilicates (quartz and feldspars), phyllosilicates (micas and clays), and carbonates (calcite and dolomite) in different percentages.

We performed frictional experiments to characterize frictional properties of the sampled material—steady-state friction, healing rate, and velocity dependence of friction—by collecting two experimental datasets under the same boundary conditions. In the first dataset, we assessed velocity dependence of friction, whereas in the second, we focused on characterization of healing properties.

The first experimental dataset was collected using the BRAVA2 biaxial apparatus at the Rock Mechanics and Earthquake Physics Laboratory, Sapienza University of Rome, and the second dataset was collected using the BRAVA biaxial apparatus hosted at the High Pressure—High Temperature Laboratory at the Istituto Nazionale di Geofisica e Vulcanologia of Rome. Both experimental apparatuses are equipped with two perpendicular, servo-controlled hydraulic pistons—the horizontal piston applying a normal load to the sample, and the vertical piston applying shear force in a double-direct shear (DDS) configuration (Figure 1). Both pistons are fitted with strain-gauge load cells with an accuracy of 0.03 MPa. Displacement of the pistons were measured using linear variable differential transducers (LVDTs) with a resolution of <0.01 μm. All displacement measurements were corrected for elastic deformation of the experimental assembly.

We deformed sampled materials using a DDS configuration, consisting of two identical layers of simulated gouge (5 mm thick) placed between three steel forcing blocks—two stationary side blocks and one central sliding block. The stationary side blocks apply normal stress, whereas the central sliding block applies shear deformation. All forcing blocks were equipped with grooves to ensure the deformation was accommodated within the gouge layer and not at the block-gouge interface.

All experiments followed a standardized procedure to ensure reproducibility and comparison among different experiments, which were performed under water-saturated conditions by submerging the experimental assembly in $CaCO_3$-rich water. To ensure full saturation of the sample, it was left under a low normal stress of 5 MPa while compacting until a steady-state thinning rate was attained. After sample saturation, normal stress was increased gradually to target normal stress and left compacting to a constant layer thickness. In each experiment, the experimental fault was deformed at three different normal stresses (20, 40, and 60 MPa) according to the following experimental procedures.

The measured steady-state shear stress of the tested materials shows a linear dependence, with applied normal stress pointing to a brittle, frictional behavior. The slope of the linear relation, represented by friction coefficient μ, ranges between μ = 0.33 and μ = 0.66, revealing a strong relation to the mineralogical composition of the tested rocks. The altered granite sample, despite having only 23% phyllosilicates, shows the lowest friction coefficient (μ = 0.33), which can be related to the presence of illite and kaolinite in the phyllosilicates fraction—among the most frictionally weak minerals. Noticeable weakening of the friction coefficient as a function of the phyllosilicate content is not linear but, rather, shows (1) marked decrease followed by (2) more gradual weakening in larger numbers of phyllosilicates.

During slide-hold-slide tests, we assessed healing properties of the tested rocks (Figure 1). Generally, frictional restrengthening upon reshear (Λμ) increases log-linearly with imposed hold time, except for phyllosilicate-rich rocks in which frictional restrengthening deviates from linearity, attaining a constant value of a hold time longer than 300 seconds. Similar to that of the friction coefficient, the healing rate of our materials decreases with increasing amounts of phyllosilicates following a nonlinear path.

Through inversion of velocity step curves, we retrieved rate and state frictional parameters—direct effect *a*, evolution effect *b*, and critical slip distance D_c (Figure 1). We can report a velocity dependence of friction described by the *a-b* parameter. We generally observe positive values of *a-b*, indicating velocity-strengthening behavior for most of the samples, with negative *a-b* values, indicative of velocity-weakening behavior and, therefore, of a potential seismogenic behavior, observed in the Atoka Dolostone, the Bone Spring Limestone, and in the intact granite. In general, we observe that the median values of *a-b* parameters increase as a function of phyllosilicate content.

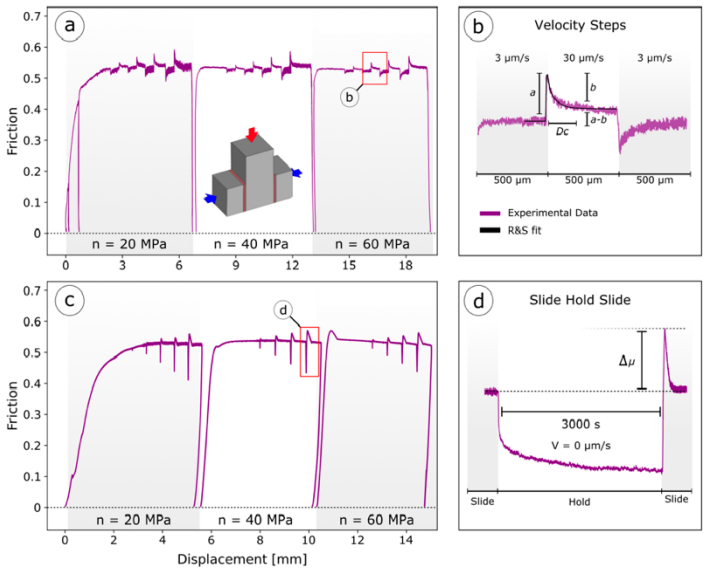

Figure 1. Description of experimental methods and procedures used in frictional experiments. (a), (b) Procedures used in first dataset, in which velocity steps were performed. Note that during run-in at 20 MPa, first 1 mm of shear displacement is characterized by two cycles of unload-reload used to enhance strain localization. (c), (d) Procedures used in second dataset, in which slide-hold-slide was performed.

Resolving depth: High-resolution earthquake location and allied studies in Texas

Heather R. DeShon, Asiye Aziz Zanjani, Vamshi Keranam, Julia Rosenblit, Yeshey Sheldon, Zhong Lu (Southern Methodist University), and Alexandros Savvaidis (BEG-UT)

Improving depth uncertainties in earthquake catalogs for induced seismic settings requires enhanced network density and geometry, combined with advanced methodologies, such as multi-event relocation techniques, complementary datasets such as differential traveltimes, statistical data-weighting methods, and machine-learning approaches to improve catalog completeness. These integrated strategies are essential to an understanding of spatial and temporal evolution of aseismic slip. We showcase two studies: application of the Hypocentroidal Decomposition (HD) method to TexNet and TXAR earthquake catalogs in the southern Delaware Basin (SDB) and the use of converted phases to constrain depth in the Midland Basin (MB). In the SDB, we relocated more than 5,000 earthquakes, triggered south of the Grisham Fault Zone, using an approach that combines multi-event, multi-phase approaches with a robust statistical index for data calibration and weighting (Aziz Zanjani et al., 2024a,b). Additionally, we compared the distribution of aseismic slip over time and space to operational fields and surface deformation derived via InSAR. SDB results indicate predominant reactivation of shallow faults within the Delaware Mountain Group and Bone Spring Formation as shallow injection units with no deep injection in this region. We demonstrated correlations among injection maxima, segmented subsidence patterns, and active seismic lineaments, while noting an absence of seismicity within diffuse, radially symmetric, production-related subsidence hotspots (Figures 1, 2). For the Midland Basin, synthetic seismograms and real data indicate two main conversion-generating interfaces: the top of the Silurian-Devonian and the top of the San Andres/Queen Formations. In real data, conversions were consistently picked between 5- and 15-km event-station distances, with all picks occurring in the crystalline basement (≥4-km depth from surface). Efforts to incorporate converted phase information into location strategies across the Permian Basin are ongoing, with initial results presented in Rosenblit (2024).

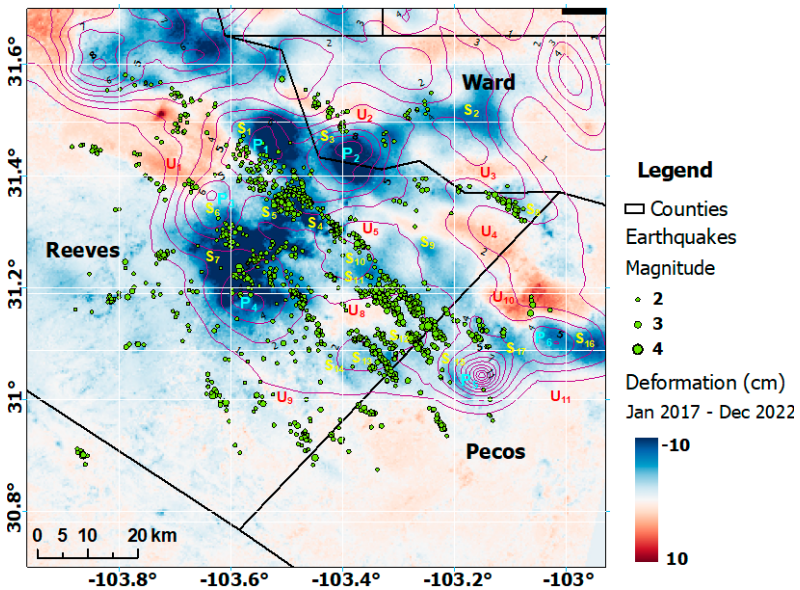

Figure 1. Comparison of cumulative shallow, vertical ground displacement from 2017 through 2022 and relocated catalog in this study (M2+) using HD. S = subsidence, U = uplift, and P = production maxima. Earthquakes scaled by magnitude. Contour lines extracted production volumes from 2017 through 2022 (from Aziz Zanjani et al., 2024a, submitted ESS).

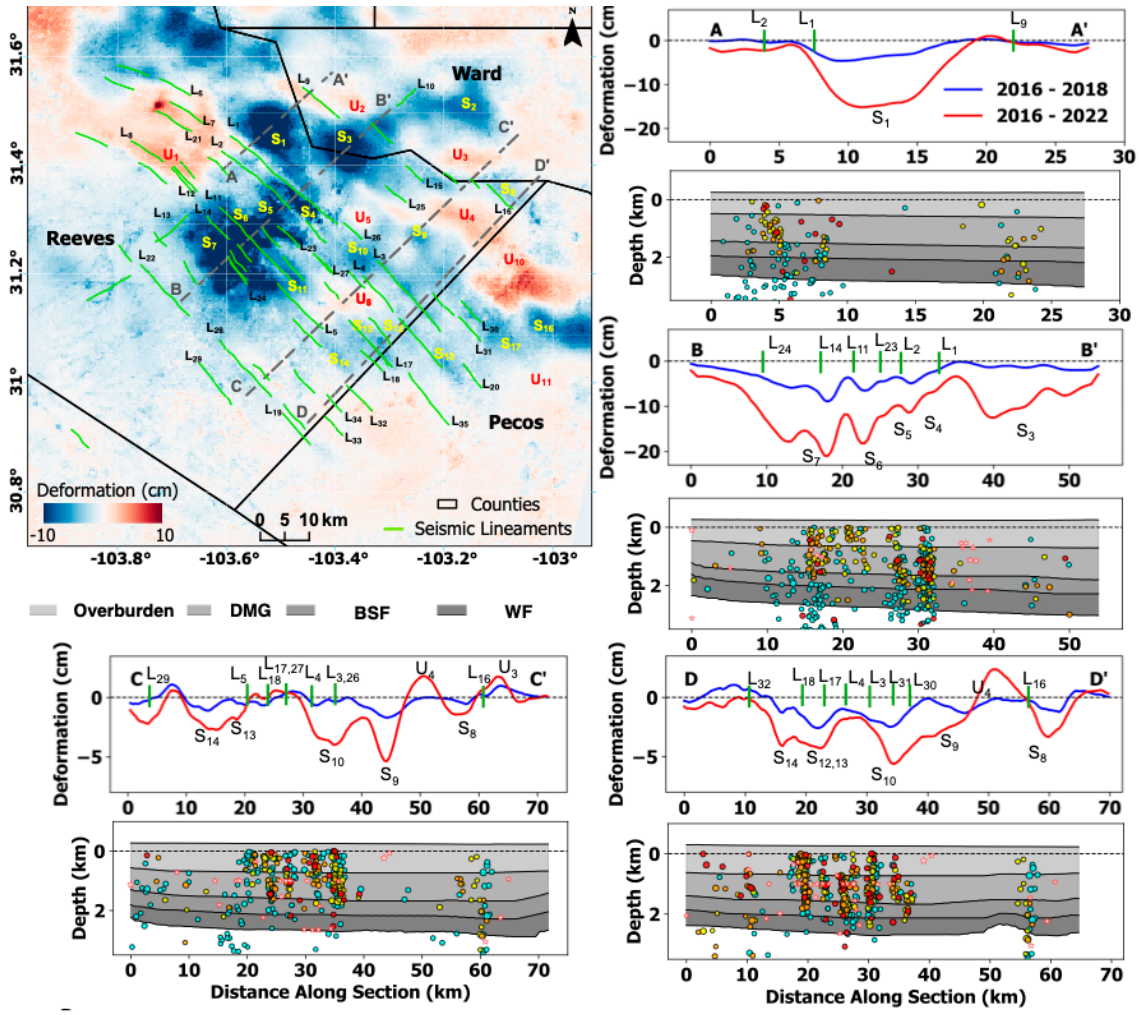

Figure 2. Progressive deformation and seismogenic source zones in southeastern Delaware Basin. Solid green lines in map view and cross section = seismic lineaments based on earthquakes (Figure 1). Cross sections shown with subsidence (S) and uplift (U) signals, labeled also in map view, shown within two different time spans (blue and red) to show changes in rate of deformation. Circles = post-2019 seismicity; stars = pre-2017 catalog from Aziz Zanjani et al. (2024b). Geologic units, including overburden, shallow injection units of Delaware Mountain Group (DMG) and Bone Spring Formation (BSF), as well as production unit of Wolfcamp Formation (WF), as indicated in legend. From Aziz Zanjani et al. (2024a, submitted ESS).

Aziz Zanjani, A., H.R. DeShon, V. Karanam, A. Savvaidis (2024a), Insights into Spatiotemporal Evolution of Induced Earthquakes in the Southern Delaware Basin Using Calibrated Relocations from the TexNet Catalog (2017-2022), submitted to *Earth and Space Science*, October 2024.

Aziz Zanjani, A., H.R. DeShon, V. Karanam, A. Savvaidis (2024b), Insights into Temporal Evolution of Induced Earthquakes in the Southern Delaware Basin Using Calibrated Relocations from the TXAR Catalog (2009–2016), *The Seismic Record*, 4 (2), 140-150, doi:10.1785/0320240011.

Rosenblit, J. (2024), Investigating Converted Phases in the Midland Basin, Texas, Using Synthetic Seismograms, M.S. Thesis, Southern Methodist University.

Numerical modeling of wave propagation in fractured medium: Explicit representation for fractures vs. effective medium

Emmanouil Parastatidis, The University of Texas at Austin; Mark W. Hildyard, University of Leeds; and Andy Nowacki, University of Leeds

Submitted to Engineering Fracture Mechanics 2024

It is well known that as seismic waves propagate through rock, they are modified by fractures in the rock, and if we can reproduce these changes successfully within fracture models, doing so will provide information on fracturing and fracture properties. Yet modeling fractures in rocks is challenging because in most cases, we need to make several assumptions about the number of fractures, their geometry, and their mechanical properties. In particular, we must make assumptions about the appropriate level of fracture detail for the model to encapsulate. A fracture is typically a discontinuity with partial contact at various positions. Although at extremely small wavelengths, the model may need to encapsulate this geometric detail of openings and contacts, at some scale we can view it as an effective fracture stiffness, even though that stiffness can vary along the length of the fracture. Similarly, once multiple fractures exist, we can model each and every fracture or attempt to represent fractures with some effective behavior. Herein we examine three models for fracture representation. The first model represents each fracture explicitly, with two explicit surfaces satisfying boundary conditions for a displacement discontinuity (Figure 1a) (e.g., Schoenberg, 1980; Shao et al., 2015). The second model is an effective medium (EM) representation that maps the properties of the collection of fractures into medium behavior (Figure 1b) (e.g., Majer et al., 1988; Ding et al., 2014; Tillotson et al., 2014). The third model is a localized effective medium (LEM) in which a thin zone of material surrounding a fracture is represented with an EM, whereas zones of material without fractures are unmodified (Figure 1c) (e.g., Coates and Schoenberg, 1995; Parastatidis et al., 2021).

For this modeling project we used the finite-difference numerical modeling code WAVE3D (M. W. Hildyard 2007), along with an experiment representing multiple parallel fractures to assess the performance of these fracture models in reproducing observed behavior. To validate the performance of each of the three fracture representations, we compared P- and S-waveforms for waves propagating parallel and perpendicular to the fractures against waveforms recorded in the experiment. First, we developed a methodology to invert a source for the experiment so that it could be applied to all three types of fracture models. This inversion was based on experimental recordings from a homogeneous medium without fractures. It had previously been found that the experiment had a nonuniform stress state influencing fracture behavior and the distribution of fracture stiffness. We therefore also developed and implemented a stress-dependent stiffness for all three fracture models so that they could be sensitive to localized stress.

Results show that waveforms from the LEM closely match those from the model with explicit fractures (Figure 2). No trade-off in switching from an explicit fracture representation to an LEM representation was observed. Both models successfully matched experimental waveforms, provided that effects due to heterogeneous stress were accounted for with stress-dependent fracture stiffness (Figure 2). Results also confirmed that it was impossible to match the experimental waveforms without heterogeneous distribution in fracture stiffness resulting from stress dependence. In contrast, a full EM representation was unable to match experimental waveforms, even with stress dependence accounted for. It had significantly less attenuation in amplitude and high-frequency content than did the other two models. The difference between the EM and the other two models resulted from the relationship between fracture spacing and wavelength. Frequency analysis showed that only wavelengths above 10 times the fracture spacing were successfully modeled by the EM representation. This work validates the use of explicit and localized fracture models in wave models, and the models can be used in forward modeling to predict the effects of fractures on waves, as well as in inversion of fracture properties from measured waveforms.

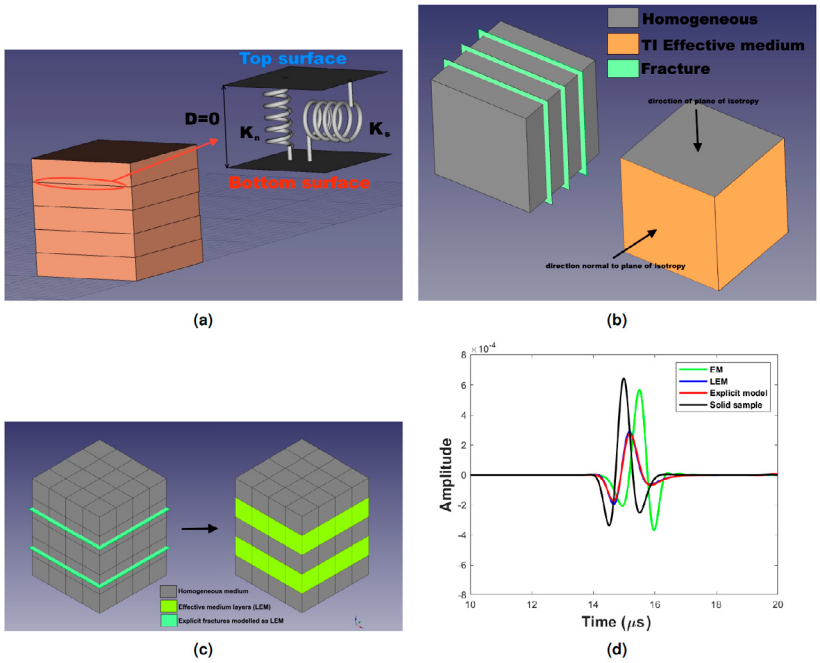

Figure 1. Schematic view of three approaches for fracture representations. (a) Linear spring contact for displacement-discontinuity model. D = distance between surfaces; K_N and K_S = normal stiffness and shear stiffness. (b) In an effective medium, fractures are mapped into material properties of the medium. Material properties in a direction perpendicular to fractures have an anisotropic behavior, and properties parallel to fractures are isotropic. (c) Zones close to predefined fracture position are anisotropic, whereas the rest are background media. The finer the mesh of the model, the thinner the LEM layer and the closer to the explicit model. (d) Example of a Ricker wave propagating through a medium with a single fracture modeled as an explicit fracture model (red), effective medium (green), a localized effective medium (blue), and a solid continuous medium (black).

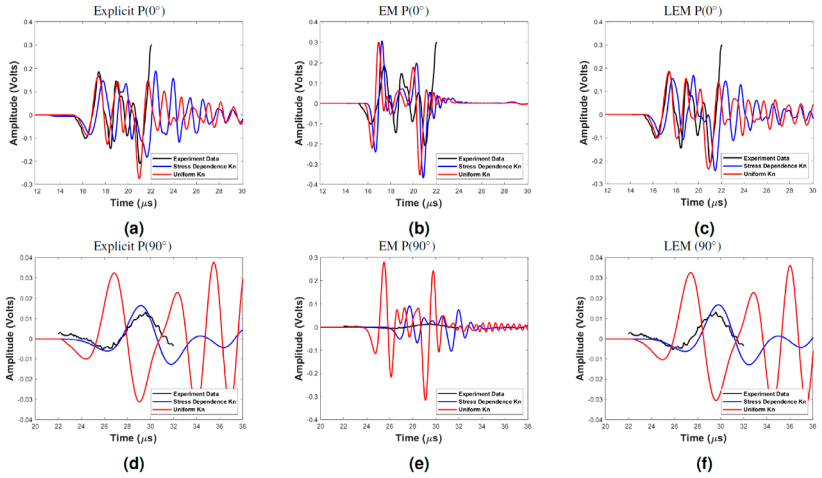

Figure 2. Comparisons of uniform and stress-dependent fracture-stiffness models with P-wave recordings. (a, d) Explicit model for propagation parallel P(0º) and perpendicular P(90º) to fractures. (b, e) EM model for propagation parallel P(0º) and perpendicular P(90º) to fractures. (c, f) LEM model for propagation parallel P(0º) and perpendicular P(0º) to fractures.

Characteristics of the Seismogenic Structures That Hosted the M4.8 New Jersey Earthquake

Dino Huang, Jess Domino, Victor Salles, Vincent O'Sullivan, Grace Burke, Yangkang Chen, and Alexandros Savvaidis

Bureau of Economic Geology, The University of Texas at Austin

On April 5, 2024, an M4.8 earthquake, and a series of aftershocks. occurred near the Tewksbury township, New Jersey. After the main shock, the Texas Seismological Network (TexNet) and seismology research team quickly mobilized and joined an effort to collaboratively monitor the aftershock sequence. This collaboration campaign includes efforts from the Lamont-Doherty Earth Observatory of Columbia University (LDEO), the United States Geological Survey (USGS), and Rutgers University, as well as TexNet (Fig. 1).

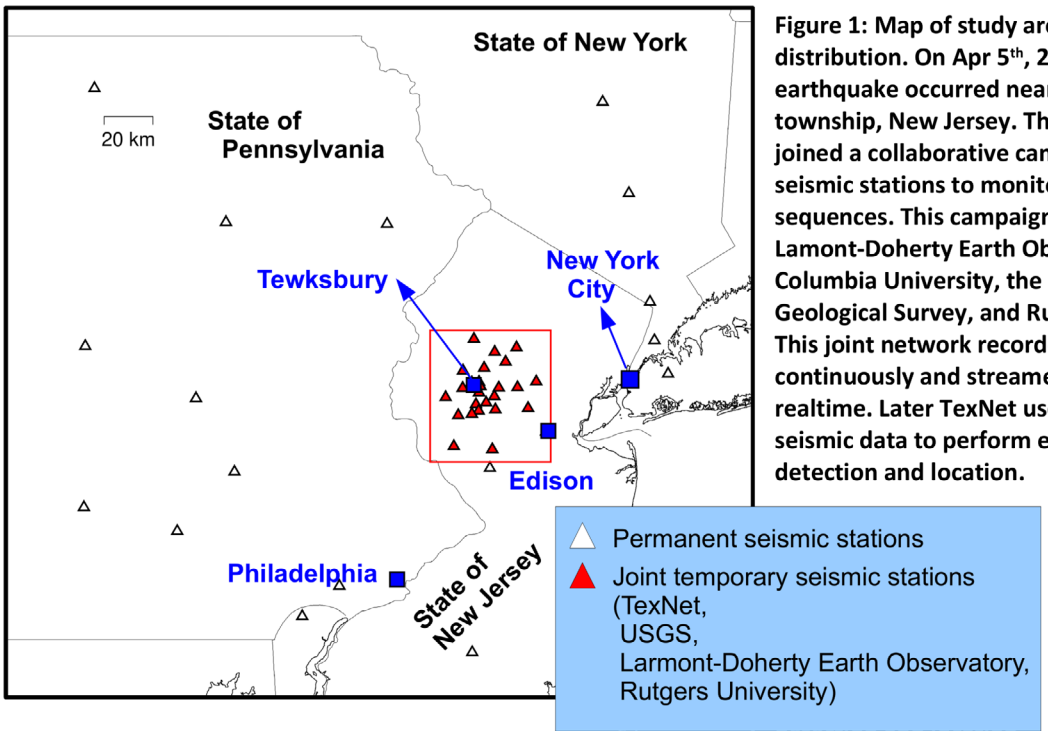

Figure 1: Map of study area and station distribution. On Apr 5th, 2024, an M4.8 earthquake occurred near the Tewksbury township, New Jersey. The TexNet has joined a collaborative campaign to deploy 6 seismic stations to monitor the aftershock sequences. This campaign includes the Lamont-Doherty Earth Observatory of Columbia University, the United States Geological Survey, and Rutgers University. This joint network recorded data continuously and streamed recorded data in realtime. Later TexNet use these recorded seismic data to perform earthquake detection and location.

In this campaign, TexNet has installed 6 monitoring stations (network code: 4N; station names are NJ10 through NJ15) to fill in the monitoring gap within the current station distribution of a permanent seismic network operated by the LDEO. Each station is equipped with a 3-component seismometer and records at high sample rates (either 250 sps or 100 sps). Additionally, at station 4N.NJ15, we deployed an accelerometer which is almost on top of the reported hypocenter of the M4.8 mainshock. An accelerometer at this site allows for recording of strong motion in proximity to the main rupture zone. Data are provided to the public and research organizations 24/7 through the TexNet data hub at The University of Texas at Austin.

After field deployment to record seismic data in realtime, TexNet used the earthquake compact convolutional transformer (EQCCT) to perform earthquake detection and to determine the preliminary earthquake location using the Central and East US velocity model. Using EQCCT, TexNet has detected nearly 400 aftershock events. To take the local velocity structure into account, we used earthquake tomographic inversion to jointly determine a 3-D local velocity model and locate the earthquake hypocenters. Later we used the relative relocation approach (i.e., hypoDD) to further delineate the earthquake hypocenters that were previously determined by tomographic inversion. The distribution of delineated hypocenters has shown that the active faulting area is located in a two distinctive depth groups of (1) 0–5 km and (2) deeper than 5 km (Fig. 2).

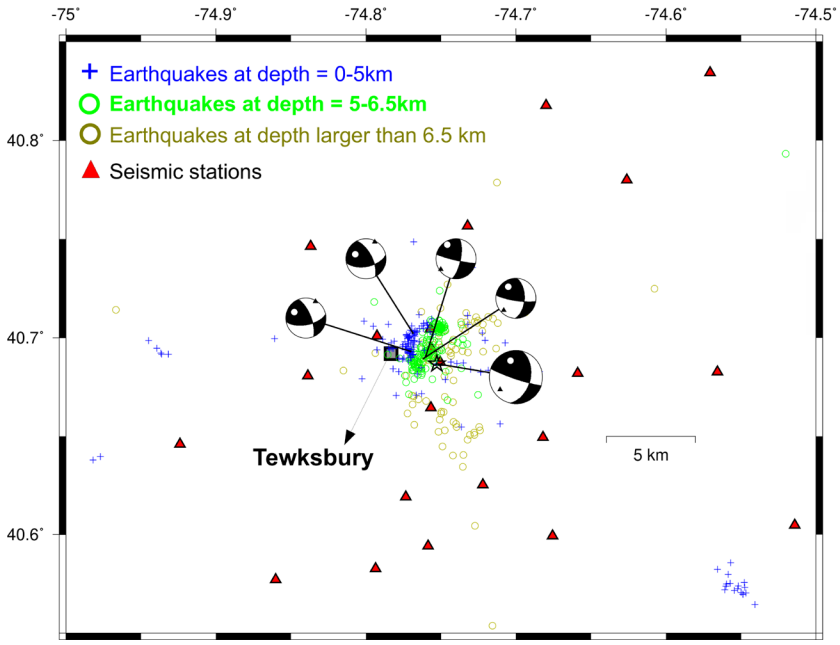

Figure 2: Delineated earthquake hypocenters and selected earthquake source mechanisms. This study used tomographic inversion to resolve a local 3-D velocity model and locate earthquake hypocenters simultaneously. Also, this study used waveform moment tensor inversion to determine earthquake mechanisms. A combination of seismicity distribution and source mechanisms suggests that the faulting sequence was hosted by a nearly northeast-southwest striking fault having a high oblique thrusting component.

They also suggest that the main shock and the aftershock sequence were hosted by a nearly northeast-southwest striking fault that has a high oblique thrusting component. Specifically, the faulting type shifted from oblique thrust to strike-slip during the period of the aftershock sequence. Throughout this field campaign, TexNet has not only enhanced its reputation but also effectively built up a close collaboration with other research agencies nationwide.

Stochastic Inversions and Site Amplification in West Texas

Bartik Pandel[1], Ellen M. Rathje[1], Alexandros Savvaidis[2], Albert R. Kottke[3]

This study builds upon our previous analyses of seismic ground motions in West Texas, emphasizing high-frequency characteristics vital for seismic design and hazard assessments. We analyzed ~6,500 recordings from earthquakes in the Delaware Basin from January 2017 to August 2023 with magnitudes ranging from 3.0 to 5.4 (Fig. 1), examining source, path, and site effects from 49 TexNet stations. Our analysis of the acceleration Fourier Amplitude Spectra (FAS) revealed magnitude-dependent stress parameters ($\Delta\sigma$) ranging from 5 to 157 bars (Fig. 1) and established a frequency-dependent quality factor $Q = 753f^{0.6}$ with near-field geometrical spreading characterized by $\gamma = 1.15$.

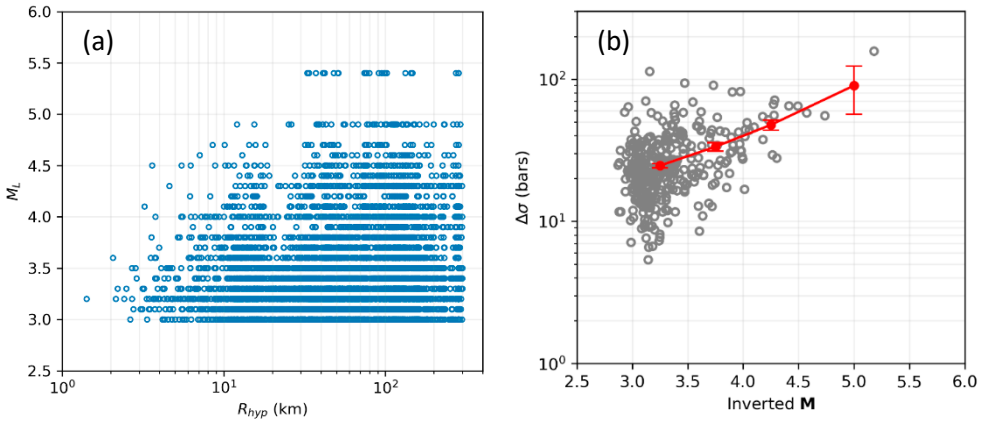

Figure 1. (a) Magnitude – distance distribution of dataset used in broadband inversions. (b) Inverted stress parameter as a function of magnitude.

Focusing primarily on the site term, we aimed to separate site amplification from the high-frequency spectral decay parameter κ_0, employing both broadband inversion techniques and band-limited slope methods. We computed κ_0 directly from the broadband inversions on acceleration FAS, as well as from classical slope methods that utilize either the acceleration FAS from M > 3.0 or displacement FAS from M < 2.0 events (Fig. 2). An important distinction in these approaches is that the inversion method solves for site-specific site amplification functions, whereas the classical slope methods utilize a theoretical site amplification function from a V_S profile computed by the square-root-impedance (SRI) method.

1. Fariborz Maseeh Department of Civil, Architectural, and Environmental Engineering, The University of Texas at Austin
2. Bureau of Economic Geology, The University of Texas at Austin
3. Pacific Gas and Electric Company

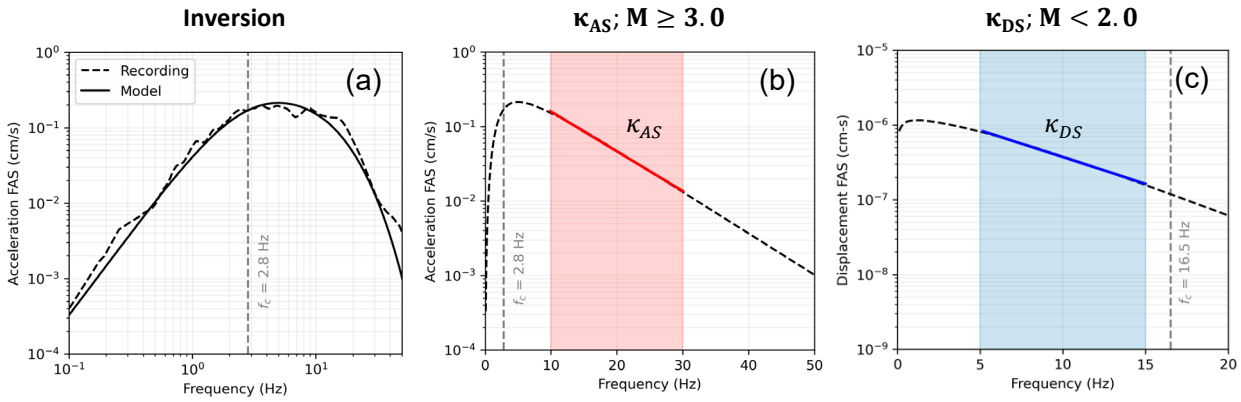

Figure 2. Methods for deriving κ_0: (a) broadband inversion, (b) band-limited slope of acceleration FAS, and (c) band-limited slope of displacement FAS.

Results demonstrated that κ_0 values from the slope of the acceleration FAS (κ_{AS}) are systematically smaller than those from the slope of the displacement FAS (κ_{DS}), on average by 0.025 s (Fig. 3a). The broadband inverted κ_0 values ($\kappa_{0,BB}$) are similar to the $\kappa_{0,AS}$ values, although the comparison is influenced by the site amplification because the inverted site amplification is often different from the computed site amplification from the SRI method. When the SRI site amplification is used in the $\kappa_{0,AS}$ calculation, $\kappa_{0,BB}$ and $\kappa_{0,AS}$ take on similar values but with significant scatter (Fig. 3b). When the inverted site amplification is used in the $\kappa_{0,AS}$ calculation, the values of $\kappa_{0,BB}$ and $\kappa_{0,AS}$ are more similar (Fig. 3c). These insights indicate the strong relationship between the assumed site amplification and κ_0, and they contribute to improved ground motion characterization and more accurate seismic hazard assessments of West Texas.

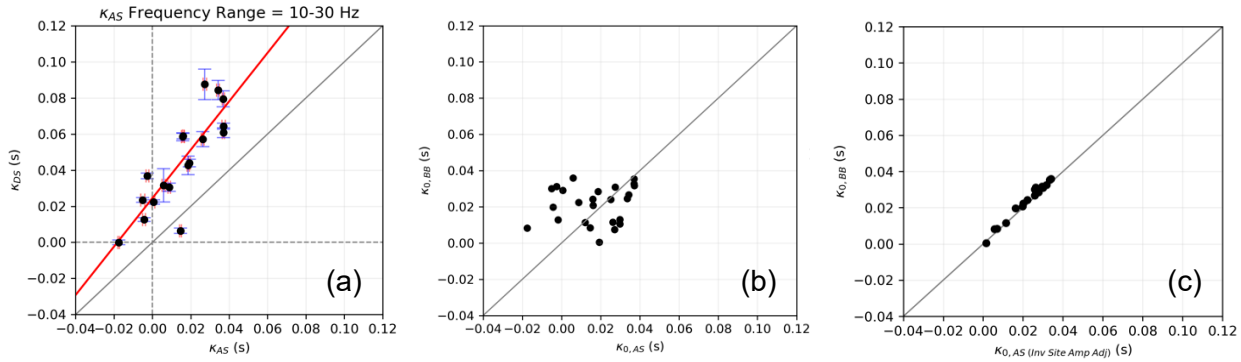

Figure 3. Comparison of κ_0 values derived using different methods.

1. Fariborz Maseeh Department of Civil, Architectural, and Environmental Engineering, The University of Texas at Austin
2. Bureau of Economic Geology, The University of Texas at Austin
3. Pacific Gas and Electric Company

Assessment of Seismic Hazard Potential for a Geothermal Field: A Case Study in West Texas

Victor Salles, Guo-chin Dino Huang, Katerine Vallejo, Peter Eichhubl, Shuvajit Bhattacharya, and Alexandros Savvaidis

Submitted to The Seismic Record

The El Paso (TX) - Ciudad Juárez (MX) metropolitan area is part of the tectonically active Rio Grande Rift system, known for its complex geological and seismic activity. This rift system is marked by Quaternary faulting, sedimentary basins, and volcanism, and it stretches from Colorado to Mexico. Some historical earthquakes (including the 1887 Mw 7.5 event in Sonora, Mexico, and the 1931 Mw 5.8 earthquake in Valentine, Texas) suggest the potential for future high-magnitude events. Recent natural low-magnitude seismicity and GPS-based geodetic studies confirm ongoing deformation, especially in the central and southern regions with high tectonic strain. In this study, we used the machine-learning-based EQCCT algorithm to detect seismicity using the Transportable Array data from 2008 to 2011. We refined event locations through manual review and relocation using NonLinLoc and hierarchical clustering with GrowClust3D. These techniques revealed seismic clusters linked to mapped faults, indicating that they are seismically active. Our findings provide new insights into the region's geological activity and lay a foundation for future seismic hazard assessments.

According to the USGS seismic catalog, historical seismicity since the early 1900s in this area shows few events associated with mapped faults. Nakai et al. (2017) located events from 2008 to 2010 in the region, also finding limited association with these structures. Both catalogs are shown in Figure 1.

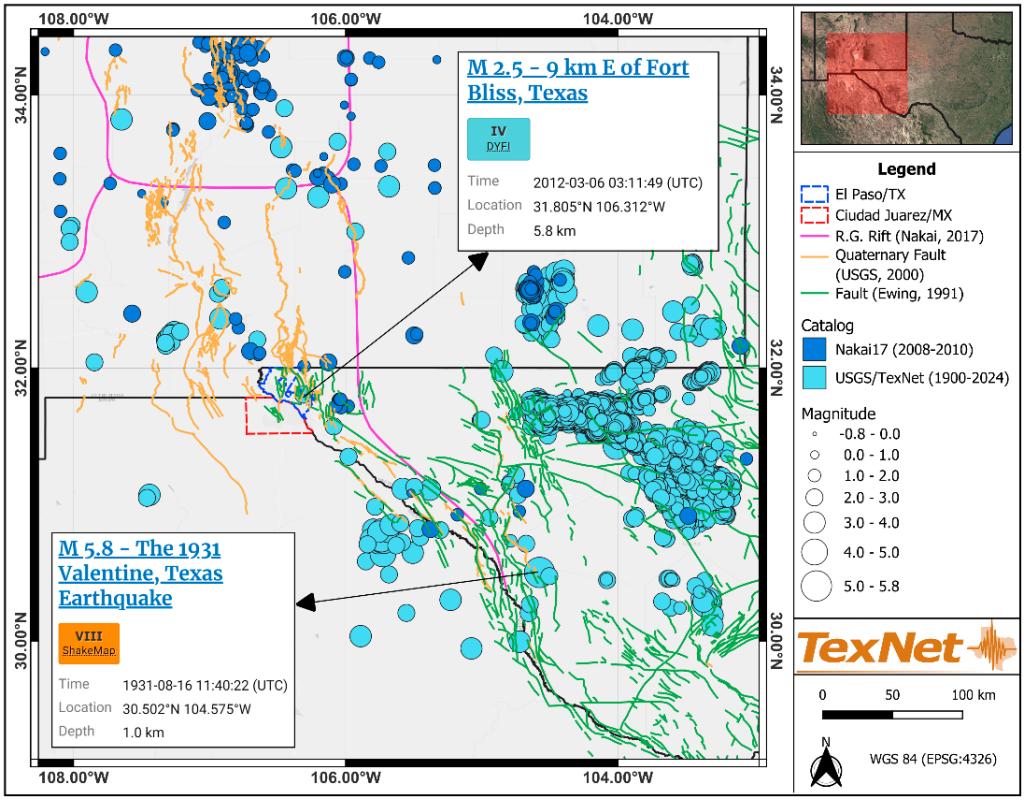

Figure 1. Seismicity map of the El Paso-Ciudad Juárez metropolitan area, incorporating data from USGS, TexNet, and previous studies.

Using EQCCT in the target area, we detected 653 events between February 17, 2008, and December 20, 2011. After manually reviewing the auto-picked arrival times and relocating all events with GrowClust3D, we confirmed 645 as real seismic events (Fig. 2). For a detailed hazard analysis, we recommend deploying an array of seismic stations across the area and nearby faults to monitor seismicity and better identify active fault zones. Developing a 3D earth model would enhance the accuracy of depth estimates for both basement top and earthquake hypocenter. In this way, it will be possible to clarify if the seismicity is into the shallow strata or inside the basement. These data are crucial for assessing hazards related to existing seismicity and potential migration of earthquake activity, especially considering ongoing anthropogenic activities like geothermal energy production.

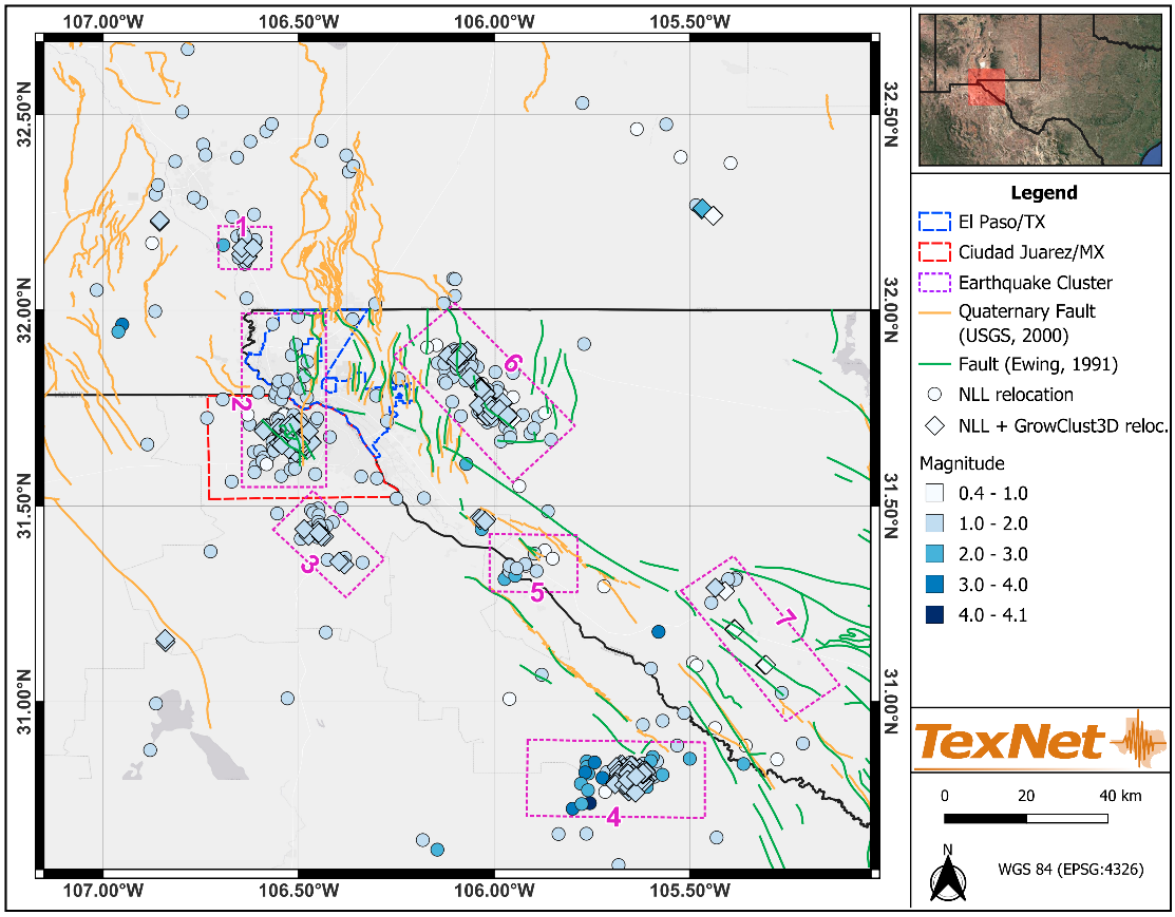

Figure 2. Seismicity located in this study, revealing seven major earthquake clusters. Clusters 1, 3, and 4 suggest the presence of previously unmapped seismogenic faults; clusters 2, 5, 6, and 7 overlap with mapped Quaternary faults.

A new Block Time-Series BOI algorithm for retrieving horizontal displacement: Application in the Delaware Basin

Xing Li

Bureau of Economic Geology, The University of Texas at Austin, Austin, Texas, U.S.A.

Geodetic measurements of interseismic deformation are essential for estimating fault slip rates and locking depths, which are critical for seismic hazard assessments. However, due to the near-polar orbits of radar satellites, conventional InSAR has limited capability in measuring the northward component of displacement. Techniques such as azimuth pixel-offset tracking, multi-aperture interferometry (MAI), and burst-overlap interferometry (BOI) are used to retrieve horizontal displacements aligned with the satellite track. Among these, offset-tracking and MAI are primarily suited for large-magnitude along-track deformations, such as those from co-seismic and post-seismic events. Burst-overlap interferometry (BOI), on the other hand, enables along-track deformation measurements by double-differentiating consecutive burst overlaps, showing significant potential to detect millimeter-level horizontal deformation along slowly moving faults. This technique is initially applied to refine the azimuth offset through the interferometric phase during fine image co-registration, known as enhanced spectral diversity (ESD). With ESD, azimuth misregistration due to orbit errors is treated as a constant value, allowing for sub-pixel accuracy (better than 0.001 pixels). However, if there is a large-scale deformation trend, such as plate motion or rapid fault slip, any deformation-induced misregistration is corrected during co-registration, leading to an underestimation of the actual deformation. For instance, with a deformation rate of 2 cm/year and a 3-year temporal baseline, the misregistration would be 0.0043 pixels, which would be removed during ESD correction, thereby excluding the deformation from the displacement field. Another limitation of ESD is that it averages the constant misregistration across all burst-overlap interferograms. If the burst-overlap interferograms are all located on one side of a fault, the displacement will be fully removed from all overlaps, resulting in a zero-mean displacement field.

To address the limitations of Enhanced Spectral Diversity (ESD) in retrieving large deformations while correcting for orbital errors, we developed a novel method called Block Time-Series Burst-Overlap Interferometry (BTSB), with the workflow outlined in Figure 1. This workflow begins by selecting two burst overlaps that cover the same region (forward and backward burst overlap stacks) and generating a subset of small baseline burst-overlap interferograms. After enhancement of the phase accuracy, we perform a time-dependent deformation inversion on the misregistration series, incorporating a linear plate motion model to estimate the mis-registration that correspond to orbital errors. We divide the entire overlap region into blocks, correct the orbital errors, and then apply a periodogram function to each block to invert the misregistration time series. Finally, we derive the velocity based on the corrected burst-overlap misregistration series.

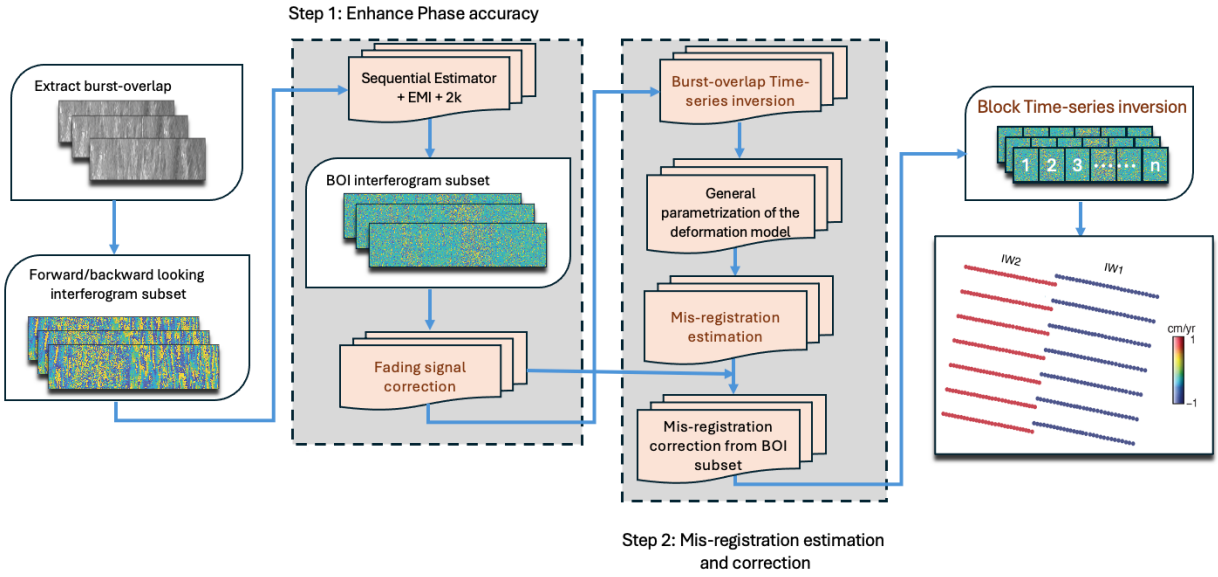

Figure 1. Schematic diagram of the workflow.

We applied the workflow in the Delaware Basin, processing Sentinel-1 ascending and descending SAR images from 2015 to 2024. Following the block time-series inversion step in Figure 1, we set the block size to be 8 km × 8 km and obtained a more accurate and smooth velocity map. Our results in Figure 2 show horizontal displacements along the satellite azimuth direction with magnitudes exceeding 1 cm/year in the middle of the Delaware Basin. Positive values indicate movement in the satellite flight direction, revealing a clear extension in the center of the basin from both orbits. The extension in the center of the basin is expected to be associated with the vertical deformation in this area. The velocities at GNSS station TXP6, projected to the ascending and descending orbits, align with our derived results.

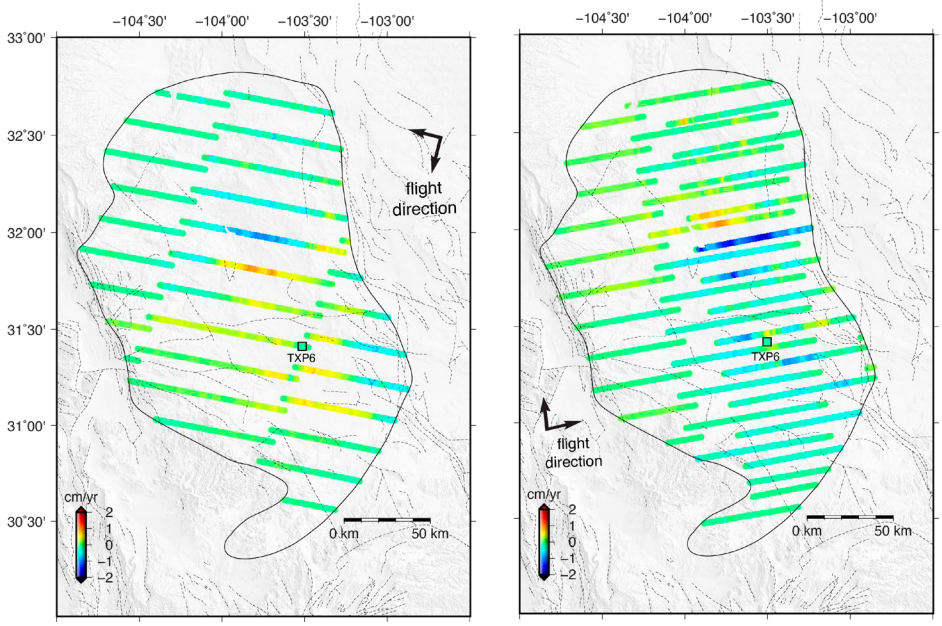

Figure 2. Horizontal displacement map along satellite azimuth direction derived from descending and ascending orbits.

Resolving Three-Dimensional Time-Series Displacements in the Delaware Basin from InSAR Measurements

Xing Li

Bureau of Economic Geology, The University of Texas at Austin, Austin, Texas

Displacement fields in the Delaware Basin have been extensively studied using Interferometric Synthetic Aperture Radar (InSAR). However, prior research has predominantly focused on the vertical and east-west components of displacement, often neglecting the north-south component. The direct approach to resolving the full 3D displacement field involves combining multiple InSAR line-of-sight (LOS) measurements from various viewing geometries. Conventional methods for retrieving horizontal displacement, including pixel-offset tracking and multi-aperture interferometry (MAI), are limited due to their low accuracy. In many regions, including the Delaware Basin, where GPS stations are sparse—particularly in highly deformed areas—combining InSAR data with GPS observations is challenging.

To address this gap, we applied a novel approach called Block Time-Series Burst-Overlap Interferometry (BTSB) along with DInSAR to resolve the 3D time-series displacements across the Delaware Basin. We processed Sentinel-1A/B ascending and descending orbit data from 2015 to 2024. For DInSAR processing, we utilized the advanced DetrendInSAR method to denoise the DInSAR ascending and descending time-series. The resulting LOS velocity maps from ascending and descending orbits (Fig. 1a, b) reveal significant subsidence patterns, with negative values highlighting areas of pronounced subsidence. Notable discrepancies between the ascending and descending fields indicate substantial horizontal deformation. For the horizontal displacements, we employed the BTSB method with Laplacian interpolation to retrieve horizontal displacements from both orbits (Fig. 1c, d). These observations, shown in Figure 1. were then decomposed into a 3D velocity map.

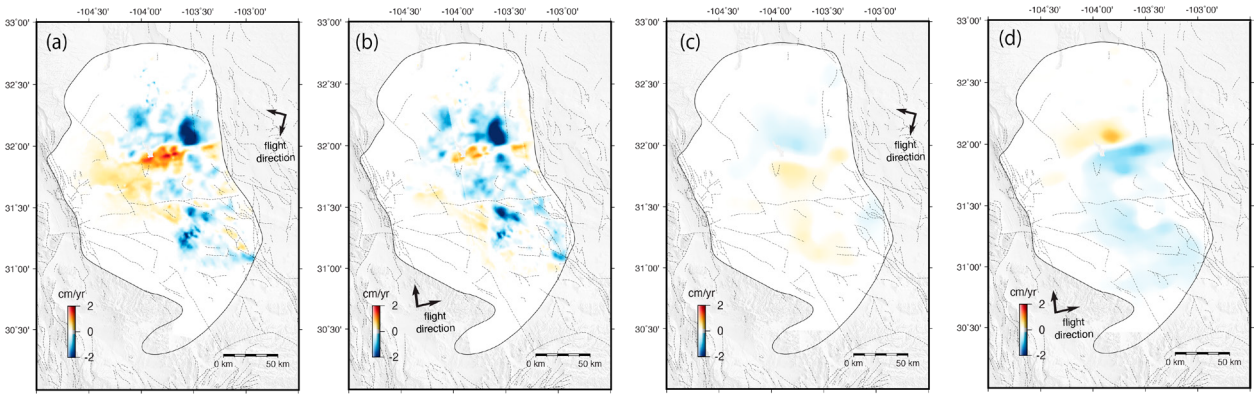

Figure 1. Velocity map from 2015 through September 2024. Panels (a) and (b) are descending and ascending velocity maps along LOS direction. Panels (c) and (d) are interpolated descending and ascending velocity maps along azimuth direction.

The resulting decomposition (Fig. 2) illustrates both the vertical and horizontal displacement components. The horizontal displacement reaches as much as 1.4 cm/year, primarily located south of the boundary between large-scale subsidence and uplift. Extension is also observed along this subsidence-uplift boundary, suggesting that the horizontal displacement is associated with vertical displacement. Comparison with GPS time-series data from stations TXP6 and TXPC shows strong correlation in the vertical and east-west components, displaying clearer trends and reduced noise relative to the GPS data. The north-south component exhibits higher noise due to its inherently low signal-to-noise ratio. Our results underscore the reliability of InSAR in capturing complex deformation patterns in areas with limited ground-based measurements, offering a robust solution for 3D displacement monitoring in the Delaware Basin.

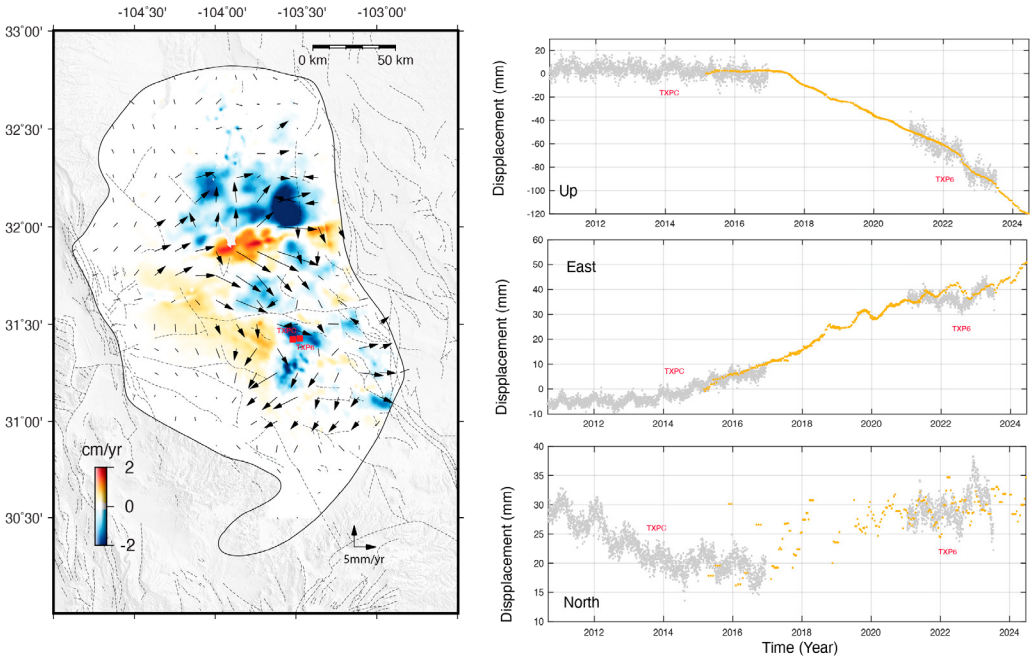

Figure 2. Decomposed 3D velocity map of the Delaware Basin from 2015 through September 2024. The arrow and the color represent the down-sampled horizontal displacement and the vertical displacement, respectively. The right column shows the comparisons between decomposed 3D time-series and GPS time-series at stations TXPC and TXP6.

TexNet injection seismicity analysis tool (TISAT): Analyzing impact of individual wells in induced seismicity in Texas and assessing quality of operator-injection data provided, Scurry-Fisher July 2024 M4+ earthquake cluster

C. Skevofilax and A. Savvaidis

Induced seismicity, or human-induced earthquakes, is a growing concern in unconventional hydrocarbon production, in which activities such as hydraulic fracturing (HF) and saltwater disposal (SWD) are commonly practiced. Industry leaders have identified these activities as contributors to earthquake inducement owing to their capacity to alter subsurface pressure and stress conditions, highlighting the need for careful monitoring and management.

The relationship between subsurface-injection activities and induced seismic events has been widely studied; however, a critical gap persists in an understanding of these interactions, primarily because of the absence of detailed temporal monitoring of individual wells' injection activities and their potential to trigger seismic events within a specific area. To address this limitation, we developed the TexNet injection seismicity analysis tool (TISAT), which offers a novel approach to bridging the understanding gap between SWD operations and their influence on seismic events, particularly those occurring near earthquake epicenters. TISAT enables researchers to visualize operator-reported daily injection activity, including injection volumes and pressures, while simultaneously calculating well bottomhole pressures in relation to seismic events recorded in the TexNet Earthquake Catalog. By providing detailed timelines of well activity near specific epicenters, TISAT facilitates identification of anomalous operational patterns that may be linked to induced seismicity. This functionality is crucial to distinguishing outlier behaviors among wells that could contribute to seismic risk, thereby aiding development of informed and proactive risk mitigation strategies.

Applying TISAT to four recent M4+ earthquakes that occurred in Scurry and Fisher Counties, Texas, in July 2024, we identified specific well activities most likely linked to these seismic events. Analysis revealed that wells with constant injection volumes exhibited minimal correlation with seismicity, whereas wells with sharp decreases followed by rapid increases in injection volumes were probable contributors. Notably, wells undergoing substantial reductions in injection volumes appeared to have played a significant role, particularly when these reductions coincided with an overall decline in regional injection activity. These findings suggest a complex interaction between gradual and abrupt changes in well operations over time and the initiation of seismic events (Fig. 1).

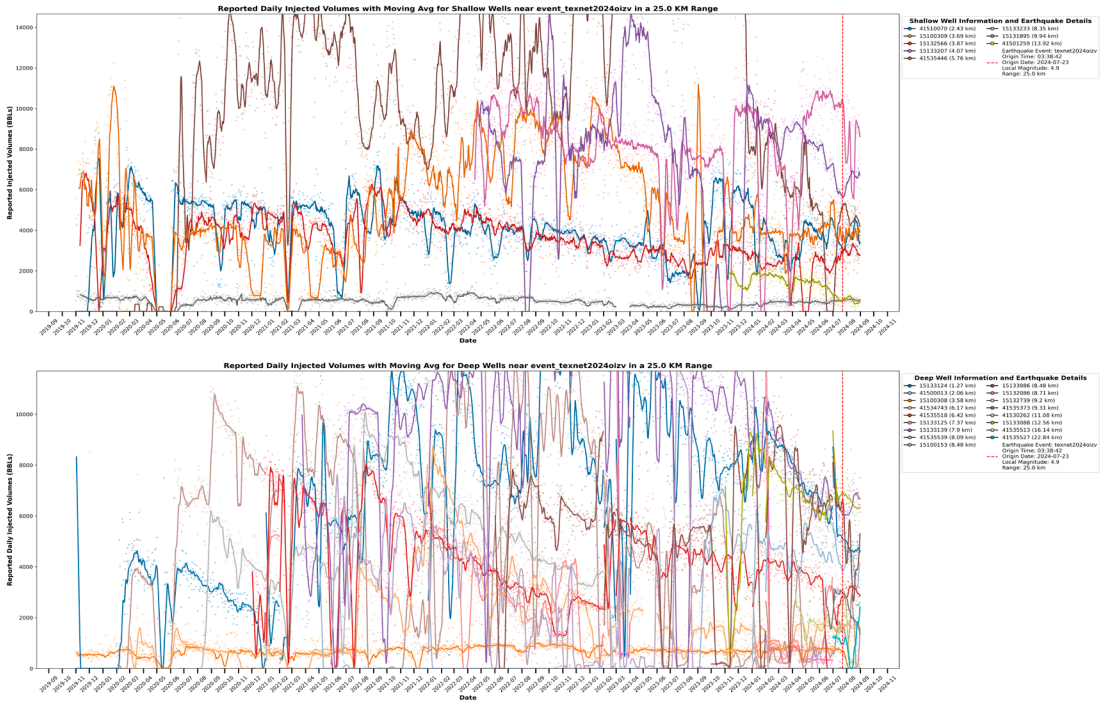

Figure 1. Reported injection volumes for shallow and deep wells near seismic event (Event ID: texnet2024oizv).

Crucially, TISAT also addresses data quality issues, including missing or inaccurate values for reported -volume injected- and -injection pressure- keys, as well as instances in which reported pressure values remain static over time when changes are expected. These issues can compromise the reliability of analytical results. To mitigate the impact of incomplete or erroneous data, we took measures to identify and exclude faulty records, as well as to provide visualizations that highlight calculations affected by missing data. Additionally, data-quality histograms were developed (Fig. 2) to enable researchers to assess the accuracy of operator-reported information, offering a clearer understanding of data accuracy. These features ensure more precise calculations and visualizations of injection activity, enhancing the robustness of analyses performed using TISAT.

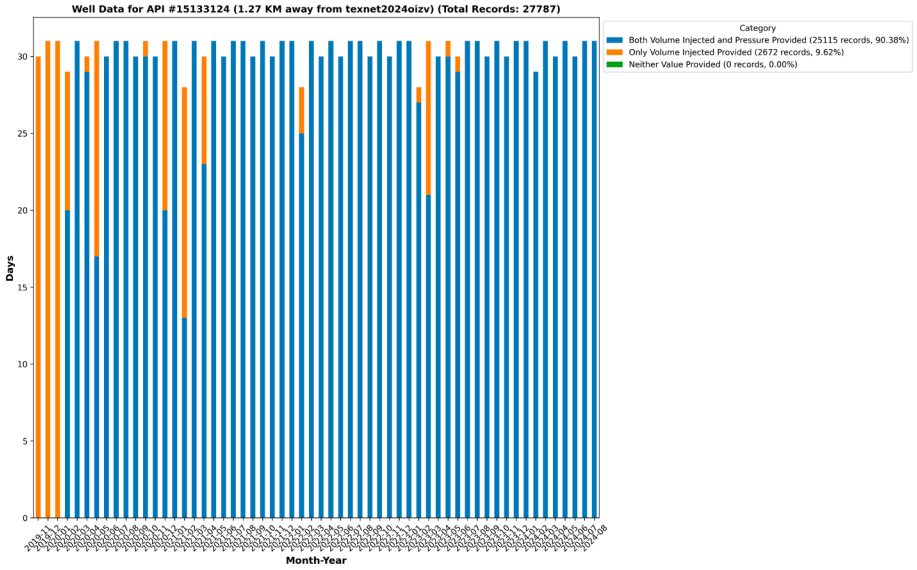

Figure 2. Quality-control histogram of reported injection-well values for API #15133124.

Intricate relationship between seismicity and injection revealed by deep-learning-detected small earthquakes

***Yangkang Chen**, The University of Texas at Austin, **Alexandros Savvaidis**, The University of Texas at Austin, **Omar M. Saad**, KAUST, **Daniel Siervo**, The University of Texas at Austin, **Dino Huang**, The University of Texas at Austin, **Yunfeng Chen**, Zhejiang University, **Iason Grigoratos**, ETH Zurich **Sergey Fomel**, The University of Texas at Austin, and **Caroline Breton**, The University of Texas at Austin*

Presented at the 4th International Meeting for Applied Geosciences and Energy (SEG-AAPG), 2024.

In the past decade, because West Texas has become a seismically active region owing to injection of industrial wastewater and hydrocarbon exploitation, the newly founded Texas seismological network has created a catalog that characterizes intense seismicity down to a magnitude of 1.5 Ml. However, analyzing numerous small-magnitude events (Ml<1.0) is prohibitively unaffordable. We therefore proposed applying an advanced deep-learning method, the earthquake compact convolutional transformer (EQCCT), to relieve the workload involved in analyzing thousands of small earthquakes per month in West Texas (Figure 1). The EQCCT method, embedded in an integrated detection and location framework to seamlessly output a complete earthquake catalog, has enabled us to detect and locate 50 times more earthquakes than previously possible. We applied an EQCCT-embedded detection and location workflow to the Culberson and Mentone earthquake zone (CMEZ) in West Texas, and association with nearby injection activities revealed an intricate correlation between rate of injected fluid volume and number of small earthquakes.

To study spatiotemporal correlation with fluid injection, we selected a target area (yellow circle in Figure 2a) in the CMEZ region that included the 31 wells operating in CMEZ in October 2022 (Figure 2a). We chose one well (well 1) that began injection immediately following the M3.5 event, and we analyzed its association with nearby seismicity. We chose an area centered around the well with a radius of 0.1° (yellow highlight) to analyze the relationship between injection (eight wells in the yellow circle) and seismicity. We plotted daily distribution of the number of detected earthquakes (Figure 2b), where we could see a generally stable distribution of number of events, although a gradual decrease occurred from 10/21/22 through 10/27/22. We plotted a magnitude-time distribution (Figure 2c) to illustrate TexNet events and EQCCT-detected small earthquakes. Note the sudden drop in number of small earthquakes on 10/27/22, and observe the good correlation between injection activities and the sudden drop in number of earthquakes. Also note that injection rate peaks on 10/27/22, whereas daily number of earthquakes (mostly small ones) has become the lowest. Traditionally, when small earthquakes are barely detectable, analyzing the influence of small-earthquake activities vs. fluid injection is difficult. Moderate- to large-earthquake activities show little dramatic change during the short-term fluid injection. However, owing to the detection of an enormous number of small earthquakes, we were able to find a distinct drop in small earthquake activities as injection rate peaked. This observation contradicts the mainstream assumption regarding the relationship between fluid-injection rate and seismicity. It is commonly thought that increased fluid injection would cause increased rates of seismicity, but this generally held claim contradicts what we have observed in this study regarding ultra-small earthquakes (e.g., M<1). The observation in this study might be explained by a lubricant effect of fluid in the earthquake-generation mechanism. The fast-injected fluid smooths faults and reduces the number of small earthquakes in the short term, whereas stress accumulates for larger earthquakes later on. This phenomenon could also be attributed to delayed triggering, which can be explained by rate of state friction laws. More research needs to be done to confirm this hypothesis, however.

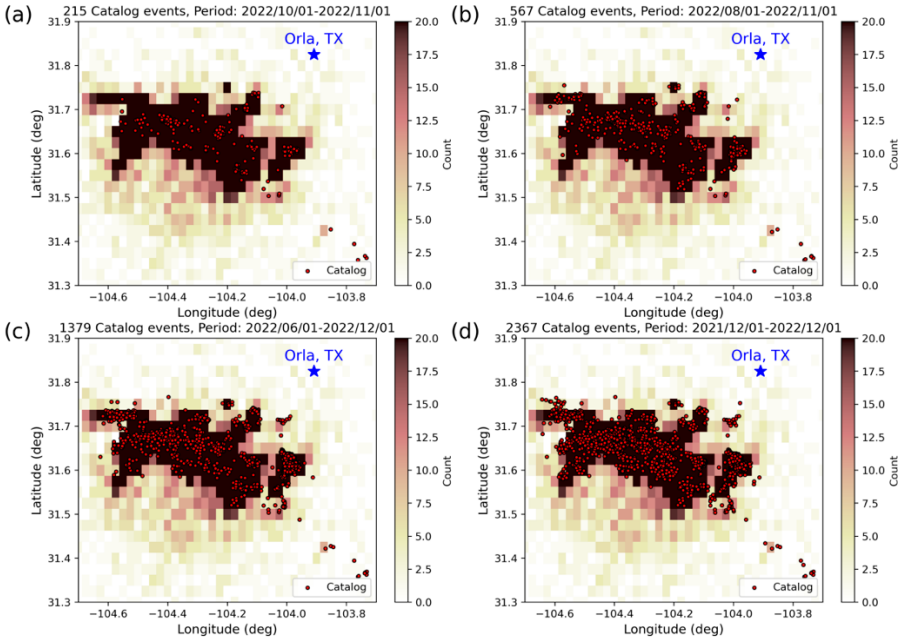

Figure 1. Detection and location results (33,319 events) of EQCCT compared with TexNet events in different periods. (a) Location comparison between EQCCT events and 1-month catalog events. (b) Location comparison between EQCCT events and 3-month catalog events. (c) Location comparison between EQCCT events and 6-month catalog events. (d) Location comparison between EQCCT events and 1-year catalog events.

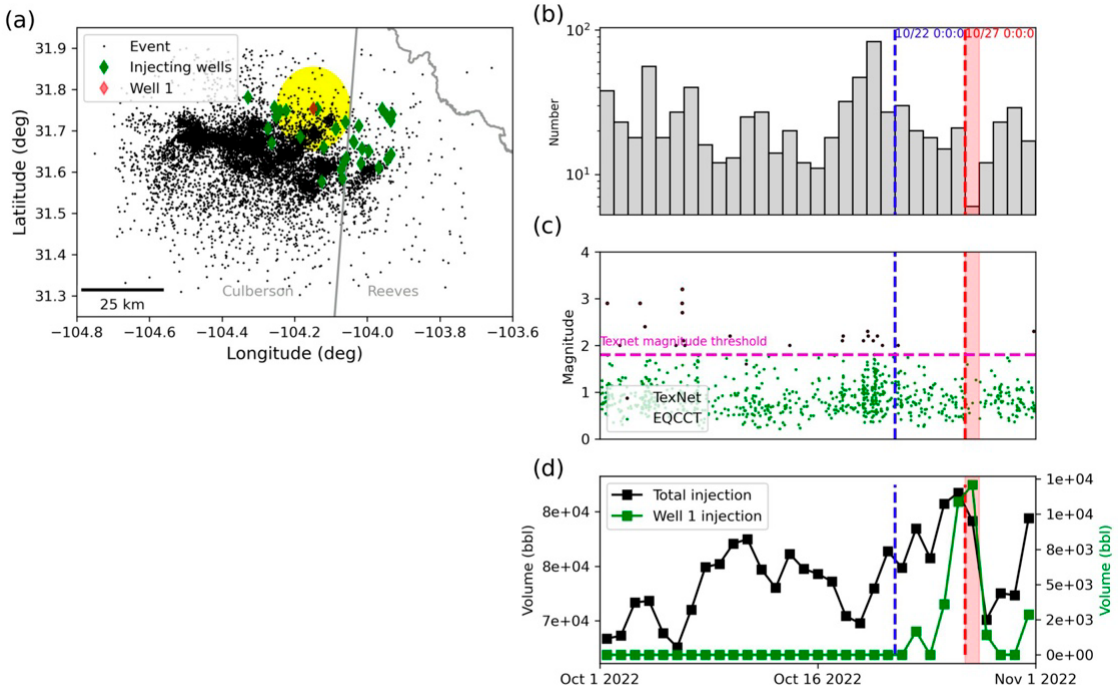

Figure 2. Association of seismicity with fluid injection. (a) Spatial distribution of detected events in October 2022. (b) Daily distribution of events. (c) Daily magnitude distribution. (d) Daily injected volumes of all wells in target area (yellow circle in a) and center well. Note strong correlation between daily seismicity and injected volumes around 10/27/22.

Study of effect of preexisting fractures in reservoir on potential for induced seismicity for hydro-storage dam projects

Emmanouil Parastatidis, The University of Texas at Austin; Mark W. Hildyard, University of Leeds; Stella Pytharouli, University of Strathclyde; Alexandros Savvaidis, The University of Texas at Austin, and Oliver Chowns, University of Leeds

Presented IMAGE2024 / To be submitted to International Rock Mechanics and Mining Sciences, 2025

In this project, we attempted to explain how various geomechanical scenarios of a geological fault, influenced by the presence of a water reservoir, can lead to reservoir-induced seismicity (RIS) under maximum water impoundment. The area we focused on was a hypothetical scenario for a future hydro-pump storage reservoir (Figure 1a). Two types of seismicity occur as a result of RIS:

- **Initial seismicity**—A mechanical response to water-level change that immediately alters the stress state (fracture-weakening-state scenario).
- **Protracted seismicity**—A hydraulic response, in which water diffuses from the reservoir into the fault line, reducing effective stresses (water weakening and fracture-fatigue scenarios). This method typically leads to the largest events (H. Gupta, 2022).

The aim of this project was to investigate the effects of loading and unloading of a nearby hydro-electric dam on seismic activity of an existing fault line. We modeled the influence of changes in Mohr-Coulomb properties, elastic properties, and background stress on different scenarios. We considered different geological conditions of the site, such as fracture fatigue and presence of fluids in the fracture. Finally, we used modeling results to explain what could encourage seismicity in this particular area.

For the modeling project, we used the finite difference numerical modeling code WAVE3D (M. W. Hildyard, 2007) to create three major model scenarios (Figure 1). The first scenario (weakened state) tests the limits of stress due to the presence of water from the dam reservoir and how this affects the balance between cohesion and shear stress. The second scenario tests the water-weakening state, assuming that the presence of water from the reservoir along with stress will saturate the fault with water, leading to a reduction in fracture cohesion. The last scenario examines fracture fatigue due to stress loading and unloading during the use of the hydro-pump scheme to produce energy. This fatigue was expressed as a weakening zone in our models, with lower elastic-material properties than those of the surrounding rock (Figure 1g, h).

We have summarized results of all modeling scenarios (Table 1), illustrating that in order for fault rupture to take place, shear stress must exceed cohesion, whereas size of the applied shear stress determines amount of displacement. In the water-weakening scenario, we tried reducing the water level and, as a result, the stress load. The models show that despite significant water-level change, the water-weakening effect has significant control over the strength condition of the fault. Such conditions create protracted seismicity, which is what generates the worst RIS cases (H. Gupta, 2022). A reduced water load created excess shear stress (ESS) directly beneath the reservoir that was higher than what the maximum load created. This difference was due to lower vertical stress, enabling regional stresses to be distributed toward the reservoir, in turn enabling greater ESS (J. L. Zhang et al, 2022), which is similar to an unloading effect. Judging from modeling results, water flow in the fault must be a priority because water weakening generates protracted seismicity. Model results also show that, although seismic-moment values indicate small levels of seismicity, their frequent occurrence could potentially lead to an accumulation of damage. Further investigation is therefore suggested at this stage, both in (1) background-seismicity monitoring prior to any such project with a dense seismic network and (2) by using more advanced 3D models.

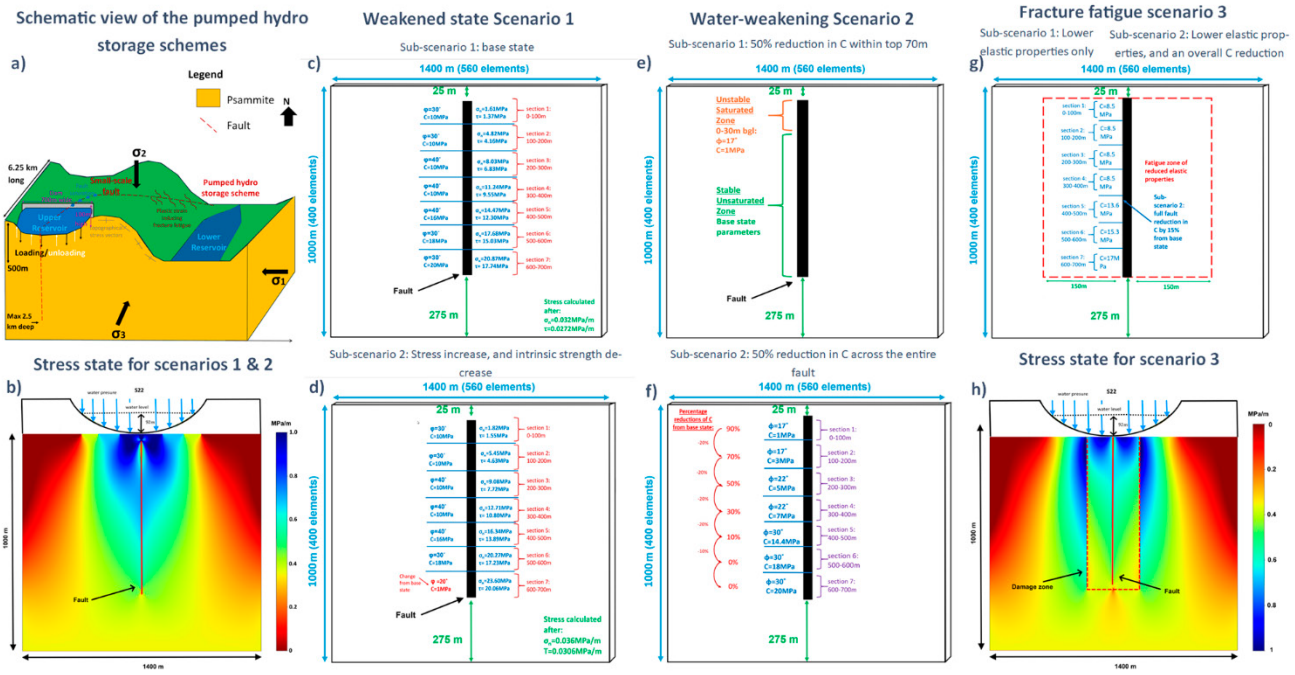

Figure 1. (a) 3D schematic view of modeled pumped hydro-storage schemes, 700 × 92 m, with theoretical water capacity of 26 billion L. (b) Stress field due to presence of water (S22 stress) at maximum water capacity of reservoir. Weakened-state Scenario 1—(c) Subscenario 1, in which cohesion is changed such that it is greater than shear stress. It is enforced because, as the fault is not constantly slipping, realism is maintained. (d) Subscenario 2, in which stress is increased with depth such that σn = 36.30 MPa/km and τ = 30.86 MPa/km—testing range of background stress that could cause failure independently from water load. Water-weakening Scenario 2—(e) Subscenario 1, which reduces cohesion to represent influence of water at top part of fault. (f) Sub-scenario 2, which tests what occurs when fault is fully saturated with water. Fracture-fatigue scenario 3—(g) Sub-scenario 1, which is used to assess ductile-strain conditions, reducing elastic properties within a 300-m zone around the fault and reducing cohesion to imitate strain-induced weakness—(h) Sub-scenario 2, in which cohesion is further reduced by 15%, as compared with that of Subscenario 1. These models provide potential scenarios and, therefore, potential outcomes, and do not definitively predict an exact location or extent of fault rupture but, rather, act as an indicator of where one is possible under conditions set.

Table 1. Summary of model results. Within water-weakened state, Subscenario 1, ESS value nearly 3 times that of fracture-fatigue Subscenario 2 data. Water-weakening effect can have significant influence on ESS and, thus, encourage greater displacement directly beneath reservoir. Water-weakened-state and fracture-fatigue scenarios linked to protracted-seismicity model, in which mechanical properties of fracture change due to presence of reservoir.

	Rapture length / total fault length	Fault displacement (m)	ESS at fault rupture segments (MPa)	Seismic moment M_o (Nm)
Weakened state 1	0	0	-0.017	-
Weakened state 2	0.27	0.9-19.4	0.1-18.8	1.89E+13
Water weakening 1	0.1	0.4	0.35	1.00E+11
Water weakening 2	0.57	1.8-12	0.20-2.5	1.89E+13
Fracture fatigue 1	0	0	-0.017	-
Fracture fatigue 2	0.27	10-18	0.7-1	1.40E+13

AEFA: Earthquake forecasting dataset for AI

Yangkang Chen, The University of Texas at Austin, Alexandros Savvaidis, The University of Texas at Austin, Yunfeng Chen, Zhejiang University, Chao Li, The University of Texas at Austin, Shanshan Yong, Peking University, Xin'an Wang, Peking University, and Omar M. Saad, KAUST

Submitted to Seismological Research Letters.

Earthquake forecasting is a challenging task aimed at predicting the occurrence of a large destructive earthquake in the short term, e.g., within days or months. With the advent of artificial intelligence (AI), this long-term, seemingly intractable problem has become surprisingly solvable, thanks to the acoustic electromagnetic to AI (AETA) initiative launched in the past decade. The AETA program has designed two anomaly-sensitive sensors—electromagnetic and geo-acoustic sensors—to continuously record signals, in hopes of extracting weak precursor signals for forecasting future earthquakes. To better define the problem, many physics-based features have first been calculated and extracted from continuous data as an input for a machine-learning-based classifier to predict whether an earthquake will occur in a certain period of time in the near future. The assumption is that the extracted features bear precursory anomalies related to physical stress or electromagnetism changes, thereby facilitating a regressional classifier learned from historical measurements and ground-truth earthquake-occurrence labels. A dataset in a 4-year recording experiment was carefully prepared as a benchmark dataset for AI studies. Earthquake forecasting enthusiasts and AI experts are encouraged to design advanced AI models for predicting earthquakes, hopefully leading to a breakthrough along this research track. A repository can be accessed at https://github.com/chenyk1990/aefa.

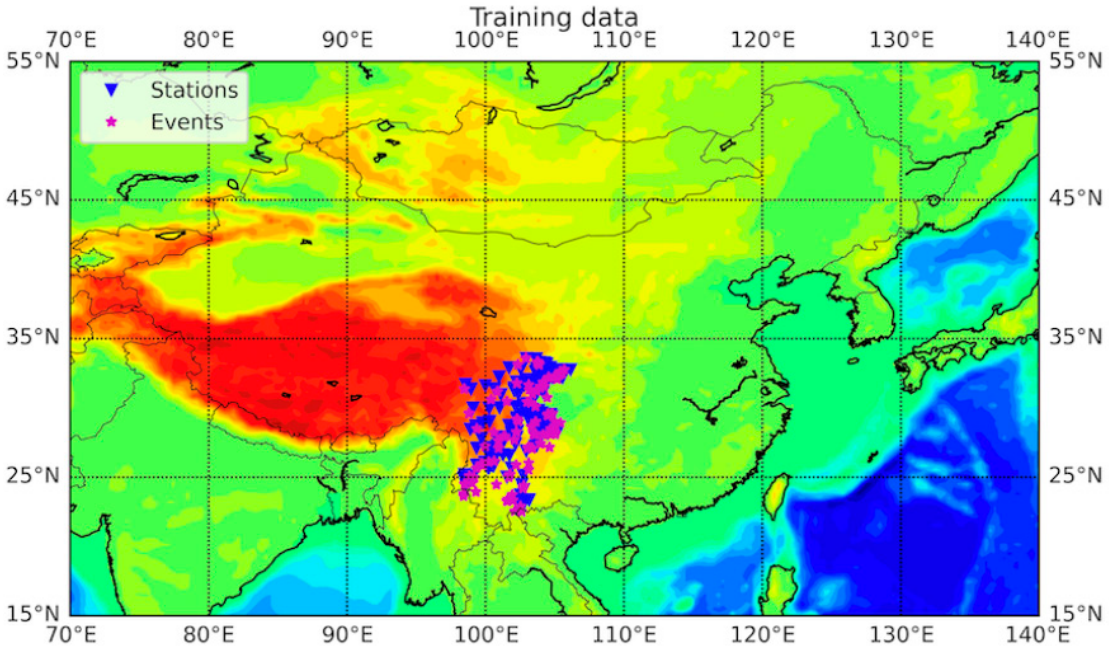

Figure 1. AEFA station and earthquake event distribution on map of AEFA training data. Station coverage in most seismically active part of West China.

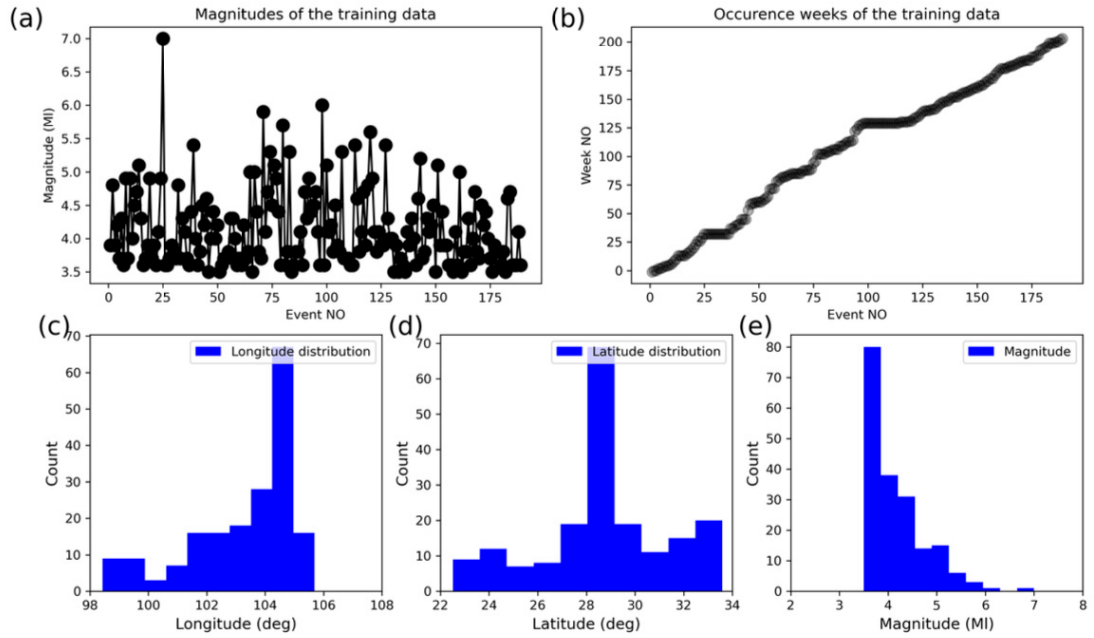

Figure 2. Event-distribution plot. (a) Magnitudes of training data. (b) Week NOs of training data. (c) Longitude distribution. (d) Latitude distribution. (e) Magnitude distribution.

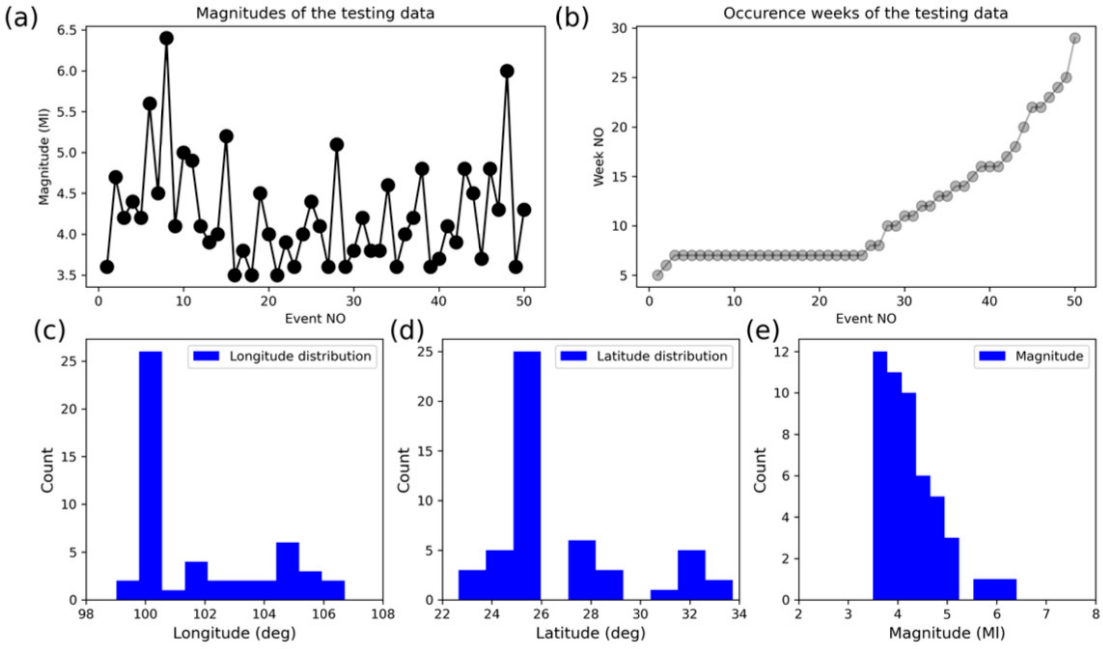

Figure 3. Event-distribution plot. (a) Magnitudes of testing data. (b) Week NOs of testing data. (c) Longitude distribution. (d) Latitude distribution. (e) Magnitude distribution.

Improvements to the TexNet Web Presence

Aaron Averett

One of the cornerstones of TexNet's strategy for collecting and distributing earthquake data to stakeholders in Texas is a series of web applications, each of which provides a unique view into TexNet's earthquake data. This system also collects information that assists TexNet scientists and the community in understanding the causes of seismicity in Texas. These web applications include, but are not limited to, the TexNet Earthquake Catalog, High Resolution Catalog, and Injection and Pressure Reporting Tool. In 2024, each of these web applications was updated or redesigned to improve usability and provide new capabilities.

As part of its efforts to continually improve availability of information to the public, TexNet has expanded its team of web software developers to a total of four, including a professional designer. One of the results of this expansion in capability has been an enterprise-wide review of TexNet's existing application designs, with the intent to improve usability. The result of this review is a new visual style, which is shared across all sites, with variations in colors and layout used to differentiate each site, and serve each site's distinct mission.

The TexNet Injection and Pressure Reporting Tool (IVRT) is a web application, developed in cooperation with the Railroad Commission of Texas (RRC), that allows well operators to submit information describing their injection activities to TexNet and the RRC. Previous mechanisms for collecting these data were limited to collecting records on a monthly basis, which was considered insufficient to properly understand the relationship between injection and seismicity. Deployment of the IVRT has allowed collection of daily records, which dramatically improves the resolution of the data and quality of the science that can be derived from it. Data collected by the IVRT are available for download by the public, with over 680,000 daily injection volume records from more than 800 wells having been collected as of November 2024.

The IVRT received a major update in March 2024 with the addition of the ability to collect bottom hole pressure data (Fig. 1). This capability was developed in order to assist operators in complying with RRC's Notice to Operators, sent on December 19, 2023, that calls for submission of measured or estimated bottom hole pressure information for certain wells. Given the diversity of equipment in the field, it was necessary to accept these data in several different formats, described in the application as methods 1, 2, and 3, corresponding to the options described in the Notice to Operators, and providing a variety of daily and quarterly reporting options.

In addition to the new bottom hole pressure reporting capability, numerous other user interface enhancements were made to improve efficiency of submission by the users, who are primarily well operators, being asked to submit daily data on a semi-voluntary basis. Such improvements include smarter pre-filling the submission forms with past data in cases where values to do not frequently change; implementation of a feature that allows data to be entered into a spreadsheet for multiple wells in advance, bypassing the need for manual data entry; and improvements to validity checking routines that occur before final submission, reducing the chances of erroneous data being entered due to human error. Finally, the site's front page, including the map symbology, was updated in order to improve legibility.

The TexNet Earthquake Catalog received numerous updates, the most significant being a revision to its visual style (Fig. 2) and addition of a new feature that allows viewing of the seismometer traces from each of TexNet's seismometer stations in real time. Previously, access to this information was limited to experts equipped with the specialized software required to retrieve it from TexNet's earthquake detection infrastructure. With the release of this updated version of the Catalog, this information can be viewed within a browser, allowing interested members of the public to observe the same signals that TexNet's seismologists do, as they are received.

TexNet remains committed to its mission of providing high-quality earthquake information to government, industry, and the public in a timely manner. Web applications such as the Catalog and IVRT to convey this information has been and will continue to be a primary tool that TexNet uses to achieve that mission. Support for these applications and others, such as the TexNet Web Tools Portal, will continue into the future.

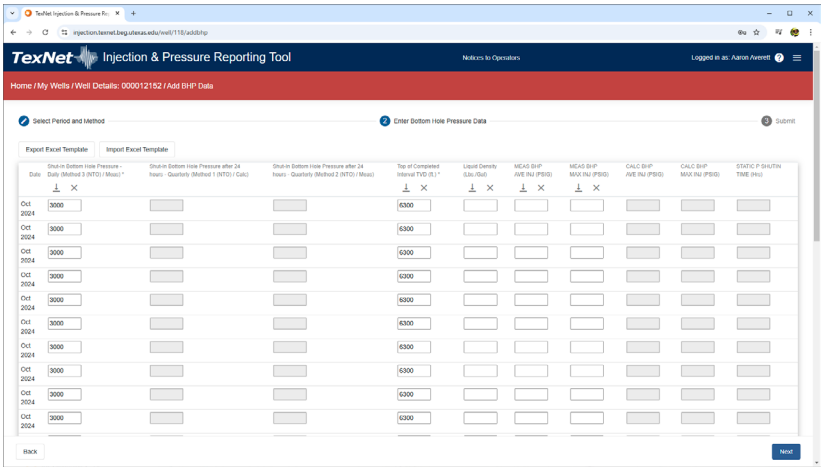

Figure 1. The Injection Pressure Reporting Tools' new bottom hole pressure input page.

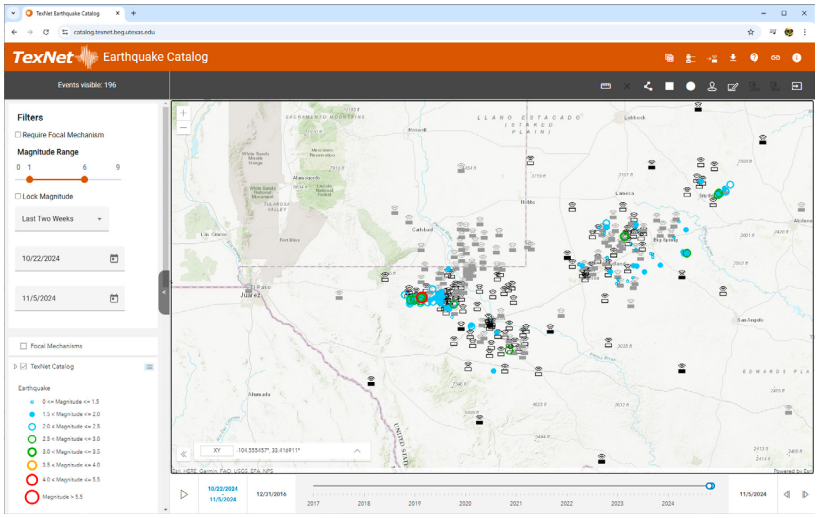

Figure 2. The new visual style of the TexNet Earthquake Catalog.

Introducing the TexNet Web Tools Platform

Aaron Averett

One of the most important products of TexNet's collaboration with its partners in industry and the academic community is a set of software tools for modeling or analyzing the relationship between seismicity and other phenomena, such as injection of water into the subsurface. Although these tools offer valuable insights, they can be difficult to use for a few reasons, the primary ones being that they often require complicated setup, specialized supporting software that is difficult or expensive to license, and may lack any sort of graphical user interface, requiring the user to employ other software in order to properly interpret the results. To address these challenges and make these tools available to all members of the community, TexNet has chosen to convert several tools into web applications that allow the user to interact with them using a browser, without the need to endure the complex setup required to run them on the user's own computer. The method chosen to accomplish this process was to build a single web application that can provide access to many different tools, with shared user accounts, data storage, and user interface elements. This application is currently in development, and will be deployed for testing in late 2024 as the TexNet Web Tools Platform.

Building a shared platform to host these tools offers several key advantages over simpler options, such as the construction of separate web applications for each tool. The primary advantage is that the user experience can be improved dramatically by allowing the sharing of user accounts and data across multiple tools, reducing the need for tedious repetitive input on the part of the user, and creating the possibility to easily use the output from one tool as the input to another. The other key advantage to this approach is that although the initial software development effort required to deploy a single tool is much greater than would be required to build an application that serves just that one, the level of effort required to support additional tools is much lower, requiring only the development of any additional features, if any, that are required for that specific tool.

The TexNet Web Tools Platform is composed of four separate layers: a client-side application, written in Typescript and making use of the Angular framework that accepts input from the user and presents the results, a server-side layer, written in C# and using ASP.NET Core that handles storage of the user's data and manages communication with the tool processes, and a third layer consisting of the tool processes themselves, along with any additional code required to adapt them to use in this environment. A fourth layer, a Microsoft SQL Server database, is used to store the application's data, which consists of both user data and the information the application requires for its own internal configuration.

The design of the platform aims to standardize the presentation of the tools by using the same basic layout to present each one (Fig. 1). The layout is customized for each tool by specifying the series of process steps that that tool contains. For each step, a set of input and output parameters can be specified, which are customizable by administrators in numerous ways, with support for several distinct data types including numbers, strings, dates, tabular datasets (which may or may not be geographic), and single records from a dataset. The interaction of these parameters with each other, both within a given step and with other steps in the process, is configurable by the administrators, giving the platform the ability to support a wide range of possible user interactions. The application also has the ability to show graphs, maps and other visual representations of the inputs or results of each step, which makes it capable of wide variety of different data visualizations.

One of the key challenges encountered during development of the Tools Platform is the execution of the tools themselves on a separate computer from the one presenting the graphical user interface. Web applications conduct communication between the client and server using the HTTP protocol, which is inherently stateless, meaning that no persistent network connection is maintained as the user interacts with the page. Instead, whenever new information is required, a new connection with the server is established, the server responds, and then the connection is terminated. If additional information is required, another connection is established. This stateless protocol presents a challenge when attempting to adapt code that was originally written to be run on the client, with immediate access to the user interface, to instead run on a remote server. Because some tool operations may take several minutes to execute, it is not possible for the network connection to remain open while the tool works. Instead, the tool code must be executed asynchronously, independent of the network connection.

To accommodate this requirement, two measures are required. The first measure involves altering the tool code to run using only information supplied to it in files or at the command line, without the need for any of its original graphical user interface. The second measure is implemented in the client and server layers, which provide the graphical user interface, management of the execution of the tool code on the server, and the communication between the two.

Initially, two software tools will be made available using the TexNet Web Tools Platform, and a third will be released in early 2025. The first is the Geostatistical Software Toolkit, or GIST, which allows the user to explore different scenarios describing the contributions of disposal well activity to seismic events. The second is the Fault Slip Potential tool, or FSP, which analyzes the potential of a set of observed or hypothetical faults to slip under varying conditions. These tools exist as standalone software at present, but they are being converted by TexNet's software development team into libraries that can then be integrated into other applications without their own graphical user interfaces. When conversion of these libraries is complete, user testing of them on the Tools Platform can begin. Limited testing is expected to begin in late 2024, and wider testing will occur in the first quarter of 2025.

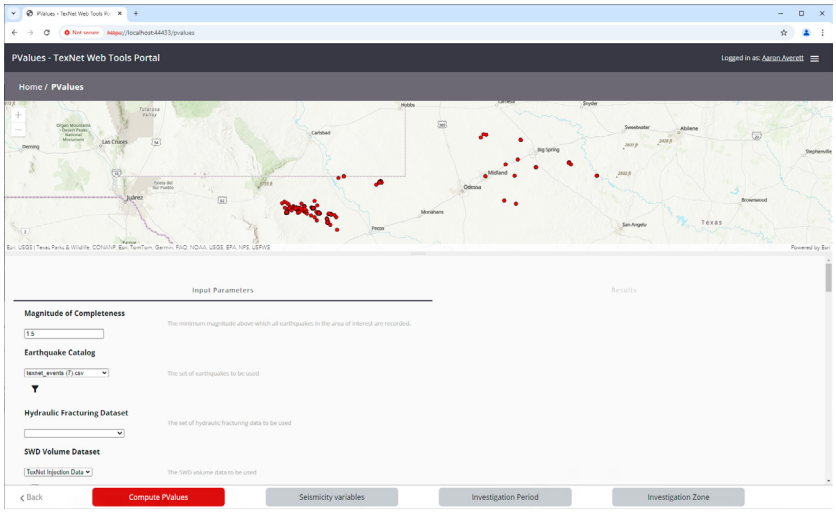

Figure 1. An early version of the TexNet Web Tools Platform's user input page.

Designing GIST's Interface from the Ground Up

Elena Kalogirou

This report details the progress of the UI/UX design and development of the Geomechanical Injection Scenario Tool (GIST), developed by TexNet in collaboration with the ExxonMobil team. The project began with initial conceptualization and whiteboarding sessions, wherein various ideas were explored to establish a foundation for the tool's design and functionality. Next was the creation of low-fidelity wireframes (Fig. 1), which were used to confirm that all necessary elements were included. As the design evolved, high-fidelity mockups were created (Figs. 2 and 3), refining the components to ensure a user-friendly experience.

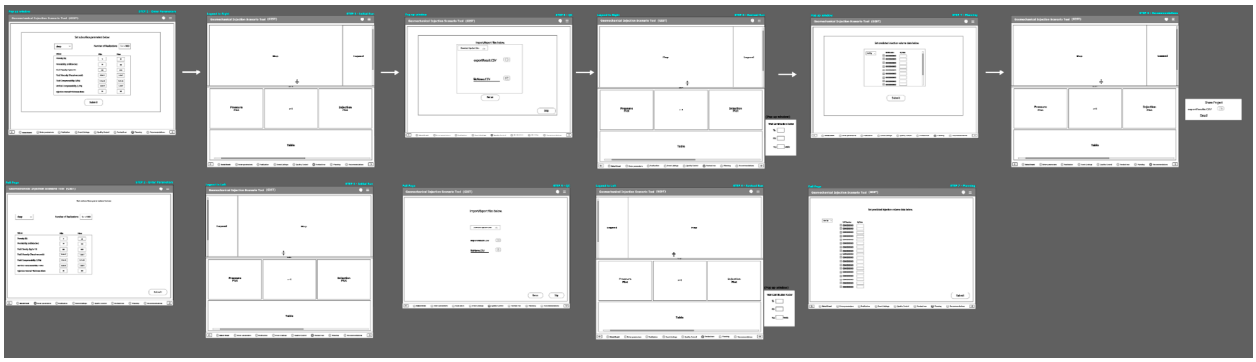

Figure 1. Low-fidelity wireframes for the GIST tool.

GIST's functionality centers on a structured five-step workflow: earthquake selection, subsurface parameter input, quality control and data correction, visualization of filtered results, and scenario forecasting for geomechanical planning. The interface is designed to incorporate user-friendly navigation through next and back arrow keys displayed by the step buttons at the bottom of the page. Data entry fields will be clearly labeled for straightforward and accessible input for users. Resulting outputs will be presented in engaging graphs, with options for fullscreen viewing and additional filtering capabilities. Users will also have the ability to easily save and reset their data inputs, with options to export outputs in PDF or CSV formats, facilitating easy sharing and further analysis of data.

Design elements such as color schemes, fonts, icons, and navigation components were carefully chosen to enhance appeal, functionality, and scalability for future needs. GIST's design will include blue as the accent color, whereas the webtools portal will be shown in gray tones, to harmonize with the accent colors of the other tools.

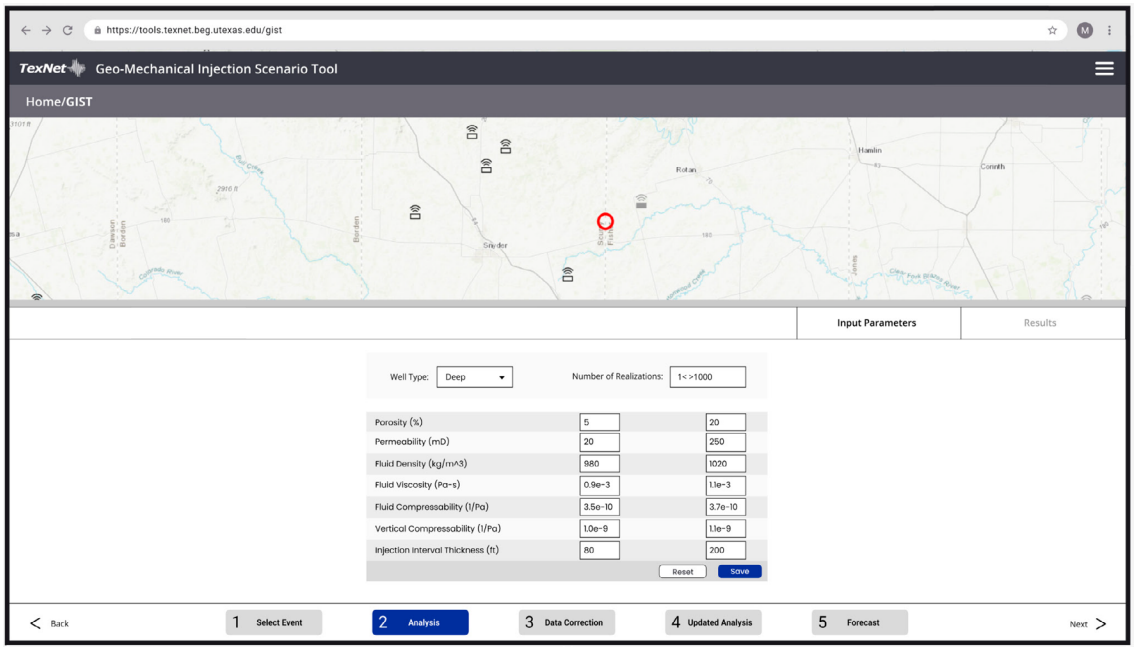

Figure 2. High-fidelity mockup of part one of second step of GIST, Analysis: Input Parameters.

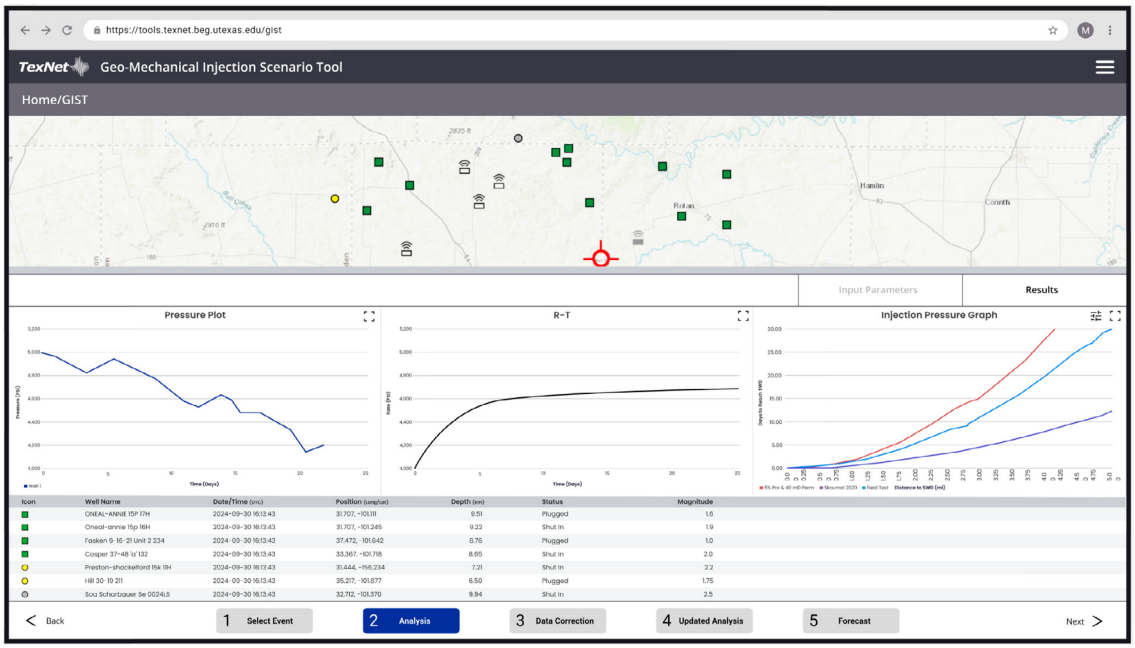

Figure 3. High-fidelity mockup of part two of second step of GIST, Analysis: Results.

This development process is an ongoing collaboration between TexNet and ExxonMobil, with feedback loops at each iteration to refine user flow, visual hierarchy, and placement of elements. Although significant progress has been made, considerable work still lies ahead. Future efforts will focus on developing the tool's functionality, optimizing performance, and ensuring that GIST meets the needs of users. Continued collaboration and feedback will be essential in achieving a final product that can facilitate a strong user interface, allowing users to navigate complex geomechanical scenarios effectively.

Development of GIST as a Web Service

Peter Sarkis

The Geomechanical Injection Scenario Tool (GIST) is a collaborative web application in development that aims to streamline the analysis of earthquake data related to well injection activities. The project started as a series of Python scripts for injection, computation, and visualization, which later evolved into a collection of Jupyter notebooks. Although these notebooks allowed users to connect various steps of GIST in one place, transitioning to a web platform offers several advantages.

One key benefit of moving to the web is the ability to provide a more tailored user experience by consolidating data entry, computations, and visualizations. Integrating GIST into the TexNet web tools portal will enable users to share data across different processes, making it easier to engage with other tools and reducing duplication for those using multiple applications. Additionally, session management features will allow users to seamlessly continue their work where they left off and revisit completed tasks. This web-based framework facilitates an iterative process, allowing for data corrections and future injection forecasts. The current project goal is to introduce GIST as a basic, viable product within the TexNet web tools, along with training materials, with additional features to follow.

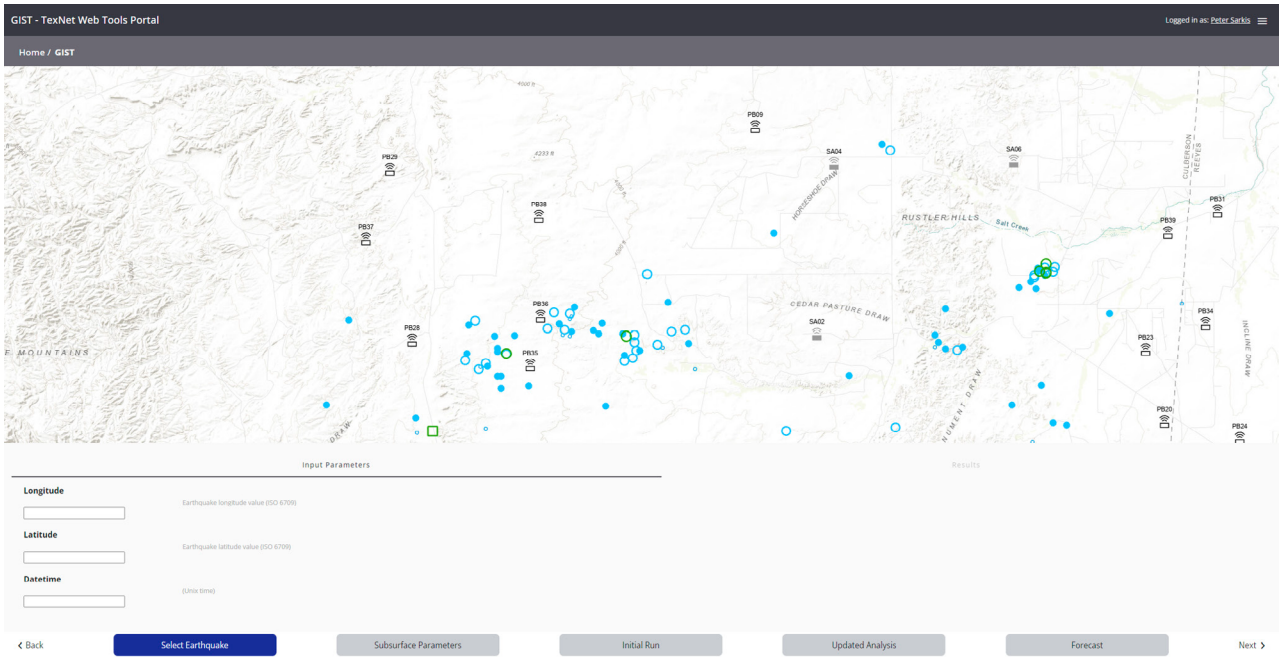

Figure 1. An early development view of GIST within the TexNet web tools shows how logged-in users can interact with the ESRI Map element to select an earthquake or manually input longitude, latitude, and date/time. Users can then initiate GIST computations, progressing through the GIST process.

Migrating to the web also broadens the potential user base. Not all users are familiar with running or modifying Jupyter notebooks, so adding a graphical user interface will make GIST accessible to a wider audience, while still providing options for experienced users. As more processes are integrated into the TexNet web tools, GIST will gain visibility, and overlapping data will be easily accessible across different tools.

Session management is a significant improvement gained from this migration. Some complex processes can take several minutes to hours to complete, so automatically saving a user's session to their personal web tools account greatly enhances usability. This allows users to leave mid-process, close the application, and resume later without losing progress. Users can also revisit past work, easily jumping back into previous sessions to review outputs.

The seismicity industry is continually evolving, necessitating that the tools we use adapt accordingly. Flexibility is a cornerstone of the TexNet web tools portal, designed to allow administrators—regardless of coding background—to access a comprehensive suite of administrative panels. This enables quick and efficient adjustments to various processes, ensuring the system remains responsive to the scientific community's dynamic needs. For GIST, this focus on flexibility and user-friendliness will be crucial as it evolves to incorporate more complex features and computational capabilities.

Beyond the advantages of a web-based platform, the TexNet team plans to implement major improvements based on user-driven requirements. The initial development of GIST and its Jupyter notebooks focused on a smaller group of users, but recent efforts have included extensive consultations with future users across various sectors. This engagement has resulted in a detailed list of specific needs and pain points.

This comprehensive feedback has been instrumental in guiding our development efforts, ensuring that the first release of the revamped GIST will be both functional and beneficial to users. By aligning the tool's capabilities with the real-world experiences and requirements of its users, we are committed to creating a resource that is effective and user-friendly, fostering a more collaborative and productive environment for those using GIST in their work.

Ultimately, numerous benefits accrue from moving an application like GIST to the web. A more customizable user experience will allow users to tailor their interactions with the tool to better suit their individual needs. The integration of session management will enhance usability, enabling users to pause and resume their work effortlessly. Additionally, the web-based platform will facilitate greater collaboration by making it easier to share data and insights across different processes and tools. By incorporating user feedback and adapting to the evolving needs of the seismicity industry, GIST is poised to become a more effective and accessible resource. This transition not only enhances the functionality of the tool but also fosters a more productive environment for all users and encourages future advancements in geomechanical injection analysis.

Enhanced User Experience Using the Fault Slip Potential Tool

Elena Kalogirou

Recognizing the need to improve the Fault Slip Potential (FSP) tool, TexNet is actively involved in a thorough redesign and redevelopment process of the application. This transformation involves transitioning the existing framework into a web-based platform that will be integrated into a broader portal. This webtools portal will house a variety of other tools aimed at supporting seismicity research and computations.

The workflow of FSP version 2.0 (Fig. 1) consists of six stages: model inputs, geomechanics, probabilistic geomechanics, hydrology, probabilistic hydrology, and integrated results. Each of these stages is critical for understanding the interactions between injection and fault stability. The steps are arranged in a tabbed format, but the design fails to provide effective guidance, possibly making it difficult for users to navigate the process clearly. Additionally, the elements within the workflow have become somewhat outdated, resulting in a range of user pain points. Slow processing speeds that hinder workflow efficiency, parameter inconsistencies that disrupt workflow, and restrictive import formats and file types further obstruct usability. Users have also reported issues with the limited capabilities of report generation in the final step of FSP. Together, these limitations indicate the need for a more modern, streamlined, and user-friendly interface.

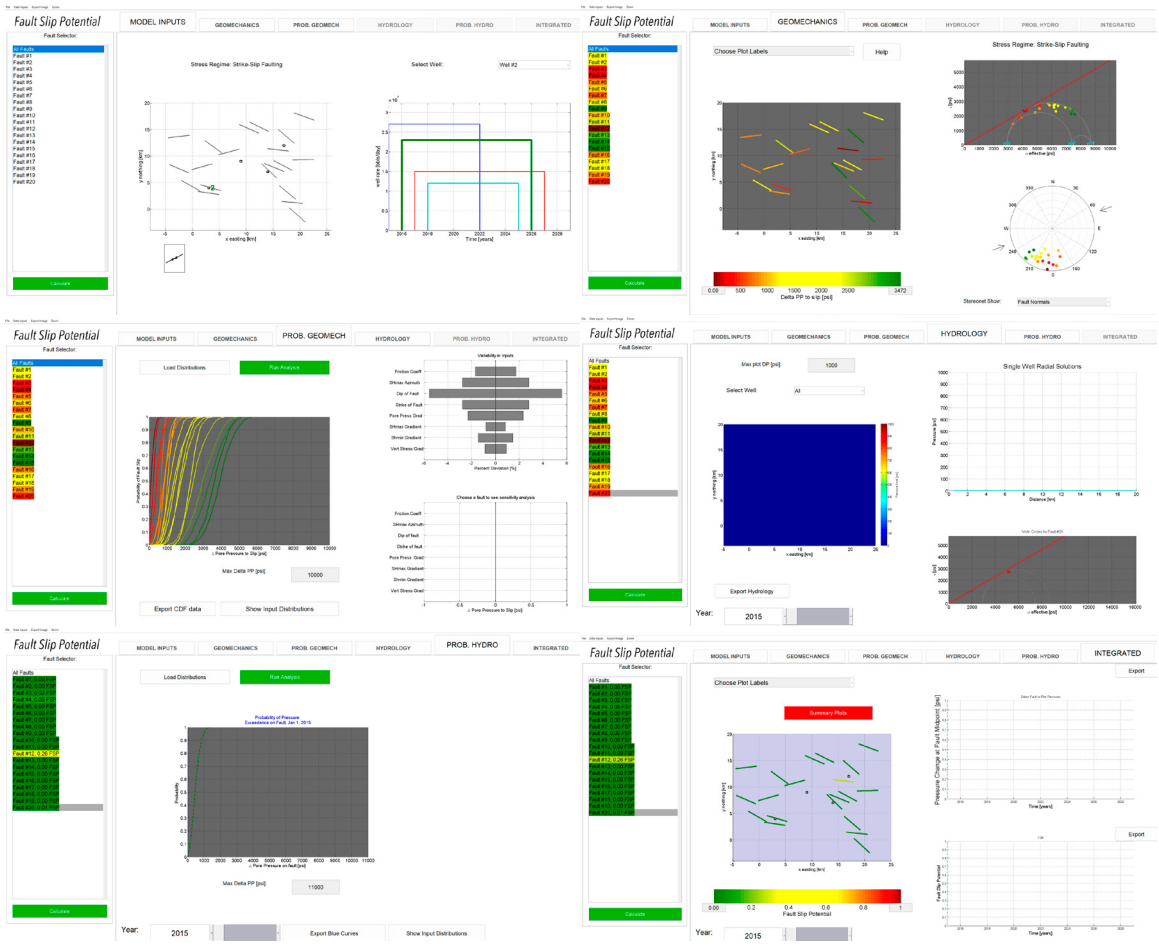

Figure 1. The six tabs featured in FSP version 2.0.

In the updated version of the FSP tool (Fig. 2), there will be a significant emphasis on organization, data visualization, and user experience. Navigation will be more intuitive for users with the addition of next and back arrows, replacing the previous tab system. This change will allow for smoother transitions between different sections of the tool. A map is also planned for further visualization, designed similarly to the interface of the Geomechanical Injection Scenario Tool (GIST). This addition will allow users to visualize geographic data more effectively, aiding in their analysis and decision-making.

The updated design of FSP will include red as the accent color, providing a distinctive look within the gray tones of the webtools portal that unifies the different tools. The new tool will incorporate cleaner, more modern elements to enhance the overall appearance and user experience. Furthermore, the addition of a toolbar will offer additional help, resources, and features that were not present in the previous version. By improving the way data are presented, the redesigned FSP tool will improve user comprehension and enable more informed decision-making regarding fault slip potential. Ultimately, these enhancements will create a more user-friendly tool that meets the evolving needs of its users.

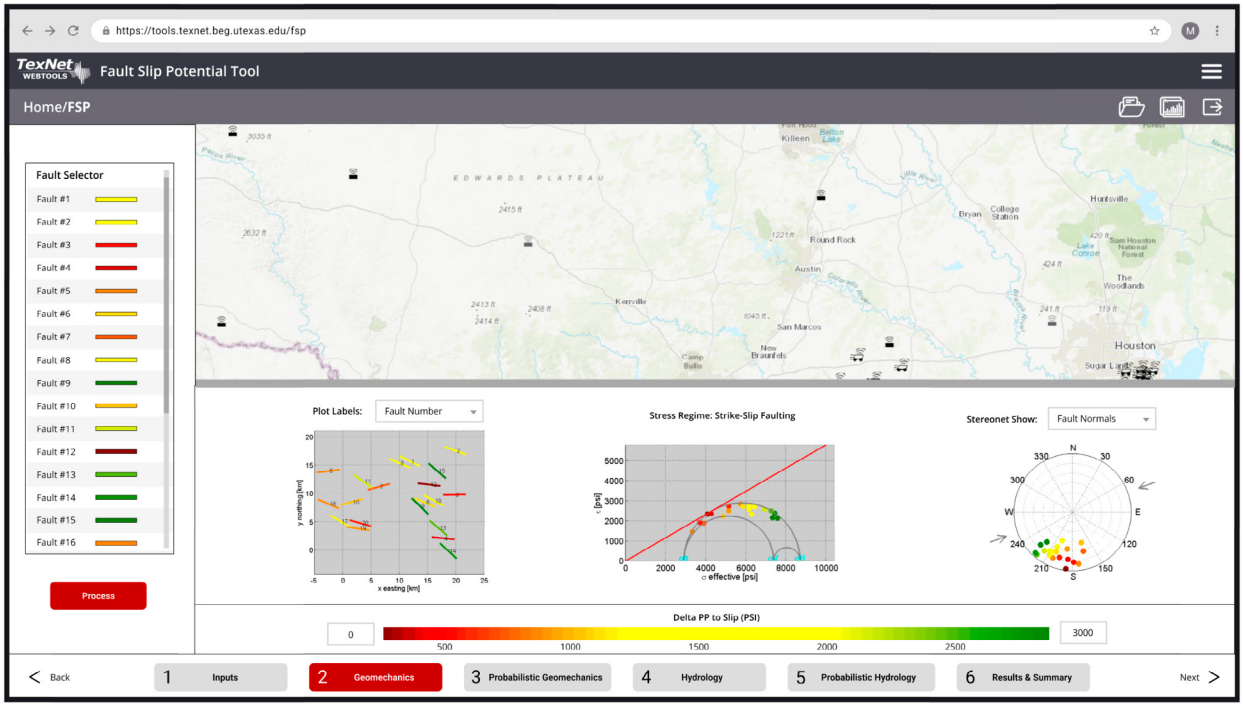

Figure 2. High-fidelity mockup of step two, Geomechanics, in FSP Version 3.0. It is important to note that the graphs displayed here have been sourced from an earlier version of the tool, as the updated visualizations are still in development.

Integrating Fault Slip Potential Tool into TexNet's Web Tools Portal for Enhanced Induced Seismicity Risk Management

Nikolaos Bakirtzis

TexNet has been making continuous efforts to expand and improve the web services it offers to its stakeholders. Part of those efforts is the current development of the Fault Slip Potential (FSP) tool, which will be integrated into TexNet's web tools portal. FSP is designed to calculate the cumulative probability of a fault exceeding Mohr-Coulomb slip criteria due to increased pore pressures from fluid injection. By incorporating a quantitative risk assessment in geomechanics and hydrology, FSP can assist operators and regulators with their decision making when they design injection operations.

Using both a deterministic and a probabilistic model, FSP provides a flexible model that has the ability to account for uncertainties in key parameters like the fault orientation, stress field, and hydrological properties. This feature allows the user to inspect how these uncertainties impact the fault stability under various injection conditions by utilizing a Monte Carlo simulation, which uses random sampling to predict possible outcomes when the inputs themselves are uncertain. The model is iteratively running using random inputs from input probability density functions (PDFs), and it aggregates the distribution of results.

FSP's workflow is a step-by-step assessment of fault slip potential. Each step focuses on a specific component of the model. This enables a clear and progressive understanding of how various factors can affect fault stability under different conditions. Figure 1 shows the workflow inside the web tools portal.

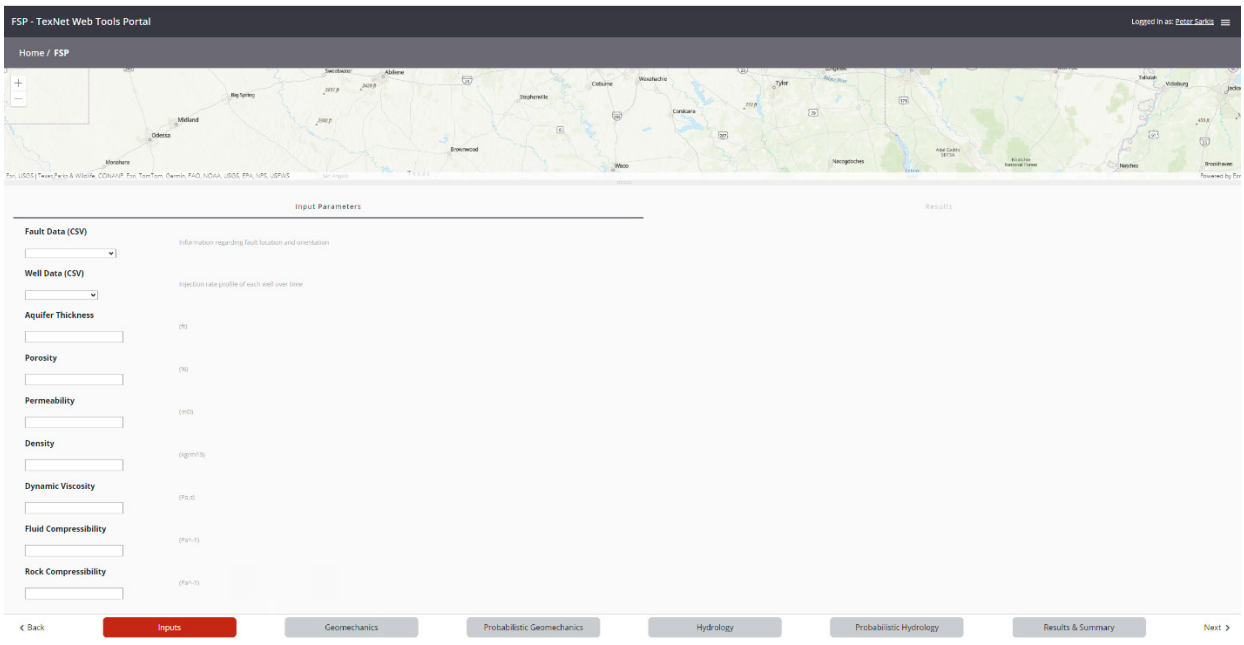

Figure 1. The systematic, step-by-step assessment of FSP, structured across the six tabs guiding the user through the full analysis process.

The Geomechanics tab allows the user to perform a geomechanical analysis without considering parameter uncertainties. The Probabilistic Geomechanics step builds on the previous tab by running the Monte Carlo simulation to produce a probabilistic distribution of pore pressures needed to induce slip on each fault. Similar to the hydrologic model, the Hydrology step assesses pore pressure changes over time due to fluid injection, assuming a uniform flow model. In Probabilistic Hydrology, the Monte Carlo simulations can be applied to the hydrology parameters, providing a probabilistic range of pressure increases on each fault based on the input uncertainties. Finally, the Summary tab combines the results from both probabilistic geomechanics and hydrologic models and displays the cumulative slip potential values across all faults.

The FSP web tool will leverage modern technologies to enhance both the computational efficiency and the visualization quality of the results. Julia, a language optimized for high-performance scientific computing, is what the core computational engine is implemented in. With this feature, we can achieve faster execution times and better handling of complex numerical models compared to other, more widely used programming languages. In addition, D3.js, a JavaScript library for dynamic and interactive visualization of data, will be used for FSP to present graphs that enhance the user's understanding of the model outputs.

Looking ahead, TexNet will expand FSP's capabilities with additional features that will increase its versatility and user-friendliness. Those features include, but are not limited to, support for a broader range of input data formats used in the industry, such as coordinate systems, Petrel files, and reported disposal volumes from TexNet, reporting features for exporting and sharing insights from the assessments, and more advanced visualization capabilities.